Helix – Coil – Transition in Solid Polypeptides

Dissertation zur Erlangung des Grades
„Doktor der Naturwissenschaften“
am Fachbereich Chemie, Pharmazie und Geowissenschaften
der Johannes Gutenberg – Universität Mainz

vorgelegt von

Mirko Dietz
geboren in Mainz

Mainz 2007

Table of Contents

Chapter 1
General Introduction

1.1 Motivation

Poly(L-glutamates) have attracted considerable attention in the past for industrial applications described in many publications and patents.[1,2] Especially, poly(L-glutamates) with short side chains, like poly(γ-methyl-L-glutamate) (PMLG), have shown high potential as industrial materials for fibers or films in fabrics and artificial leather production.[3] Poly(L-glutamates) with longer alkyl chains, like poly(γ-octadecyl-L-glutamate) (PSLG), were intensively studied for effects of the side chain crystallization and their liquid crystalline properties.[4,5] Poly(γ-benzyl-L-glutamate) (PBLG), which was synthesized in the current work as precursor for poly(L-glutamic acid) (PLGA), was the first polymer found to exhibit liquid crystalline behavior.[6-8] Block and graft copolymers containing L-glutamate units have also been suggested as resin and membranes for ion exchange, particularly in biological applications, while the chirality of peptide chains has been exploited in chromatography for the resolution of stereoisomers of DL-α-amino acids.[9-11] PLGA did not yet find much utilization in industrial processes. A new promising purpose for PLGA would be its application as coating material for the printing plate in a commercial offset printing device.

Offset printing is the most widely used printing technique to produce large volumes of documents. The equipment and initial set-up cost are relatively high, but the actual printing process provides low cost document production. Offset printing, shown schematically in Figure 1.1, is a high quality indirect printing process. The plate cylinder is covered by the printing plate consisting of a flexible hydrophilic aluminum or Zn plate, 0.1-0.5 mm thick, with a hydrophobic coating. To transfer the image to be printed on this plate, the coating at the non-image areas of the plate is removed by a photochemical or thermal process by exposing it to laser irradiation (direct imaging). The nonprinting areas on the printing plate have therefore a hydrophilic surface to improve the wetting by water. The formed etched images possess a lipophilic/hydrophobic surface character to improve the wetting by fatty printing inks. The mutual repulsion between water and inks assures constant sharp borders between the areas. For printing, a water-impregnated roller (dampening) is applied first to the plate to maintain the water film in the nonimage area before ink is spread on the plate by the ink rollers shown in Figure 1.1. The inked plate transfers ink from the image to a rubber blanket covered offset cylinder (intermediary surface), which further transfers the image to the substrate (paper) by using an impression cylinder.[12]

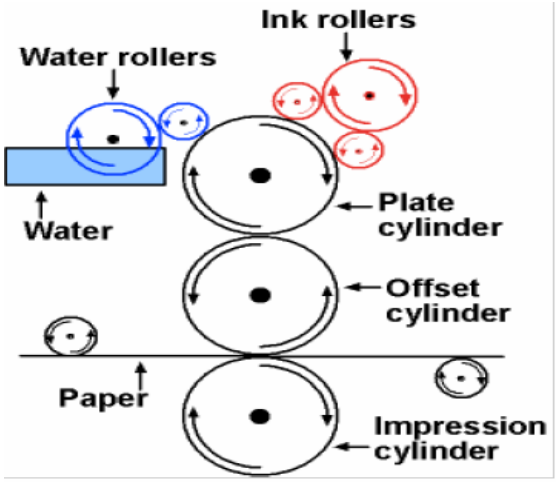

Figure 1.1: The offset printing process.[13]

The described offset printing process could be improved by investigating new low cost coating materials for the printing plate. The required change in wettability should be accessible by annealing defined places of the coating by a laser. A new promising compound for this purpose could be PLGA if a temperature induced solid state conformational transition is possible. The principle, shown in Figure 1.2, assumes a transition between the hydrophilic α-helix and the hydrophobic coil conformation. The different arrangement of the hydrophilic carboxylic acid groups in the side chains would lead to an altered surface wettability. PLGA was chosen due to its well studied precursor PBLG, which is easily prepared on a large scale. The monomer L-glutamic acid is low-cost and has found widespread use as food additive in the form of its sodium salt. Amino acids with an amide group in the side chain (L-glutamine and L- asparagine) were not chosen because these groups stabilize the helical structure through additional hydrogen bonding. It would be expected that polymers based on these amide bearing monomers would exhibit higher melting temperatures of the helix and could shift the required thermal transition to exceed the degradation temperature of the polypeptide.

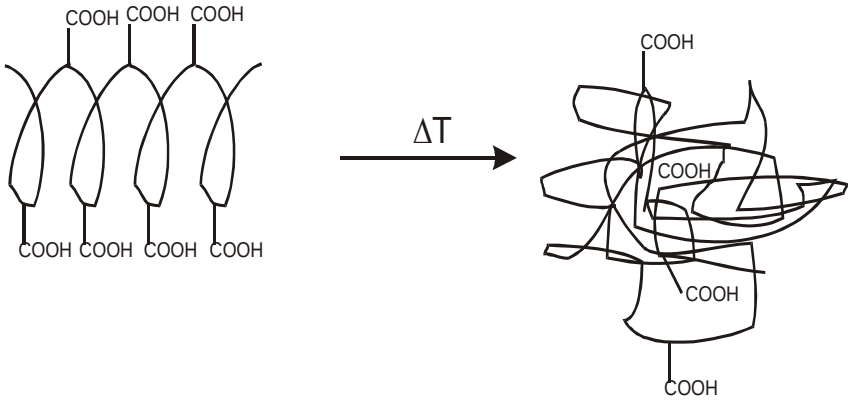

Figure 1.2: Temperature induced helix-coil transition of poly(L-glutamic acid) (PLGA).[14]

1.2 Structure and scope of the thesis

Each chapter of this thesis, with the logical exception of the general introduction (*Chapter 1*) and the conclusive chapter (*Chapter 9*), consists of different possible subdivisions like introduction, synthesis, characterization, conclusion etc.

Chapter 1 describes the motivation and the fundamental background of the helix-coil transition including the different suitable detection techniques. The following first part of the work, *Chapter 2-5*, focuses on the synthesis and characterization of the NCA monomers (*Chapter 2*), the poly(γ-alkyl-L-glutamates) (*Chapter 3*), PLGA (*Chapter 4*), and poly(cysteic acid) (*Chapter 5*). The system development to characterize PLGA by capillary electrophoresis is included in *Chapter 4*. All characterizations conducted for the compounds as powder are described here.

The different approaches to obtain oriented or ordered fiber or film systems mostly based on PLGA are summarized in the second part of the work (*Chapter 6-8*). *Chapter 6* describes the film preparations of PLGA from TFA solutions on silica and glass substrates before the solvent was changed in *Chapter 7* to different hydrogen bonding disrupting solvent systems like DMF, DMA etc. *Chapter 8* consists of the different fiber extrusion attempts for PLGA, PSCBC, and PSBC.

The scope of the dissertation was based on preliminary results of the diploma thesis, which focused on spin-coating of PLGA solutions in TFA on glass.[15] Drop-cast films should be investigated to avoid the induced orientation on the outside region of substrates by centrifugal forces during the spin-coating process. Another disadvantage of spin coating was that no thick bulk films could be prepared by this technique. The films of the present work should exhibit, if possible, a uniform thickness around 5 µm to be suitable to use them as coating material for printing plates. One of the first challenges was to determine a method to obtain uniform reproducible films. The choice of solvent and the evaporation conditions were investigated before films were prepared and analyzed. It was important to determine if long range or only short range order was present in the solid state.

1.3 Helix-Coil Transition

1.3.1 Structure and Geometry

The primary structure of polypeptides refers to the sequence of the amino acids in the polymer chain. The convention for the designation of the order of amino acids is that the N-terminal end (free amino group) is to the left and represents the number one.

The secondary structure of polypeptides describes the three dimensional arrangement of the local segments, whereby the α-helix is a common conformation in proteins. The polypeptides self-assemble in the α-helix conformation driven by formation of intramolecular hydrogen bonds between every main chain C=O and N-H group to a peptide bond 4 residues away yielding a regular, stable arrangement. The peptide planes are roughly parallel with the helix axis and the dipoles within the helix are aligned. All C=O groups point in the same direction and all N-H groups point into the opposite direction. The side chains point outward from the helix axis and are generally oriented towards the N-terminus. The right-handed helical structure repeats itself every 5.4 Å along the helix axis, known as the helical pitch, and has 3.6 residues per turn. The axial translation of the monomer residues is thereby 1.5 Å. Although there are other helical structures possible, the α-helix is the most common due to its stability and packing properties

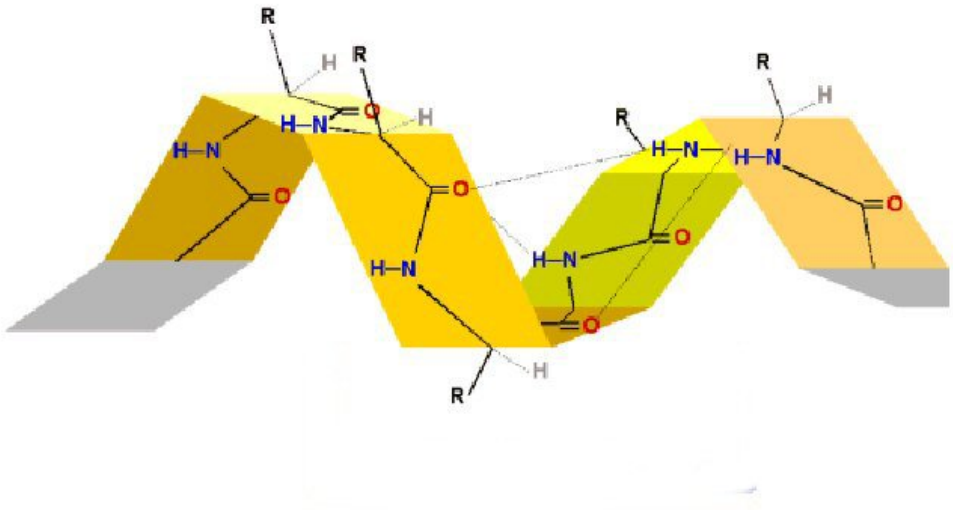

Figure 1.3: The α-helix turn with 3.6 residues.[15a]

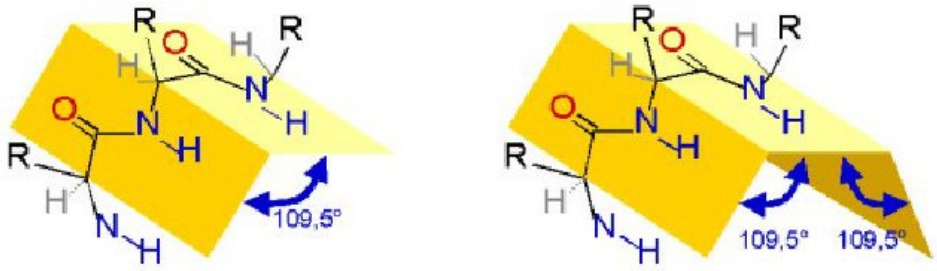

Figure 1.4: The α-helix structure along two (left) and three (right) amide bonds.[15a]

The β-pleated sheet is the second most common form of regular secondary structures in proteins. The chains can be either parallel or antiparallel. In parallel sheets adjacent peptide chains proceed in the same direction, whereas in antiparallel sheets adjacent chains are aligned in opposite directions. The linearity of the intermolecular hydrogen bonds in an antiparallel β-sheet is responsible for the higher stability as compared to a parallel β-sheet. The polypeptides with side chains having branches or a hetero atom (oxygen or sulfur) attached directly to the β-carbon form the β-sheet structure exclusively. The branching causes enough steric hindrance of the side chains to inhibit the formation of the helical structure. Poly(L-valine) for example exhibits a β-sheet in contradiction to poly(L-leucine) which adopts α-helix even if it is a homologue of valine with one additional methylene group. The propensity of the polypeptides including a heteroatom, like poly (L-cysteine) and poly (L-serine), to form a β-sheet cannot be attributed to steric factors. It appears that the β-sheet is the thermodynamically stable state then.

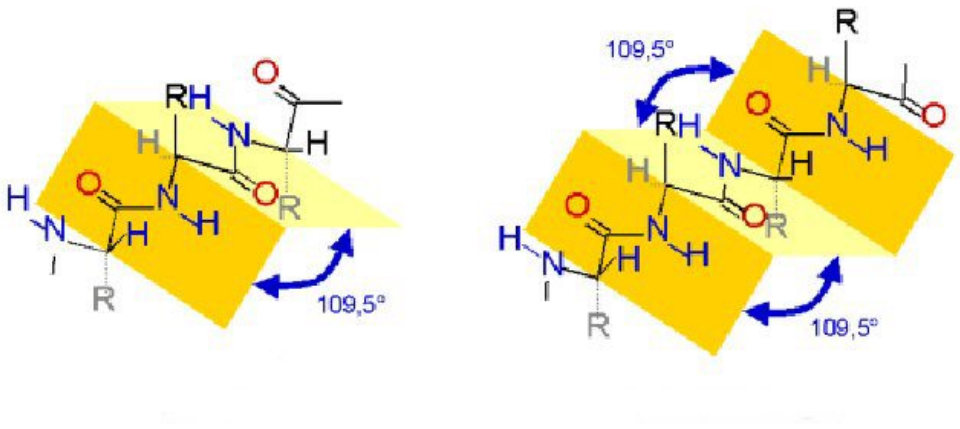

Figure 1.5: The β-sheet structure along two (left) and three (right) amide bonds.[15a]

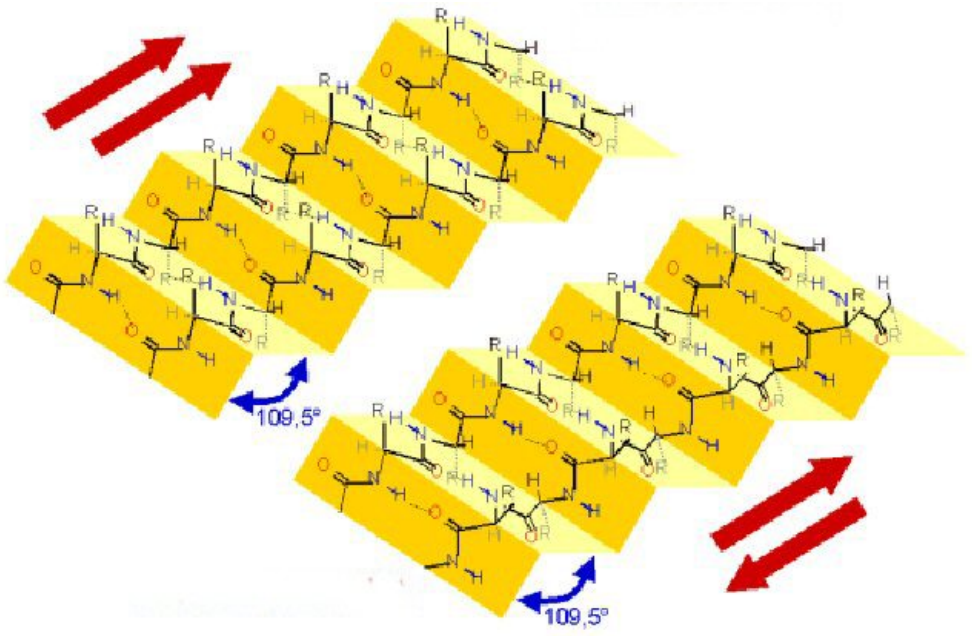

Figure 1.6: The β-parallel (left) and β-antiparallel (right) pleated sheet structure.[15a]

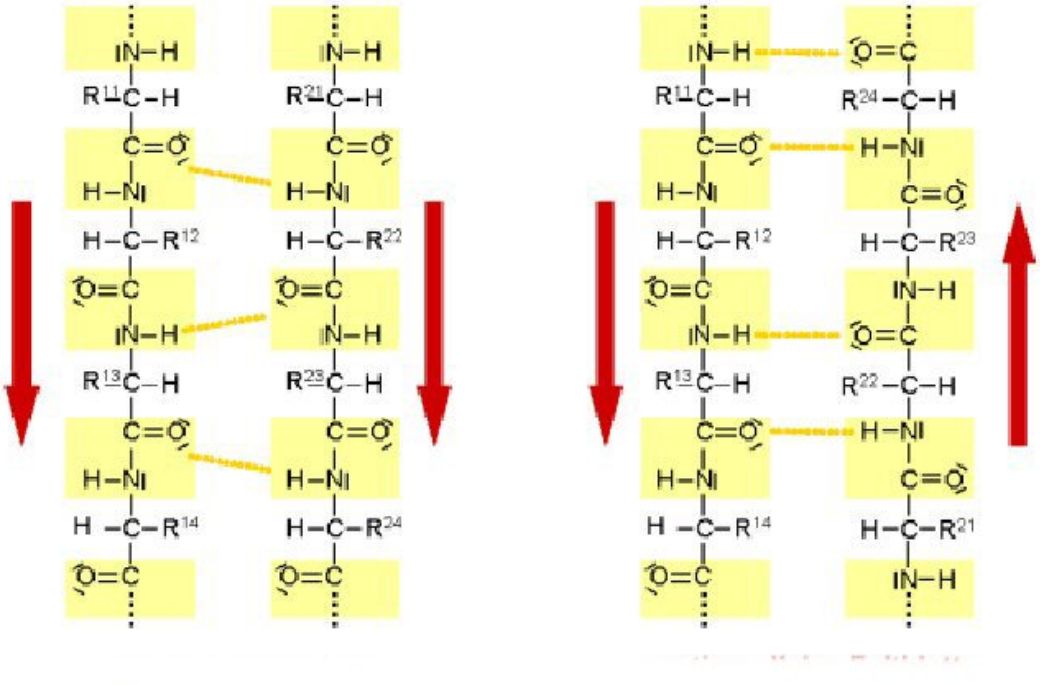

Figure 1.7: The β-parallel (left) and β-antiparallel (right) pleated sheet structure.[15a]

Besides the "natural" preference for one of the two ordered hydrogen bonded structures, numerous researchers investigated the dependence of the secondary structure from the degree of polymerization as another key parameter.[16-19] It was found that at relatively short polymer chain lengths (5-10 units) an antiparallel β-sheet structure is preferred even for a normally helical polypeptide. If the chain length is increased, there is a definite preference for the α-helix which predominates. This phenomenon was confirmed in the past by Blout et al. for PBLG.[16] His group proved that the β-sheet of PBLG is only obtained for low molecular weights. Prepared films of these materials exhibit a mixture of α- and β-forms, whereby the fraction of the β-form exhibited a strong dependence on the nature of the solvent.

The goal to obtain a helix to coil transition in the solid state was based on the known occurrence of such a phenomenon in solution. The transition of an ordered to a disordered state in solution is dependent on the pH of the aqueous solution (if water soluble), on the solvent, and on the temperature. These different parameters will be discussed and explained in the following part of this chapter as the detection techniques are described. The same parameters as for a helix-coil transition are also valid for a sheet-coil transition as was shown for PSBC.[20] This transition was observed at a percentage of 40% DCA in $CHCl_3$. The conformation was detected by different techniques like ORD, IR and viscosity. The viscosity changed only slightly in contradiction to a helix-coil transition where a higher decrease in the viscosity can be observed. The conformation of PSBC in the solid state was previously shown to be of β-sheet type with antiparallel arrangement of adjacent chains.[21,22]

1.3.2 Crystallization model

The first published crystal growth hypothesis for polypeptides was reported by Komoto and Kawai.[23] Figure 1.8 illustrates why growing oligopeptides are poorly soluble according to Komoto. The oligomers that precipitate in the early stage of polymerization possess exclusively the antiparallel β-structure. These β-sheet structures form ribbon-like crystals. A small fraction, however stays in solution and these fully solvated chains continue chain growth in the α-helical structure when DP exceeds 10. Backfolding of growing chains on the surface of β-sheet lamellae creates a serious problem for the preparation of high-molar-mass polypeptides. These chains fold back forming a interchain antiparallel sheet, which finally deactivates the living chain ends before all monomers are consumed due to steric hindrance (physical death of the polymerization).[24]

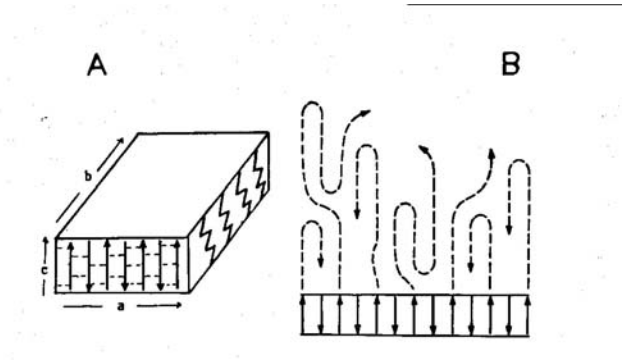

Figure 1.8: [23]

A: Scheme of the precipitation of antiparallel β-sheet crystals of oligopeptides (DP>4).

B: Scheme of "physical death" of amino endgroups by further chain growth.

Electron micrographs revealed that the oligomeric β-sheets precipitating from the reaction mixture were ribbon-like crystals, which slightly thickened with increasing conversion, but did not change their form. Komoto concluded that the chain growth continued on the surface of these crystals, whereby some individual chains grew faster than others.[25,26]

Kricheldorf [27] postulated a modified crystallization model, shown in Figure 1.9, which contradicted the kinetically controlled crystal growth hypothesis of Komoto and Kawai.[23] At DP > 3 the growing oligomers associate and begin to precipitate in the form of β-sheet lamellae. For steric reasons the rate of chain propagation is retarded, whereas the soluble fraction grows faster until the minimum DP for the coil-helix transition is reached. The α-helices begin to precipitate, but fast chain propagation continues until all monomers are consumed. Hence, most chains growing on the surface of the β-sheet lamellae do not have a chance to reach the α-helical conformation. The β-sheet lamellae serve maybe as nuclei for the crystallization of α-helix crystals.

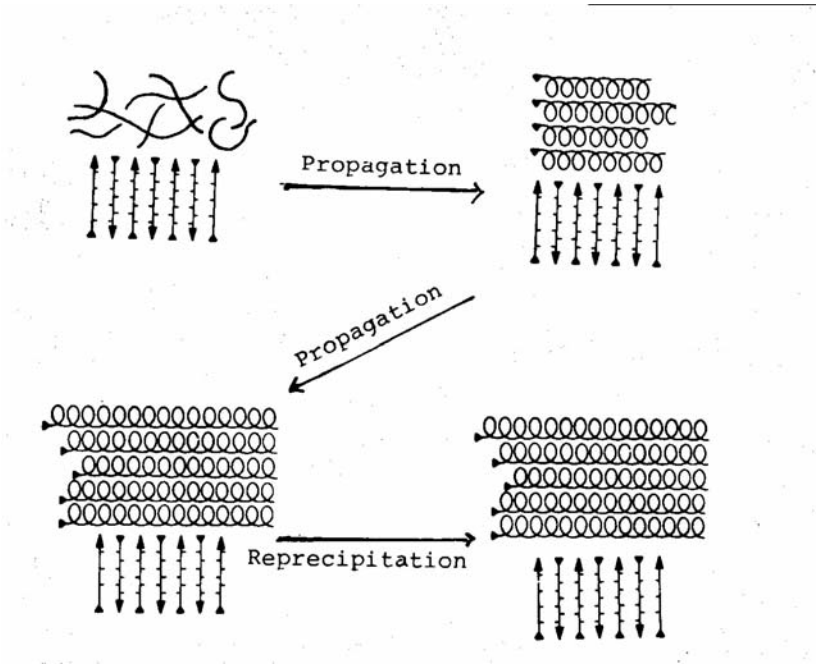

Figure 1.9: Scheme of the secondary structures in primary amine initiated polymerizations of α-helix-forming polypeptides.[27]

Mixtures of helix and sheet structures obtained were previously analyzed by various groups to gain a better understanding of the helix and β-sheet conformations. The first series of experiments attempted to determine if the mixture of secondary structures could be changed by simple reprecipitations in a suitable solvent system. Kricheldorf et al. increased the helical part of PMLG by 20-30 % by reprecipitation from TFA/diethylether, which remained constant upon further reprecipitations. It was assumed that a part of the chains were forming sheets, even if they were long enough to form helices.[27] Other polypeptides like poly(leucine) and poly(phenylalanine) confirmed the substantial increase of the amount of α-helix crystals by reprecipitation. Repeated reprecipitation did not change as well the ratio further, indicating that after the first reprecipitation a thermodynamically stable situation was reached. Obviously these samples contained a substantial fraction of thermodynamically unstable β-sheets in

addition to stable ones. Kricheldorf et al. did not determine by solid state NMR a dependence of the α-helix/ β-sheet ratio on the nature of the solvent for poly(alanine) in contradiction to the previous studies with PMLG. Various samples of poly(alanine) were reprecipitated and the ratio remained unchanged. Neither the nature of the nonsolvents nor the temperature influenced the ratio. The β-sheet fractions were thermodynamically stable.

These observations can be rationalized by assuming that the oligomeric β-sheets precipitating in the first stage of the polymerization continue a slow chain growth on their surface. However, in contrast to Komoto and Kawai, Kricheldorf [27] postulated, as shown in Figure 1.10, that this slow chain growth mainly yields a new β-sheet structure and not α-helical chains. Also, when individual chains of the thickening β-sheet lamellae are long enough to take on the α-helical conformation, they remain in the β-sheet structure (parallel or antiparallel), because the energy of activation to break all the hydrogen bonds cannot be reached. After dissolution in TFA and precipitation from a helical non-solvent, the longer chains of β-sheet lamellae assume the α-helical conformation, whereas the shorter chains precipitate again in the β-sheet structure. To what extent the superficial chain growth of the β-sheet lamellae can compete with the faster growth of the α-helical fraction will depend on the nature of the NCA, on the solvent, and on the temperature.

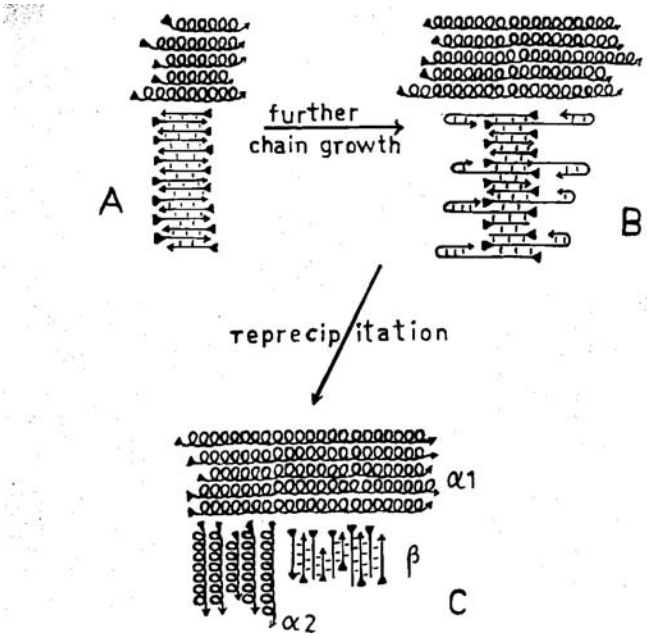

Figure 1.10: Scheme of the secondary structures in primary amine initiated polymerizations, illustrating formation and conformational change of thermodynamically unstable β-sheets.[27]

Kricheldorf did not succeed to synthesize amorphous polypeptides, possessing a coil structure, in different ways, namely polymerizations in the melt and in the solid state. Polymerizations in the melt only served to increase the amount of the byproducts by 20 % without causing a change of the helical secondary structure. Polymerizations in the solid state at – 15°C led to short chain lengths with thermodynamically unfavorable mixtures of β-sheet and α-helix without the appearance of a coil structure. Recrystallizations transformed the mixtures to a stable equilibrium of β-sheet and α-helix.[28]

Blout et al. used a mixture of α-helix and β-sheet structures of PBLG (DP < 20) to confirm that the proportion of β-sheet increases with decreasing DP.[29,30] The β-sheet fraction was successfully extracted from the mixtures by virtue of their solubility in 98% formic acid. The formic acid soluble fraction consisted completely of β-sheets according to IR spectroscopy. Low viscosities led in the past to the conclusion that the β-sheets consisted of very low molecular weight materials. The formic acid insoluble fraction was proven to be helical. Bamford et al. followed the assumption that further formic acid treatment could produce more β-sheets from the α-helical fraction; this was proven to be incorrect.[31] Kricheldorf attempted this transition from α-helix to β-sheet by annealing a mixture of secondary structures in formic acid up to 280°C in vacuo. The ratio of the α-helix to β-sheet by IR spectroscopy remained constant, which illustrated that there is no α-β or β-α transition occurring by formic acid treatment.[29,30]

Ando et al. examined the influence of different precipitation methods on blockcopolymers consisting of a helical part (γ-benzyl-L-glutamate) and a β-sheet part (γ-methyl-L-glutamate). The α-helix / β-sheet ratios were set up by different molar fractions of the comonomers to obtain different initial ratios. The helical block could be successfully elongated from 35 to 85% totally by reprecipitation from HFIP/diethylether. The secondary structures in the resulting copolymers were investigated and quantified by IR spectroscopy and solid state NMR.[32] Kricheldorf et al. confirmed the assumptions of Ando et al. through intensive studies on the synthesis of blockcopolypeptides by batchwise copolymerizations of a helical and a sheet comonomer. The sheet block was observed to be partially helical to varying extents.[33,34]

1.3.3 Detection Techniques

The secondary structure of polypeptides can be elucidated utilizing the following techniques: IR Spectroscopy, Raman Spectroscopy, X-ray Diffraction (XRD), Circular Dichroism (CD), and ^{13}C- or ^{15}N-NMR Solid State CP/MAS-Spectroscopy, and in some limitations ^{1}H and ^{13}C-NMR. Each method possesses characteristic advantages and disadvantages, which are carefully taken into account in this chapter. The elucidation of secondary structures becomes more challenging when more than one conformation is present.

CD-Spectroscopy:

A common method for protein characterization is far ultraviolet (170-250 nm) circular dichroism. A pronounced double minimum at 208 and 222 nm indicates α-helical structure, whereas a single minimum at 204 nm or 217 nm reflects random-coil or β-sheet structure, respectively. The method is particularly useful for the characterization of the helical structure even if a quantification of different secondary structures is not feasible.[35] CD and ORD studies have been accomplished for poly (glutamates), PSCBC, and PSBC e.g. in mixtures of 1,2 dichloroethane with 10% DCA.[35] Solution studies are strongly limited due to the UV cut-off of the solvent system, which should not exceed 200 nm. The polypeptide backbone is weakly UV active in the range of 180-210 nm, which inhibits the use of the most common organic solvents ($CHCl_3$, Dioxane, THF, etc.) for polypeptides.

PBLG and PLGA are not soluble in most of the low UV frequency absorbent solvents like 2-butanol, ethanol, n-hexane, H_2O, or methanol. Detailed CD studies were not conducted due to the focus of this work on the solid state. It should still be noted that this technique is very important in protein chemistry of the liquid state.

CD measurements were used to study the coil-helix transition of different alkali metal salts of PLGA in different aqueous organic solvents. The dependence of the helical content on the volume percent of EtOH in water is shown in Figure 1.11, clearly illustrating that a transition was observable. The data were taken from reference 36.

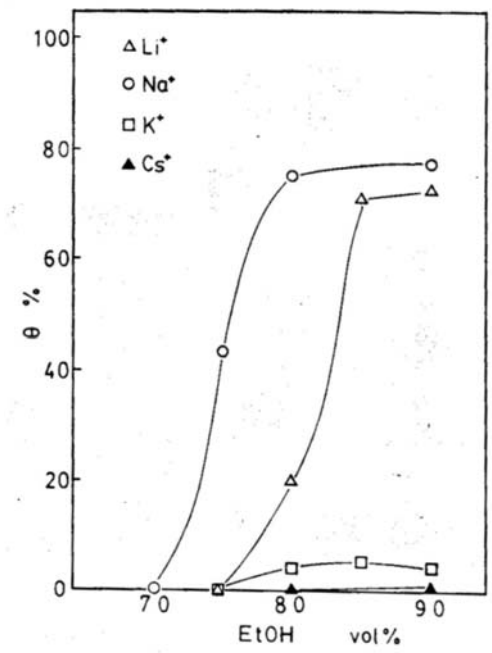

Figure 1.11: Solvent-induced coil-helix transition of PLGA alkali salts in aqueous EtOH.[36]

Fourier Transformed Infrared Spectroscopy (FT-IR):

Once the typical spectroscopic features of an individual secondary structure are known, IR spectroscopy enables a rapid and convenient identification of the secondary structures.[37]

Miyazawa and Blout established a basis, shown in Table 1.1, for correlating the observed Amide I and II frequencies and dichroism with the α-helical, parallel-chain pleated sheet, antiparallel-chain pleated sheet and random conformations of polypeptides and proteins.[38] It has been determined that polypeptide chains may exist in extended conformations. In the fully extended conformation of polypeptides interchain hydrogen bonds may be formed satisfactorily only when the polypeptide chains are antiparallel. However, in this conformation steric hindrance between β-carbon atoms of adjacent chains is appreciable.

The localized vibrations, like the Amide I and II vibrations have been treated by first-order perturbation theory.[39] A general equation for the frequency of a localized vibration of an infinite helical chain has been derived.

$$\nu(\delta,\delta') = \nu_0 + \sum_s D_s \cos(s\delta) + \sum_{s'} D_s' \cos(s'\delta') \qquad (1.1)$$

The first term ν_0 is the unperturbed frequency; the second and the third term are due to the intrachain and interchain vibrational interactions. δ is the phase angle between adjacent group motions in the chain and the coefficient D_s is determined by the potential and kinetic energy interactions between the s*th* neighbors in the chain; δ' and D_s' pertain to the interactions through interchain hydrogen bonds and have meanings similar to those of δ and D_s, respectively. The results of the calculations together with the observed values are listed in Table 1.1.

The schematic representations for the parallel- and antiparallel-chain pleated sheets are shown in Figure 1.12 and 1.13, where the arrows represent the transition moment associated with the in-plane vibrations of the peptide group; the phase angles in parentheses after the ν represent in-phase motions (0), and out-of-phase motions (π) relative to the C-N direction. The first number represents the phase angle of the adjacent intrachain peptide group and the second that of the phase angle of the interchain peptide group. The plus or minus signs represent the components of the transition moments perpendicular to the plane of the paper, the former pointing upward and the latter pointing downward. A description of the vibrations is exemplary done for the antiparallel-chain pleated sheet.

Antiparallel-chain pleated sheet:

It has been found that there are three kinds of infrared active vibrations. The ν (0,π) vibration gives rise to a band with parallel dichroism whereas the ν (π,0) and ν (π,π) vibrations give rise to bands with perpendicular dichroism. Two Amide I bands, 1685 and 1632 cm^{-1}, have been observed. The weak parallel band at 1685 cm^{-1} has been assigned to the ν (0,π) vibration and the strong perpendicular band at 1632 cm^{-1} to the ν (π,0) vibration. The perpendicular ν (π,π) band was not observed. In fact its intensity is expected to be even weaker than the weak band ν (0, π) at 1685 cm^{-1}. The Amide II band at 1530 cm^{-1} shows parallel dichroism and is assigned to the ν (0,π) vibration. The two expected perpendicular bands, ν (π,0) and ν (π,π) have not been observed yet. It should be noted that the calculated ν (π,π) frequency of 1550 cm^{-1} is not much different from the strong perpendicular amide II frequency (1545 cm^{-1}) of the α- helix.

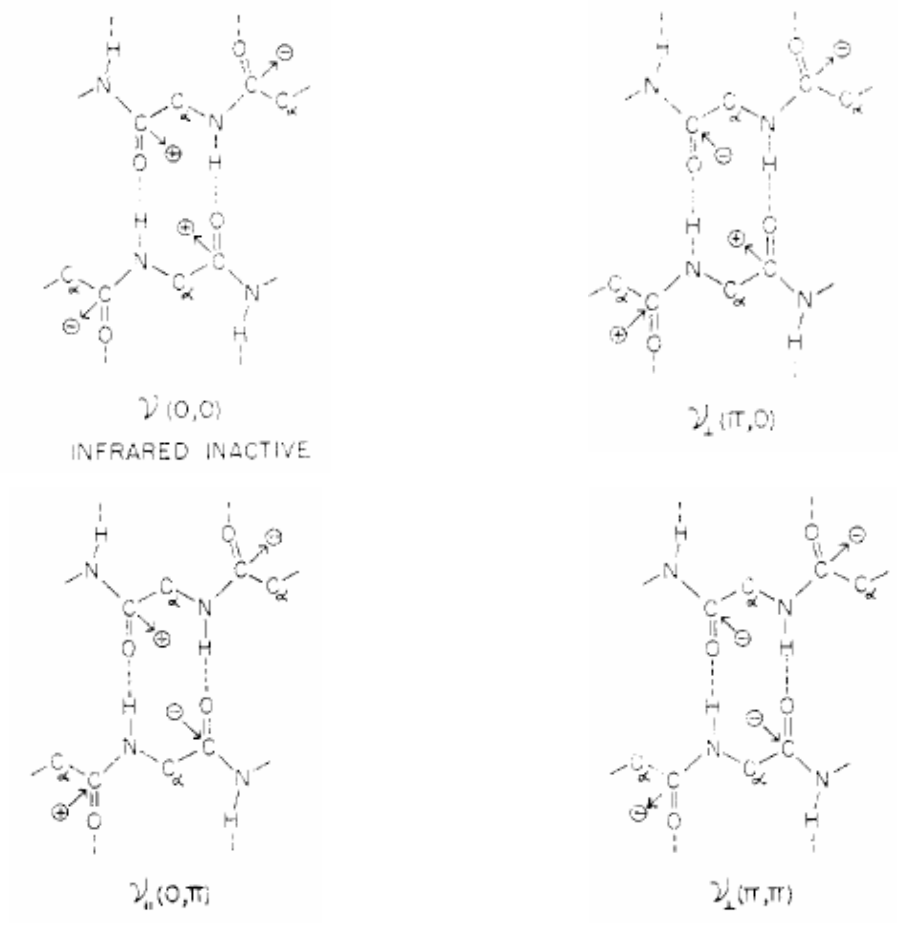

Figure 1.12: The vibrational modes of the antiparallel-chain pleated sheet.

Parallel-chain pleated sheet:

The ν (0,0) vibration gives rise to a parallel band whereas the ν (π,0) vibration gives rise to a perpendicular band.

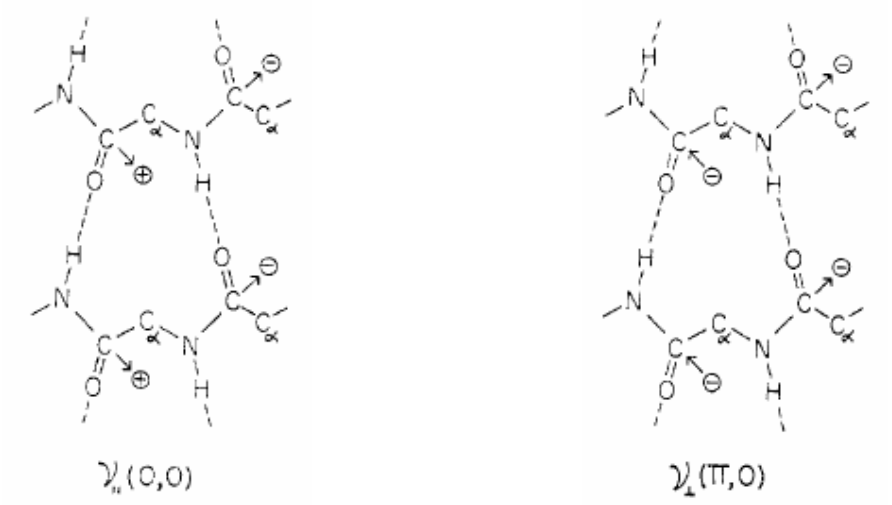

Figure 1.13: The vibrational modes of the parallel-chain pleated sheet.

It is possible to differentiate between parallel- and antiparallel-chain pleated sheets. Both conformations show a perpendicular Amide I band ν (π,0) at 1630 cm^{-1}. However, the parallel Amide I band ν (0, π) at 1695 cm^{-1} is observed characteristically only for the antiparallel-chain pleated sheet.

Random coil structures have nearly no frequency shifts due to the interchain or intrachain interactions (equation 1). The bands around 1730 cm^{-1} occur due to the ester C=O stretching modes. PLGA cast from dioxane-water gave helical structure with the corresponding Amide I and II band vibrations at 1650 and 1550 cm^{-1}.

The Amide I band is associated to C=O stretching. The Amide II band has a composite character. It is associated mostly with NH deformation (bending) and partially with CN stretching.[31] The vibrational band around 3300 cm^{-1}, so called Amide A, arises due to NH stretching, which is not sensitive to main chain or side chain conformation, but exhibits sensitivity to the strength of hydrogen bonding to other carbonyl groups. The band disappears if the hydrogen is substituted by an alkyl group.[40] The Amide A, I, and II bands are pure backbone modes with no sensitivity to the side chain structure, while the remaining Amides III (1257 cm^{-1}), IV, V, VI and VII are coupled with the side chain. The Amide V mode (719 cm^{-1}) depends on the main chain conformation, hydrogen bond strength, and side chain structure.

Table 1.1:
Observed and calculated IR frequencies (cm^{-1}) of the Amide I and II bands of polypeptides in various conformations.

Conformation	**Designation**	**Amide I** *(observed)*	**Amide I** *(calculated)*	**Amide II** *(observed)*	**Amide II** *(calculated)*
Random Coil		1656 (s)	1658	1535 (s)	1535
α-Helix	$\nu_{\parallel}(0)$ $\nu_{\perp}(2\pi/n)$	1650 (s) 1652 (m)	1650 1647	1516 (w) 1546 (s)	1516 1540
β-Parallel-chain pleated sheet	$\nu_{\parallel}(0,0)$ $\nu_{\perp}(\pi,0)$	1645 (w) 1630 (s)	1648 1632	1530 (s) 1550 (w)	1530 1550
β-Antiparallel-chain pleated sheet	$\nu_{\parallel}(0,\pi)$ $\nu_{\perp}(\pi,0)$ $\nu_{\perp}(\pi, \pi)$	1685 (w) 1632 (s)	1685 1632 1668	1530 (s)	1530 1540 1550

n is the number of peptide groups per turn of the helix and the observed intensities are indicated as follows: s = strong, m = medium, w = weak.

Blout was able to classify most of the common polypeptides according to their preferred secondary structure by IR. On the other hand, IR spectroscopy can cause problems for a quantification of complex secondary structures, because of different shapes and extinction coefficients of the IR bands of the different conformations.[27]

FTIR has proven to be very useful for the detection of IR dichroism in oriented liquid crystalline solutions, cast films, and fibers by means of polarized IR radiation which delivers helpful information about the orientation of individual groups relative to the chain axis. Blout et al. pioneered the use of polarized infrared radiation for studying IR dichroism of flowing polymer solutions of PBLG and PLGA.[41,42] They developed techniques to make quantitative observations of the dichroism of dilute polymer solutions subjected to flow conditions by using polarized IR radiation. A series of experiments were conducted covering a wide range of molecular weights, concentrations and flow gradients. The molecular orientation necessary for the observation of dichroism was produced by letting the polymer solutions flow through a modified IR liquid cell. Inside of the optical cell used, a wide range of velocity gradients from zero at the center of the cell to a maximum value at the cell wall were present. The bands showed different sensitivity to IR dichroism, which was consistent for all helical systems (PBLG in different solvents, PLGA in a dioxane-D_2O [90-10] mixture) analyzed. The failure to observe significant dichroism with sodium poly(L-glutamate) is consistent with the view that electrostatic repulsion must destroy the helical configuration and force these molecules into random configurations.[43,44] The N-H stretching (3300 cm^{-1}) and the Amide I band (1650 cm^{-1}) showed parallel dichroism; the Amide II band (1550 cm^{-1}) perpendicular dichroism. If the dipoles would be perfectly oriented parallel to the axis of the helix, they would all exhibit identical relative density changes. The changes of the Amide I band are smaller by a factor 0.65, indicating that the Amide I band is only an imperfectly oriented parallel absorber. Blout et al. used IR dichroism also for the identification of the α-helical conformation and to differentiate between it and the β-sheet conformation based on the work of Ambrose and Bamford.[45,37]

Selective deuteration was found to be another important effective source to obtain conformational information. Blout et al. investigated a procedure to measure the rate of hydrogen-deuterium (H-D) exchange of the NH of the backbone of polypeptides. They had chosen PLGA as test compound in helical and random conformation.[46] The material was dissolved in a dioxane-D_2O mixture (1:1) and a time dependent IR measurement has proven a decrease in the intensity of the Amide II band (1550 cm^{-1}), which shifts from 1550 to 1450 cm^{-1} upon deuteration.[47] It is advantageous to analyze the decrease of 1550 instead of the increase of the 1450 cm^{-1} band due to potential overlap with CH deformation bands at 1450 cm^{-1}. The Amide I band did not change in intensity upon

deuteration but shifted to lower frequency by about 10 cm^{-1}. The random coil conformation exchanged very rapidly (10 min) whereas the helical conformation required many hours for a complete exchange. The hard-to-exchange NH hydrogens ranged from less than 10% to about 60%. Blout finally established this method to search for large parts of coil (fast) or helix (slow) in unknown proteins.[46] Selective deuteration was carried out later for oriented films of polyamides (PA66) to study the molecular orientation. The difference in diffusion of D_2O in the crystalline phase (extremely slow) compared to the amorphous phase for crystallinity was utilized in investigations to elucidate orientation.[48]

Fourier Transformed Raman Spectroscopy (FT-Raman):

In the structural characterization of polypeptides and proteins, Raman spectroscopy was always a suitable technique due to the problems associated with obtaining an infrared spectrum in native (usually aqueous) environments. Raman spectroscopy has several significant advantages like a weak interference with bands from water, no necessary pretreatment of the samples, and the measurement is non-destructive.

The choice of the laser source to record a reliable FT-Raman spectrum is decisive. A visible laser source was determined to be unsuitable for proteins, because this laser source delivered enough energy to induce energetic excitation which led to electronic transitions. The pure compound spectrum will not be obtained with the presence of a fluorescent impurity because the fluorescent emission is so efficient (high quantum yield) that its intensity would completely obscure the Raman spectrum of the polypeptide. Another possible problem can arise even if an impurity does not fluoresce. It may cause local heating due to photon absorption, which can induce degradation or denaturation of the protein. The investigation of the less powerful NdYAG laser excitation (1.064 µm) in the near IR region overcame these problems because photons with such a low energy cannot induce fluorescence, but it is still sufficient to induce Raman scattering. The frequency regime of the stokes-shifted Raman scattering using NdYAG laser is considerable lower than for an argon ion laser. The lower frequency leads according to Equation 1.2 to much less intense scattering, which can be compensated by using higher incident laser powers.[49]

$$I_s \propto \bar{\nu}_s^{\,4} \qquad (1.2)$$

I_s = Scattering intensity

$\bar{\nu}_s$ = Wavenumber of the scattered light

Raman spectra are sensitive to small changes of the secondary structure of polypeptides yielding reliable results. The Amide II band does not exhibit sensitivity in Raman, in contradiction to IR. The Amide I, III, and the skeletal C-C vibrations were established as the main vibrational bands applied for the detection and quantification of secondary structures as shown in Table 1.2.[50] The weak line of the β-sheet form at 1290 cm^{-1} is usually difficult to see, because it is considerably weaker than the other one at 1230 cm^{-1} and there is considerable overlap with weak side-chain frequencies in this region of the spectra of proteins.[51] The Amide I frequency is only about one-third as sensitive to conformational change as the Amide III, so this small difference might arise from other factors than hydrogen bonding. The Amide III vibration represents a complicated mixture rather than a simple group motion.[51]

Table 1.2: Observed Raman frequencies (cm^{-1}) of the Amide I, II, and C-C skeletal bands of polypeptides in various conformations.[51]

Conformation	Amide I	Amide III	Skeletal C-C
Random Coil	1655 (s)	1243-1253 (m)	950 (s)
α-Helix	1650 (s)	1265-1300 (m)	930 (s)
β-sheet	1666-1669 (s)	1229-1235 (s) 1289-1295 (w)	Not observed
The observed intensities are indicated as follows: s = strong, m = medium, w = weak.			

The PLGA helix-coil transition of PLGA in solution was followed in dependence of pH, temperature and solvent composition by Raman spectroscopy.[52,53] Raman spectra of PLGA as the free acid or as the corresponding calcium, strontium, barium, and sodium salts were reported by Fasman and reviewed by Krimm and Sengupta.[54-56]

Initial studies in the solid state were executed with poly(glycine) and poly(alanine) to avoid that the amide III band frequently overlaps with vibrational modes caused by side chain groups. The helical structure of poly(alanine) in the solid state was detected by the Amide I band at 1655 cm^{-1}. The three Amide III vibration modes at 1265, 1275, and 1283 cm^{-1} were assigned as A, E_1, and E_2 in the $C_{18/5}$ group to which the helix belongs.[57,58,51]

The most studied helical polypeptide, PBLG, exhibited the Amide I and III frequencies around 1650 and 1294 cm^{-1}, respectively. The Amide III band could be detected as a weak but definite line at 1280 cm^{-1} that shifted to 961 cm^{-1} upon deuteration. Surprisingly, the Amide III frequency in PBLG was significantly higher than in poly(alanine) leading to the conclusion that the side chain contributes to a strengthening of the helix due to enhanced hydrogen bonding.[57,59]

The polypeptides scatter with a lower intensity than the corresponding monomers. The average intensity ratio of equivalent bands in the former and the latter equaled 1:3, shown in literature by a comparison of methionine with poly(methionine).[51]

Nuclear Magnetic Resonance Spectroscopy (NMR):

The helix-coil transition of PBLG was first investigated in $CDCl_3$/TFA-d by several authors.[60,61] ^{1}H-NMR studies showed that the highest detection sensitivity of a transition between the ordered helical and the disordered coil structure exhibited a downfield shift of 0.5 ppm for the α-CH signal during the transition (3.9 to 4.6 ppm). The ^{13}C-NMR spectrum showed upfield shifts of 3.0 ppm for both the α-carbon and the C=O (amide) carbon (56.3 to 53.2 and 173.1 to 171.1). It was confirmed by ORD studies. Bradbury et al. reported a detailed parameter study of the helix-coil transition in solution. The observed transitions depended on the solvent and the temperature and are presented in Figure 1.14. It has to be noted that a solution of PBLG containing 10% TFA exhibited the transition from coil to helix by heating from 4°C up to 50°C.[62]

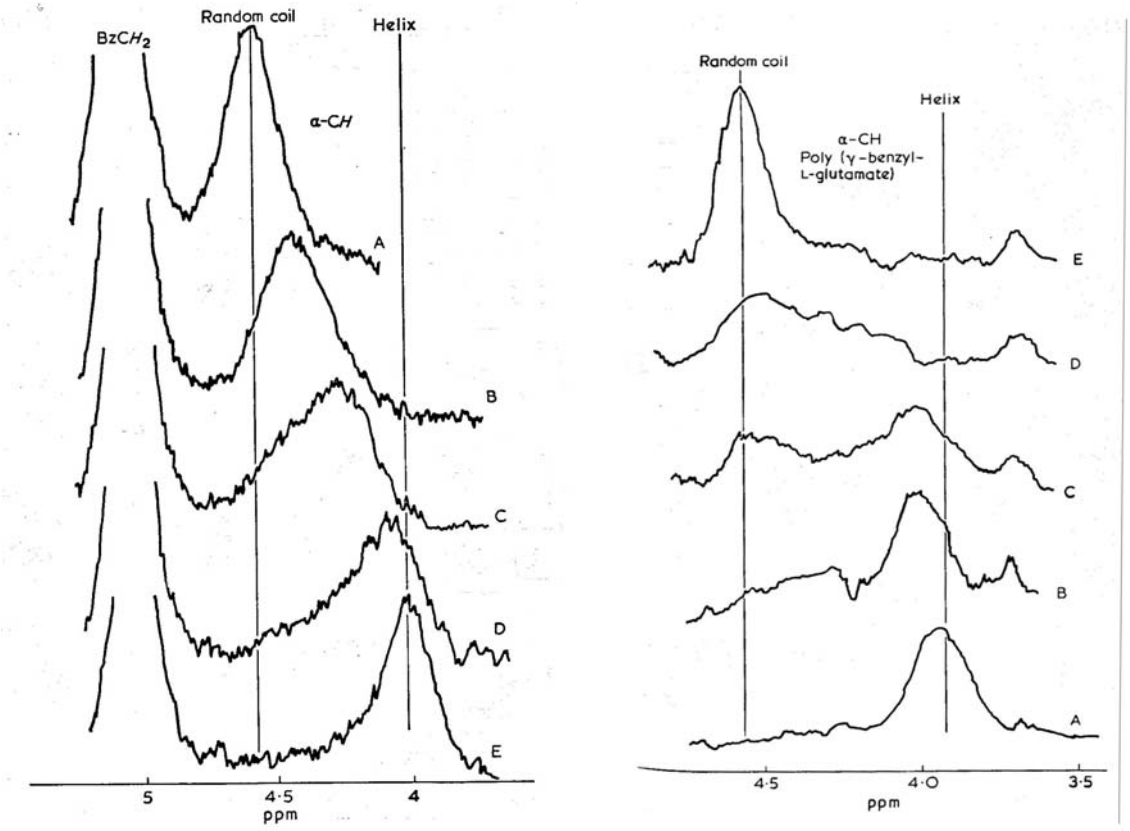

Figure 1.14: 100 MHz ^{1}H-NMR spectra of PBLG.[62]

Left: Temperature induced coil-helix transition in 12:88% $CDCl_3$/TFA-d.
A (5°C); B (16°C); C (19°C); D (26°C); E (38°C)

Right: Solvent induced helix-coil transition in $CDCl_3$/TFA-d at 22°C. TFA content:
A (1% TFA); B (3.5%); C (5.5%); D (7.8%); E (11.1%)

A helical solvent often induces problems for the analysis due to aggregation which decreases the resolution of the NMR spectra. The aggregated helical structure of PSLG as example was disrupted in $CDCl_3$ by adding TFA-d to obtain a reasonable resolution.[63]

Similar conditions were investigated for a β-sheet-coil transition of Poly(S-benzyl-L-cysteine) (PSBC) in mixtures of $CDCl_3$/DCA-d.[64] The relatively broad peaks in pure $CDCl_3$ sharpened significantly by adding DCA-d until 25 % DCA-d content was reached. The downfield chemical shift of the α-CH peak indicated a higher mobility of the respective protons. Further increase of the DCA-d content did not improve the resolution and the spectrum remained indistinguishable from those in pure DCA-d. ORD studies in 1,2-dichloroethane/DCA mixtures confirmed the β-sheet-coil transition.[65]

Mandelkern et al. investigated the pH dependence of the helix-coil transition of PLGA in 0.2 M NaCl solution in D_2O. The pD value was changed continuously from 5 to 8 to induce the transition. The corresponding ^{1}H-NMR spectra are shown in Figure 1.15.[66]

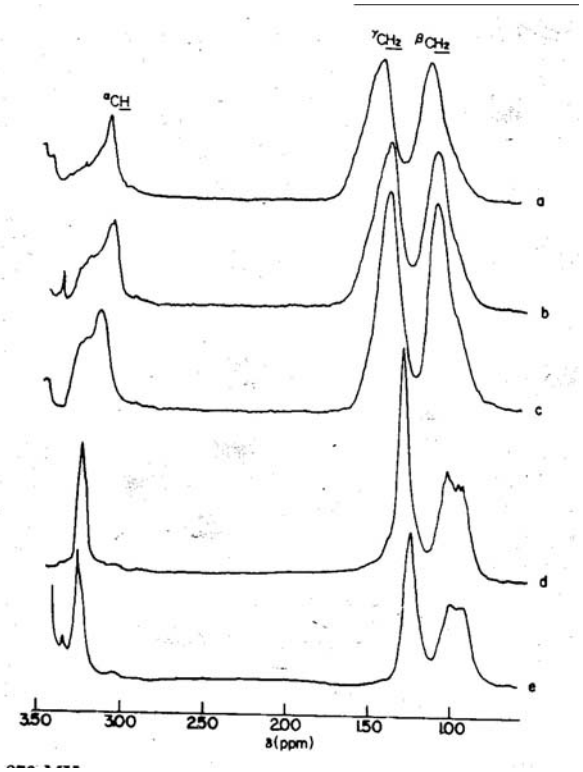

Figure 1.15: The 270 MHz ^{1}H-NMR of PLGA in 0.2 M NaCl in D_2O.[66]
The pD values and number of scans are as follows.
a) 4.65/256 b) 5.00/150 c) 5.15/150 d) 5.95/256 e) 7.70/128

The aggregation in helical solvents leads also to erroneous integration results for the resonance of the α-CH peak area. The addition of a strong acid causes a complete helix-coil transition and results in an increase of the relative area of the peak. The integration ratio of benzyl CH_2/ α-CH in the helical state is less than the expected value of 2. A reliable integration can only be conducted in the coil state, as proven for PBLG [67-69] and the copolymers of the corresponding benzyl and methyl esters.[70]

Solid State NMR Spectroscopy:

^{13}C NMR CP/MAS spectroscopy was first applied to elucidate secondary structures of polypeptides by Saito [71,72] and Kricheldorf [73,74]. Numerous studies were reported by Kricheldorf [75-77] and Ando [78] about the interpretation of the ^{13}C-NMR and ^{15}N-NMR chemical shifts.[27] Chemical shifts of the different conformations were established for many polypeptides by ^{13}C NMR CP/MAS spectroscopy. The most interesting chemical shifts for the current work are summarized in Table 1.3. Only the CO (main chain), α-C, and β-C signals exhibit a sensitivity to the nature of the secondary structure. The α-C signal depends strongly on the nature of the side chain.

Table 1.3: Observed ^{13}C-NMR CP/MAS spectroscopy shifts (ppm) of the different carbons of polypeptides in various conformations.[77]

Polypeptide	Conformation	CO Main Chain	α-C	β-C	γ-C	CO Side Chain	Ester group
PLGA	Sheet	171.9	52.7	29.9	29.9	174.8	
NaPLGA	Sheet	172.6	51.3	30.9	30.9	180.0	
PMLG	Helix	175.9	47.0	26.3	29.7		51.1 (CH_3)
	Sheet	172.2	51.2	29.8	29.8	172.0	51.1 (CH_3)
PBLG	Helix	175.4	56.8	25.9	30.3		136.0, 128.0, 65.8
	Sheet	172.2	51.1	29.7	29.7	172.2	136.0, 128.0, 65.8

The technique has the limitation that it does not allow a differentiation between the different types of β-sheets. Kricheldorf proved that ^{13}C-NMR CP/MAS spectra allow distinguishing two different crystalline secondary structures, namely the α-helix and the antiparallel β-sheet structure. A helical peptide was mixed with an equal amount of a β-sheet peptide (valine, glycine). Signal intensities proportional to the mole fractions of the two secondary structures were detected. The CO and α–C signals parallel the mole

fractions regardless of the nature of the peptide. It was successfully confirmed that quantitative investigations of the secondary structures of copolypeptides and proteins were feasible.[79]

X-Ray Diffraction (XRD):

X-ray and to a lesser extent electron diffraction played an important role in the past decades in the elucidation of secondary structures in polypeptides or proteins. The pioneering work of Pauley and Corey initiated the investigations of different conformations by XRD.[80-86] The research group of Courtaulds Ltd. applied XRD in combination with IR for comprehensive studies of polypeptides.[87-96] Most of the interpretations were focused on oriented samples, i.e. extruded fiber or cast films.[97,98] Powder patterns, for the most part, did not give rise to reliable data, as shown by Komoto et al. for poly(leucine).[99] Several years ago, the α-helix was demonstrated by XRD in a few synthetic polypeptides[100-104] and was recently shown to be a basic structural element of proteins.[105] Bamford [106] and Perutz [107] analyzed a characteristic 1.15 Å meridional reflection for the α-helix, the origin of which has been explained in section 1.3.1. Temperature dependent XRD studies were focused on fibers or oriented cast films composed of PBLG, PMLG or the corresponding copolymers, which proved that the helix expanded with temperature.[108-114] Both X-ray and electron diffraction do not allow a quantification of composite secondary structures. The reflexes of the minor component were difficult to detect and their intensities were not necessarily proportional to the mole fractions.[27] The XRD pattern of most polypeptides showed only one or two signals and a quantitative evaluation of the diffuse signals was not reliable.[115]

References:

[1] A. Akamatsu, K. Matsushita, S. Kaizumi, *German Pat. 2352332*, **1974**

[2] W. H. Daly, D. Poché, I. I. Negulesco, *Prog. Polym. Sci.*, **1994**, *19*, 79-135

[3] H. Block, *Poly (gamma-benzyl-L-glutamate) and other glutamic acid containing polymers, Vol. 9*, Gordon and Breach, **1983**

[4] D. S. Poché, *Ph.D. Dissertation*, Louisiana State University, **1990**

[5] J. Watanabe, T. Nagase, *Polymer J.*, **1987**, *19*, 781

[6] C. Robinson, J.C. Ward, R. B. Beevers, *Disc. Faraday Soc.*, **1958**, *25*, 29

[7] C. Robinson, *Trans. Faraday Soc.*, **1956**, *52*, 571

[8] A. Elliot, E. J. Ambrose, *Discuss. Faraday Soc.*, **1950**, *9*, 246

[9] S. Ebihara, A. Okata, *Chem. Abstr.*, **1976**, *85*, 47308

[10] H. Iwase, *J. Chromatogr.*, **1974**, *93*, 233-237

[11] H. Kiniwa, Y. Doi, T. Nishikaji, N. Ogata, *Makromol. Chem.*, **1987**, *188*, 1841

[12] K. W. Klemm, R. Kübler, *Printing Inks_Ullmann Encycl. of Industr. Chem.*, **1998**

[13] http://en.wikipedia.org/wiki/Offset_printing

[14] J. Gutmann, *MPI Mainz*, **2003**

[15] M. Dietz, *Diploma Thesis*, **2004**, Mainz, *MPIP Mainz*

[15a] Homepage *University Erlangen*

[16] E. R. Blout, A. Asadourian, *J. Am. Chem. Soc.*, **1956**, *78*, 955

[17] M. Idelson, E. R. Blout, *J. Am. Chem. Soc.*, **1957**, *79*, 3948

[18] P. Doty, R. D. Lundberg, *J. Am. Chem. Soc.*, **1956**, *78*, 4810

[19] J. C. Mitchell, A. E. Woodward, P. Doty, *J. Am. Chem. Soc.*, **1957**, *79*, 3955

[20] H. Maeda, T. Inoue, M. Tsunoda, S. Ikeda, *Bull. Chem. Soc. Japan*, **1973**, *46*, 2708

[21] E. R. Blout, C. D. Lozé, S. M. Bloom, G. D. Fasman, *J. Am. Chem. Soc.*, **1960**, *82*, 3787

[22] R. D. B. Fraser, B. S. Harrap, T. P. Mc Rae, F. H. C. Stewart, E. Suzuki, *J. Mol. Biol.*, **1965**, *14*, 423

[23] T. Komoto, K. Y. Kim, Y. Minoshima, M. Oya, T. Kawai, *Makromol. Chem.,* **1972**, *168,* 261

[24] H. R. Kricheldorf, D. Müller, *Int. J. Biol. Macromol.*, **1983**, *5*, 171

[25] T. Komoto, K. Y. Kim, M. Oya, T. Kawai, *Makromol. Chem. (Suppl. 1),* **1975**, *175*, 283

[26] T. Komoto, K. Y. Kim, M. Oya, T. Kawai, *Makromol. Chem. (Suppl. 1)*, **1974**, *175*, 301

[27] H. R. Kricheldorf, *α-Aminoacid-N-carboxy-anhydrides and related heterocycles. Syntheses, Properties, Peptide Synthesis, Polymerization*, Chap. 1 and 2, Springer, **1987**

[28] H. R. Kricheldorf, D. Müller, *Polymer Bulletin*, **1983**, *10*, 513

[29] E. R. Blout, A. Asadourian, *J. Am. Chem. Soc.,* **1956**, *78*, 955

[30] R. D. B. Fraser, W. C. Price, *Nature*, **1952**, *170*, 490

[31] C. H. Bamford, W. E. Hanby, F. Happey, *Proc. Roy. Soc.*, **1951**, *206*, 407

[32] A. Shoji, T. Ozaki, H. Saito, R. Tabeta, I. Ando, *Macromolecules*, **1984**, *17*, 1472

[33] H. R. Kricheldorf, D. Müller, *Polymer Bulletin*, **1982**, *8*, 495

[34] H. R. Kricheldorf, D. Müller, Förster, Polymer Bulletin, 1982, 8, 487

[35] K. Raghavendra, V. S. Ananthanarayanan, *Int. J. Peptide Protein Res.*, **1981**, *17*, 412

[36] M. Satoh, Y. Fujii, F. Kato, J. Komiyama, *Biopolymers*, **1991**, *31*, 1

[37] C. H. Bamford, A. Elliott, W. E. Hanby, *Synthetic Polypeptides*, Academic Press, New York, **1956**, 295

[38] T. Miyazawa, E. R. Blout, *J. Am. Chem. Soc.*, **1961**, *83*, 712

[39] T. Miyazawa, *J. Chem. Phys.*, **1960**, *32*, 1647

[40] H. Block, *Polymer Monographs*, Gordon and Breach, **1983**, *9*

[41] G. R. Bird, E. R. Blout, *J. Am. Chem. Soc.*, **1958**, *81*, 2499

[42] E. R. Blout, C. D. Lozé, S. M. Bloom, G. D. Fasman, *J. Am. Chem. Soc.*, **1960**, *82*, 3787

[43] E. R. Blout, M. Idelson, *J. Am. Chem. Soc.*, **1956**, *78*, 497

[44] M. Idelson, E. R. Blout, *J. Am. Chem. Soc.*, **1958**, *80*, 4631

[45] E. J. Ambrose, A. Elliott, *Proc. Roy. Soc. (London)*, **1951**, *A 205*, 47

[46] E. R. Blout, C. D. Lozé, A. Asadourian, *J. Am. Chem. Soc.*, **1960**, *83*, 1895

[47] H. Lenormant, *Ann. Chim.,* **1950**, *5*, 459

[48] A. Garton, M. K. Phibbs, *Makromol. Chem. Rapid Comm.*, **1982**, *3*, 569

[49] G. Xue, *Prog. Polym. Sci.*, **1997**, *22*, 313

[50] S. Krimm, *Vibrational spectra and structure*, **1987**, *16*, Chapter 1

[51] M. C. Chen, R. C. Lord, *J. Am. Chem. Soc.*, **1974**, *96*, 4750

[52] J. L. Koenig, B. Frushour, *Biopolymers*, **1972**, *11,* 1871

[53] Y. Sugawara, I. Harada, H. Matsuura, T. Shimanouchi, *Biopolymers*, **1978**, *17*, 1405

[54] G. D. Fasman, K. Itoh, C. S. Liu, R. C. Lord, *Biopolymers,* **1978**, *17*, 1729

[55] P. K. Sengupta, S. Krimm, S. L. Hsu, *Biopolymers*, **1984**, *23*, 1565

[56] P. K. Sengupta, S. Krimm, *Biopolymers*, **1985**, *24*, 1479

[57] D. Gani, P. J. Hendra, W. F. Maddams, C. Passingham, I. A. M. Royaud, H. A. Willis, V. Zichy, M. E. A. Cudby, *Analyst*, **1990**, *115*, 1313

[58] J. F. Rabolt, W. H. Moore, S. Krimm, *Macromolecules*, **1977**, *10*, 1065

[59] J. L. Koenig, P. L. Sutton, *Biopolymers*, **1971**, *10*, 89

[60] J. A. Ferretti, B. W. Ninham, *Macromolecules,* **1970**, *3*, 30

[61] L. Paolillo, T. Tancredi, P. A. Temussi, E. Trivellone, *J. Chem. Soc. Chem. Comm.,* **1972**, 335

[62] E. M. Bradbury, C. Crane-Robinson, P. G. Hartman, *Polymer*, **1973**, *14*, 543

[63] D. S. Poché, W. H. Daly, P. S. Russo, *Macromolecules*, **1995**, *28*, 6745

[64] V. S. Ananthanarayanan, K. R. K. Easwaran, *Current Science*, **1974**, *43*, 241

[65] R. D. B. Fraser, B. S. Harrap, T. P. Mc Rae, F. H. C. Stewart, E. Suzuki, *J. mol. Biol.*, **1965**, *14*, 423

[66] H. J. Lader, R. A. Komoroski, L. Mandelkern, *Biopolymers*, **1977**, *16*, 895

[67] D. I. Marlborough, K. G. Orrell, H. N. Rydon, *Chem. Comm.*, **1965**, *21*, 518

[68] F. J. Joubert, N. Lotan, H. A. Scheraga, *Biochemistry*, **1970**, *9*, 2197

[69] J. B. Milstien, J. A. Ferretti, *Biopolymers*, **1973**, *12*, 2335

[70] T. Hiraoki, A. Tsutsumi, K. Hikichi, M. Kaneko, *Polymer J.*, **1976**, *8*, 429

[71] H. Saito, R. Tabeta, A. Shoji, T. Ozaki, I. Ando, *Macromolecules*, **1983**, *16*, 1050

[72] H. Saito, R. Tabeta, A. Shoji, T. Ozaki, I. Ando, *Macromolecules*, **1984**, *17*, 457

[73] H. R. Kricheldorf, D. Müller, *Makromol. Chem.*, **1983**, *184*, 1407

[74] H. R. Kricheldorf, M. Mutter, F. Maser, D. Müller, *Biopolymers*, **1983**, *22*, 1357

[75] D. Müller, J. Stulz, H. R. Kricheldorf, *Makromol. Chem.*, **1984**, *185*, 1735

[76] H. G. Förster, D. Müller, H. R. Kricheldorf, *Int. J. Biol. Macromol.*, **1983**, *5*, 101

[77] D. Müller, H. R. Kricheldorf, *Macromolecules*, **1983**, *16*, 615

[78] I. Ando, H. Saito, T. Tabeta, A. Shoji, T. Ozaki, *Macromolecules*, **1984**, *17*, 457

[79] D. Müller, H. R. Kricheldorf, *Polymer Bulletin*, **1981**, *6*, 101-108

[80] L. Pauling, R. B. Corey, *Proc. Natl. Acad. Sci. USA*, **1951**, *37*, 235

[81] L. Pauling, R. B. Corey, *Proc. Natl. Acad. Sci. USA*, **1951**, *37*, 729

[82] L. Pauling, R. B. Corey, H. R. Branson, *Proc. Natl. Acad. Sci. USA*, **1951**, *37*, 205

[83] H. L. Yakel, L. Pauling, R. B. Corey, *Nature (London)*, **1952**, *169*, 920

[84] L. Pauling, R. B. Corey, *Nature (London),* **1953**, *171*, 59

[85] L. Pauling, R. B. Corey, *Proc. Natl. Acad. Sci. USA*, **1953**, *39*, 247

[86] L. Pauling, R. B. Corey, *Proc. Natl. Acad. Sci. USA*, **1953**, *39*, 253

[87] C. H. Bamford, L. Brown, A. Elliott, *Nature (London)*, **1952**, *169*, 157

[88] C. H. Bamford, W. E. Hanby, F. Happy, *Proc. R. Soc. London A,* **1951**, *205*, 30

[89] C. H. Bamford, L. Brown, A. Elliott, *Nature (London)*, **1953**, *171*, 1149

[90] C. H. Bamford, L. Brown, A. Elliott, *Nature (London)*, **1954**, *173*, 27

[91] C. H. Bamford, L. Brown, A. Elliott, *Nature (London)*, **1955**, *176*, 396

[92] L. Brown, I. F. Trotter, *Trans. Faraday Soc.*, **1956**, *52*, 537

[93] A. Elliott, B. R. Malcolm, *Trans. Faraday Soc.*, **1956**, *52*, 528

[94] A. Elliott, B. R. Malcolm, *Proc. R. Soc. London Ser. A*, **1959**, *249*, 30

[95] E. M. Bradbury, L. Brown, A. R. Downie, A. Elliott, W. E. Hanby, T. R. R. McDonald, *Nature (London)*, **1959**, *183*, 1736

[96] E. M. Bradbury, A. R. Downie, A. Elliott, W. E. Hanby, *Proc. R. Soc. London Ser. A*, **1960**, *259*, 110

[97] S. Mori, M. Iwatsuki, *Kobunshi Kagaku*, **1973**, *30*, 365

[98] A. Elliott, G. D. Fasman, *Poly-alpha-amino acids*, **1967**, New York

[99] T. Komoto, K. Y. Kim, M. Oya, T. Kawai, *Makromol. Chem. (Suppl. 1)*, **1975**, *175*, 283

[100] C. H. Bamford, W. E. Hanby, F. Happey, *Proc. Roy. Soc. (London)*, **1951**, *205 A*, 30

[101] C. H. Bamford, L. Brown, A. Elliott, W. E. Hanby, I. F. Trotter, *J. Am. Chem. Soc.*, **1953**, *141 B*, 49

[102] C. H. Bamford, L. Brown, A. Elliott, W. E. Hanby, I. F. Trotter, *Nature*, **1954**, *173*, 27

[103] M. F. Perutz, *J. Am. Chem. Soc.*, **1951**, *167*, 1053

[104] H. L. Yakel, *Acta Cryst.*, **1953**, *6*, 724

[105] J. C. Kendrew, R. E. Dickerson, B. E. Strandberg, R. C. Hart, D. R. Davies, D. C. Phillips, V. C. Shore, *Nature*, **1960**, *185*, 422

[106] C. H. Bamford, W. E. Hanby, F. Happey, *Proc. Roy. Soc. London Ser. A*, **1951**, *205*, 30

[107] M. F. Perutz, *Nature*, **1951**, *167*, 1053

[108] H. Obata, S. Ogawa, *J. Polym. Sci.*, **1964**, *7*, 1415

[109] D. A. D. Parry, A. Elliott, *J. Mol. Biol.*, **1967**, *25*, 1

[110] A. Elliott, *J. Mol. Biol.*, **1965**, *11*, 821

[111] N. Matsushima, K. Hikichi, *Polymer J.,* **1978**, *10*, 437

[112] N. Matsushima, K. Hikichi, A. Tsutsumi, M. Kaneko, *Polymer J.*, **1976**, *8*, 88

[113] N. Matsushima, K. Hikichi, A. Tsutsumi, M. Kaneko, *Polymer J.*, **1975**, *7*, 44

[114] T. Kanamori, K. Itoh, A. Nakajima, *Polymer J.*, **1970**, *1*, 524

[115] H. R. Kricheldorf, D. Müller, *Polymer Bulletin*, **1981**, *6*, 101

Chapter 2
Monomers (NCA)

2.1 Starting materials

All compounds used for the syntheses of NCAs were commercially available except octadecyl glutamate. The esterification of L-glutamic acid to obtain γ-ester derivatives using primary alcohols with long, saturated carbon chains (8-21 C atoms) was patented by Wassermann et al. in 1966. [1] The synthesis of different mono alkyl esters of glutamic or aspartic acid was performed by reactions of a primary alkyl alcohol of at least 8 carbon atoms with the glutamic or aspartic acid in the presence of a strong acid catalyst. A tertiary alcohol was used as cosolvent.

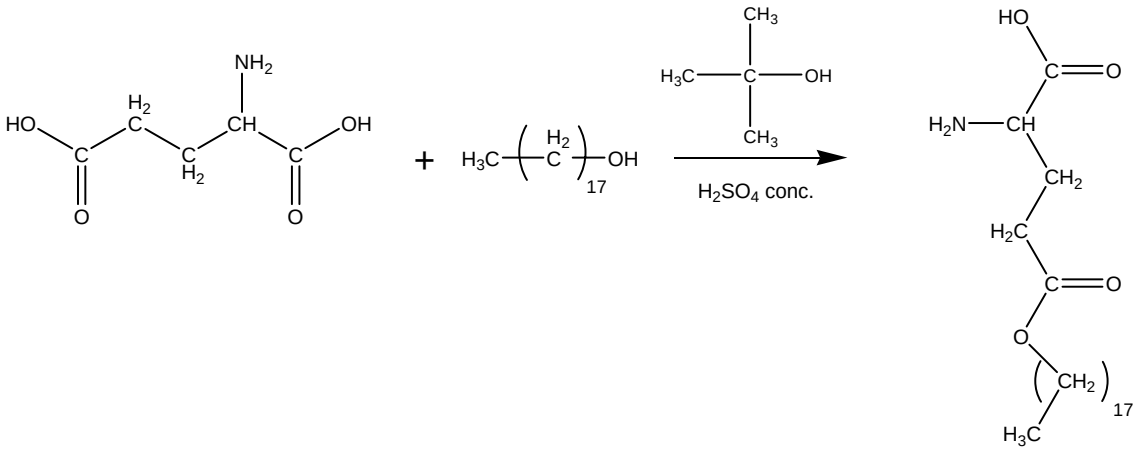

Figure 2.1: Synthesis of octadecyl-L-glutamate (MD-1-10).

A mixture of 14,7 g (0,1 mol) glutamic acid, 200 ml tertiary butyl alcohol and 108,2 g (0,4 mol) octadecanol was stirred at 45°C before 8 ml concentrated sulfuric acid was added dropwise. The reaction was stirred for one hour at 65°C before 7 ml triethylamine was added at once to neutralize the free sulfuric acid. 25 ml water, 350 ml ethanol and a second portion of triethylamine (16 ml) were still given to the reaction solution. The colorless suspension was filtered after 30 minutes and the precipitate recovered. The crude product was suspended in 300 ml hot methanol, filtered on a coarse fritted glass Buchner funnel and washed excessively by diethylether. After drying to constant weight in vacuo, the product was purified by recrystallization in a 1:1 mixture of hot n-butanol/water (the solvent mixture is not miscible at room temperature).

Yield: 19 g (48%), white crystals

M.P.: 173-175°C Literature: 169-170°C [2] 168-178°C [1]

The low solubility inhibited any NMR characterization. A solid MALDI-TOF measurement, shown in Figure 1, could be conducted for the first time. The signal identification is listed in Figure 2.3. There were three side products of much lower intensity present except the desired main product.

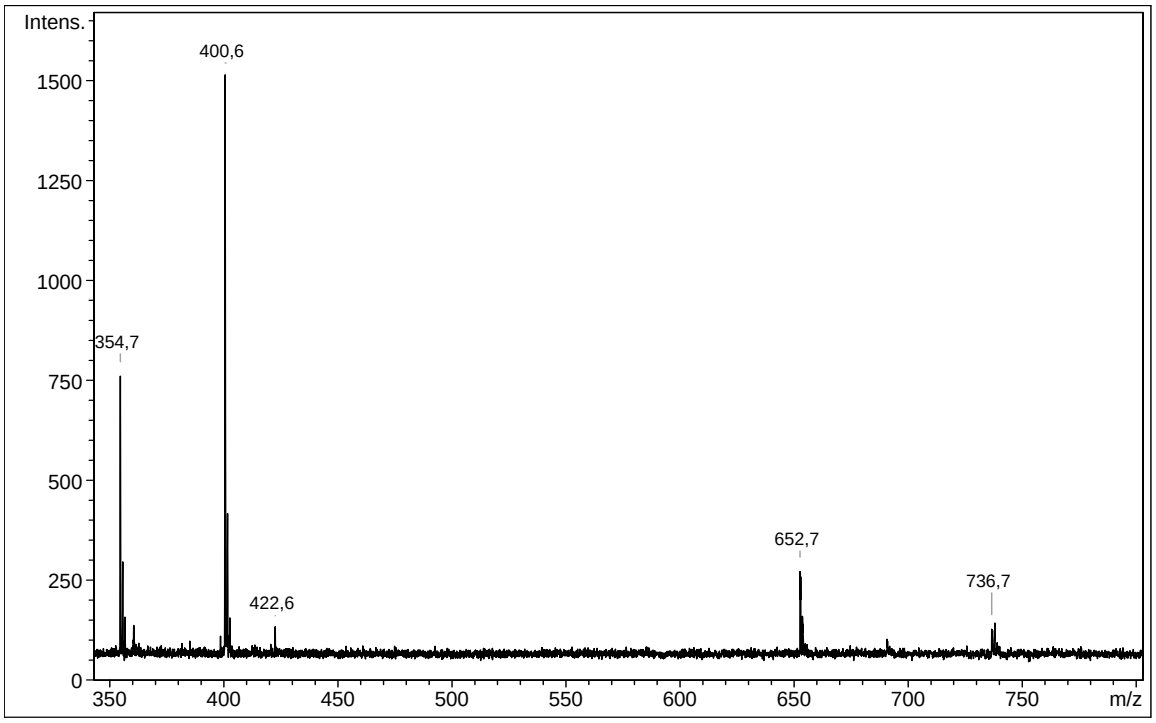

Figure 2.2: MALDI-TOF spectrum of γ-octadecyl-L-glutamate, measured as powder.

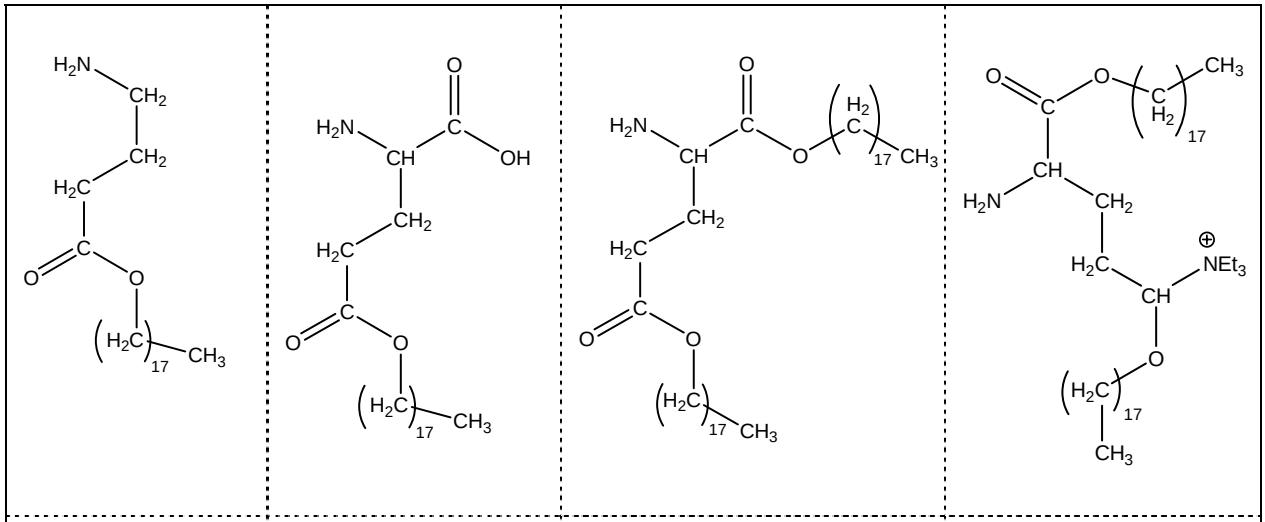

4-amino-butyric acid octadecyl ester	γ-octadecyl glutamic acid	γ-octadecyl octadecyl glutamate	Side product
354.7	400.6	652.7	736.7

Figure 2.3: Identification of the MALDI-TOF signals in Figure 2.2.

2.2 Introduction

Hermann Leuchs was the first to establish a synthetic procedure to obtain a new class of cyclic compounds, which were called the "Leuchs anhydrides." The unintentional formation of anhydrides (N-carboxyanhydrides) was observed during attempts to purify N-ethoxycarbonyl or N-methoxycarbonyl amino acid chlorides by distillation. Leuchs and coworkers published three fundamental papers in 1906, 1907 and 1908, describing the synthesis and properties of α-amino acid N-carboxyanhydrides (NCAs).[1-3]

This first successful method is still a versatile and attractive route used today for the synthesis of NCAs. Amino acids are converted to NCAs by the cyclization of N-alkoxycarbonyl acyl halides upon heating in vacuo as shown in Figure 2.4.

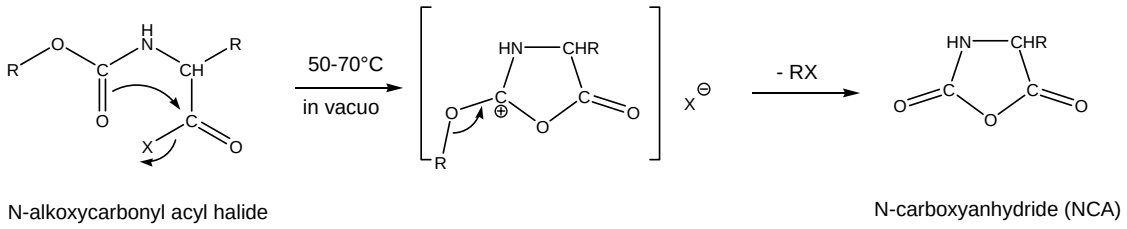

Figure 2.4:
Thermal cyclization of N-alkoxycarbonyl acyl halides to NCAs according to the method of Leuchs.[1-3]

The acid halide group is attacked in the rate-determining step by the carbonyl oxygen of the urethane group displacing the halide. However, the rate-determining step of the mechanism is highly discussed in literature, like the possibility of a nucleophilic attack of the halide ion on the alkoxy group to give an alkyl halide.[4-11]

Leuchs conducted the reaction first with thionylchloride as reagent for the chlorination of the N-alkoxycarbonyl amino acids, because it was advantageous due to gaseous byproducts. The main residual problem with this procedure was the still relatively high cyclization temperature, which came close to the point, where several NCAs began to decompose.[9]

In the search for better chlorination reagents, Ross and coworkers applied the more reactive phosphorus pentachloride, which allowed the usage of lower temperatures.
Although the synthesis was successful, it has to be pointed out that phosphorus oxide trichloride, formed as a byproduct, may affect the crystallization of the NCAs leading to purification issues.[10]

The most suitable reagent for the synthesis of NCAs according to the Leuchs method is phosphorus tribromide. The system can be even modified with reaction temperatures down to room temperature in the case of N-benzyloxycarbonyl amino acylbromides because the bromide ion is more nucleophilic than the chloride ion in protic solvents and the benzyl group more electrophilic than the alkyl groups. It was shown that the rate of cyclization increases in the following order of N-alkoxycarbonyl groups:

ethyl<methyl<allyl<benzyl [11, 12]

An example of an alternative route to obtain NCAs is the well known "Curtius rearrangement" presented in Figure 2.5. The substituted malonic diester is partially hydrolyzed and the resulting mono acid converted to the corresponding hydrazide. The hydrazide is treated with nitrous acid in the presence of ether to give the azide. Refluxing the labile azide in ether causes cyclization and the evolution of nitrogen. The Curtius syntheses yield exclusively the racemic amino acid NCAs or, under hydrolytic conditions, the free amino acids.[9]

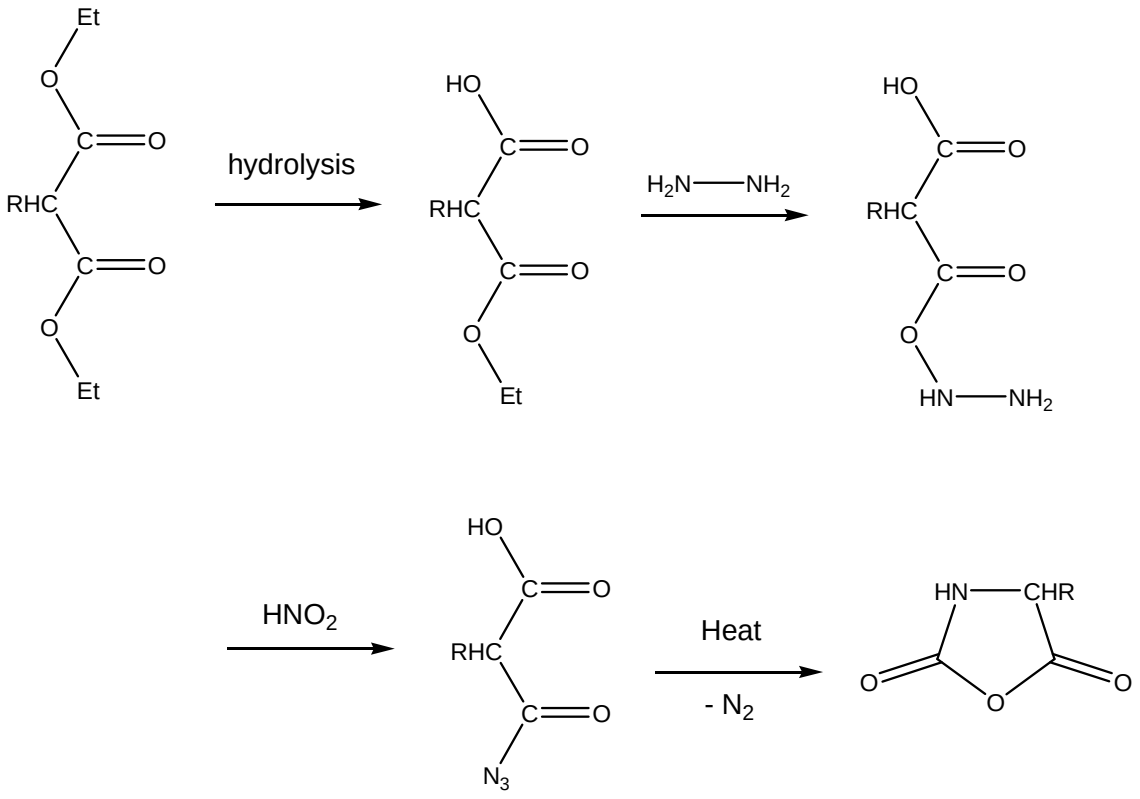

Figure 2.5: The Curtius rearrangement.

After achieving the NCAs by intermediate syntheses of an N-alkoxy or aryloxycarbonyl compound, many groups sought a new "direct" conversion method by using free α-amino acids as reagent.

The Fuchs-Farthing method allowed the synthesis of NCAs where the free α-amino acids react directly with phosgene.[13-15] It became the easiest and the most widely used approach for the synthesis of α-amino acid anhydrides.[16-22] It is remarkable that no racemization occurs if an optically pure amino acid isomer is used in the synthesis.[9, 23]

The synthetic scheme is shown in Figure 2.6.

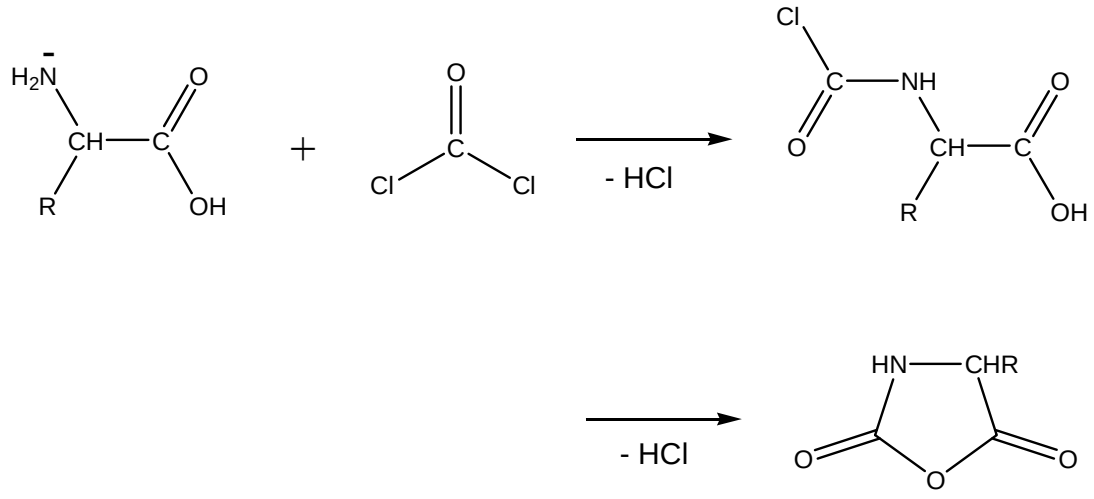

Figure 2.6: The Fuchs-Farthing method: Phosgenation of free amino acids.

The amino acid or its hydrochloride is suspended in an inert and dry low boiling point solvent (like tetrahydrofuran (THF), dioxane or ethyl acetate) and is allowed to react heterogeneously with phosgene as a cyclizing reagent. Hereby, the phosgene gas was either passed directly into the reaction solution or added as a solution. The reaction mechanism involves the intermediate formation of N-chloroformyl amino acids. Hydrochloric acid is a byproduct of this method and plays a tremendous role in the discussion of the possible side reactions. The NCA ring can be cleaved by the hydrochloric acid and further phosgenation of the formed amino acid chloride hydrochloride yields α-isocyanato acid chlorides (Figure 2.7). Under extreme conditions (large excess of hydrochloric acid and phosgene) they can even become the main product. [24]

Kricheldorf reported that large scale reactions of NCAs (>0.5 mol) should be conducted in a boiling mixture of THF (or dioxane) and methylene chloride (approximately 1:1) because hydrochloric acid is less soluble in this mixture than in pure ethers.[9]

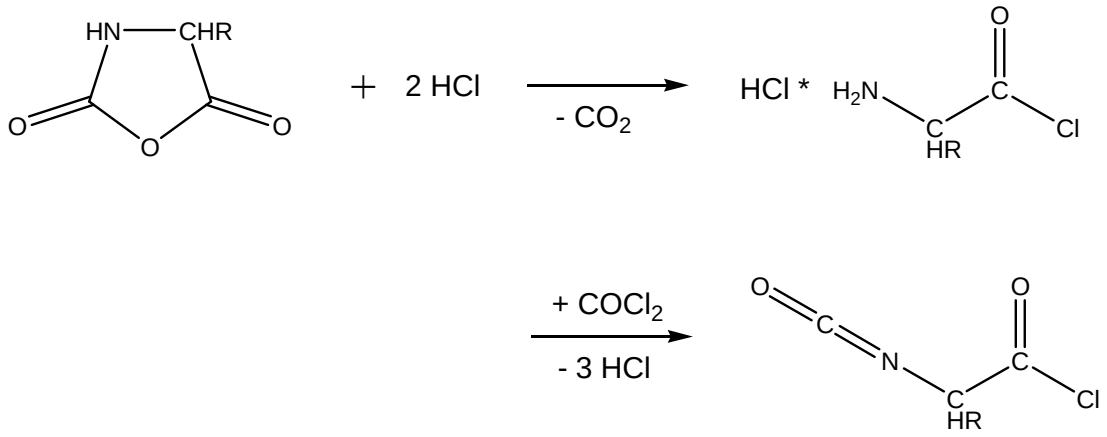

Figure 2.7: Side reactions of the NCA synthesis.

These α-isocyanato acid chlorides and their precursors, the N-chloroformyl amino acid chlorides, are the main contaminants of NCAs prepared by phosgenation of free amino acids. Therefore, the amount of added phosgene is very important in the reaction. Goodman et al. [25] and Daly et al. [26] have utilized stock solutions of phosgene in toluene or benzene as a more accurate way of metering the necessary amount of phosgene to avoid a large excess of phosgene gas.

If the amino acid has functional groups which are too unstable to survive direct phosgenation, three rarely used methods have been reported in the literature. These methods avoid the formation of hydrochloric acid [9]:

1) phosgenation of amino acid copper complexes [27]
2) phosgenation of N-trimethylsiloxycarbonyl amino acid trimethylsilylesters [28]
3) treatment of N-carboxy amino acid sodium salts with phosgene or thionyl chloride [16]

The high toxicity of phosgene and high numbers of side products led to the use of safer compounds for the phosgenation of amino acids. In 1973, Iwakura and coworkers reported trichloromethyl chloroformate "Diphosgene," which is a colorless liquid, as a substitute for phosgene.[29] However, the advantage of using a calculated amount of liquid diphosgene is offset by the very slow decomposition of diphosgene to phosgene (4-6 hours at 60°C). Without this decomposition of diphosgene prior to the reaction with the amino acids, the formation of the NCAs is usually unsuccessful.[29] Katakai and Iizuka

modified therefore the procedure of Iwakura and coworkers in 1985. It was shown that activated charcoal accelerated the dissociation of the diphosgene molecule to obtain reasonable reaction rates.[30] The amount of diphosgene needed for a complete reaction should be theoretically half an equivalent. Experimentally, however, Katakai and Iizuka pointed out that a 40% excess of diphosgene is required for total amino acid conversion.[30]

Daly and Poché pioneered the use of the crystalline solid substitute bis (trichloromethyl) carbonate "triphosgene" which became available in 1988.[31] This derivative was first described as general phosgenation reagent by Eckert and Forster.[32] The intramolecular decomposition mechanism for triphosgene, which does not require a catalyst, was already established by Hales and coworkers in 1957.[33] Daly and Poche reported the synthesis of γ-esterified L-glutamate NCAs with alkyl chains consisting of 2-18 C atoms or a benzyl group. The solubility of the γ-alkyl-L-glutamate HCl salts in water decreases with increasing the number of C atoms in the alkyl group. A stubborn emulsion was observed between the ethyl acetate/water phases if the procedure is used to purify NCAs with long (> 8 C atoms) alkyl groups. HCl and a possible small quantity of γ-alkyl-L-glutamate HCl salt, remaining after reaction as impurities, can be removed by washing them into the water layer.

Triphosgene can be synthesized by complete photochlorination of dimethyl carbonate in carbon tetrachloride solution.

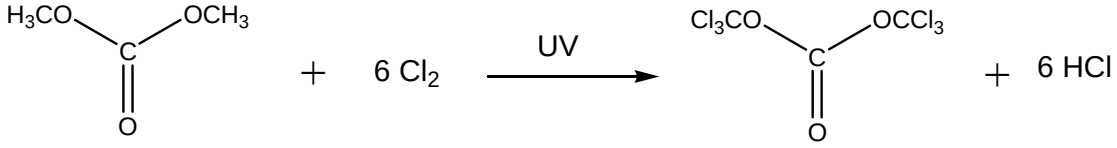

Figure 2.8: Synthesis of Triphosgene by photochlorination of dimethyl carbonate.

The problems previously mentioned for pure phosgene gas (excess) can be minimized by utilizing diphosgene or triphosgene. The reaction conditions, times, and yields are comparable to that of Fuchs-Farthing reactions. Triphosgene has an additional advantage in that it is soluble in the most often applied solvents for NCA purification which facilitates its removal from the NCA product.[31]

2.3 Synthesis

Two general procedures for the NCA syntheses were used in this work.

Diphosgene method:

A synthetic procedure modified from the literature was used for the synthesis of the desired NCA monomers.[29, 30, 34]

The amino acid and the activated charcoal were first suspended in THF under argon before a 40 % excess of diphosgene was added. The mixture was stirred at 55°C until the amino acid dissolved completely. The phosgenation reaction proceeded for an hour at 55°C for all amino acids used in this work. Thus, the reaction time was now as short as in the phosgene stock solution method.[35] The activated charcoal was then removed by filtration through celite placed on a glass filter. The filtrate was reduced and the residual oil crystallized upon addition of hexane.

Triphosgene method:

A synthetic procedure modified from the literature was used for the synthesis of the desired NCA monomers.[31]

Typically the reaction was performed by suspending the amino acid in anhydrous ethyl acetate (less hygroscopic as compared to THF). The mixture was then heated under argon to reflux before 1/3 equivalents of triphosgene were added, leading to a completely homogeneous solution of the corresponding NCA within 4-5 hours. If a clear solution has not formed, a small quantity of triphosgene was added. The reaction solution was then chilled to 0° C before it was washed first with chilled de-ionized water, followed by cold 0,5 % w/v $NaHCO_3$ (aq). For these washing procedures low temperatures and a fast performance are necessary to avoid hydrolysis of the NCA. The ethyl acetate solution was dried with $MgSO_4$ and was concentrated to about 1/3 of its original volume by a rotary evaporator. The temperature of the water bath of the evaporator was kept below 30°C to minimize or eliminate decomposition reactions due to residual water. The NCA was isolated by crystallization induced by the addition of hexane. The resulting suspension was stored at – 20°C overnight to assure complete crystallization.

Purification for both methods:

All the impurities mentioned before are decisive for choosing a suitable purification. The NCA should be highly pure in order to achieve well defined and pure polypeptides by the subsequent polymerization. Otherwise, the possible side products can react electrophilic and thus effect the polymerization. However, Kricheldorf pointed out that NCAs containing small amounts of acid chlorides are more stable on storage, because the acid chloride protects the NCAs from attack by traces of moisture.[9, 36] Highly purified NCAs must be used within a few days after the last purification step.

Because most NCAs are easily crystallizable compounds in contrast to the above-mentioned contaminants, a series of two or three crystallization steps from suitable mixtures, most widely used is EtOAc/n-hexane, have to be done. [37] Therefore the NCA monomers in this work were all purified three times by reprecipitation in ethyl acetate / hexane in a ratio of 1:4, which was found to be the most suitable mixture.

Synthesis:

All desired NCA monomers were successfully synthesized during this work by applying procedures previously described. The different glutamate NCAs were synthesized by the triphosgene reaction. However, it was not possible to obtain the methyl glutamate NCA by using this route, which was also observed by Daly and Poche. The synthesis of the methyl glutamate was attempted with triphosgene, but was met with little success (MD-1-8, marked as failed in Table 2.1). The recovery of the methyl glutamate NCA was found to be difficult because the proposed purification (washings) were identified to be not suitable. A highly stubborn emulsion resulted, which was not possible to break up by common methods like adding of ethanol or salting out. The second attempt using triphosgene (MD-1-9) was performed without the different washings. The NCA was precipitated out directly from the reaction solution by adding n-hexane. Here, the product was obtained but was very impure as shown by NMR. Therefore the methyl glutamate was synthesized by the diphosgene method and was obtained without any problems. The small scale reactions, which have shown the lowest yields, were test reactions to explore the applicability of the different methods. Afterwards, all reactions could be carried out to recover the product in high yields. As would be expected, at a certain point the up- scaling of the reaction leads to a lower yield.

Table 2.1: Experimental data of NCA syntheses.

Sample No.	Reactant	m [g] M [mol] Reactant	Solvent	Procedure	Product	m [g] M [mol] Product	Yield [%]
MD-1-1	γ-benzyl-L-glutamate	25.0 0.11	EtOAc	Triphosgene	γ-benzyl-L-glutamate NCA	16.2 0.06	58.4
MD-1-40	γ-benzyl-L-glutamate	25.0 0.11	EtOAc	Triphosgene	γ-benzyl-L-glutamate NCA	21.5 0.08	77.1
MD-1-8	γ-methyl-L-glutamate	10.0 0.06	EtOAc	Triphosgene	γ-methyl-L-glutamate NCA	Reaction failed*	---
MD-1-9	γ-methyl-L-glutamate	10.0 0.06	EtOAc	Triphosgene	γ-methyl-L-glutamate NCA	9.7 0.05*	83.3
MD-1-25	γ-methyl-L-glutamate	4.4 0.03	THF	Diphosgene	γ-methyl-L-glutamate NCA	0.8 0.004	16.3
MD-1-29	γ-methyl-L-glutamate	16.0 0.10	THF	Diphosgene	γ-methyl-L-glutamate NCA	15.8 0.08	84.8
MD-1-52	γ-methyl-L-glutamate	20.0 0.12	THF	Diphosgene	γ-methyl-L-glutamate NCA	17.7 0.09	75.7
MD-1-11	γ-octadecyl-L-glutamate	10.0 0.03	EtOAc	Triphosgene	γ-octadecyl-L-glutamate NCA	7.5 0.002	70.2
MD-1-51	γ-octadecyl-L-glutamate	8.0 0.02	THF	Diphosgene	γ-octadecyl-L-glutamate NCA	6.4 0.015	74.7
MD-1-41	S-carbobenzoxy-L-cysteine	2.5 0.01	THF	Diphosgene	S-carbobenzoxy-L-cysteine NCA	1.4 0.005	49.3
MD-1-42	S-carbobenzoxy-L-cysteine	2.5 0.01	EtOAc	Triphosgene	S-carbobenzoxy-L-cysteine NCA	1.2 0.004	43.7
MD-1-49	S-carbobenzoxy-L-cysteine	9.5 0.04	THF	Diphosgene	S-carbobenzoxy-L-cysteine NCA	8.9 0.03	84.7
MD-1-60	S-carbobenzoxy-L-cysteine	20.0 0.08	THF	Diphosgene	S-carbobenzoxy-L-cysteine NCA	15.8 0.06	72.1
MD-1-59	S-benzyl-L-cysteine	20.0 0.10	THF	Diphosgene	S-benzyl-L-cysteine NCA	19.2 0.08	85.5

*Explained in the interpretation before

2.4 Characterization

IR spectroscopy:

The stretching modes of the two carbonyl groups were considered to be characteristic of the mixed anhydride structure. Their frequencies (1855 ± 5 cm^{-1} and 1780 ± 5 cm^{-1}) indicative of NCA ring formation were present in all NCA samples prepared. The lower frequency at 1780 cm^{-1} corresponds to the CO-2, because of the delocalized electrons around the oxygen and the delocalized electron pair of the nitrogen. Alkyl substituents in the 4-position, i.e., the nature of the amino acid, do not have a noteworthy influence on the frequencies of both CO-bands. The different frequencies of CO-2 and CO-5 suggest that the latter group is more reactive than the former one. This suggestion is supported by a variety of experimental results.[9]

NMR-spectroscopy:

The chemical identification of the compounds was accomplished by ^{1}H and ^{13}C NMR. The corresponding data are listed in Tables 2.2 and 2.3. The signal patterns of NCAs in general do not display unusual features. α-Amino acid NCAs differ from most other α-amino acid derivatives by having a greater down-field shift of the C_α proton (0.2-0.5 ppm). Alkyl or aryl groups attached to the nitrogen do not have a significant influence on the C_α proton. The carbonyl signal in carbon NMR is not sensitive to the nature of the side chain.[37]

Table 2.2: ^{13}C NMR chemical shift δ (ppm, relative to external TMS) in $CDCl_3$.

NCA of	α-CO	N-CO	α-C	β-C	γ-C	CO (ester)	C (ester group)
γ-benzyl-L-glutamate	169.42	151.94	56.94	26.92	29.82	172.40	67.12 (CH_2) 135.24 128.61 [m] (phenyl)
γ-methyl-L-glutamate	169.41	151.83	56.99	26.92	29.61	173.07	52.27 (CH_3)
γ-octadecyl-L-glutamate	169.51	152.10	56.96	26.94	29.61	172.71	65.56 31.94 28.51 25.89 22.71 14.13 29.60 [m]
S-benzyl-L-cysteine	168.01	151.81	57.60	32.77	---	---	37.06 (benzylic CH_2) 137.14 128.99 127.81 (phenyl)
S-carbobenzoxy-L-cysteine	167.92	151.74	57.84	31.82	---	170.18	70.36 (benzylic CH_2) 134.36 128.80 [m] (phenyl)

Table 2.3: ^{1}H NMR chemical shift δ (ppm, relative to external TMS).

NCA of	Solvent	NH	α-CH	β-CH_2	γ-CH_2	Protons (ester group)
γ-benzyl-L-glutamate	$CDCl_3$	6.57 (s)	4.37 (t) (J = 6 Hz)	2.26 (m) (J = 7 Hz) 2.13 (m) (J =7 Hz)	2.60 (t) (J = 7 Hz)	7.36 (s) (aromatic, 5H) 5.14 (s) (benzylic CH_2)
γ-methyl-L-glutamate	$CDCl_3$	6.64 (s)	4.41 (t) (J = 6 Hz)	2.29 (m) (J = 6 Hz) 2.13 (m) (J =7.2 Hz)	2.57 (t) (J = 6.6 Hz)	5.14 (s) (methyl CH_3)
γ-octadecyl-L-glutamate	$CDCl_3$	6.56 (s)	4.40 (t) (J = 6 Hz)	2.26 (m) (J = 6 Hz) 2.12 (m) (J =7.3 Hz)	2.55 (t) (J = 6.5 Hz)	4.09 (t) (J= 6.8 Hz, CH_2) 1.62 (t) (J= 6.8 Hz, CH_2) 4.09 (s) (15*CH_2) 0.88 (t) (J= 6.3 Hz, CH_3)
S-benzyl-L-cysteine	$CDCl_3$	6.27 (s)	4.30 (dd) (J = 7.5, 3.75 Hz)	2.26 (dd) (J = 14.4, 3.6 Hz) 2.13 (dd) (J = 14.4, 7.2 Hz)	---	7.32 (s) (aromatic, 5H) 3.77 (s) (benzylic CH_2)
S-carbobenzoxy-L-cysteine	$CDCl_3$	6.13 (s)	4.64 (t) (J = 4.5 Hz)	3.50 (dd) (J = 15.0, 3.9 Hz) 3.20 (dd) (J = 15.0, 4.8 Hz)	---	7.37 (s) (aromatic, 5H) 5.28 (s) (benzylic CH_2)

Elemental analysis:

Elemental analysis was conducted for γ-methyl-L-glutamate NCA and γ-octadecyl-L-glutamate NCA. The results listed in Table 2.4 and 2.5 agree with the theoretical values for each atom according to common error margins depending on the applied analytical methods.

Table 2.4: Elemental analysis of γ-methyl-L-glutamate NCA (MD-1-29).

Elements	Theoretical [%]	Experimental [%]	Deviation [%]
C	44.92	43.74	2.63
H	4.85	4.46	8.04
N	7.49	7.07	5.61
O	42.74	44.71	4.61

Table 2.5: Elemental analysis of γ-octadecyl-L-glutamate NCA (MD-1-11).

Elements	Theoretical [%]	Experimental [%]	Deviation [%]
C	67.76	68.54	1.15
H	10.12	10.21	0.89
N	3.3	3.26	1.21
O	18.82	18.10	3.83

Mass spectrometry:

Mass spectrometry analysis was attempted to elucidate the chemical structure of the obtained NCAs even if there was never published a mass spectral analysis of NCAs in the literature before. Two different ionization methods, electrospray (ESI) and field desorption (FD), were attempted for the investigation of the NCAs. The main hindrance in the characterization by mass spectrometry for these compounds is their thermal instability even under mild conditions. The ESI-mass spectral data are listed in Tables 2.6, 2.7 and 2.8. The specimens were prepared in $CHCl_3$ with TFA as a protonation agent. The measurements were conducted at 120° C. The temperature was determined as too high for the thermal unstable NCAs and induced degradation. The possible degradation products are illustrated in Figure 2.9, which represents different decarboxylation steps during an oligomerization process. The confirmation, that the NCAs were not already oligomerized during the sample preparation or even before, was successfully achieved by the FD-mass measurement of γ-benzyl-L-glutamate NCA where the same solution in $CHCl_3$ without TFA was applied. There was no evidence for any kind of degradation product because it shows just one mass signal for the unchanged NCA, given in Table 2.9, which was absent in the ESI-Mass spectra.

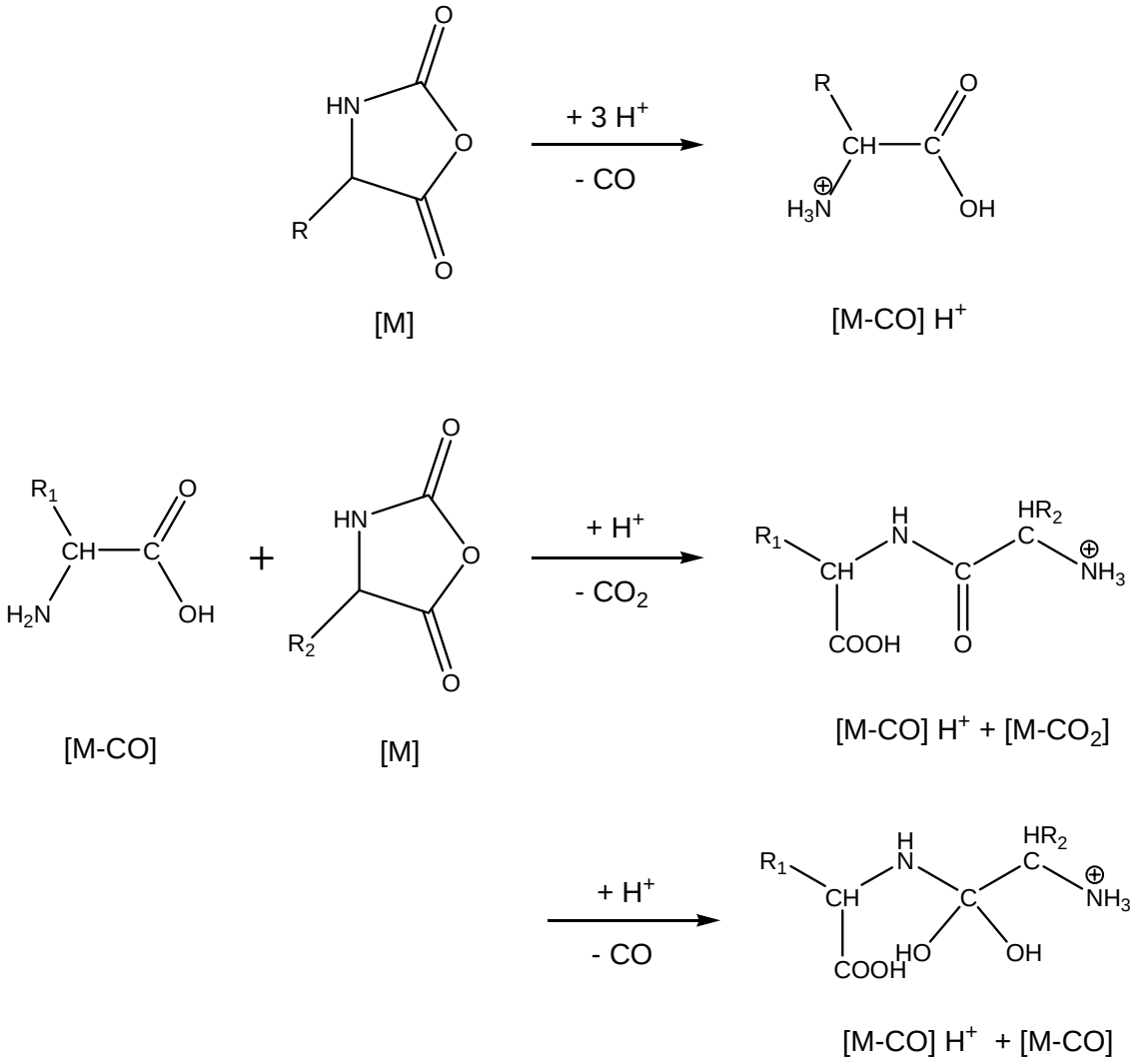

Figure 2.9: ESI-Mass reactions which took place in situ during the measurement.

Table 2.6: ESI-MASS of S-carbobenzoxy-L-cysteine NCA, 120° C in $CHCl_3$/TFA.

M/Z (Mass / Charge)	Intensity [%]	Identification
256	5.60	[M – CO] H^+
493	100.00	[M-CO] H^+ + [M-CO_2]
511	2.19	[M-CO] H^+ + [M-CO]
730	21.05	[M-CO] H^+ + 2 [M-CO_2]
967	8.59	[M-CO] H^+ + 3 [M-CO_2]
985	3.56	[M-CO] H^+ + 2 [M-CO_2] + [M-CO]
1204	4.73	[M-CO] H^+ + 4 [M-CO_2]
1222	2.28	[M-CO] H^+ + 3 [M-CO_2] + [M-CO]

Table 2.7: ESI-MASS of S-benzyl-L-cysteine NCA, 120° C in $CHCl_3$/TFA.

M/Z (Mass / Charge)	Intensity [%]	Identification
405	85.69	[M-CO] H^+ + [M-CO_2]
598	100.00	[M-CO] H^+ + 2 [M-CO_2]
791	36.93	[M-CO] H^+ + 3 [M-CO_2]
809	1.08	[M-CO] H^+ + 2 [M-CO_2] + [M-CO]
984	18.69	[M-CO] H^+ + 4 [M-CO_2]
1002	12.51	[M-CO] H^+ + 3 [M-CO_2] + [M-CO]
1177	5.44	[M-CO] H^+ + 5 [M-CO_2]
1195	18.28	[M-CO] H^+ + 4 [M-CO_2] + [M-CO]
1388	14.47	[M-CO] H^+ + 5 [M-CO_2] + [M-CO]
1581	7.19	[M-CO] H^+ + 6 [M-CO_2] + [M-CO]
1774	1.46	[M-CO] H^+ + 7 [M-CO_2] + [M-CO]

Table 2.8: ESI-MASS of γ-benzyl-L-glutamate NCA, 120° C in $CHCl_3$/TFA.

M/Z (Mass / Charge)	Intensity [%]	Identification
238	65.66	[M–CO] H^+
266	15.07	MH_3^+
286	5.44	M + Na^+
439	48.62	[M-CO_2] H^+ + [M-CO_2]
457	27.26	[M-CO] H^+ + [M-CO_2]
461	54.16	[M-CO_2] + [M-CO_2] + Na^+
477	2.14	[M-CO] + [M-CO_2] + Na^+
505	6.30	[M-CO_2] + M + Na^+
676	100.00	[M-CO] H^+ + 2 [M-CO_2]
704	1.72	M + H^+ + 2 [M-CO_2]
720	3.07	[M-CO] H^+ + [M-CO_2] + M
895	10.84	[M-CO] H^+ + 3 [M-CO_2]
899	22.53	4 [M-CO_2] + Na^+
943	13.72	3 [M-CO_2] + M + Na^+
1114	10.29	[M-CO] H^+ + 4 [M-CO_2]
1158	2.16	[M-CO] H^+ + M + 3 [M-CO_2]
1162	1.32	Na^+ + M + 4 [M-CO_2]

Table 2.9: FD-MASS of γ-benzyl-L-glutamate NCA, $CHCl_3$.

M/Z (Mass / Charge)	Intensity [%]	Identification
263	100.00	M^+

The FD-mass spectral data of older NCA samples did not show similar results. There were several signals detected, summarized in Tables 2.10-2.14, indicating an oligomerization of the NCA monomers by water molecules as shown in Figure 2.10. The oligomerization confirms that the NCA molecules cannot be stored for a long time under inert atmosphere in a freezer without attracting water from the atmosphere. The low storage stability of the NCAs was also reported by Kricheldorf et al.[3]

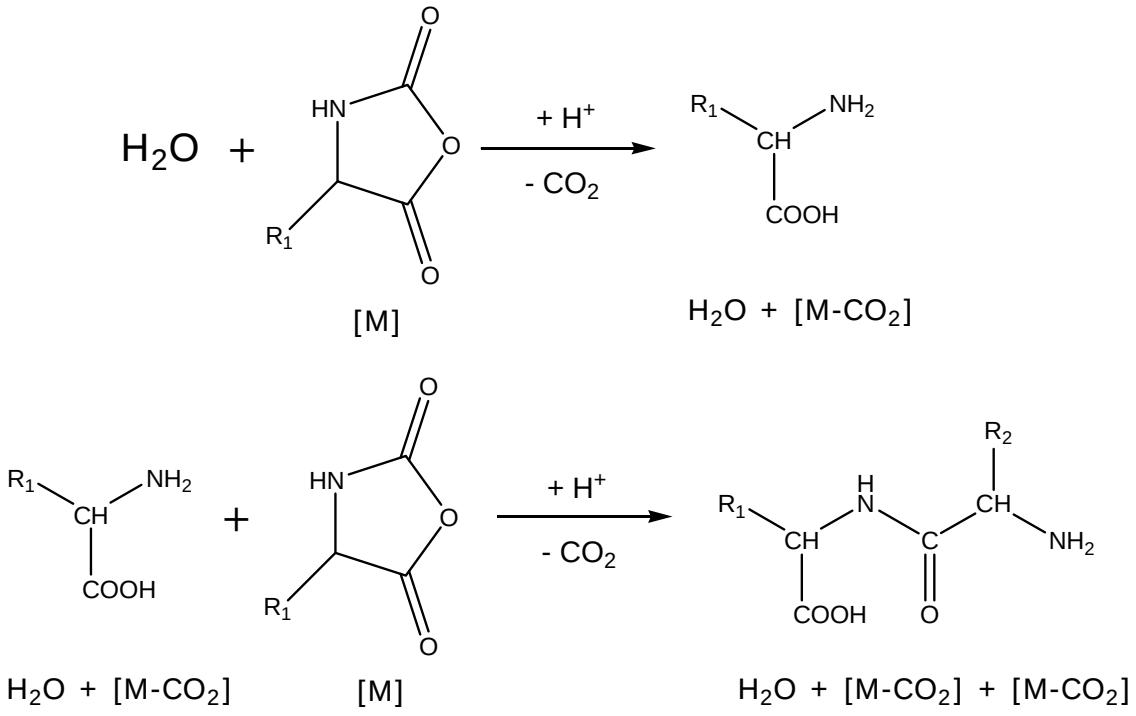

Figure 2.10: FD-Mass detected oligomerized NCA monomers initiated by water.

Table 2.10: FD-MASS of S-carbobenzoxy-L-cysteine NCA, $CHCl_3$.

M/Z (Mass / Charge)	Intensity [%]	Identification
256	100.00	[M-CO_2] + H_2O
281	10.43	NCA
475	40.47	2 [M-CO_2]
493	26.51	2 [M-CO_2] + H_2O
730	49.17	3 [M-CO_2] + H_2O
966	2.19	4 [M-CO_2] + H_2O

Table 2.11: FD-MASS of γ-methyl-L-glutamate NCA, $CHCl_3$.

M/Z (Mass / Charge)	Intensity [%]	Identification
143	7.57	[M-CO_2]
171	2.70	[M-CO] + H^+
188	100.00	NCA
332	21.62	2 [M-CO] + H^+
450	4.86	3 [M-CO_2] + H_2O

Table 2.12: FD-MASS of γ-octadecyl-L-glutamate NCA, $CHCl_3$.

M/Z (Mass / Charge)	Intensity [%]	Identification
400	20.92	[M-CO_2] + H_2O
426	5.91	NCA
761	19.13	2 [M-CO_2]
807	100.00	
851	23.11	3 [M-CO_2], Na^+

Table 2.13: FD-MASS of S-benzyl-L-cysteine NCA, $CHCl_3$.

M/Z (Mass / Charge)	Intensity [%]	Identification
386	100.00	2 [M-CO_2]
405	8.60	2 [M-CO_2] + H_2O
493	15.51	3 RP, S
598	6.82	3 [M-CO_2] + H_2O
686	7.23	4 RP, S
791	7.09	4 [M-CO_2] + H_2O

Table 2.14: FD-MASS of γ-benzyl-L-glutamate NCA, $CHCl_3$.

M/Z (Mass / Charge)	Intensity [%]	Identification
109	20.24	Benzyl alcohol
157	88.74	
239	100.00	[M-CO_2] + H_2O
439	12.94	2 RP

In conclusion, the diphosgene route was found to be more versatile than the triphosgene route and could be applied successful to all of the molecules investigated in contradiction to the latter one, which failed for γ-methyl-L-glutamate NCA. Additionally, the general reaction conditions and results were better due to higher yields, higher purity and less time consumption. The synthesis of the different cysteine NCAs confirmed these results. The NCAs could be successfully characterized by different techniques like NMR, IR and mass spectrometry. The obtained mass spectral data were the first ever obtained for this compound class, but it exhibited only reliable results if the NCA molecules were freshly synthesized. Atmospheric water initiated the longer stored NCAs and polymerized them even during storage under inert atmosphere at low temperatures. The resulting oligomers could be qualitatively proven by FD-mass spectroscopy.

References:

[1] D. Wassermann, J. D. Garber, F. M. Meigs, *U.S. Patent 3285953*, **1966**

[2] K. Mathauer, *Dissertation*, **1991**, University Mainz

[3] H.R. Kricheldorf, *α-Aminoacid-N-carboxy-anhydrides and related heterocycles. Syntheses, Properties, Peptide Synthesis, Polymerization*, Chap. 2, Springer, **1987**

Chapter 3
Polymerization of the NCAs

3.1 Introduction

α-Amino acid NCAs possess four reactive centers (two electrophilic (the carbonyl groups C2 and C5), and two nucleophilic (the NH and the α-CH group)).
This rich reactivity of the NCA monomers is responsible for the complex chemistry of this class of compounds.[1]

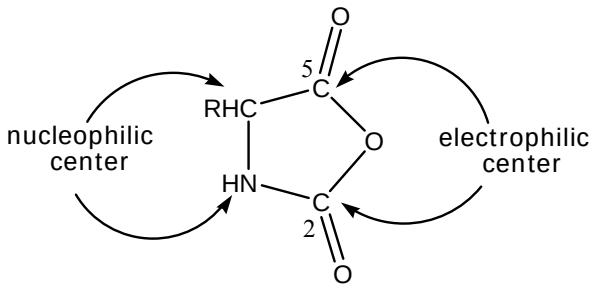

Figure 3.1: Multiple reactivity of a NCA.

Bamford summarized the first decades of research on the polymerization of NCAs in 1956. These first polymerization experiments had been carried out under the following conditions.

1) Exposing the solid NCA to water vapor.
2) Heating the NCA above its melting point.
3) Allowing the NCA to polymerize in solution, with or without the application of heat and the addition of an initiator.

Exposing NCAs to water vapor was not commonly used and was shown to lead to diketopiperazines by Wessely and Sigmund in 1926. In the second method, the reactant was initially fluid, but later became a hard glass. After these two unsuccessful and ineffective methods, the third one (polymerization in solution) were promising.[2]

It was shown after the reports of Bamford that the most suitable conditions for polypeptide synthesis is the polymerization of α-amino acid NCAs in solution using a base or generally speaking a nucleophile as initiator. This pathway is shown in Figure 3.2.

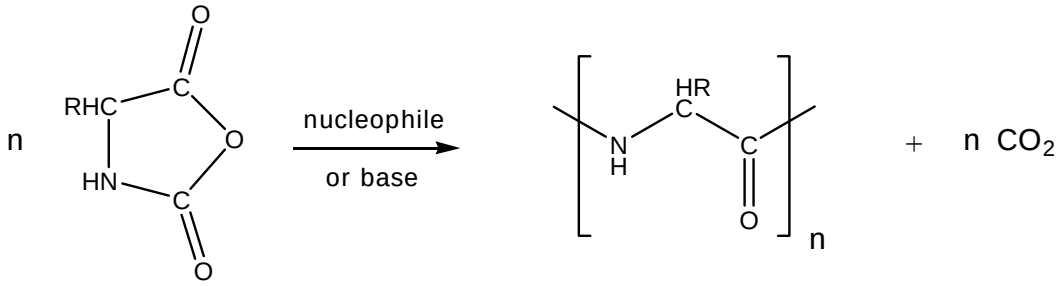

Figure 3.2: NCA polymerization initiated by a nucleophile or a base.

The method shown in Figure 3.2 involves the simplest reagents, and high molecular weight polymers can be prepared in both good yields and large quantities with no detectable racemization at the chiral centers. The considerable number of NCAs that have been synthesized (> 200) allows for exceptional diversity in the types of polypeptides which can be prepared.[1] Since the 1940s, the polymerization of NCA monomers has become the most common and economical technique used for the large scale preparation of high molecular weight polypeptides. Although more recently solid phase reactions (i.e. Merrifield-type reactions) have become popular, these reactions are better suited for step-wise synthesis of oligomers and can produce only small amounts of high molecular weight materials.[3-6]

Optimal polymerization conditions were often determined empirically for each single NCA. Therefore, no universal initiators or conditions exist for the preparation of high molecular weight polymers from any given NCA monomer. This is due in part to the different properties of the individual NCAs and their polymers (e.g. solubility), but is also strongly related to the different side reactions which may occur during the polymerization.

The solvent plays an important role in the polymerization and the choice of the proper solvent for the polymerization for a given NCA monomer can be challenging for several reasons. The first criterion is that the NCA monomer and the resulting polypeptide should be soluble in the chosen medium and at the same time the solvent should not act as an initiator during the polymerization. Unfortunately, many inert organic solvents for the NCA do not dissolve the respective polypeptide and vice versa. If the polymer suffers from low solubility in a particular solvent, the polymer will precipitate before a high molecular weight can be achieved. The purity of the solvent is another important criterion for successful polymerizations. The solvent must be stable, easy to dry, and readily available free from other reactive species, which can inhibit the polymerization to high molecular weight. Consequently, many solvents were examined in literature as media for

the polymerization of NCAs. Some of them were found to be disadvantageous because of undesired effects, like the ability of alcohols to react as an initiator.
The rate of polymerization depends as well on the quality of the solvent used - notably its dielectric constant, because it stabilizes or destabilizes ionic intermediates.

The role of the initiator has been under discussion for decades. The choice of the initiator greatly influences the mechanism by which the polymerization will proceed. Several classes of initiators were studied for the effective polymerization of monomers including radicals, salts and acids. All experiments with such initiators, except dry HF at ambient temperature, were unsuccessful.[7] With the exception of the application of heat (thermal polymerization), the following are the four most important classes of initiators: protic nucleophiles, aprotic nucleophiles, aprotic bases, and organometallic compounds. The interaction of NCAs with each of these four classes of initiators was investigated by several authors and was later reviewed by Kricheldorf.[8-18]

The efficiency of an initiator is roughly correlated to its nucleophilicity / basicity ratio with respect to the specific monomer that is to be polymerized. Most commonly, primary amines are utilized because they are more nucleophilic than basic. Tertiary amines or alkoxides, which are more basic than nucleophilic, are utilized to produce polymers of very high molecular weights that cannot be obtained with a primary amine. Kricheldorf and coworkers investigated the initiation of polymerization by amines, especially focusing on secondary amines which showed a great deal of tertiary base character.[19] Factors like steric hindrance must also be considered if a secondary amine is to be used for the initiation of the reaction.

The reactivity of the initiator compared to that of the active chain end (amino or carbamate group) is decisive for kinetic studies. Once an initiator molecule reacts with an NCA monomer, it is no longer active in the polymerization and the resulting primary amine, carbamate, or NCA anion end group is free to undergo a variety of undesired side reactions which are discussed later in this chapter. The mechanism of the polymerization, which is dependent upon the identity of the initiator, has been investigated intensively and has been the subject of considerable controversy in the last five decades.[20-22]

There are several difficulties associated with the elucidation of the polymerization mechanism.

1) The multiple reactive sites of a NCA.
2) The low solubility of most oligo-and polypeptides in organic solvents (precipitation of growing oligopeptides affects the reactivity of the active endgroups and changes the kinetics of the polymerization).
3) Conformation changes of the resulting polypeptide from sheet to helix influence the rate of propagation.
4) Due to the heterogeneity of most reaction mixtures the method for kinetic studies had been the measurement of the CO_2 evolution. The results are unreliable because side reactions causing CO_2 evolution cannot be avoided.

The two most likely pathways of NCA polymerization are the so-called amine and activated monomer (AM) mechanisms. A given system can switch back and forth between the amine and the AM mechanisms many times during a polymerization; a propagation step for one mechanism is a side reaction for the other, and vice versa. The mechanisms are named after the two different chain growth reactions which follow the different initiation reactions.

An inherent problem in conventional NCA polymerizations is the inability to control reactivity of the growing polymer chain end during the course of the polymerization.
Deming and coworkers investigated the use of an organometallic catalyst to control the polymerization. The organometallic catalyst caps the end of the polymeric chain and acts as a chaperone to control the propagation steps. This initial research by Deming and coworkers eventually led to the development of controlled living anionic ring-opening polymerization of NCAs to polypeptides of narrow polydispersities. To date, there are no other viable methods for the preparation of polypeptides via the NCA monomers with a low polydispersity. The group of Hadjichristidis claims that the lack of control is only depending on the purity of the system and has published a “High vacuum technique”. The method of Hadjichristidis has not yet been accepted by the scientific community.[3-6]

For this work, the traditional polymerization technique was chosen because the catalysts of Deming are not commercially available and their synthesis is very time consuming. Another down side of the preparation of the needed catalysts is the toxicity of the required phosphine ligands.

Molecular weight distribution (MWD):

Waley and Watson hypothesized that the anionic polymerization of NCAs should proceed with narrow weight distributions like olefins.[23] Narrow distributions would require nearly identical propagation rates for all chains. This was not observed, however, due to the broad distribution of end-group reactivities of the propagating species in the NCA polymerization.

High molecular weight polymers of exclusively beta sheet forming amino acids have not been reported. Long chains with low polydispersity (PD) can only be prepared from a handful of soluble and mostly helix forming peptides. Consequently the bulk of the recent publications discuss the polymerization of NCAs to poly (γ-alkyl-glutamates) and poly (N-Z-lysine).

The PD does not depend solely on the reactivity of the initiator, the solubility and secondary structures of the growing peptide chains are also important. Low PD can only be obtained for polypeptides soluble in inert reaction media. For the vast majority of natural amino acids, the rapid precipitation of the oligo- and polypeptides from the reaction medium leads to high PDs.[24] As a consequence of these diverse initiation and propagation steps the molecular weight distribution is broader than the Poisson type and can be bimodal when protic initiators are used.[25]

Primary amine (protic) mechanism:

A free primary amine attacks as a nucleophile at the C5 atom of the NCA monomer and opens the ring. The resulting carbamic acid decarboxylates to give a free amino end group which then acts as a propagation center. The polymerization mechanism first proposed by Wessely and later by Waley and Watson is shown below in Figure 3.3:[20, 21, 23, 26, 27]

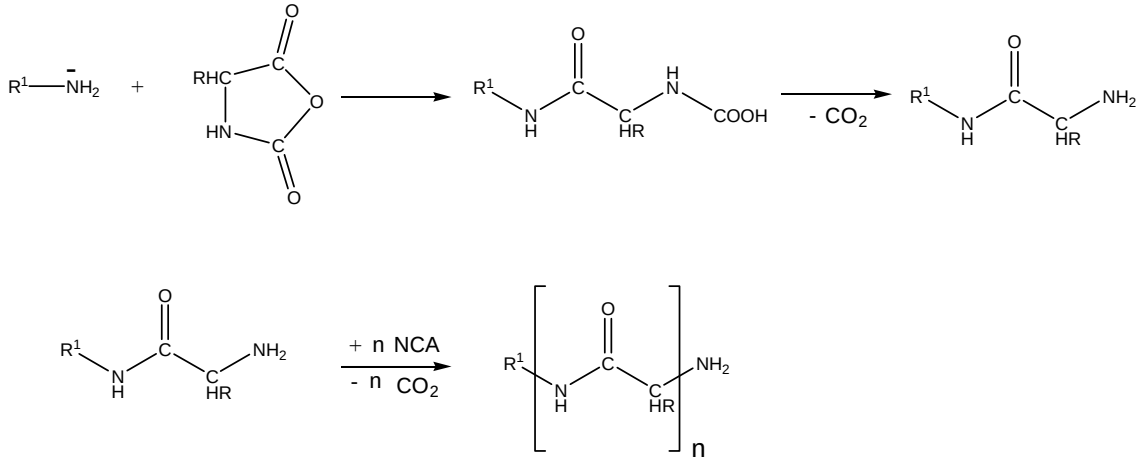

Figure 3.3: Primary amine mechanism for the polymerization of NCAs.

Primary amine initiated ring opening polymerizations (ROP) of NCAs are the most widely used approach for the preparation of polypeptides. The polymer grows linearly with monomer conversion under the ideal assumption that side reactions are absent.
The degree of polymerization (DP) can be easily controlled by variation of the molar ratio [M]/[I] ([M] and [I] represent the initial NCA and initiator concentrations, respectively) up to 100. N-Hexylamine and benzylamine are commonly used in the literature as initiators.[20, 21, 28, 29, 30]

Primary aliphatic amines and sterically unhindered secondary amines are more nucleophilic than the active chain ends; therefore, the initiation step is faster than the propagation step. Since the primary amine initiators become the terminus of each polymer chain, primary diamines yield polypeptides with a single disruption of the helix at the initiator site (broken rod structure).[31] All initiator molecules are incorporated into the growing peptide chain. Some kinetic investigations have established second order kinetics with the use of primary amine initiators of the form: - d[M]/dt = k[M][I] for the polymerization of benzyl glutamate NCA. The kinetics of the polymerization of benzyl glutamate NCA has been investigated in a variety of different solvents with numerous base initiators. Evolution of CO_2 was the preferred method of monitoring the reaction progress.

Carbamate mechanism:

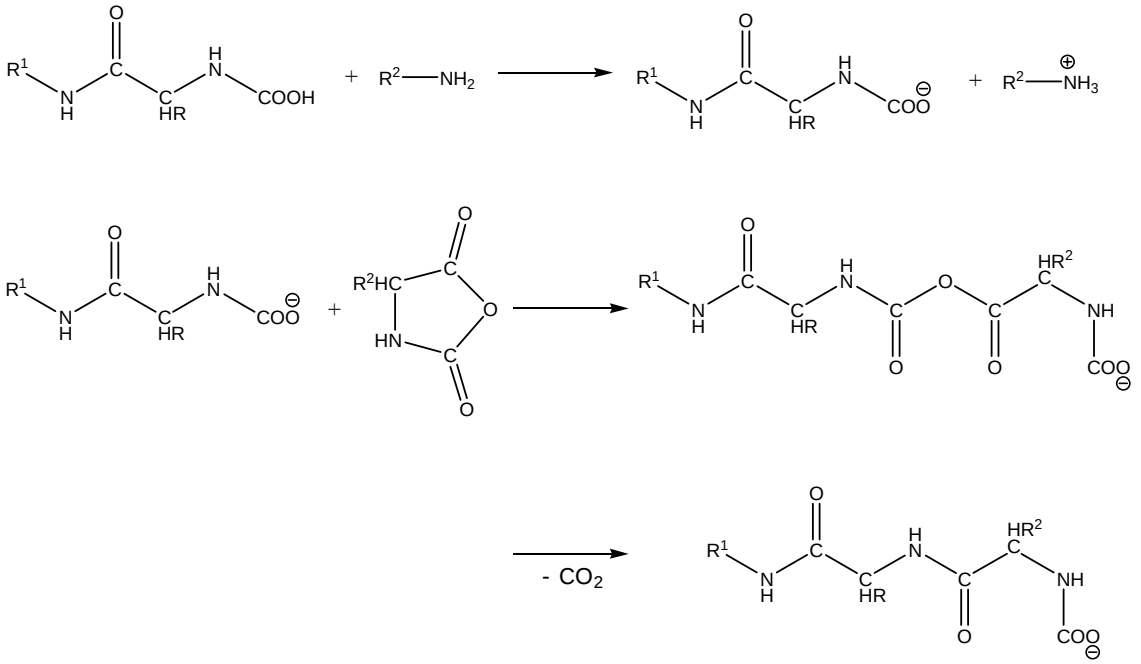

Figure 3.4: Carbamate mechanism.

The carbamate polymerization mechanism was first formulated by Idelson and Blout.[32] Harwood proposed later a modified improved version of the Idelson-Blout mechanism in which the carbamate anion of a growing chain reacts under decarboxylation with a NCA molecule.[32,33] The mechanism shown in Figure 3.4 represents the initiation step in which the initiator amine as well as the amino end groups of the growing chains deprotonate the intermediate carbamic acids preventing their decarboxylation. The propagation reaction proceeds via the carbamate groups. They attack nucleophilic on the NCA C5 atom and produce the intermediate anhydride which decarboxylates under the polymerization conditions to produce peptide bonds.

Activated Monomer (AM or aprotic) mechanism:

The highest molecular weights in NCA polymerization were obtained with trialkylamines, especially triethylamine.[1,34,35] The AM (activated monomer) mechanism is shown in Figure 3.5.

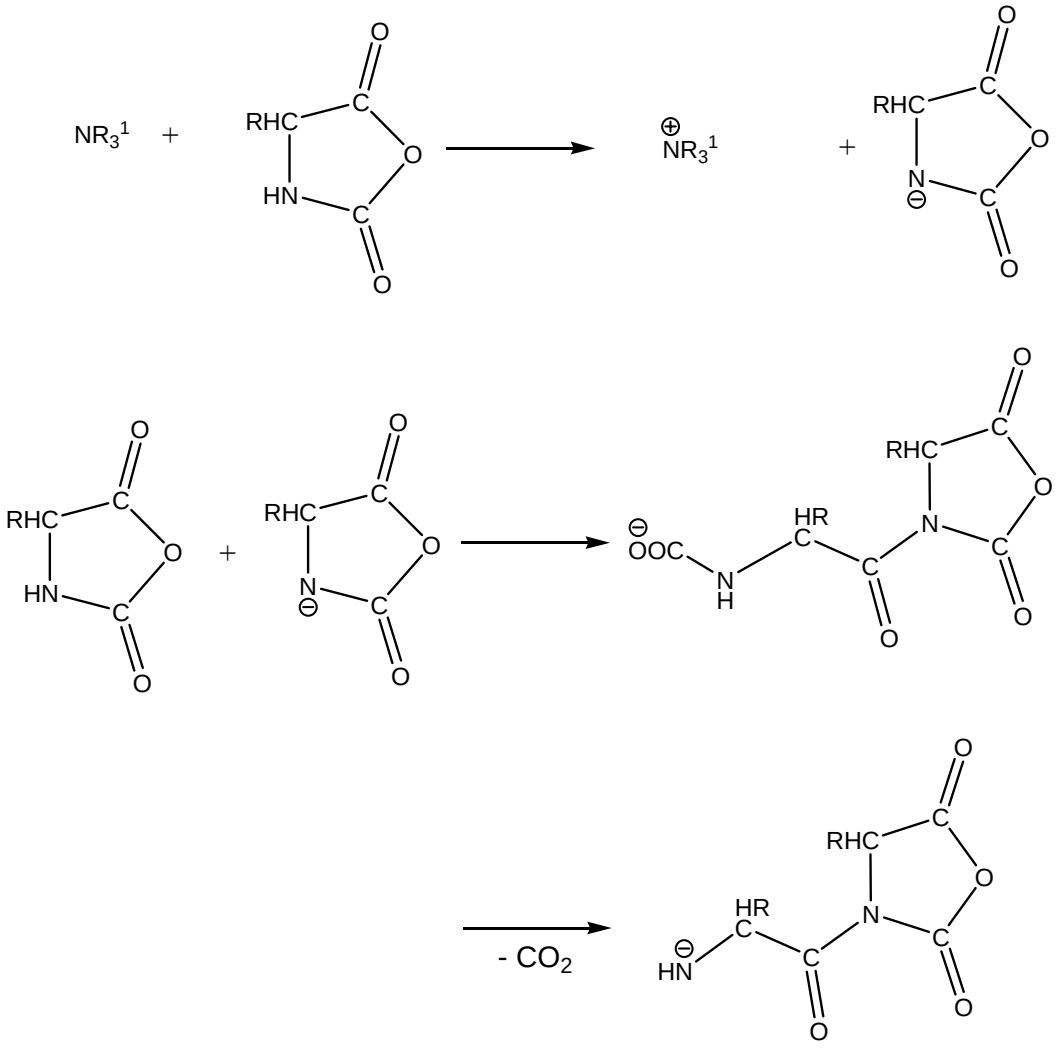

Figure 3.5: Activated Monomer (AM) mechanism.

Tertiary amines, alkoxides (i.e. aprotic initiators) and to some extent secondary amines act as bases and deprotonate the NCA to create a powerful nucleophilic NCA anion. The deprotonation of the NCA is followed by the nucleophilic attack of the NCA anion on another NCA monomer (or the NCA anion). The nucleophilic NCA bifunctional dimer with a highly electrophilic N-acyl NCA group at one end and a nucleophilic carbamate group at the other end. Decarboxylation yields a free amino end group which attacks nucleophilic on the next NCA molecule to continue the polymeric chain growth. This reaction pathway, first proposed by Bamford, is known as the activated monomer polymerization mechanism.[36] The amine mechanism differs from the previously described mechanism in that the amine is not incorporated into the polymer. The intermediate "active" monomer actually initiates chain growth.

NCA polymerizations initiated by strong bases also leads to an enhancement of the molecular weight (i.e. M_w of resultant polypeptide is much higher than that predicted by the initial [M]/[I] ratios even for [M]/[I]=100 or less). The molecular weight is independent of the monomer/initiator ratio in contrast to the amine mechanism. This enhancement is due to post-polymerization chain coupling, which requires a high mobility of peptide chains.[37]

Since most of the polypeptides strongly associate and even precipitate from less polar reaction mixtures, polycondensation is not always observed in the presence of strong bases when short polymerization times are used. Chain coupling is favored in solvents that minimize the helical conformations within a growing polypeptide chain.[37]

Initiation of NCAs with alkoxides (usually as an alcoholic solution) also produces high molecular weight polypeptides if the initial [M]/[I] ratio is high and rapid propagation occurs.[34] In this case both initiation and propagation may depend on the concentration of NCA and alcohol.[14] Figure 3.6 shows the equilibrium which can be shifted according to Le Chatelier´s Principle.

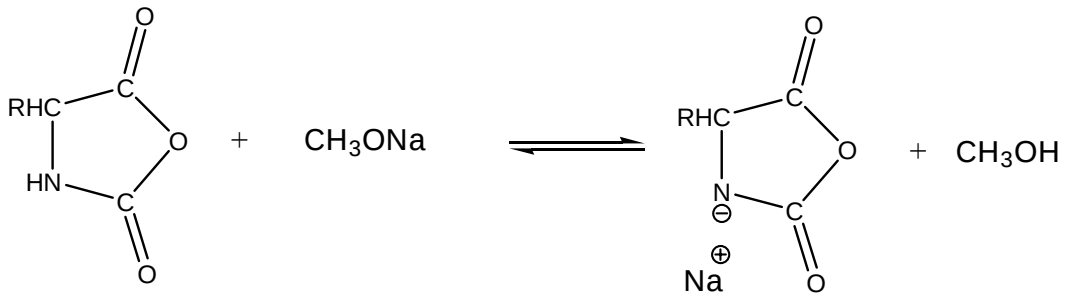

Figure 3.6: Equilibrium between methoxide and the alcohol solution.

Some remarks for the copolymerization of NCAs:

The sequence of residues in the resulting copolymer will depend on the relative rates of polymerization of the monomers. A mixture of NCAs will in general lead to a random copolymer, of which the overall composition can be calculated by the molar ratio of the NCAs used. The distribution of α-amino acid residues in the polymer chain will not be known. Sometimes block copolypeptides with compositions different than those predicted by monomer feed compositions have been reported. They had considerable homopolymer contamination most probably due to the very different reactivities of the monomers.

Side reactions:

One general possibility for a side reaction is the nucleophilic attack on the C2 atom, shown in Figure 3.7, leading to a substituted urea.

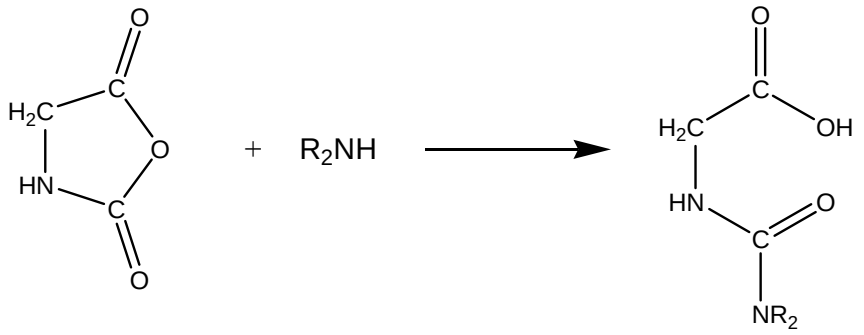

Figure 3.7: Side reaction of the nucleophilic attack on the C2 atom of an NCA.

It has only been observed in the polymerization of glycine and it appears therefore to be of negligible significance in the polymerization of glutamic acid ester NCAs.[2]

An intramolecular termination step, which is characteristic for polyglutamates, is formulated in Figure 3.8.

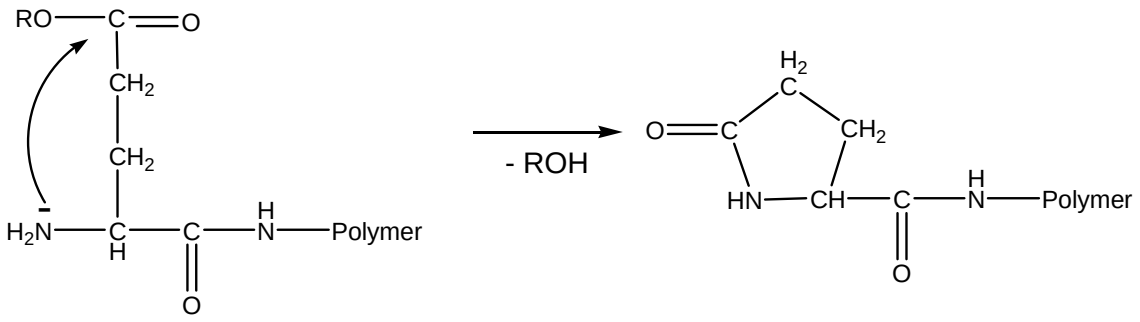

Figure 3.8: Intramolecular termination reaction for polyglutamates.[1]

Another possible side reaction is the condensation between bifunctional intermediate "activated" monomers which is shown in Figure 3.9.

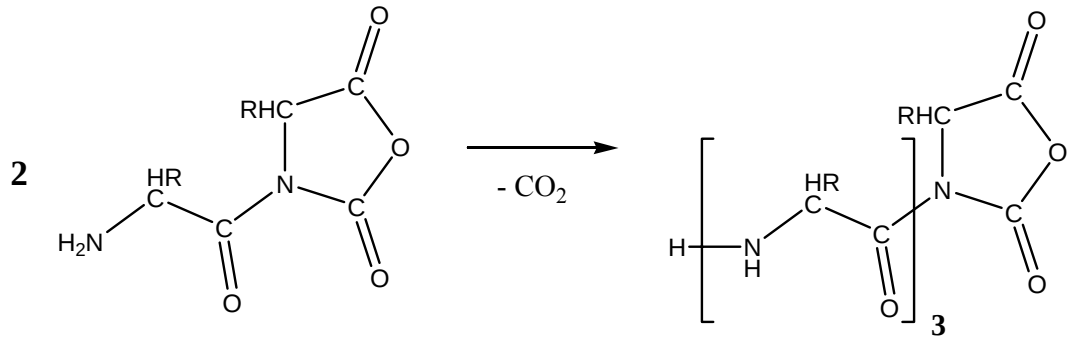

Figure 3.9: Condensation of two bifunctional activated monomers (side reaction).

Another undesired side reaction, which is a termination reaction, leads to a cyclic peptide. This cyclization of the intermediates, shown in Figure 3.10, has only been reported to form during the polymerization of the glycine NCA (cyclohexaglycine).

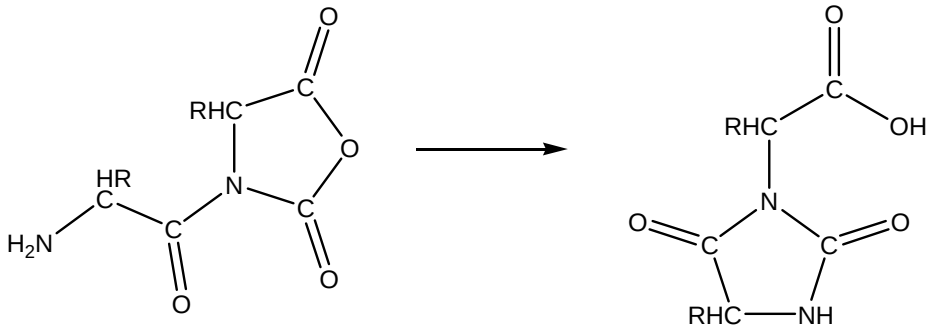

Figure 3.10: Cyclization of the intermediate activated monomers (side reaction).

3.2 Synthesis

All polymerizations carried out as part of this study are listed in Table 1 together with the important experimental conditions. These parameters are discussed later in this chapter. All non-aqueous reactions were performed under argon. All reactions were monitored by Thin-Layer-Chromatography (TLC) using a methanol/chloroform (8:2) eluent system and Ninhydrin as a staining agent for visualization. The molecular weight determination for the obtained polypeptides was found to be a challenging task and it will be discussed separately in the following chapter, which will include the techniques of viscosimetry, gel permeation chromatography (GPC), dynamic and static light scattering. The thermal behavior was analyzed by thermal gravimetric analysis (TGA) and differential scanning calorimetry (DSC). The obtained powders were also analyzed due to their chemical structure (IR) and crystallinity (XRD). A general working procedure for a polymerization of NCAs according to the "Amine mechanism" follows [38]:

Homopolymerizations:

γ-benzyl-L-glutamate NCA (2.00 g, 7.6 x 10^{-3} mol) were dissolved in 20 ml of dry THF. The required volume of the primary amine was then added to the stirred solution. The primary amine was dried prior to use by reflux over CaH_2 followed by vacuum distillation. After half an hour the viscosity of the reaction solution increased and the evolution of carbon dioxide bubbles were observed. After stirring for 5 days, the polymer was precipitated into water. The white powder was freeze-dried to remove residual water.

Copolymerizations:

The copolymerizations were conducted in a similar manner as the homopolymerizations. The different monomers (NCAs) were mixed in the desired ratio and dissolved in the reaction medium prior to the addition of the initiator. The polymers were precipitated in methanol and the white precipitate was excessively washed by methanol.

Table 3.1: Experimental data for polymerizations at 25°C.

Sample No.	NCA Monomer	m [g] M [mmol] NCA	Initiator	Time [days]	DP	Polymer	m [g] Polymer	Con-version [%]
MD-1-2	γ-benzyl-L-glutamate NCA	16.0 60.9	3-methoxy-propylamine	5	80	Poly (γ-benzyl-L-glutamate)	13.1	98.3
MD-1-45	γ-benzyl-L-glutamate NCA	21.0 79.9	n-hexylamine	5	100	Poly (γ-benzyl-L-glutamate)	14.3	81.8
MD-1-30	γ-methyl-L-glutamate NCA	2.0 10.6	3-methoxy-propylamine	5	60	Poly (γ-methyl-L-glutamate)	1.4	92.0
MD-1-31	γ-methyl-L-glutamate NCA	0.4 2.1	3-methoxy-propylamine	5	60	Poly (γ-methyl-L-glutamate)	0.3	98.6
MD-1-58	γ-methyl-L-glutamate NCA	10.0 53.2	n-hexylamine	3	60	Poly (γ-methyl-L-glutamate)	7.5	98.6
MD-1-32	γ-methyl and γ-octadecyl-L-glutamate NCA	1.0 5.3 --- 1.0 2.4	3-methoxy-propylamine	5	60	Copolymer (methyl-octadecyl) 30.5 % octadecyl	1.4	84.5
MD-1-33	γ-methyl and γ-octadecyl-L-glutamate NCA	1.0 5.3 --- 0.5 1.2	3-methoxy-propylamine	5	60	Copolymer (methyl-octadecyl) 18.0 % octadecyl	1.1	91.0
MD-1-34	γ-methyl and γ-octadecyl-L-glutamate NCA	0.5 2.7 --- 1.0 2.4	3-methoxy-propylamine	5	60	Copolymer (methyl-octadecyl) 47.0 % octadecyl	1.0	78.3
MD-1-53	γ-methyl and γ-octadecyl-L-glutamate NCA	1.0 5.3 --- 1.0 2.4	n-hexylamine	3	60	Copolymer (methyl-octadecyl) 30.5 % octadecyl	1.1	66.4

MD-1-54	γ-methyl and γ-octadecyl-L-glutamate NCA	2.0 10.6 --- 1.0 2.4	n-hexylamine	3	60	Copolymer (methyl-octadecyl) 18.0 % octadecyl	2.2	91.0
MD-1-55	γ-methyl and γ-octadecyl-L-glutamate NCA	1.0 5.3 --- 2.0 4.7	n-hexylamine	3	60	Copolymer (methyl-octadecyl) 47.0 % octadecyl	2.1	82.2
MD-1-56	γ-methyl and γ-octadecyl-L-glutamate NCA	2.0 10.6 --- 0.5 1.2	n-hexylamine	3	60	Copolymer (methyl-octadecyl) 10.0 % octadecyl	2.2	100.0
MD-1-24	γ-octadecyl-L-glutamate NCA	2.0 4.7	3-methoxy-propylamine	3	60	Poly (γ-octadecyl-L-glutamate)	1.5	83.7
MD-1-57	γ-octadecyl-L-glutamate NCA	1.5 3.5	n-hexylamine	3	60	Poly (γ-octadecyl-L-glutamate)	1.1	81.8
MD-1-46	S-carbobenzoxy-L-cysteine NCA	2.0 7.1	n-hexylamine	5[a]	100	Poly (S-carbobenzoxy-L-cysteine)	1.0	60.0
MD-1-50	S-carbobenzoxy-L-cysteine NCA	8.0 28.5	n-hexylamine	5[b]	100	Poly (S-carbobenzoxy-L-cysteine)	2.8	41.0
MD-1-62	S-carbobenzoxy-L-cysteine NCA	15.5 55.2	n-hexylamine	10	100	Poly (S-carbobenzoxy-L-cysteine)	11.0	84.7
MD-1-61	S-benzyl-L-cysteine NCA	19.0 80.2	n-hexylamine	10	100	Poly (S-benzyl-L-cysteine)	10.7	69.4

[a]: The last hour at 40°C.

[b]: Polymerization temperature was 50°C.

The ring-opening anionic polymerizations in this work were carried out following the standard conditions for NCA polymerizations which are described above in the general procedure given.[37-43] All polymerizations were initiated by a primary amine (n-hexyl amine or 3-methoxy-propylamine) following the “Amine mechanism” in dry THF. The polymers were precipitated in methanol or water. The polymers were purified further by several washings with methanol.

The different poly(glutamate)s were obtained in high conversions (over 80%, mostly even over 90%). The reaction time and initiator used was shown to have little influence on the yields obtained for the methyl and octadecyl ester. The decrease of conversion from 98.3 to 81.8 % for the polymerizations of the benzyl ester can therefore only depend on the increase of the amount of starting material used because it is known that an up scaling of a reaction often leads to reduced yields.

The synthesis of poly(S-carbobenzoxy-L-cysteine) and poly(S-benzyl-L-cysteine) has so far not been thoroughly investigated. In fact, only two synthetic articles exist from Berger, Noguchi, and Katchalski from the middle of the 1950s.[44-48] At the time of these preliminary reports, the characterization techniques for NCAs and the resulting polypeptides synthesized by anionic ring opening polymerization of these cyclic compounds were limited. The only method of characterization was elemental analysis.
An improved synthetic approach for the sulfur containing NCAs and the preliminary characterization of the resulting poly(cysteine)s was successfully achieved in the course of this work. After investigation of the most suitable synthetic route for the NCAs (see section 2.3) the polymers obtained can now be compared to the analogous and well characterized poly(glutamate)s.

Due to the lack of information for the polymerization of the cysteine derivatives, several parameters, which may influence the polymerization, were investigated. First the influence of the polymerization temperature was analyzed on poly(S-carbobenzoxy-L-cysteine). To examine the effects of temperature all of the other reaction conditions were kept constant except for the reaction temperature. The reaction conducted at 50° C for five days showed a conversion 20% lower than the polymerization, which was run for four days at room temperature and one day at 40° C. The conversion of 60% was still low compared to the poly(glutamate)s. It was assumed that elevated temperatures had adverse effects upon the conversion of the polymerizations. Therefore, another polymerization was run at room temperature, this time for 10 days. The expected influence on the conversion was proven with an increase of the conversion to 85 %. These conditions were used for poly(S-benzyl-L-cysteine) as well; however, the conversion was a little bit lower. This lower conversion of the polymerization might be caused by the lower reactivity of the S-benzyl-L-cysteine NCA or the increased amount of starting material, which has already shown to lead to lower yields. This study seems to indicate that the concentration of NCA can be raised up to a maximum of about 60 mmol without having negative influence on purity and yield. If the limiting value is surpassed, the yield decreases by 20% as the amount of NCA is increased to 80 mmol of NCA.

The copolymerizations have shown a correlation between conversion and copolymer composition. The higher the content of octadecyl group containing NCAs is, the more the conversion decreases. This trend was found for two series of copolymerizations with different initiators. No influence on the physical properties was observed due the identity of the initiator.

Table 3.2: Molecular weights of NCAs and polymeric repeating units.

	γ-methyl-L-glutamate	γ-octadecyl-L-glutamate	γ-benzyl-L-glutamate	Carbobenzoxy-L-cysteine	S-benzyl-L-cysteine
Mass NCA [g]	188	425	263	281	237
Mass repeating unit [g]	143	381	219	237	193

The conversion of the polymerizations was calculated according to equation 3.1:

$$\left(\frac{m_{Polymer} * M_{NCA}}{U_{Polymer} * m_{NCA}} \right) * 100 = Conversion\,[\%] \qquad (3.1)$$

$m_{Polymer}$ = Total Mass Polymer obtained

M_{NCA} = Molecular Mass NCA

m_{NCA} = Total Mass NCA used

$U_{Polymer}$ = Mass of the repeating unit of the obtained polymer

For the copolymerizations an average for M_{NCA} and $U_{Polymer}$ was calculated before according to equations 3.2 and 3.3:

$$M^{o}{}_{NCA} = P_{Methyl} * M_{NCA,\,Methyl} + P_{Octadecyl} * M_{NCA,\,Octadecyl} \qquad (3.2)$$

$$U^{o}{}_{Polymer} = P_{Methyl} * U_{Polymer,\,Methyl} + P_{Octadecyl} * U_{Polymer,\,Octadecyl} \qquad (3.3)$$

P_{Methyl} / P_{Methyl} = Percentage of the different esters (100% = 1; 0% =0)

3.3 Characterization

NMR-Spectroscopy:

^{1}H-NMR and ^{13}C-NMR spectra were obtained for all polymers prepared in this work. The low solubility drastically limits the choice of a suitable NMR solvent. PBLG is an exception, and it is highly soluble in a variety of common organic solvents, and therefore one of the most studied synthetically synthesized peptides. TFA is a necessary additive to disrupt aggregation, which even occurs in hydrogen bond interrupting solvents like DMF. Therefore, DMF should be avoided if possible as NMR solvent. The NMR data summarized in Tables 3.3 and 3.4 do not contain any unexpected results and will not be discussed further. The newly investigated poly(cysteine)s were characterized successfully as well.

Table 3.3: ^{13}C NMR chemical shift δ (ppm, relative to external TMS) of the obtained polypeptides.

Polymer	Solvent	NH-CO (main chain)	α-C	β-C	γ-C	CO (ester)	C (Ester group)
Poly (γ-benzyl-L-glutamate) ***PBLG***	$CDCl_3$ + TFA-d	175.81	55.75	29.10	32.31	178.26	70.85 (CH_2) 136.62 130.81 (phenyl)
Poly (γ-methyl-L-glutamate) ***PMLG***	$CDCl_3$ + TFA-d	173.44	53.52	27.12	30.04	176.64	53.06 (CH_3)
Poly (γ-octadecyl-L-glutamate) ***PSLG***	$CDCl_3$ + TFA-d	173.40	53.62	27.20	29.92	176.33	67.35 32.15 28.35 25.78 22.83 13.88 29.92 (octadecyl)
Poly (S-benzyl-L-cysteine) ***PSBC***					---	---	
Poly (S-carbobenzoxy-L-cysteine) ***PSCBC***	DMF-d	171.05	54.26	Signal is covered by the solvent	---	171.42	70.20 (benzylic CH_2) 136.72 129.68 129.57 (phenyl)

Table 3.4: ^{1}H NMR chemical shift δ (ppm, relative to external TMS) of the obtained polypeptides.

Polymer	Solvent	NH	α-CH	β-CH_2	γ-CH_2	Protons (Ester group)
Poly (γ-benzyl-L-glutamate) ***PBLG***	TFA-d	---	4.71	2.20 2.01	2.51	7.28 (aromatic, 5H) 5.13 (benzylic CH_2)
Poly (γ-methyl-L-glutamate) ***PMLG***	$CDCl_3$ + TFA-d	---	4.70	2.23 2.05	2.57	3.77 (methyl CH_3)
Poly (γ-octadecyl-L-glutamate) ***PSLG***	$CDCl_3$ + TFA-d	---	4.60	2.13 1.96	2.47	4.06 (CH_2) 1.58 (CH_2) 1.21 (15*CH_2) 0.80 (CH_3)
Poly (S-benzyl-L-cysteine) ***PSBC***	$CDCl_3$ + TFA-d	---	4.39	2.66	---	7.13 (aromatic, 5H) 3.54 (benzylic CH_2)
Poly (S-carbobenzoxy-L-cysteine) ***PSCBC***	DMF-d	8.48	4.74	3.50 3.30	---	7.40 (aromatic, 5H) 5.28 (benzylic CH_2)

IR spectroscopy:

PBLG and PSCBC were measured as KBr pellets and the observed IR frequencies at 3293, 1734, 1654, and 1542 cm^{-1} for PBLG and 3283, 1711, 1635, and 1514 cm^{-1} for PSCBC are consistent with the literature α-helical for PBLG [1] and antiparallel β-sheet for PSCBC.[49-52]

Raman spectroscopy:

Table 3.5: Observed experimental Raman frequencies (cm^{-1}) of Amide I and II bands.

Polypeptide	Conformation	Amide I	Amide III
PMLG	β-pleated sheet + α-Helix	1671 (s) 1695 (w)	1231 (s) 1297 (m)
PSLG	α-Helix	1659 (s)	1295 (s)
PSCBC	β-pleated sheet	1677 (s)	1239 (w)
PSBC	β-pleated sheet	1671 (m)	1239 (s)
PBLG	α-Helix	1650 (s)	1295 (m)

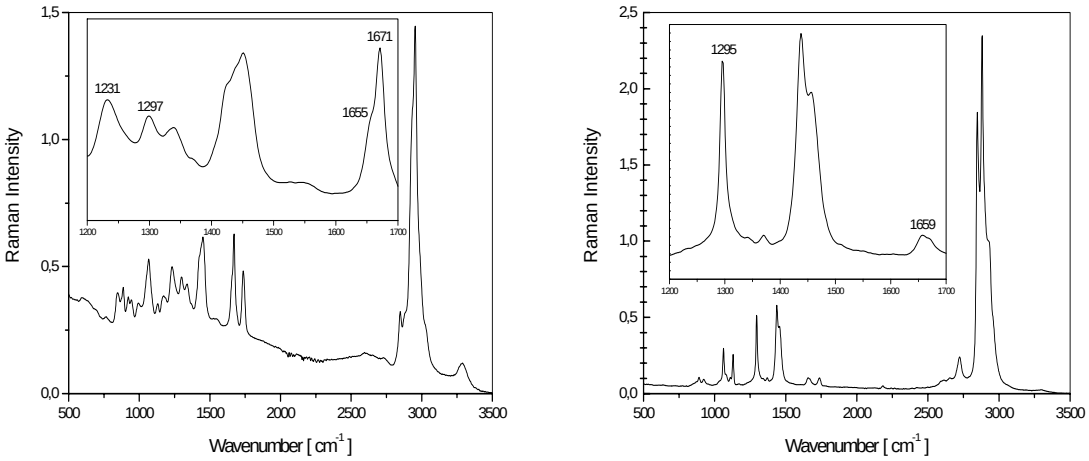

Figure 3.11: FTIR Raman spectrum of PMLG (left) and PSLG (right).

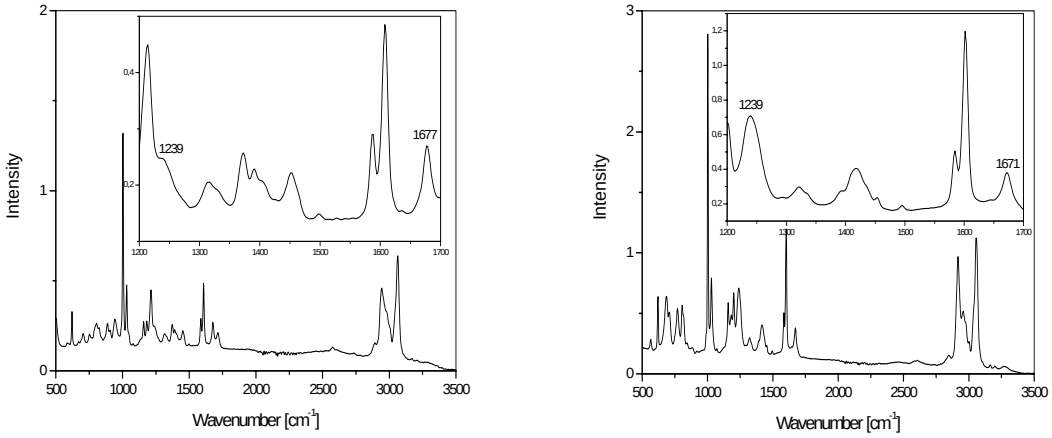

Figure 3.12: FTIR Raman spectrum of PSCBC (left) and PSBC (right).

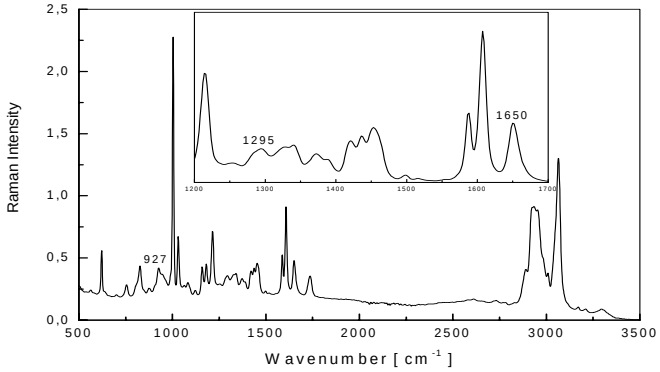

Figure 3.13: FTIR Raman spectrum of PBLG.

The observed experimental Raman bands are summarized in Table 3.5. All samples were measured as powders and the assignment of the secondary structures was based on literature values. Notable is the β-sheet structure for the polypeptides containing a heteroatom in the side chain (sulfur) or of PMLG and the different PLGA batches PP8 and PP9 which supports the previously discussed crystallization model including a competition between helix and β-sheet even if the chemical structure of the side chain prefers commonly a helical arrangement. The prepared films cannot be measured in the FT-Raman device because of the choice of substrates. Silica and glass fluorescent too strongly and yield a very broad halo.

Solid state NMR:

The solid state NMR spectra of PSCBC and PSBC are shown for the first time and the chemical shifts are elucidated to a β-sheet structure in both systems. This is in agreement with the general expectations for S-containing polypeptides.

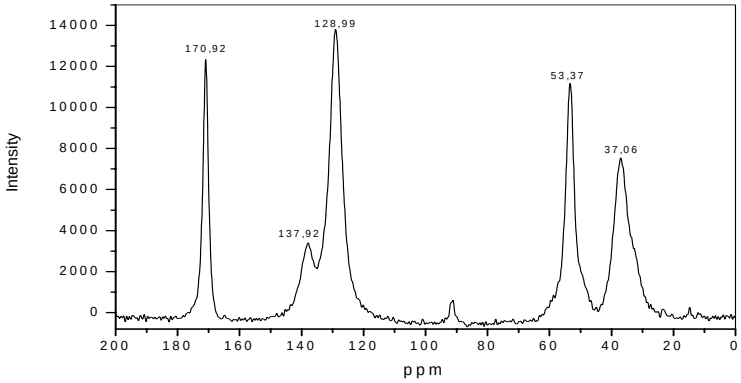

Figure 3.14: Solid state NMR spectrum of PSBC powder.

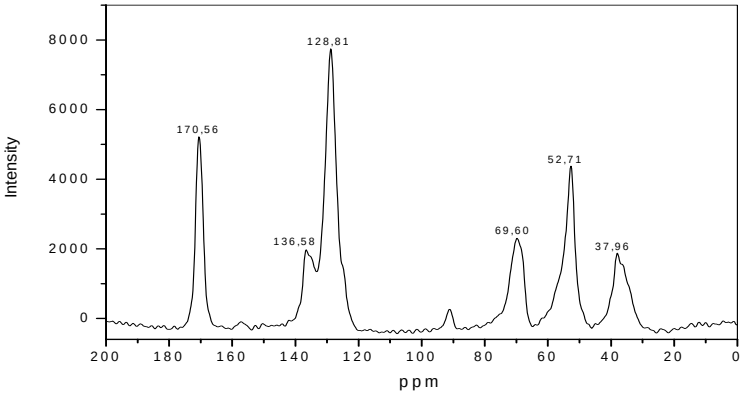

Figure 3.15: Solid state NMR spectrum of PSCBC powder.

The main chain CO (amide) and C_α peaks appear at 176.2 and 57.4 ppm, respectively.[53,54] The structure and the dynamics of PSLG with a long alkyl chain investigated further in the solid state and in the liquid crystalline state as a function of temperature.[55,56]

Mass spectrometry:

The use of mass spectrometry as characterization tool to elucidate the chemical structure of the prepared polymers was attempted. It should be mentioned that there are no mass spectra data available in literature for the polypeptides of the present work. The reason is that the protonation of the polymeric chains does not occur only at a single site. Multiple charges are possible and cause, together with the broad molecular weight distribution, mass spectra with a uncountable number of signals. Different techniques like FD (field desorption) and ESI (electrospray ionization) were however attempted and met with little success.

Analysis by MALDI-TOF (matrix assisted laser desorption ionization-time of flight) proved to be more fruitful. MALDI is a soft ionization method leading dominantly to singly charged ions regardless of the molecular mass and circumvents the problem of multiple charges. The MALDI technique for peptides was invented in the late 1980s by Karas and Hillenkamp to enable mass spectrometric analysis of large biomolecules.[57,58] Fragmentation of the sample ions does not usually occur. In the positive ionization mode used, the protonated molecular ions are normally dominant, but they can be accompanied by salt adducts.

The technique was originally limited to small organic molecules such as amino acids, Hillenkamp and Karas extended it to larger peptides with masses over 20 kDa. Consequently, Tanaka was the first to report the successful application of the technique for larger proteins and received the Nobel Prize in 2002. He dissolved the proteins in a suspension of ultra fine metal powder and glycerol so that the intact macromolecules could be ionized.[59]

The polymers were dissolved in the present work in a dithranol matrix and potassium trifluoroacetate was used as a dopant in TFA. This matrix was first reported by Kricheldorf for poly(alanine), poly(sarcosine) and poly(phenylalanine).[60-63] He discovered the cyclization reaction between the polymeric chain ends (called backbiting) and explained it as a result of a different polymerization mechanism. Kricheldorf and coworkers attempted to gain further insight into the mechanism and proposed several different alternatives to the known mechanism.

The MALDI data are summarized with the corresponding signal correlations to the different possible products in Tables 3.6-3.18. The MALDI spectrum itself is shown in Figures 3.17-3.21. To our knowledge these spectra and their interpretation are the first reported for PBLG, PMLG, PSLG, PLGA, PSCBC, PSBC, and the different copolymers of methyl and octadecyl glutamate. Cyclization was already reported for polyamides by Montaudo et al. and was further discussed by Pasch.[64,65] Other products detected beside the regular linear polymer are the following.

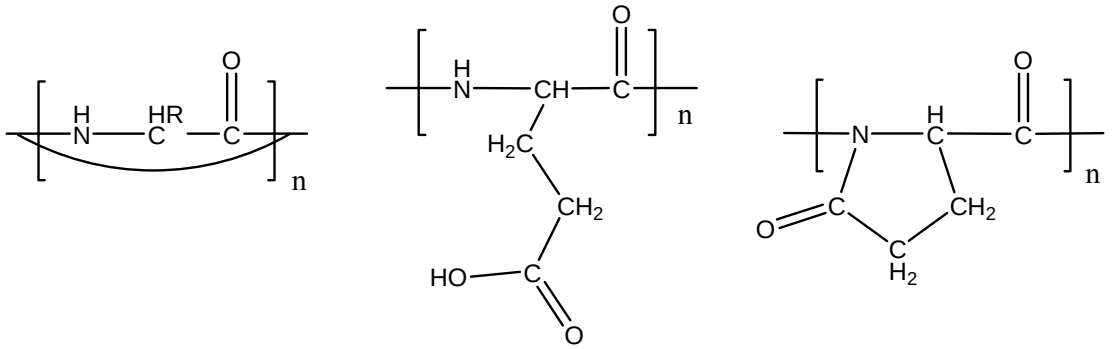

Figure 3.16: The different possible products detectable in MALDI.

B: Both ends of the polymeric chains cyclize under release of the initiator molecule.
S: The side chain ester group is saponified.
C: Cyclization occurs inside of a repeating unit and forms a stable five ring.

All of the MALDI spectra support the back-biting (**B**) as reported by Kricheldorf and coworkers. The poly(glutamate)s and PSCBC have the further possibility of exhibiting saponification (**S**) of the ester group in the side chain, or cyclization (**C**) inside of the side chain. PSBC can not cyclize in the side chain due to the lack of an electrophilic carbonyl group. The spectrum shows nearly no backbiting and most of the signals are due to sodium or potassium as cation.

PMLG: The mass of a repeat unit is ca. 143 Da.

Table 3.6: Masses (Da) of PMLG in TFA with dithranol as matrix and potassium trifluoroacetate as a dopant.

DP	4	5	6	7	8	9	10	11	12	13	14	15
S												
C					3							
B	no	yes	yes	yes	no	yes	yes	yes	yes	yes	yes	yes
Mass	675	717	860	1002	1151	1287	1431	1569	1719	1858	2002	2143

DP	17	17	18	19	20	22	22	24	25	25	27	28
S								11		1		
C	8					5			5		5	5
B	no	yes	yes	yes	yes	yes	yes	yes	yes	yes	yes	yes
Mass	2281	2430	2573	2713	2858	2993	3142	3281	3423	3562	3708	3850

DP	30*	30	30	31	32	33	34	36	36	37	39	39
S			1	1	1	1	1					
C	9	5						5	4	4	5	4
B	yes	yes	yes	yes	yes	yes	yes	yes	no	no	yes	no
Mass	3987	4136	4276	4417	4563	4705	4847	4996	5126	5270	5426	5556

*: These masses were achieved by Na^+ additive **: These masses were achieved by K^+ additive

Table 3.7: Masses (Da) of PMLG in DMF with dithranol as matrix and potassium trifluoroacetate as a dopant.

DP	12	13	14	15	16	17	18	19	20	21	22	23
S												
C												
B	yes	yes	yes	yes	yes	yes	yes	yes	yes	yes	yes	yes
Mass	1715	1857	2001	2145	2289	2431	2573	2717	2861	3004	3147	3291

DP	24	25	26	27	28	29	30	31	33	34
S										
C										
B	yes	yes	yes	yes	yes	yes	yes	yes	yes	yes
Mass	3434	3577	3720	3864	4008	4151	4294	4435	4722	4866

Solid phase Maldi, matrix TCNQ:

DP	4*	7	7**	8*	10*
S					
C	3	5	5		
B	no	yes	yes	yes	yes
Mass	603	846	885	1167	1453

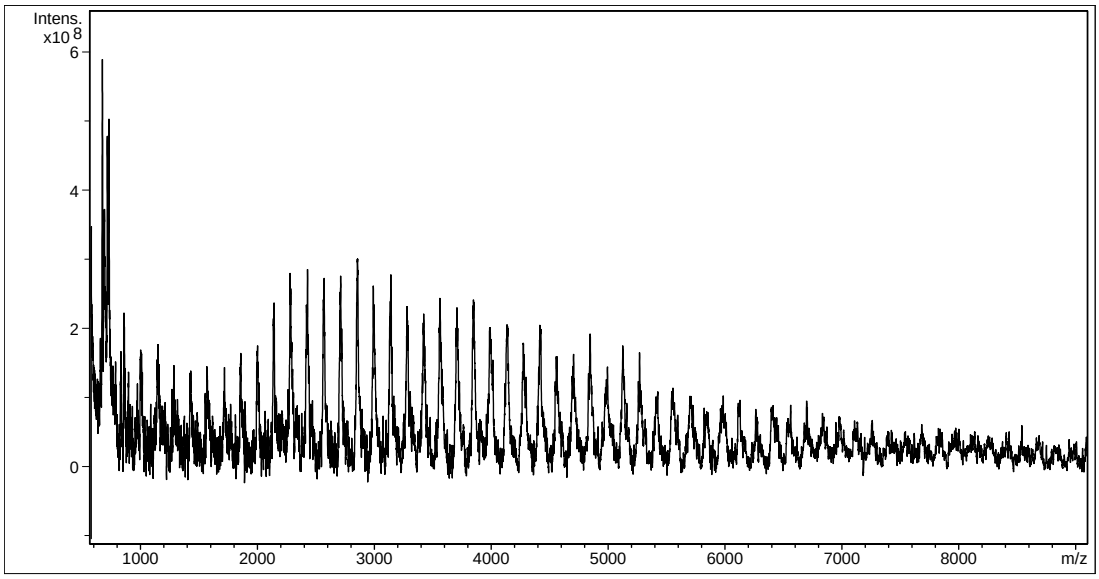

Figure 3.17: MALDI-TOF mass spectrum of a poly(γ-methyl-L-glutamate) (MD-1-58), measured in TFA as matrix and potassium trifluoroacetate as a dopant.

The matrix containing DMF instead of TFA has less saponified or cyclized chains. The solid measurement shows more cyclizations.

PBLG: The mass of a repeat unit is ca. 219 Da.

Table 3.8: Masses (Da) of PBLG in TFA with dithranol as matrix and potassium trifluoroacetate as a dopant.

DP	4	4	5	5*	5	5*	4	4	5	6	6*	6**
S	2	3	1	1	4	4		1	3	4	4	4
C	2	1	4	4	1	1	1			2	2	2
B	no	no	no	no	no	no	yes	yes	yes	no	no	no
Mass	585	599	676	699	732	754	770	786	824	842	865	881

DP	6	8	9	18	17	18	19	20	20	21	21	22
S	3	2	2	3	3	3	3	4	3	3	3	4
C		1	1	2			2	2	2	2	2	2
B	no	yes	yes	yes	no	yes	no	no	no	yes	no	no
Mass	1146	1465	1683	3460	3553	3671	3777	3907	3998	4118	4214	4344

DP	22	23	23	23	24	25	25	26	26	27	27	28
S	3	3	3	4	3	3	2	3	2	4	3	4
C	2	2	2		2	2	2	2	2	2	2	2
B	no	yes	no	no	no	yes	yes	yes	yes	no	no	no
Mass	4437	4555	4655	4780	4872	4995	5099	5209	5318	5440	5527	5658

*: These masses were achieved by Na^+ additive **: These masses were achieved by K^+ additive

Table 3.9: Masses (Da) of PBLG in DMF with dithranol as matrix and potassium trifluoroacetate as a dopant.

DP	5**	5**	6**	6**	7**	7**	8**	8**	9**	9**	10**	16**
S												
C	1		1		1		1		1		1	
B	no	no	no	no	no	no	no	no	no	no	no	yes
Mass	1128	1236	1348	1456	1567	1675	1787	1895	2006	2114	2226	3543

DP	17**	18**	19**	20**	21**	22**	23**	25**	26**	27**	28**	29**
S												
C												
B	yes	yes	yes	yes	yes	yes	yes	yes	yes	yes	yes	yes
Mass	3763	3981	4201	4423	4641	4859	5078	5518	5737	5958	6176	6396

DP	30**	31**	32**	33*	34**	35**	36**	37**	38**	39**	40**	41**
S												
C												
B	yes	yes	yes	yes	yes	yes	yes	yes	yes	yes	yes	yes
Mass	6614	6835	7054	7275	7492	7712	7933	8151	8368	8589	8811	9027

*: These masses were achieved by Na^+ additive **: These masses were achieved by K^+ additive

Table 3.10: Masses (Da) of PBLG, solid phase Maldi with DCTB as matrix and potassium trifluoroacetate as a dopant.

DP	4	6	6	5**	5**	6**	7**	10	8**
S	4		4					5	
C		3		1					
B	no	yes	no	no	no	no	no	yes	no
Mass	615	991	1051	1128	1237	1455	1676	1740	1894

Table 3.11: Masses (Da) of PBLG, solid phase Maldi with TCNQ as matrix and potassium trifluoroacetate as a dopant.

DP	4	4	3	5	5**	6	6**
S	2	3		1	1	4	4
C	2		1	4	4	1	1
B	no	yes	no	no	no	yes	yes
Mass	586	603	647	677	716	846	885

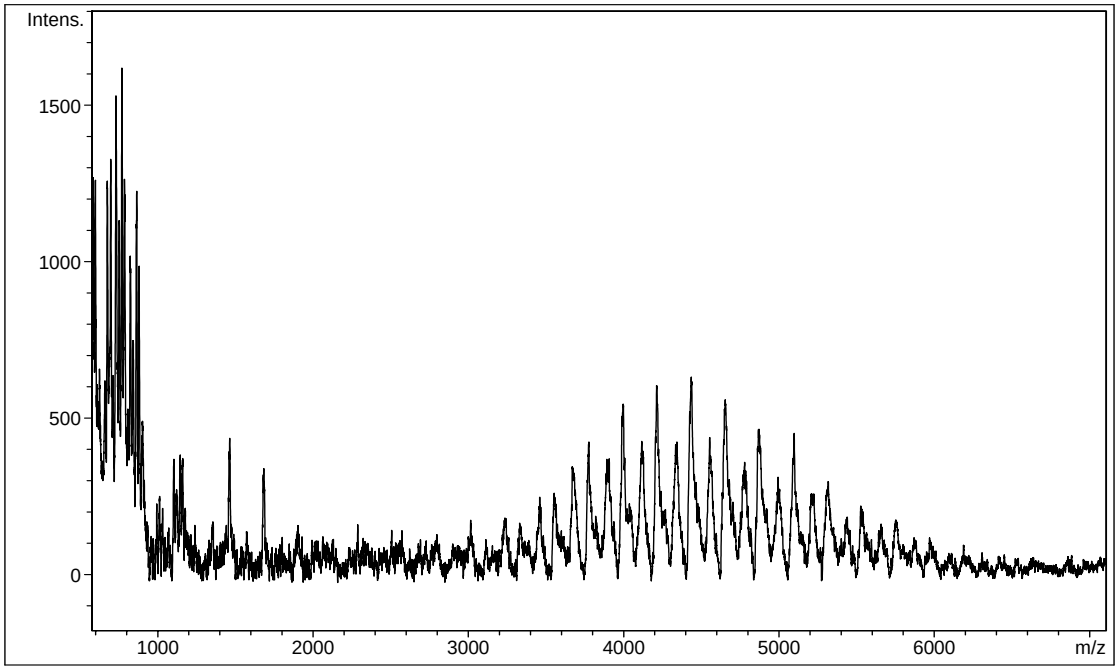

Figure 3.18: MALDI-TOF mass spectrum of a poly(γ-benzyl-L-glutamate) (MD-1-45), measured in TFA with dithranol as matrix and potassium trifluoroacetate as a dopant.

DMF as matrix shows backbiting and exclusively potassium doping but nearly no saponifications or cyclizations in contrast to TFA wherein hydrogen doping is dominant. The solid phase Maldi spectra show signals in a much narrower m/z range than the liquid Maldi.

PSLG: The mass of a repeat unit is ca. 381 Da.

Table 3.12: Masses (Da) of PSLG in TFA with dithranol as matrix and potassium trifluoroacetate as a dopant.

DP	5	3	5	10	8	6	8	6	7	9	10	8
S	2		1	10		1	1	1	1	4		1
C	2		2		6	2	4	1	2	1	6	2
B	no	yes	no	yes	yes	no	yes	no	no	yes	no	no
Mass	965	1145	1217	1289	1434	1600	1721	1865	1983	2153	2295	2364

DP	15	10	11	10	11	10	12	13	12*	13	14	16*
S	13	1	3	2	4	3	4		4	1	3	3
C		4	3	2	1		1	6		4	3	5
B	yes	no	no	no	no	no	yes	no	yes	no	no	yes
Mass	2438	2582	2727	2868	3013	3156	3300	3438	3588	3726	3869	4020

DP	14	14	15	16	17*	16	17*	16	17*	17	16
S	4	3	4		7	1	2	2	3	3	2
C	1	1	1	6		4	4	2	2	1	
B	no	yes	yes	no	yes	no	no	no	no	yes	yes
Mass	4157	4308	4441	4585	4736	4872	5023	5156	5309	5448	5593

*: These masses were achieved by Na^+ additive **: These masses were achieved by K^+ additive

Table 3.13: Masses (Da) of PSLG in DMF with dithranol as matrix and potassium trifluoroacetate as a dopant.

DP	4	3	3	5*	5	4	4**	6	4	5	5	5
S	4	2	3	5	2	2	2	2	1	1	2	3
C					3	1	1	4	2	3	2	1
B	no	yes	yes	yes	no	yes	yes	no	no	yes	yes	yes
Mass	619	640	657	668	696	751	789	805	833	843	859	883

DP	5	6	6	6**	6**	6*	6**	5	6
S	4		2	2	3			1	1
C		5	3	3	2	5	5	2	2
B	yes	yes	yes	yes	yes	no	no	no	no
Mass	898	937	975	1013	1029	1067	1082	1215	1596

Table 3.14: Masses (Da) of PSLG, solid phase Maldi with DCTB as matrix and potassium trifluoroacetate as a dopant.

DP	4	5	6	7	8	8**	9	9**	10	10**	11	11**
S	1	1	1	1	1	3	1	3	1	3	1	3
C	2	2	2	2	2		2		2		2	
B	no	no	no	no	no	no	no	no	no	no	no	no
Mass	834	1215	1597	1979	2362	2430	2744	2812	3126	3195	3508	3577

DP	12	12**	13	13**	14	14**	15	15**	16	16**	17	17**
S	1	3	1	3	1	3	1	3	1	3	1	3
C	2		2		2		2		2		2	
B	no	no	no	no	no	no	no	no	no	no	no	no
Mass	3890	3959	4271	4341	4653	4723	5034	5104	5417	5486	5799	5868

DP	18	18**	19	19**	20	20**	21	21**	22	22*	23	23**
S	1	3	1	3	1	3	1	3	1	3	1	3
C	2		2		2		2		2		2	
B	no	no	no	no	no	no	no	no	no	no	no	no
Mass	6182	6250	6562	6633	6945	7014	7328	7395	7708	7778	8089	8160

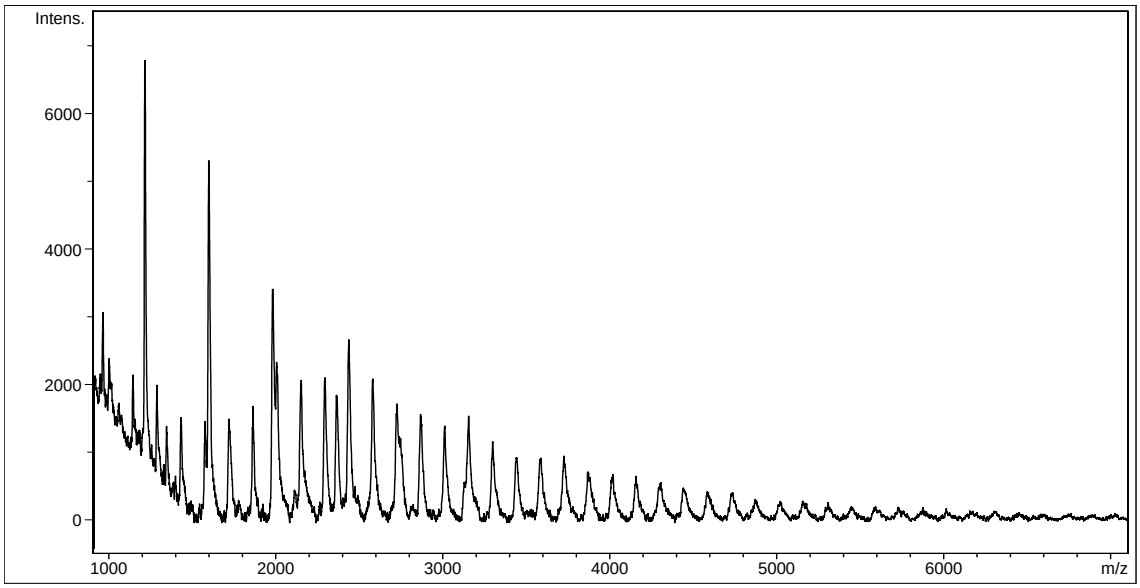

Figure 3.19: MALDI-TOF mass spectrum of a poly(γ-octadecyl-L-glutamate), measured in TFA with dithranol as matrix and potassium trifluoroacetate as a dopant.

There is not a big difference between TFA and DMF as matrix. The backbiting is not present at all.

PSCBC: The mass of a repeat unit is ca. 237 Da.

Table 3.15: Masses (Da) of PSCBC in TFA with dithranol as matrix and potassium trifluoroacetate as a dopant.

DP	4	4	3	3	4	4	6	7	8	9	10	13	12	13	17
S	3	4				2	2	2	2	2	4	1	4		13
C			1		2		3	2	2	2		7		3	
B	yes	yes	no	yes	yes	yes	no	yes	yes	yes	yes	yes	yes	yes	no
Mass	677	584	705	625	732	771	1022	1262	1502	1738	2009	2243	2484	2760	2961

*: These masses were achieved by Na^+ additive **: These masses were achieved by K^+ additive

Table 3.16: Masses (Da) of PSCBC in DMF with dithranol as matrix and potassium trifluoroacetate as a dopant.

DP	3**	4	4*	4*	5	5	5*	6	6*	6	6*	6**	7*	8*	8*
S		2	2	3		1	1	2	2	2	2	2	2	1	2
C		1	1		2	1	1	2	2	1	1	1	1	2	1
B	yes	no	no	no	yes	yes	yes	yes	yes	no	no	no	no	no	no
Mass	751	765	789	805	975	991	1013	1028	1051	1236	1257	1275	1494	1717	1734

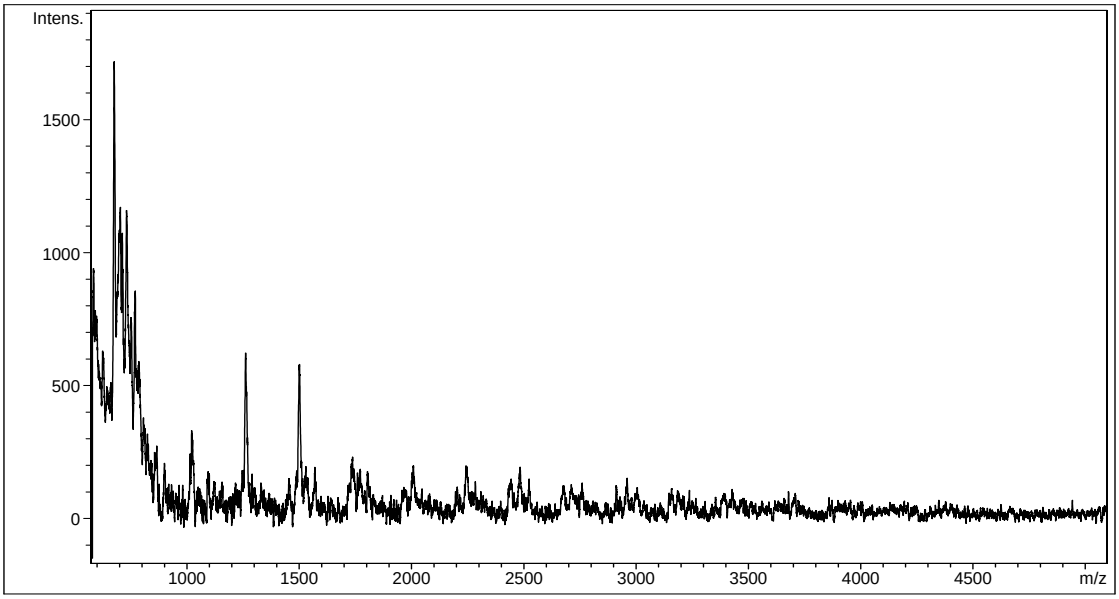

Figure 3.20: MALDI-TOF mass spectrum of a poly(S-carbobenzoxy-L-cysteine) initiated with hexylamine in THF at 20° C (MD-1-62).

There is again not a big difference between TFA and DMF as matrix, but the detected molecular weight range is narrower for DMF.

PSBC: The mass of a repeat unit is ca. 193 Da.

Table 3.17: Masses (Da) of PSBC in TFA with dithranol as matrix and potassium trifluoroacetate as a dopant.

DP	3			6**	7**	7**	8**	8**	9**	9**	10**	10**
S				5	5	4	5	4	5	4	5	4
B	no			no	no	no	no	no	no	no	no	no
Mass	676	712	731	846	1040	1129	1237	1323	1428	1518	1625	1711

DP	11*	11**	12**	12**	13**	14**
S	5	4	5	4	4	5
B	no	no	no	no	no	no
Mass	1816	1907	2010	2096	2294	2401

*: These masses were achieved by Na^+ additive

**: These masses were achieved by K^+ additive

Table 3.18: Masses (Da) of PSBC in DMF with dithranol as matrix and potassium trifluoroacetate as a dopant. Solid phase Maldi, matrix TCNQ with the same spectrum:

DP	8	8*	9*	9*	10*	10*	11*	11*	12*	12*	13*	13*	14*	14*
S	7	6	7	6	7	6	7	6	7	6	7	6	7	6
B	no	no	no	no	no	no	no	no	no	no	no	no	no	no
Mass	1013	1125	1230	1318	1423	1511	1617	1706	1812	1900	2005	2093	2199	2288

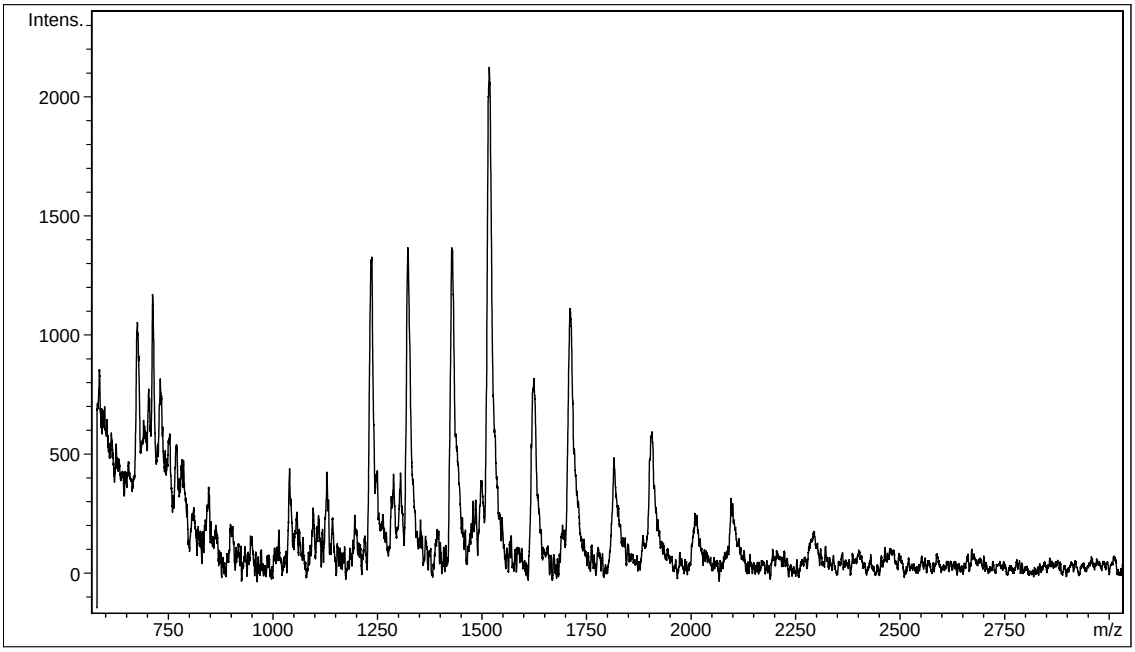

Figure 3.21: MALDI-TOF mass spectrum of a poly(S-benzyl-L-cysteine) initiated with hexylamine in THF at 20° C (MD-1-61).

There is no backbiting at all present in the spectra, but here are existing more saponified chains for DMF than for TFA.

PSCBC shows mostly backbiting in contrast to PSBC due to higher stability under acidic conditions. PBLG and PSLG have a more or less equal fraction of backbiting (~50%) and show a higher amount of totally saponificated or cyclized side groups compared to PMLG. PMLG exhibits a large degree of backbiting.

These high degrees of backbiting in nearly all samples means that nearly all initiator amine groups have been removed from the polymer. If Kricheldorf was correct that the cyclization is a result of a different polymerization mechanism, then it should be possible to observe a different NMR spectrum. The initiator signals would not be visible. The initiator to main chain integration, commonly used to estimate the degree of polymerization, would lead to erroneous results. Furthermore, if Kricheldorf´s assumption is correct, then the saponified and cyclized side chains should be in the polymers present prior to the sample preparation for the MALDI measurements. This can be contradicted by NMR. In both cases the ester group in the side chain will be released and therefore will be absent in the NMR. The integration of the main chain NMR signals to the side chain signals, like the benzyl group, have shown that there is not a large amount of saponification or cyclization present in the polymers.

Therefore the change in the structure may depend on the dissolution of the polymers in TFA, a highly acidic solvent, which induces the cleavage of the acid labile ester groups. The amount of these reactions shows the order in the stability for the different poly(glutamate)s: PMLG > PBLG > PSLG
Further studies in a less acidic solvent should give a confirmation for this assumption, but the obtained spectra are not clearly confirming this approach. All measurements analyzed were recorded in the reflectance mode because the linear mode had shown worse resolution.

Solubility:

Statistic copolymers have a better solubility than homopolypeptides. The solubility increases with the acidity of the solvent. The more acidic the more is the main chain getting protonated and the less is the main chain capable to form secondary structures.
Solubility of the glutamic acid and of the aspartic acid in water is just depending on the pH (ionization of the side chain). Homopolypeptides in general low soluble in non acidic solvents.

Molecular weight characterization of the polymers:

The insolubility of most of the homopolypeptides in inert solvents prevents reliable characterization with any kind of common polymer characterization technique like gel permeation chromatography (GPC), dynamic and static light scattering or viscosimetry.[66] However, a broad variety of analytical methods have been applied to determine the molecular weight or MWD of polypeptides. These methods can be subdivided into four groups:

1.) Viscosity measurements, which do not give absolute molecular weights.
2.) Quantitative endgroup analyses, e.g. formerly done by titration reactions with chromophores, or NMR spectroscopy.
3.) Physical measurements, such as vapor pressure osmometry (VPO), membrane osmosis, cryoscopy, light scattering, or ultracentrifuge.
4.) Chromatographic methods, e.g. gel permeation chromatography (GPC)

In particular, information on the MWD of polypeptides is quite rare, because GPC is not applicable to most polypeptides and fractionated precipitation combined with methods suitable for the determination of the absolute molecular weight is time consuming.

Endgroup analysis was applied at the beginning to determine the degree of polymerization and the molecular weight if the polymerization mechanism meets the following requirements:

1) Each initiator molecule initiates the growth of only one chain
2) Termination steps must be absent or must occur in all chains in the same way.
3) Formation of cyclopeptides must be absent

Probably the first method used for endgroup determination was the conversion of the free amino endgroup with nitrous acid to nitrogen, according to Van Slyke.[67] Later, an attractive alternative was conducted by Sela and Berger through the titration of the amino endgroups by means of perchloric acid or by sodium methylate using thymol blue as indicator.[68,69] The indicator/solvent systems for the former one were crystal violet/glacial acetic acid or thymol blue/DMF. If the polypeptides were water soluble, the end point was also able to determine by potentiometry, whereas conductometric measurements were advantageous in organic solvents such as methanol/m-cresol.[70,71] Another route involved their dinitrophenylation by means of 2,4-dinitrofluorobenzene.
A more convenient method for the determination of amino endgroups was established by Shoji and coworkers.[72] They compared the intensity of the ^{1}H-NMR signal of the protonated amino endgroup with the signal intensities of either CO-NH or C_α protons in DCA or TFA. The problem was the partial overlapping of the NH of the main chain with the NH_3^+ signal even in the case of oligomers. If the polymer adopted various conformations (e.g. helices, sheets or coils) in solution, splitting of the peptide signal completely obscured the endgroup. Therefore, endgroup analysis by ^{1}H-NMR spectroscopy of initiator fragments became widely used if primary amines were used as initiators for the preparation of polypeptides with defined DPs.[73-75] This method was used in this work for the calculation of the degree of polymerization by integrating initiator alkyl signals versus polymer backbone signals.

The physical methods used for the determination of absolute molecular weights are cryoscopy, vapor pressure osmometry (VPO), membrane osmometry, light scattering, and ultracentrifuge. The application of all these methods suffers from the insolubility of most polypeptides or from association, in the cases where solution occurs. Thus, PBLG, which has been known for a long time for its outstanding solubility in various solvents, was the most frequent subject of physical molecular weight measurements. There are only a few cryoscopic measurements reported in the literature.[76] MWDs are usually broad. Therefore, membrane osmotic measurements run a high risk of overestimating the molecular weight due to loss of the low molecular weight fraction. Aggregation causes the same problem. In a way to avoid the problem they tried a use of acidic solvents such as TFA and MSA, which prevent aggregation, suitable membranes are not

available. In other words, the M_n determined by their first osmotic measurements are far too high. The addition of hydrogen bond breaking solvents was reported.[77] The molecular weight measurements and IR spectra of Blout and Doty demonstrated for the first time that living polymerizations of NCAs do not necessarily result in a Poisson distribution and that the polymerization kinetics, MWD, and secondary structure of the polypeptides are interdependent.

PMLG, PSLG and the corresponding copolymers:

The compositions of the copolymers were calculated based on integrations of the ^{1}H-NMR spectra and were found to be consistent with the theoretical calculations. The molecular weight was determined by two different methods. The first method compares the integration of the initiator and the polymer backbone peaks in the ^{1}H-NMR spectra to obtain the molecular weight. The calculated degree of polymerization (DP) was in agreement with the applied monomer/initiator ratio during polymerization. It should be noted, however, that this method becomes less accurate with increasing DP. Other common characterization methods for polymers, like gel permeation chromatography (GPC) and static light scattering (SLS), met with little success due to low solubility, low molecular weights, and tendency of the polymers to aggregate. Viscosimetry was applied as a second method to determine the molecular weights. Dichloroacetic acid, a solvent known to lead to a non-helical polymer conformation, was used as the eluent to avoid aggregation. The measurements were carried out at 25 °C using an Ubbelohde capillary viscosimeter. Two different Mark-Houwink equations were taken into account for calculating M_η:

$$[\eta] = 2{,}78 * 10^{-5} M^{0{,}87} \qquad (3.4)^{[78]}$$

$$[\eta] = 29 * 10^{-5} M^{0{,}74} \qquad (3.5)^{[79]}$$

Both systems are valid for DCA at 25°C, but for different polymers.

Equation 3.4 was investigated by Doty et al. for the polypeptide poly-γ-benzyl-L-glutamate (PBLG) which is the most often cited reference for homopolypeptides in viscosimetry studies even if the polymeric structure is less or more slightly different. It was used in our work to analyze the accuracy of the range of obtained molecular weights depending on the Mark-Houwink parameters for these biopolymers. Equation 3.5 was achieved by Tanaka et al. especially for Poly-γ-methyl-L-glutamate (PMLG). The results, listed in Table 3.19, exhibit a large difference for PMLG by applying both sets of Mark-Houwink parameters. In comparison to the expected theoretical values for M_η, the PMLG equation seems to provide more realistic data. There are no Mark-Houwink parameters

published for the different copolymers and Poly-γ-stearyl-L-glutamate (PSLG) itself in this solvent system. Therefore the other values of M_η were achieved by calculations according to equation (3.6).

$$M_\eta = \left[\left(\frac{M_{\eta,PMLG} * f_{PSLG}}{M_{R(PMLG)}} \right) * M_{R(PSLG)} \right] + f_{PMLG} * M_{\eta,PMLG} \qquad (3.6)$$

$M_{\eta,PMLG}$ = Viscosity average molecular weight of PMLG

$M_{R(PMLG)}$ = Molecular weight of the repeating unit of PMLG

$M_{R(PSLG)}$ = Molecular weight of the repeating unit of PSLG

f_{PSLG} = Molare fraction of the octadecylester unit in the polymer ($0 \leq f \leq 1$)

f_{PMLG} = Molare fraction of the methylester unit in the polymer ($0 \leq f \leq 1$)

Table 3.19: Characterization Data for polymers.

Polymer	Methyl [a]	Octadecyl [a]	M_n [b]	M_η [c]	M_η [d]	DP_{th} [e]
Copolymer	69,5	30,5	13000	13425 *	51746 *	60
Copolymer	82	18	11000	11572 *	44606 *	60
Copolymer	53	47	15000	15870 *	61170 *	60
Copolymer	90	10	10000	10387 *	40037 *	60
PSLG	0	100	23000	23726 *	91456 *	60
PMLG	100	0	8700	8905	34326	60

[a] Percentage of the monomer unit in the polymer [%]

[b] Number average molecular weight

[c] Viscosity average molecular weight according to equation 2

[d] Viscosity average molecular weight according to equation 1

[e] Degree of polymerization by the monomer-initiator ratio

* These values were achieved by calculations according to equation 3

PBLG (MD-1-2): [80]

The characterization in order to achieve an accurate way of measuring the exact molecular weight and to get some hints about the molecular weight distribution as well were examined to be extremely difficult due to the lack of solubility of most of the polypeptides which were synthesized in this work. An exception is PBLG which is therefore most often used in literature for all kind of studies belonging to poly(glutamates) because it shows a remarkable solubility in a lot of common organic solvents and offers therefore the highest potential for systematical studies. Most of the researchers did not do any kind of further studies with other poly(glutamates) which results in a real limited literature even if the field of polypeptides is involved generally since nearly 100 years.[81] All common techniques of polymer characterization were successfully employed to obtain reliable values for the molecular weight and the molecular weight distribution. These experiments were all performed in DMF because this system has shown the ability to break up the aggregation which takes place highly intense in other solvents due to hydrogen bonding. Viscosimetry was conducted successfully in DMF at 25 °C. GPC was attempted in DMF with little success. PBLG has an UV absorbance maximum at 258 nm belonging to the phenyl ring.[1] Dynamic and static light scattering (DLS and SLS) were done successfully in DMF to determine the M_w and the A_2 value which can be nicely correlated to the literature values found. The hindrance of aggregation could be solved for PBLG by stirring of the polymer solution for 24 h at 60°C. The success of this approach was determined by DLS which shows a bimodal distribution if aggregation occurred. Viscosimetry experiments were performed at 60°C with an Ubbelohde viscosimeter using seven different concentrations between 10 and 7 g/l. The data (not shown) were analyzed by the Huggins method and delivered an intrinsic viscosity [η] of 0.24052 dl/g.

Table 3.20: Solubility of PBLG.

Solvent	DMSO	DMF	DCM	Nitrobenzene	2-butanol	EtOH	Toluene
Result	+	+	+	+	-	-	-
Solvent	THF	MeOH	H_2O	$CHCl_3$	TFA	DCA	n-hexane
Result	0	-	-	+	+	+	-

DLS and SLS measurements, shown in Figures 3.22-3.25, have given the following values. dn/dc = 0.1143 ml/mg M_w=45000 g/mol $A_2=3.029*10^{-7}$ mol*dm^3/g^2

$<R_g^2>_z^{1/2}$ = 13.8 nm

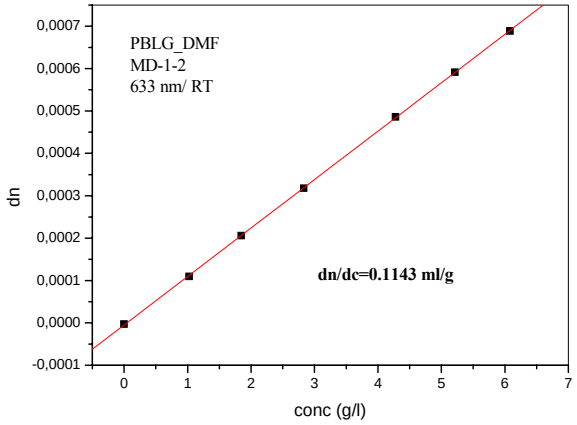

Figure 3.22: dn/dc determination for PBLG (MD-1-2) in DMF at RT.

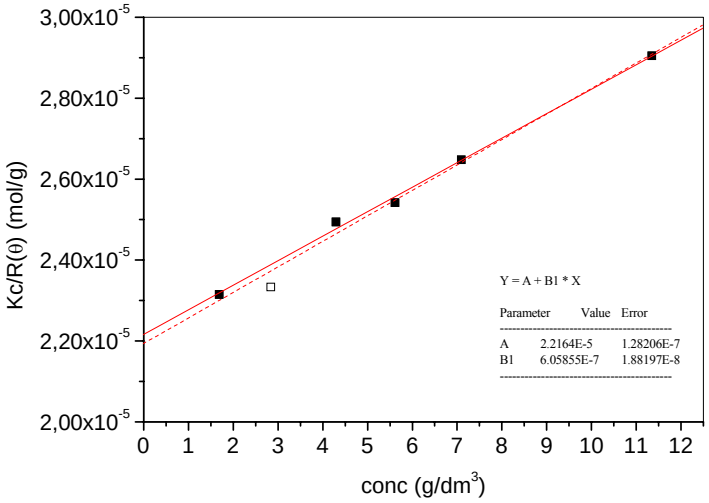

Figure 3.23: Zimm plot for PBLG (MD-1-2) in DMF at RT.

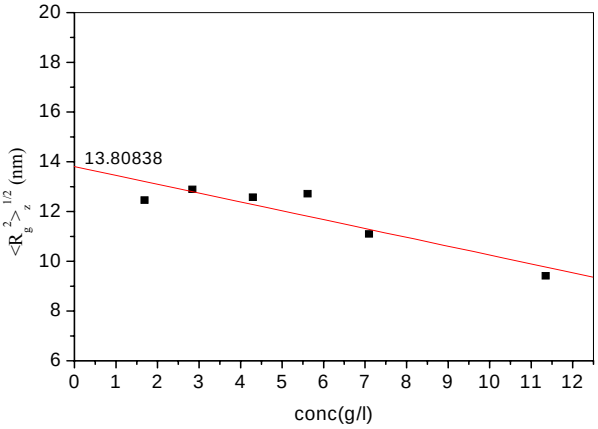

Figure 3.24: $<R_g^2>_z^{1/2}$ (radius of gyration) calculation for PBLG (MD-1-2) in DMF at RT.

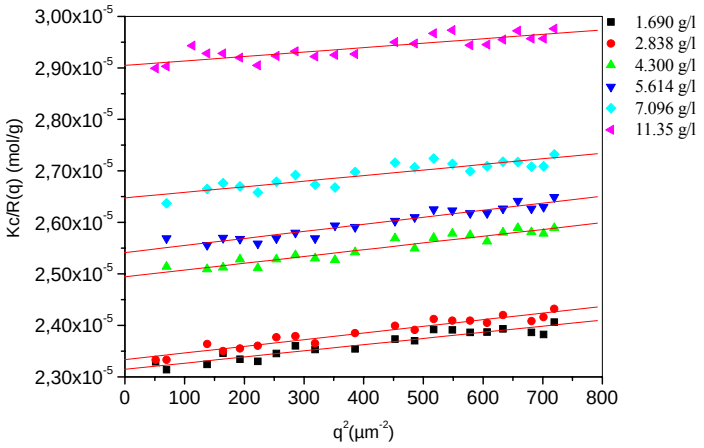

Figure 3.25: SLS for PBLG (MD-1-2) in DMF at RT.

PBLG (MD-1-45):

The characterization was conducted by viscosimetry using an Ubbelohde viscosimeter in DMF. The use of filtered DMF was detected to be inconvenient because of the relatively high deviation of the values of each concentration which should be ideally nearly constant. Therefore DMF was freshly distilled prior to use with the result of obtaining reliable, consistent, and constant values. A drying tube has to be placed on the top of the viscosimeter to avoid soaking up water from the atmosphere. Viscosimetry experiments were performed after 24 h at 60°C with an Ubbelohde viscosimeter using seven different concentrations between 10 and 4 g/l. The data (not shown) were analyzed by the Huggins method and delivered an intrinsic viscosity [η] of 0.55255 dl/g. DLS and SLS measurements (not shown) are similar to Figures 3.22-3.25 and have given the following values after stirring for 24 h at 60°C.

dn/dc=0.1089 ml/mg (633 nm), Mw=75400 g/mol, A_2=3.752*10^{-7} mol*dm^3/g^2

Additionally GPC could be successfully performed in DMF at 60°C with Gram columns 3000, 2000 and 1000. The UV and RI signal were normalized in Figure 3.26 and showed the same behavior. The following results could be achieved by GPC calibrated against PS.

Table 3.21: GPC results of PBLG (MD-1-45) in DMF at 60°C.

	M_w	M_n	D
UV	75416	51791	1.46
RI	74920	47615	1.57

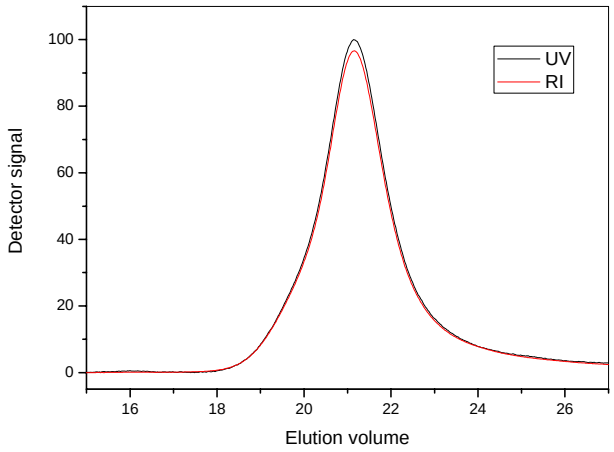

Figure 3.26: Elution volume of PBLG (MD-1-2) in GPC (DMF at 60°C).

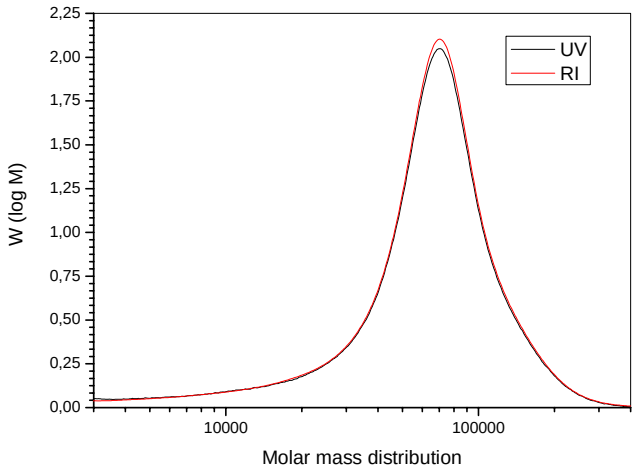

Figure 3.27: Molecular weight distribution of PBLG (MD-1-2) in GPC (DMF at 60°C).

PSBC (MD-1-61):

Poly(S-benzyl-L-cysteine) (MD-1-61) was purified by soxhlet extraction for 2 days in methanol because the NCA is nicely soluble in this solvent. A total loss of 11,7 % was observed by this procedure.

Table 3.22: Solubility of PSBC.

Solvent	DCA	NMP	$CHCl_3$/TFA	DMF	$CHCl_3$	MeOH	THF	TFA	TMU	DMA	Toluene	DMSO
Result	+	+	+	-	-	-	-	-	-	-	-	-

PSCBC (MD-1-50):

PSCBC (MD-1-50) was purified by soxhlet extraction for 2 days in methanol because the NCA is nicely soluble in this solvent. A loss of 18,8 % was observed by the purification procedure. The aggregation could not be broken up to allow a molecular weight characterization by light scattering. Dynamic light scattering was attempted to check for aggregation and the following systems were determined to be unsuitable. All salts (LiF, LiBr and LiCl) were dried in a vacuum oven at 130°C prior to use for 48 h.

Table 3.23: DLS results of the attempts to break up aggregation of PSCBC (MD-1-50).

System	Result
3 g/l (DMF)	**AGGREGATION**
3 g/l (DMF + 10 % HFIP)	
3 g/l (DMF + 5 % HFIP), USB at 50°C for 24h	
2.5 g/l (DMF + 10 folded excess of LiCl)	
1 g/l (DMF + 10 folded excess of LiCl), USB at 50°C for 24 h	
1 g/l (DMF + 10 folded excess of LiBr)	
1 g/l (DMF + 10 folded excess of LiBr), USB at 60°C for 24 h	
1 g/l (DMF + 10 folded excess of LiF)	
1 g/l (DMF + 30 folded excess of LiF)	

Table 3.24: Solubility of PSCBC.

Solvent	DMF	$CHCl_3$/TFA	NMP	DMSO	DCA	TMU	DMA	FA	AcOH	HCOOH
Result	**+**	**+**	**+**	**0**	**0**	**0**	**0**	**-**	**-**	**-**
Solvent	Et_2O	Dioxane	EtOAc	n-hexane	$CHCl_3$	MeOH	THF	TFA	Toluene	HFIP
Result	**-**	**-**	**-**	**-**	**-**	**-**	**-**	**-**	**-**	-

PMLG (MD-1-58):

Table 3.25: Solubility of PMLG (MD-1-58).

Solvent	HFIP	DMSO	DCA	Toluene	DMF	EtOAc	Dioxane	THF
Result	**+**	**+**	**+**	**-**	**-**	**-**	**-**	**-**
Solvent	ACN	Isopropanol	NMP	FA	HCOOH	AcOH	$CHCl_3$	DMA
Result	**-**	**-**	**-**	**-**	**-**	**-**	**-**	**-**

Table 3.26: DLS results of the attempts to break up aggregation of PSCBC (MD-1-50).

System	Result
1 g/l (DMSO)	**AGGREGATION**
5 g/l (HFIP)	
10 g/l (HFIP)	
5 g/l (HFIP + 10 folded excess of LiBr), USB at 60°C for 24 h	

Copolymers:

Table 3.27: Solubility of the different copolymers (Methyl-co-octadecyl-L-glutamate).

Solvent	THF	$CHCl_3$/FA	$CHCl_3$	Toluene	DMF	DMSO	DCA	TFA
Result	**-**	**-**	**-**	**-**	**-**	**-**	**+**	**+**

PSLG (MD-1-24):

GPC in THF was unsuccessful and DLS has shown in THF and $CHCl_3$ a strong aggregation behavior.

XRD pattern (powder):

The XRD powder patterns of the synthesized polymers are listed in the next Figures 3.28-3.30 to demonstrate that they all possess an amorphous character with the exception of PSLG which has order based on the side chain crystallization of the long aliphatic octadecyl chain.

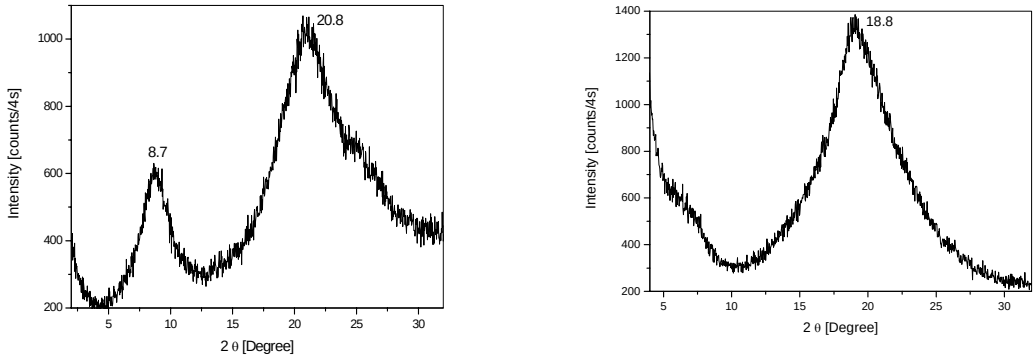

Figure 3.28: XRD of MD-1-28 (left) and MD-1-32 (right) as powder; 0.03 step scan with 4s.

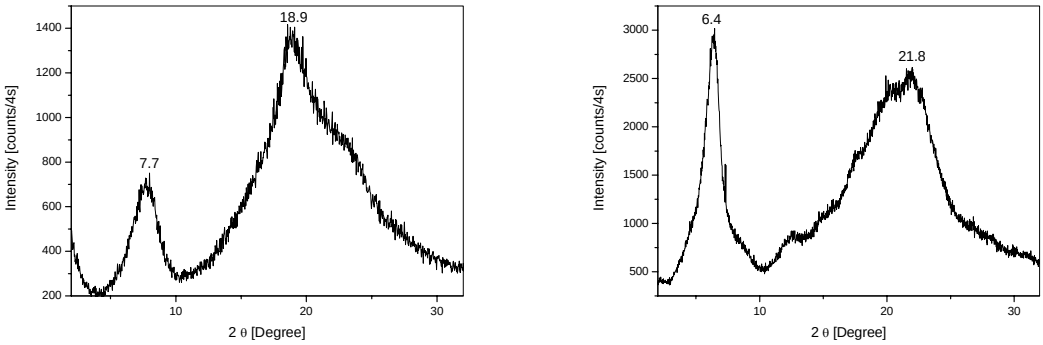

Figure 3.29: XRD of PMLG (left) and PBLG (right) as powder; 0.03 step scan with 4s.

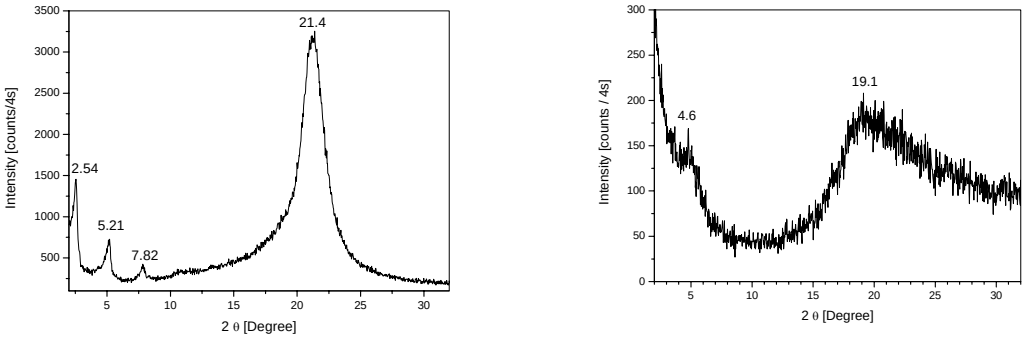

Figure 3.30: XRD of PSLG (left) and PSCBC (right) as powder; 0.03 step scan with 4s.

Thermal gravimetric analysis (TGA):

Each polymer was analyzed by thermal gravimetric analysis (TGA). Table 3.28 summarizes the determined degradation temperatures, where a significant mass loss occurred by annealing the sample in a small aluminum pan. The mass percentage at the onset of the degradation is given to control if there was any residual solvent or other high volatile impurity in the sample present.

Sample Name **Sample Synonym**	**Onset of Degradation** **T_d [°C]**	**Mass at the onset of degradation** **[%]**
PSCBC *MD-1-50*	200	94
PSCBC *MD-1-46*	200	96
PBLG *MD-1-45*	280	98
PBLG *MD-1-2*	280	98
PSBC *MD-1-61*	250	96
PMLG *MD-1-31*	280	100
PMLG *MD-1-30*	260	96
PSLG *MD-1-24*	240	96
PSLG-PMLG 30.5 / 69.5 % (w/w) *MD-1-32*	280	98
PSLG-PMLG 18 / 82 % (w/w) *MD-1-33*	280	98
PSLG-PMLG 47 / 53 % (w/w) *MD-1-34*	280	97
PBLG-PLGA 70 / 30 % (w/w) *MD-1-26*	240	95

PBLG-PLGA 45 / 55 % (w/w) *MD-1-27*	230	90
PBLG-PLGA 20 / 80 % (w/w) *MD-1-28*	225	91

Table 3.28: Thermal degradation temperatures determined by TGA (Heating rate: 10 K/min, N_2, 25-900°C).

All TGA curves showed high percentages between 94 and 100 %. If the different copolymers of PBLG and PLGA are compared with the homopolymers there are remarkable changes observable. The percentages and the degradation temperatures were decreasing dependent on the extent of the saponification. The decrease is enhancing from MD-1-26 to MD-1-27 and MD-1-28. The higher the PLGA fraction became the more water was attracted to the side chain due to the hygroscopic character of the acid. The different degradation temperatures in general depended on the different stabilities of the side chain protective groups.

In conclusion, the different polypeptides could be successfully synthesized following the "Amine mechanism" for low molecular weight polymers with a maximum DP of 100. The polymers were characterized by NMR, XRD, solid state NMR, TGA, DSC, IR and mass spectrometry with special focusing on the MALDI-TOF technique.

References:

[1] H.R. Kricheldorf, *α-Aminoacid-N-carboxy-anhydrides and related heterocycles. Syntheses, Properties, Peptide Synthesis, Polymerization*, Chap. 2, Springer, **1987**

[2] C. H. Bamford, A. Elliott, W. E. Hanby, *Synthetic Polypeptides,* **1956**, Chap. 2

[3] T. J. Deming, *Polym. Prep.,* **1996**, *37*, 435-436

[4] T. J. Deming, *J. Polym.Sci. Polym. Chem.,* **2000**, *38*, 3012-3018

[5] T. J. Deming, *Adv. Mater.,* **1997**, *9(4)*, 299-311

[6] T. J. Deming, *Adv. Drug Delivery Rev.,* **2002**, *54*, 1145-1155

[7] K. D. Kopple, J. J. Katz., *J. Am. Chem. Soc.,* **1956**, *78*, 6199-6205

[8] H. Block, *Poly (gamma-benzyl-L-glutamate) and other glutamic acid containing polymers, Vol. 9*, Gordon and Breach, **1983**.

[9] W. H. Daly, D. Poche, *Polym. Prep.,* **1989**, *30*, 107-108

[10] J. C. Smith, R. W. Woody, *Biopolymers,* **1973**, *12*, 2657-2665

[11] O. Tanaka, K. Hanabusa, *Polym. J.,* **1988**, *20*, 861-868

[12] E. Iizuka, K. Hanabusa, *J. Polym. Sci. Polym. Lett. Ed.,* **1984**, *22*, 559-564

[13] Y. Imanishi, *Pure Appl. Chem.,* **1981**, *53*, 715-727

[14] H. Sekiguchi, *Pure Appl. Chem.,* **1981**, *53*, 1689-1714

[15] M. Goodman, E. Peggion, *Pure Appl. Chem.,* **1981**, *53*, 699-714

[16] S. Sasaki, T. Nakamura, I. Uematsu, *J. Polym. Sci. Polym. Phys.,* **1979**, *17*, 825

[17] S. Sugai, K. Kamashima, J. Noguchi, *J. Polym. Sci.,* **1966**, *4*, 183-198

[18] A. Abe, T. Yamazaki, *Macromolecules,* **1989**, *22*, 2138-2145

[19] T. Nakahara, K. Motomura, *Bull. Chem. Soc. Jpn.,* **1967**, *40*, 495-497

[20] W. R. Krigbaum, H. Hakemi, R. Kotek, *Macromolecules,* **1985**, *18*, 965-973

[21] H. Ringsdorf, P. Tschirner, *Makromol. Chem.,* **1987**, *188*, 1431-1445

[22] I. Uematsu, Y. Uematsu, *Adv. Polym. Sci.,* **1984**, *59*, 37-74

[23] S. G. Waley, J. Watson, *Proc. R. Soc. London Ser. A,* **1949**, *199*, 499

[24] H. R. Kricheldorf, *Angew. Chem. Int. Ed.,* **2006**, *45*, 5752-5784

[25] P. G. Magagnini, F. Andruzzi, G. Benetti, *Macromolecules,* **1980**, *13*, 12-15

[26] F. Wessely, *Z. Physiol. Chem.,* **1925**, *146*, 72

[27] W. D. Fuller, M. S. Velander, M. Goodman, *Biopolymers,* **1976**, *15*, 1869-1871

[28] J. M. Catala, R. W. Lenz, *Eur. Polym. J.,* **1983**, *19*, 1043-1046

[29] Q. F. Zhou, R. W. Lenz, *J. Polym. Sci. Polym. Chem. Ed.,* **1983**, *21*, 3313-3320

[30] R. W. Lenz, *Polym. J.,* **1985**, *17*, 105-115

[31] V. E. Eskin, *Macromolecules,* **1991**, *24*, 3319-3323

[32] M. Idelson, E. R. Blout, *J. Am. Chem. Soc.,* **1958**, *80*, 2387

[33] H. J. Harwood, *Ring-Opening Polymerization, ACS Symp.,* **1985**, *286*, Chap. 5

[34] R. H. Karlson, E. R. Blout, *J. Am. Chem. Soc.,* **1956**, *78*, 941-946

[35] M. Hashimoto, J. Arimoto, *Bull. Chem. Soc. Jpn.,* **1966**, *39*, 2707-2713

[36] C. H. Bamford, H. Block, *Polyamino Acids, Polypeptides and Proteins,* **1969**

[37] W. H. Daly, D. Poche, Negulescu, II, *Progress in Polymer Science* **1994**, *19*, 79

[38] D. S. Poche, M. J. Moore, J. L. Bowles, *Synthetic Communications* **1999**, *29*, 843

[39] W. H. Daly, D. Poche, *Tetrahedron Letters* **1988**, *29*, 5859.

[40] D. S. Poche, W. H. Daly, P. S. Russo, *Macromolecules* **1995**, *28*, 6745.

[41] W. H. Daly, D. S. Poche, P. S. Russo, Negulescu, II, *Journal of Macromol. Sci.-Pure and Appl. Chem.,* **1994**, *A31*, 795.

[42] E. R. Blout, R. H. Karlson, P. Doty, B. Hargitay, *J. Am. Chem. Soc.,* **1954**, *76*, 4492.

[43] P. Doty, R. D. Lundberg, *J. Am. Chem. Soc.,* **1957**, *79*, 2338.

[44] A. Berger, J. Noguchi, E. Katchalski, *J. Am. Chem. Soc.,* **1956**, *78*, 4483.

[45] M. Frankel, D. Gertner, *J. of the Chem. Soc.,* **1961**, 463.

[46] A. Berger, J. Kurtz, E. Katchalski, *J. Am. Chem. Soc.* **1957**, *76*, 5552

[47] D. Ben-Ishai, E. Katchalski, *J. Org. Chem.* **1951**, *16*, 1025

[48] E. Katchalski, M. Sela, *Adv. Protein Chem.* **1957**, *13*, 264

[49] D. Kapoor, N. K. Misra, P. Tandon, V. D. Gupta, *J. Polym. Sci. Part B Polym. Phys.*, **1999**, *37*, 3269

[50] H. Maeda, T. Inoue, M. Tsunoda, S. Ikeda, *Bull. Chem. Soc. Jpn.*, **1973**, 46, 2708

[51] E. R. Blout, C. D. Lozé, S. M. Bloom, G. D. Fasman, *J. Am. Chem. Soc.*, **1960**, *82*, 3787

[52] R. D. B. Fraser, B. S. Harrap, T. P. Mc Rae, F. H. C. Stewart, E. Suzuki, *J. mol. Biol.*, **1965**, *14*, 423

[53] M. Tsukahara, T. Yammanobe, T. Komoto, J. Watanabe, I. Ando, I. Uematsu, *J. Mol. Struct.*, **1987**, *159*, 345

[54] E. Katoh, H. Kurosu, S. Kuroki, I. Ando, *J. Mol. Struct.*, **1994**, *326*, 145

[55] T. Yamanobe, M. Tsukahara, T. Komoto, J. Watanabe, I. Ando, I. Uematsu, K. Deguchi, T. Fujito, M. Imanari, *Macromolecules*, **1988**, *21*, 48

[56] M. Yamaguchi, A. Tsutsumi, *Polymer J.*, **1990**, *22*, 781

[57] F.Hillenkamp, M. Karas, R.C. Beavis, B.T. Chait., *Anal. Chem.*, **1991**, *63*, 1193

[58] M. Karas et al., *Anal. Chem.*, **1985**, *57*, 2935

[59] M. Tanaka et al., *Rapid Commun. Mass Spectrom.*, **1988**, *2*, 151-153

[60] H.R. Kricheldorf, C. Lossow, G. Schwarz, *Macromolecules*, **2005**, *38*, 5513-5518

[61] H.R. Kricheldorf, C. Lossow, G. Schwarz, *J. Polym. Sci. Polym. Chem.*, **2006**, *46*, 4680-4695

[62] H.R. Kricheldorf, C. Lossow, G. Schwarz, *Macromol. Chem. Phys.*, **2005**, *206*, 282-290

[63] H.R. Kricheldorf, C. Lossow, G. Schwarz, *Macromol. Chem. Phys.*, **2004**, *205*, 918-924

[64] G. Montaudo, M.S. Montaudo, C. Puglisi, F. Samperi, *J. Polym. Sci. Polym. Chem.*, **1996**, *A34*, 439

[65] H. Pasch, W. Schrepp, *MALDI-TOF mass spectrometry of synthetic polymers*, **2003**, 138

[66] H. R. Kricheldorf, *α-Aminoacid-N-carboxy-anhydrides and related heterocycles. Syntheses, Properties, Peptide Synthesis, Polymerization*, Chap. 1 and 2, Springer, **1987**

[67] D. D. Van Slyke, *J. Biol. Chem.*, **1929**, *83*, 425

[68] M. Sela, A. Berger, *J. Am. Chem. Soc.*, **1955**, *71*, 1893

[69] M. Sela, A. Berger, E. Katchalski, *Analyt. Chem.*, **1953**, *25*, 1554

[70] C. H. Bamford, A. Elliot, W. E. Hanby, *Synthetic Polypeptides*, **1956**, 295

[71] R. D. Lundberg, P. Doty, *J. Am. Chem. Soc.*, **1957**, *79*, 3961

[72] A. Shoji, T. Kawai, A. Nishioba, *Macromolecules*, **1977**, *10*, 1292

[73] H. R. Kricheldorf, K. Bösinger, *Makromol. Chem.*, **1976**, *177*, 1243

[74] H. R. Kricheldorf, D. Müller, *Makromol. Chem.*, **1983**, *184*, 1407

[75] H. R. Kricheldorf, D. Müller, H. Förster, *Biopolymers*, **1983**, *22*, 1357

[76] R. Heyns, W. Walter, H. F. Grützmacher, *Liebigs Ann. Chem.*, **1957**, *609*, 209

[77] F. Eirich, E. Katchalski, *Adv. Protein Chem.*, **1951**, *6*, 166

[78] P. Doty, J. H. Bradbury, A. M. Holtzer, *J. Am. Chem. Soc.,* **1956**, *78*, 947

[79] S. Tanaka, N. Akio, *Bull. Inst. Chem. Res. Kyoto Univ.,* **1976**, *54*, 229

[80] J. Watanabe, I. Uematsu, Polymer, 1984, 25, 1711

[81] P. Doty, J. H. Bradbury, A. M. Holtzer, *J. Am. Chem. Soc.*, 1956, 78, 947

Chapter 4
Poly (L-glutamic acid)

4.1 Introduction

The synthesis of poly(L-glutamic acid) (PLGA) has been achieved by different approaches. The synthesis of the NCA of L-glutamic acid was attempted by direct phosgenation of L-glutamic acid or indirectly by saponification of γ-benzyl-L-glutamate NCA. The polymerizations of the previously mentioned NCAs with various initiators like pyridine, triethylamine, benzylamine and sodium methoxide gave low yields of PLGA (<20%) with pyroglutamic acid as a major side product.[1] As a second approach, the saponification of the more readily available poly(glutamates) was attempted to obtain the free acid. Hanby and coworkers reported for the first time the hydrolysis of poly-γ-methyl-L-glutamate (PMLG) under alkaline conditions with ethanolic KOH followed by aqueous KOH. Extensive racemization combined with an incomplete saponification leaded to copolymers.[2,3] These observations were confirmed by the group of Bruckner.[4,5] They attempted to suppress the known tendency of peptides and proteins to rapidly racemize under alkaline hydrolysis conditions by the use of freshly prepared copper (II) hydroxide.[6] Green and Stahmann succeeded in hydrolyzing the corresponding ethyl ester (PELG) in higher conversions without a notable degree of racemization.[7] However, commercially produced PLGA is still generally prepared by the alkaline hydrolysis of PMLG and is supplied as the sodium salt and stated to be the L-isomer even if the question of the extent of racemization could not yet been clarified.

The lack of retention of the optical configuration during the alkaline hydrolysis of poly(glutamates) made the investigation of better other procedures necessary. Hanby and coworkers showed and analyzed the ineffectivity of a catalytic hydrogenation of PBLG with Pd/C due to the steric hindrance of such a heterogeneously catalyzed reaction on a polymer substrate. Sodium in liquid ammonia was effective in removing the benzyl groups from PBLG but included again considerable racemization.[3]

Phosphonium iodide in glacial acetic acid was used for the preparation of poly (aspartic acid),[8] poly-L-lysine hydroiodide,[9] and PLGA.[3,10,11] However, Blout and coworkers could not confirm and reproduce the results of the Hanby group[3] by using the iodide approach.[10,11] The Berger group studied the mechanism of the reaction and claimed that the reaction represented a non-hydrolytic alkyl oxygen ester cleavage, brought about by hydrogen iodide instead of a reduction process. The hydrogen iodide resulted from the reaction of phosphonium iodide and residual water from glacial acetic acid, but the

dangerous handling and preparing of phosphonium iodide limited its applicability for larger scale reactions. [12]

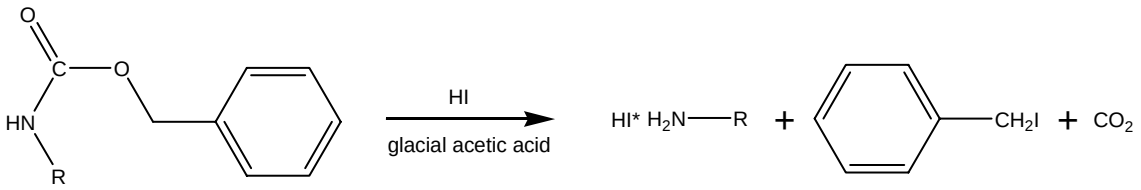

Figure 4.1: Non-hydrolytic cleavage of carbobenzyloxy groups from nitrogen atom containing peptide side chains by hydrogen iodide.[9,12]

Katchalski and coworkers first reported the saponification to PLGA under acidic conditions.[13] They prepared high molecular weight PLGA from PBLG at ambient temperature without significant cleavage of peptide bonds. Hydrogen bromide (HBr) was used to affect complete debenzylation of PBLG to PLGA in several solvents under anhydrous conditions, like benzene, liquid sulfur dioxide, nitromethane and TFA. Under these conditions racemization was found to be minimal. A detailed study of these different debenzylation methods was published by Idelson and Blout.[14] The suitability of the solvents depended on two properties: 1) the solvent must be a good solvent for PBLG 2) the solvent should not react with HBr. Nitromethane, once commonly used for saponifications of PBLG, was found to react with HBr to bromine and methyl ammonium bromide. Glacial acetic acid with HBr, in which high molecular weight PBLG is not soluble and lower molecular weight PBLG shows extensive peptide bond cleavage, was also found to be unsuitable. The saponification proceeds normally to completion within a few hours. The resulting PLGA, with nearly complete conversion, was shown to be free of benzyl ester groups by measurements of their ultraviolet absorption spectrum in the region in which benzyl groups absorb (230-270 nm).[15]

4.2 Synthesis

The saponification procedure chosen in this work is shown in Figure 4.2 and pointed out in the further discussion.

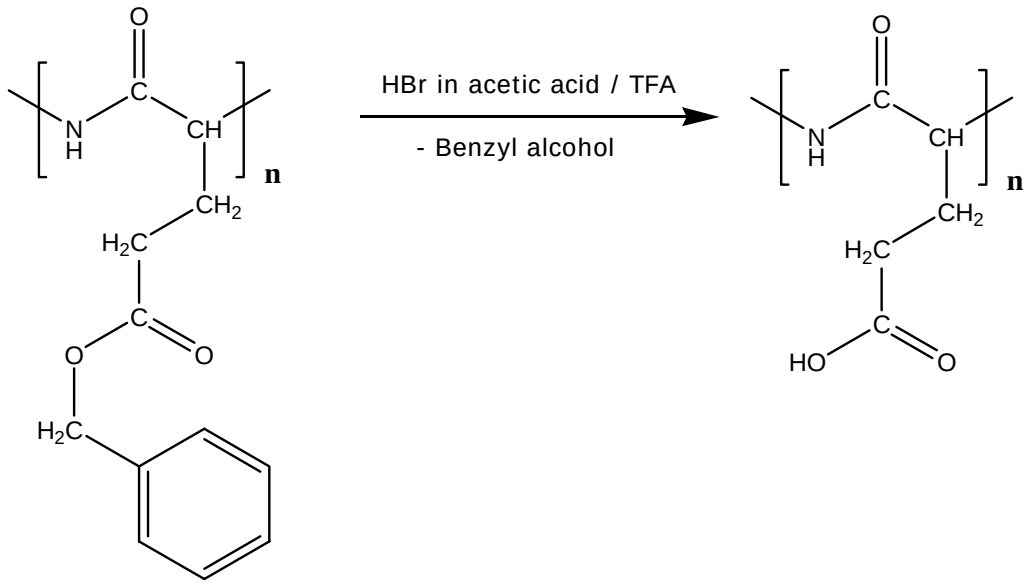

Figure 4.2: Saponification reaction of PBLG to PLGA.[13]

PBLG (10 g) (MD-1-45) was dissolved in 250 ml of TFA under argon. It was stirred at room temperature until the polymer dissolved completely. A four fold molar excess of 5.7 M HBr solution in acetic acid was then added to the reaction solution. After one hour the reaction was quenched with the addition of 200 ml of diethylether. The suspension stirred for one hour to ensure complete precipitation and was filtered and washed excessively by diethylether. The product obtained had a tan tint, which indicated residual HBr. The polymer was purified by soxhlet extraction with acetone for 2 days. Afterwards the polymer was dried in vacuo for 7 hours to remove diethylether. 6.2 g of pure white powder (PLGA, MD-1-48) was obtained after the purification corresponding to near quantitative conversion.

^{1}H-NMR (alkaline D_2O) [ppm]: 3.81 (α-CH), 1.75 (γ-CH_2), 1.55 and 1.44 (β-CH_2)

^{13}C-NMR (alkaline D_2O) [ppm]: 181.60 (C=O, side chain), 173.85 (C=O, backbone), 54.09 (α-CH), 33.58 (γ-CH_2), 28.19 (β-CH_2)

4.3 Characterization

The saponification kinetics for the conversion of PBLG to PLGA has not been previously reported. PBLG (MD-1-2) was used in all experiments as the starting material. The general procedure took one hour to obtain complete conversion from the ester to the free acid group.[13] The aim of these kinetic studies was to investigate if the conversion follows an exponential or a linear relation between reaction time and conversion. The saponification progress was monitored by ^{1}H-NMR spectroscopy and the conversion was calculated by integrating the CH_2 signal of the benzyl group versus the CH signal of the polypeptide backbone. The highest possible ratio two represents no conversion (pure PBLG) and decreases theoretically, depending on the reaction time, to zero, for complete conversion (pure PLGA).

General saponification procedure:

0.2 g PBLG (MD-1-2, DP =80) was dissolved at room temperature in 2 ml of TFA. 0.64 ml 5.7 M HBr in acetic acid was then added as reagent under argon. The reaction was quenched after certain time intervals by precipitating the polymer through the addition of 10 ml of diethylether. The solution was allowed to stir for 3 h at room temperature to ensure complete precipitation. The NMR spectra were recorded for all samples in deuterated DMF. The decreased solubility of the obtained copolymers (partially saponificated PBLGs) in DMF was a confirmation of the successful progress of the reaction. PBLG can be easily dissolved in DMF without heating in contrast to PLGA which exhibit lower solubility. Figure 4.3 and Table 4.1 show that the conversion is nearly complete after 36 minutes when the ester percentage has decreased to 9%. Therefore the one hour period, which is generally taken, should be sufficient to ensure a nearly quantitative conversion of PBLG to poly (glutamic acid) and the linear time dependence can be taken into account as valid.

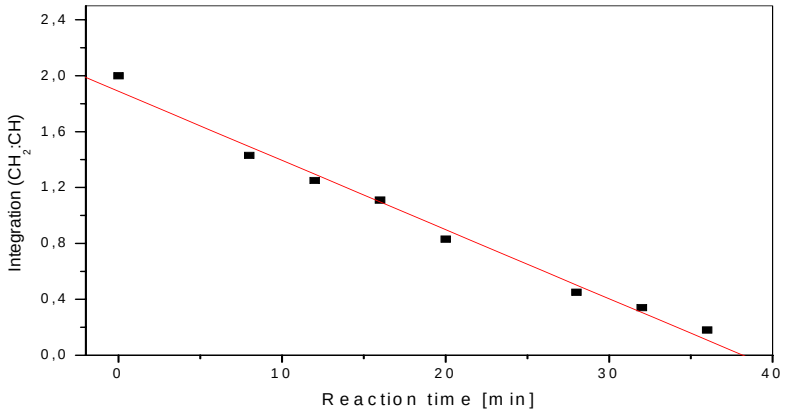

Figure 4.3: Saponification series from PBLG (MD-1-2) to PLGA.

Table 4.1: Saponification series of PBLG to PLGA.

Integration ratio (CH_2:CH)	Reaction time [min]	Ester percentage [%]
2.00	0	100.00
1.43	8	71.43
1.25	12	62.50
1.11	16	55.56
0.83	20	41.67
0.45	28	22.73
0.34	32	17.24
0.18	36	8.77

Purification:

Several attempts were made to identify a better method to purify the synthesized PLGA. Soxhlet extraction proved to be a very useful purification tool due to the limited solubility of PLGA. Table 4.2 clearly shows that strong hydrogen bond disrupting solvents are required to dissolve PLGA.

Table 4.2: Solubility of PLGA.

Solvent	DMF	Pyridine/H_2O	DMSO	DMA	TMU	NMP	TFA	EtOH	MeOH
Result	+	+	+	+	+	+	+	-	-
Solvent	H_2O	Pyridine	DCA	EtOAc	THF	HCOOH	HFIP	$CHCl_3$	Toluene
Result	-	-	-	-	-	-	-	-	-

The light yellow powder was successfully purified by extracting with acetone after 3 days to give a fine white powder. The brown soxhlet residue was analyzed, after evaporation of acetone, by NMR spectroscopy. The NMR spectra in alkaline D_2O confirmed that a large portion of oligomers were washed out, which is clearly observable by comparing the crude PLGA (PP10), the purified PLGA (PP10) and the soxhlet fraction. The different NMR spectra are shown in Figures 4.4-4.6 where the signals of the initiator are significantly decreasing by the purification. Capillary electrophoresis confirmed this observation by showing a large decrease of the number of oligomeric signals, which is shown in the following chapter 4.4. The yield of the purification was approximately 70 % for all batches.

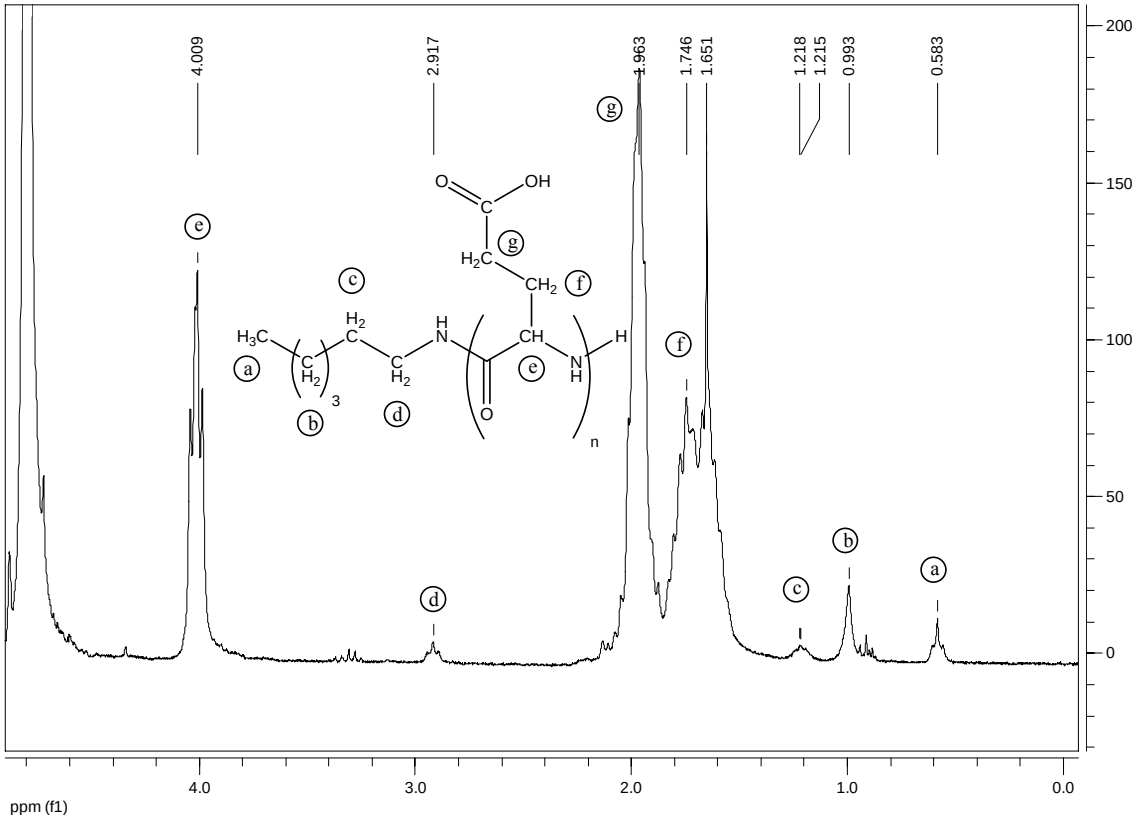

Figure 4.4: NMR (in alkaline D_2O) of crude PLGA (PP10).

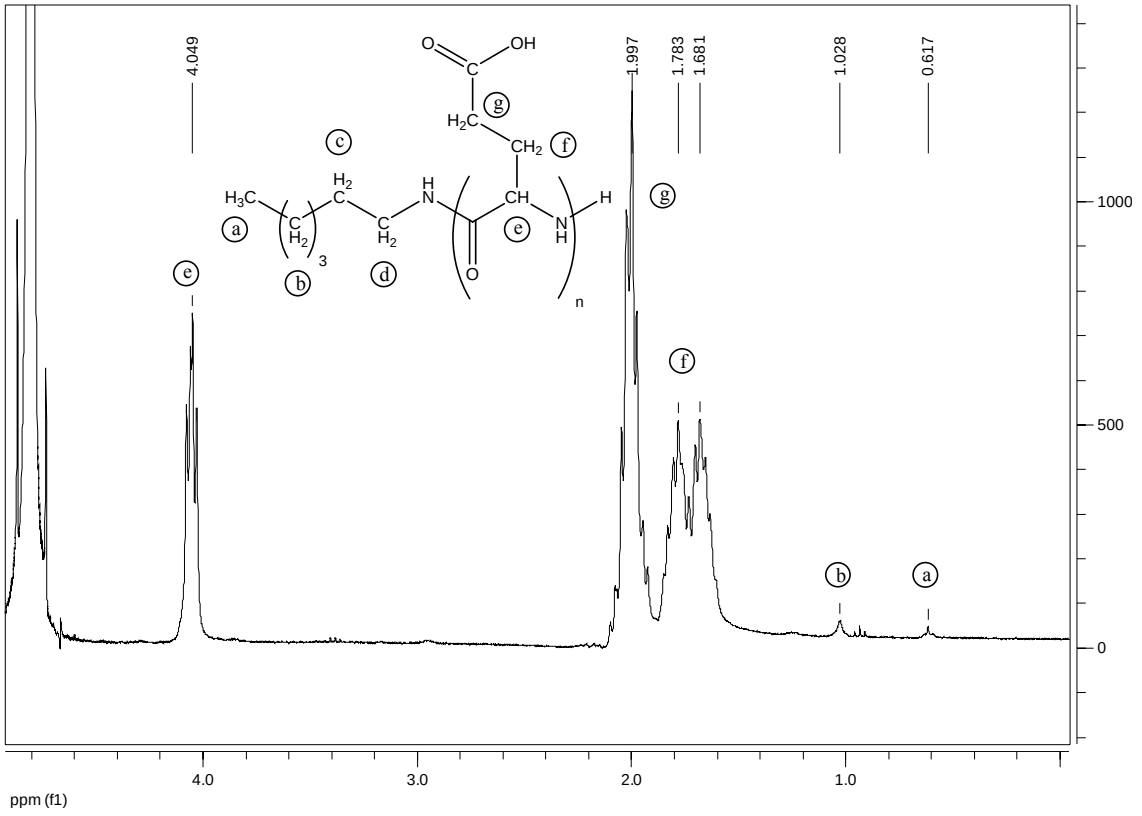

Figure 4.5: NMR (in alkaline D_2O) of purified PLGA (PP10).

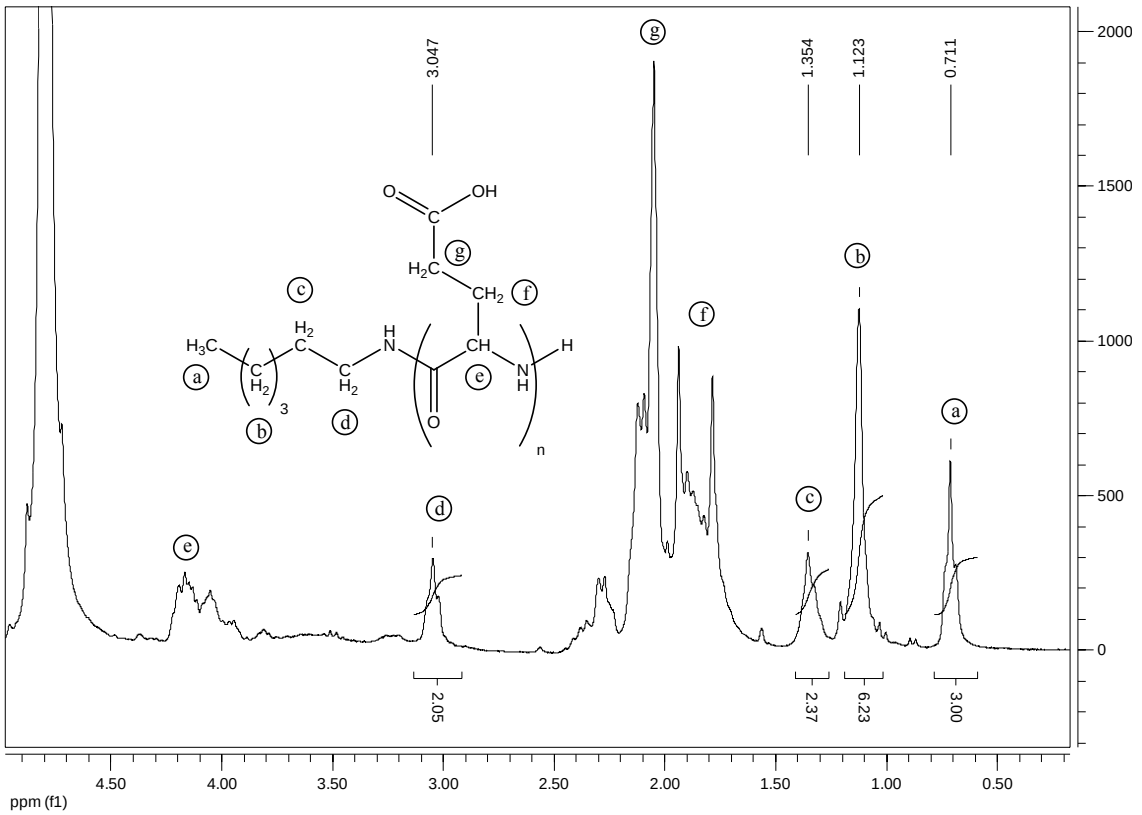

Figure 4.6: NMR (in alkaline D_2O) of the soxhlet residue of PLGA (PP10).

Elemental analysis:

PLGA (MD-1-48) was further analyzed by elemental analysis by "Analytische Laboratorien, Prof. Dr. H. Malissa und G. Reuter GmbH" and compared to the theoretical percentages of the elements.

Table 4.3: Elemental analysis of PLGA.

Elements	Theoretical [%]	Experimental [%]	Deviation [%]
C	46.51	46.31	0.4
H	5.43	5.89	7.8
N	10.85	9.83	9.4
O	37.21	37.96	2.0

None of the possible cyclization reactions, which are discussed in the MALDI section of this chapter, would explain a change of the nitrogen percentage.

Raman spectroscopy:

The observed experimental Raman bands for different PLGA samples are listed in Table 4.4. All samples were measured as powders and the assignment of the secondary structures was based on the literature values given in chapter 1.3.3. The secondary structure was indicated as β-sheet.

Table 4.4: Observed experimental Raman frequencies (cm^{-1}) of Amide I and II bands.

Polypeptide	Conformation	Amide I	Amide III
PLGA, PP8 pur.	β-pleated sheet	1670 (s)	1235 (s)
PLGA, PP9	β-pleated sheet	1671 (s)	1234 (s)

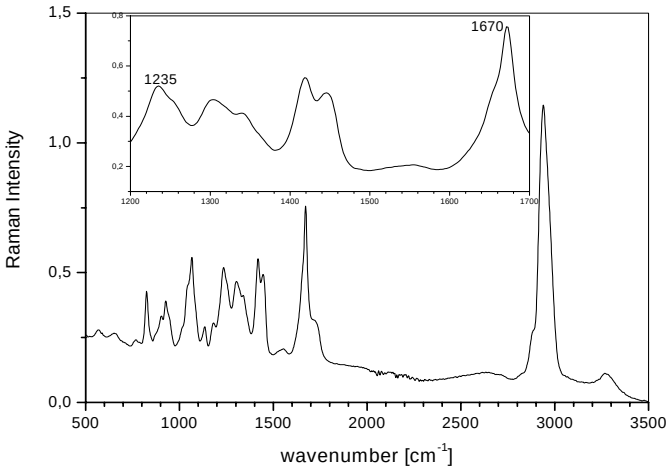

Figure 4.7: FTIR Raman spectrum of PLGA (PP8).

XRD powder pattern: The purification by soxhlet did not change the XRD pattern at all.

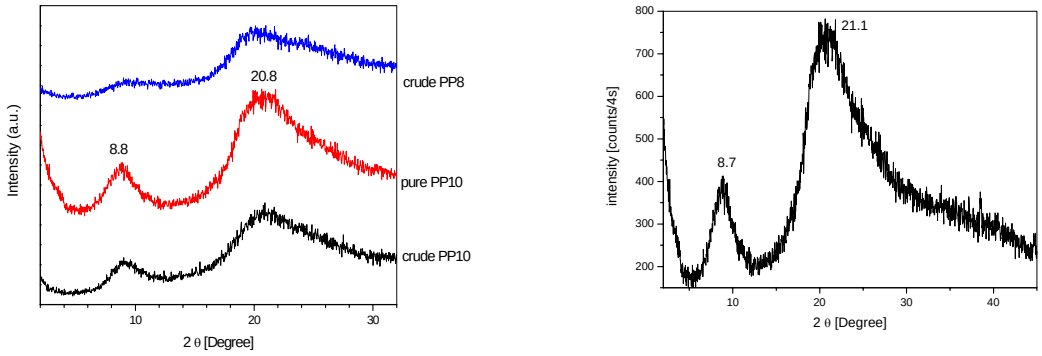

Figure 4.8: XRD of PLGA purified compared with crude PLGA powder (left) and PLGA [PP10 purified] powder (right); 0.03 step scan with 4s.

MALDI-TOF spectroscopy:

The MALDI-TOF spectra of PLGA, shown in Figure 4.9 and 4.10, were measured successfully for the first time. The analysis of the signals is given in Tables 4.5 and 4.6. The mass of the repeat unit is 129 g/mol. All the measurements were recorded in the reflectance mode, which was provided higher resolution than the linear mode. Solid samples with DCTB and TCNQ as matrix were attempted as well, but the analysis did not provide any reliable data. Compared to the MALDI-TOF spectrum in TFA, the spectrum in DMF exhibits fewer cyclizations inside of the polymeric side chains even if both ends of the polymer chain are still cyclized by "backbiting". The increased number of cyclized units in the TFA system depends strongly on the high acidity of this solvent. The use of TFA during the sample preparation for the MALDI-TOF measurement may induce side chain cyclization.

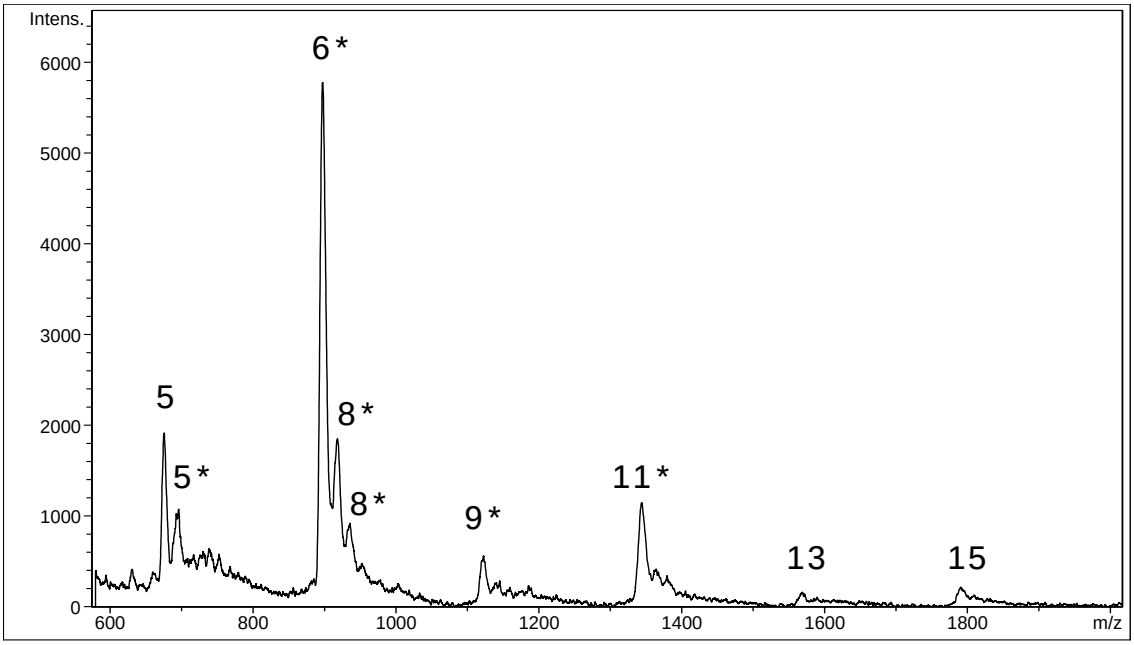

Figure 4.9: MALDI-TOF mass spectrum of poly (L-glutamic acid) sodium salt (MD-1-48) measured in TFA with dithranol as matrix and potassium trifluoroacetate as dopant.

Table 4.5: Masses (Da) of K^+-doped oligomeric PLGA sodium salt measured in TFA with dithranol as matrix and potassium trifluoroacetate as a dopant.

DP	5	5*	6*	8*	8*	9*	11*	13	15
C	4	4		5	4	1	3	6	8
B	no	no	no	yes	yes	yes	yes	yes	yes
Mass	675	696	897	918	936	1122	1344	1569	1791

*: These masses were achieved by Na^+ additive.

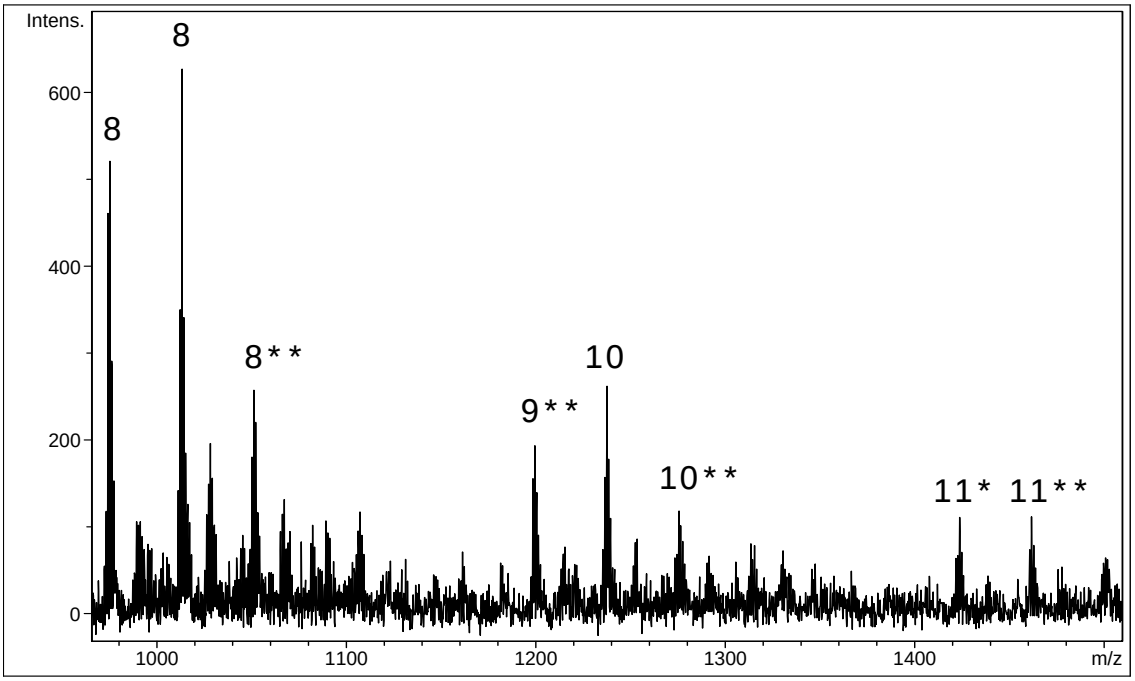

Figure 4.10: MALDI-TOF mass spectrum of poly (L-glutamic acid) (MD-1-48) measured in DMF with dithranol as matrix and potassium trifluoroacetate as dopant.

Table 4.6: Masses (Da) of K^+-doped oligomeric PLGA measured in DMF with dithranol as matrix and potassium trifluoroacetate as dopant in DMF.

DP	8	8	8**	9**	10	10**	11*	11**
C	3	1	1		3	3	1	
B	yes	yes	yes	yes	yes	yes	yes	yes
Mass	975	1013	1051	1199	1238	1276	1424	1462

**: These masses were achieved by K^+ additive

<u>Sodium salt dialysis and molecular weight characterization:</u>

The sodium salt of PLGA was obtained by the following procedure.

PLGA (533 mg, MD-1-48) was dissolved in 0.1 M NaOH to form the sodium salt. The excess sodium ions were removed by dialysis against distilled water with a dialysis membrane cutoff of 500 M_w. The deionized water was changed daily and the sodium ion removal was meanwhile monitored by conductivity measurements. The dialysis was finished after 5 days and yielded 460 mg of the sodium salt of PLGA. The attempted analysis of the PLGA sodium salt by GPC (suprema max column, 25°C, 0.1 M $NaNO_3$ as eluent) did not succeed because the sample did not elute from the column. Another GPC experiment (TSK columns, 60°C, 0.1 M $NaNO_3$ as eluent) was successful; giving the following results: M_n= 9 000 g/mol, M_w= 28 000 g/mol, PDI= 3.15 (calculated against PEO).

Molecular weight determination of the free acid PLGA:

It was attempted by light scattering in DMF, as was done with PBLG. The dn/dc determination for PLGA (PP6) was accomplished and plot was linear, but it was not possible to continue with DLS and SLS because the obtained value of 0.0606 ml/g was well below the detection limits. Removal of the benzyl groups reduced the contrast between the solvent and the polymer. GPC of PLGA (PP6 and MD-1-48) in DMF was attempted, but initially the polymer remained adsorbed on the TSK column, while utilizing an eluent mixture of 80% (v/v) 0.1 M $NaNO_3$ and 20% (v/v) ACN. The polymer also kept adsorbed on a GRAM column with a 0.1 M $NaNO_3$ eluent system. Finally, a TSK column with a 0.1 M $NaNO_3$ eluent system at 25°C, allowed for the successful analysis giving M_n=34 000, M_w= 50 000, and PDI=1.5 (calculated against PEO).

Thermal analysis and endotherm discussion:

The TGA trace exhibited a substantial weight loss step at 230°C, which is clearly assigned to the onset of the thermal decomposition of the sample. The first 8 % of mass loss corresponds to water due to not shown TGA-MS measurements. It was found to be very difficult to remove water from the polymer due to its high hygroscopicity. This could explain the analytical results of the elemental analysis, where the hydrogen and oxygen content is increased whereby the carbon and nitrogen content is decreased.

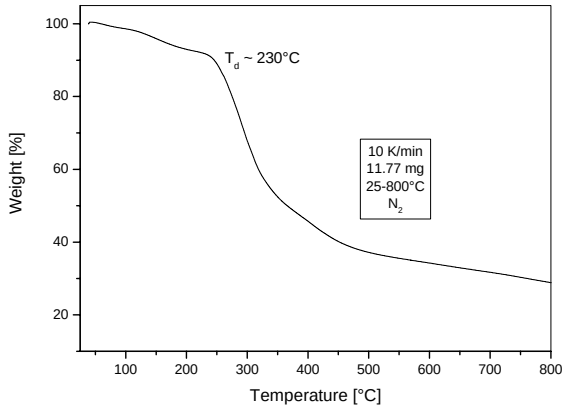

Figure 4.11: TGA analysis of PLGA (MD-1-48).

Figure 4.12 shows the DSC trace of PLGA powder (PP10) and Figure 4.13 shows the DSC trace of a PLGA film (PP8, drop-cast from a 10% (w/w) DMA solution on silica). Both thermograms exhibited only one main feature, a broad and intense endothermic peak (approximately between 0°C and 100°C). The enthalpy associated to the endotherm was found to be 98.11 J/g as calculated from the integrated area of the experimental peak. This value represents 12.66 kJ per mol of peptide groups in the polymer. The non-reversible endotherm was not dependent upon the film preparation method. In

conclusion, the endotherm cannot represent a melting of the side chains as it is known for PSLG where the side chain crystallize if the alkyl ester chain exceeds a length of 10 carbon atoms. If the DSC (Figure 4.12) and the TGA (Figure 4.11) graphs are compared in the temperature range of the endotherm, there is no sign of significant mass loss in the TGA which would indicate a change in the chemical structure. ^{1}H-NMR and ^{13}C-NMR measurements of the polymer before and after heating showed no change. A change of the chemical structure could therefore be excluded from the discussion. The origin of this endotherm could not be elucidated by the exclusive use of DSC and had to be sought by other experiments which give complementary information.

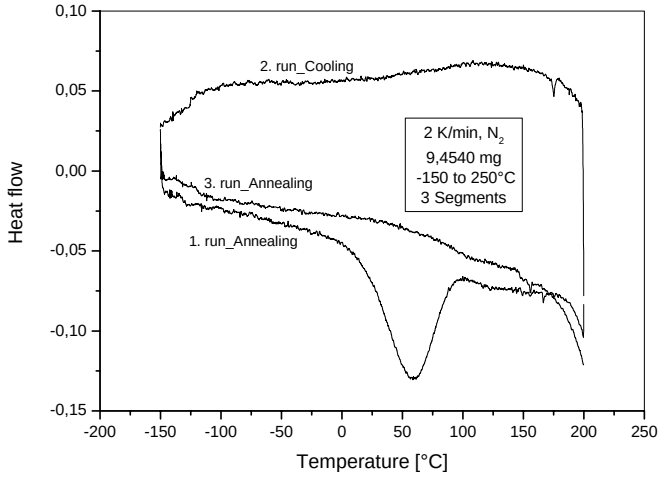

Figure 4.12: DSC trace of PLGA powder (PP10).

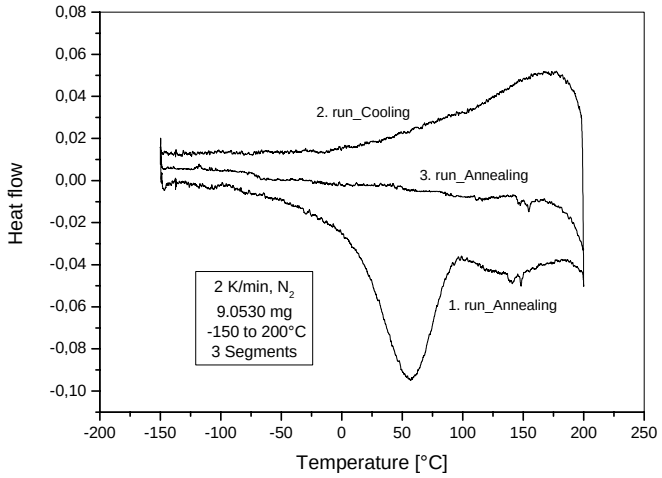

Figure 4.13: DSC trace of a PLGA film (PP8 purified, drop-cast from 10% (w/w) DMA solution at RT).

WAXD was also used to investigate the endothermic transition. WAXD should have shown any melting of conventional microcrystalline regions existing in the solid PLGA or in the cast film of PP8 purified, but the X-ray diffraction patterns in Figure 4.14 and 4.15 excluded the presence of crystalline regions within the sample, as only the amorphous halos were observed in the temperature dependent WAXD experiment.

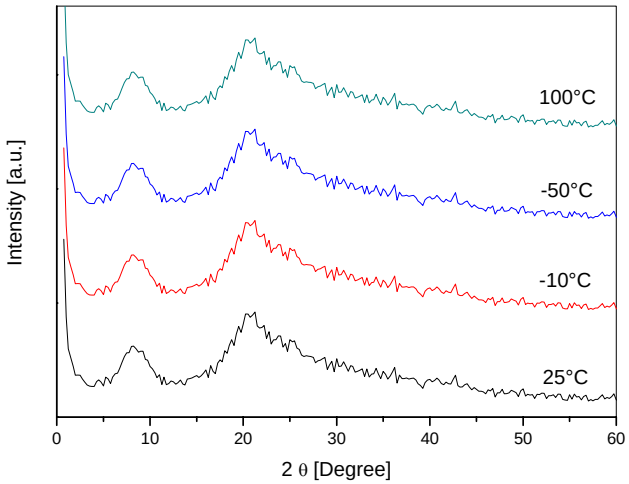

Figure 4.14: Temperature dependent XRD of PLGA (powder).

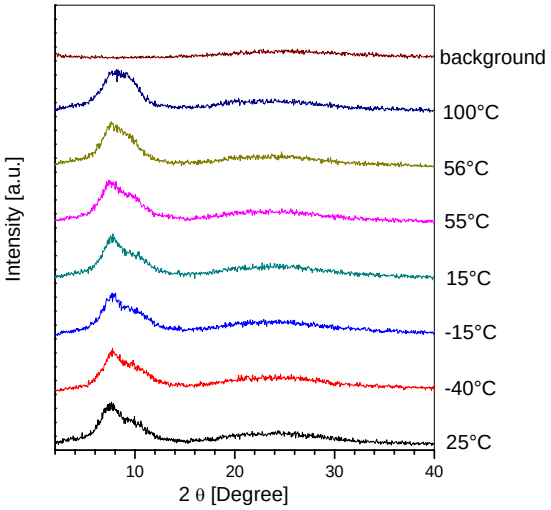

Figure 4.15: Temperature dependent XRD of PLGA (PP8, drop-cast film from 10% (w/w) DMA solution at RT).

Figure 4.16 shows the temperature dependent solid-state NMR, which was undertaken to obtain information about the endothermic transition, but the helical structure (see the secondary structure discussion in Chapter 1.3.3 for solid-state NMR) was constant.

Intensity changes and signal narrowing at higher temperatures are commonly obtained and do not influence the interpretation of the spectra.

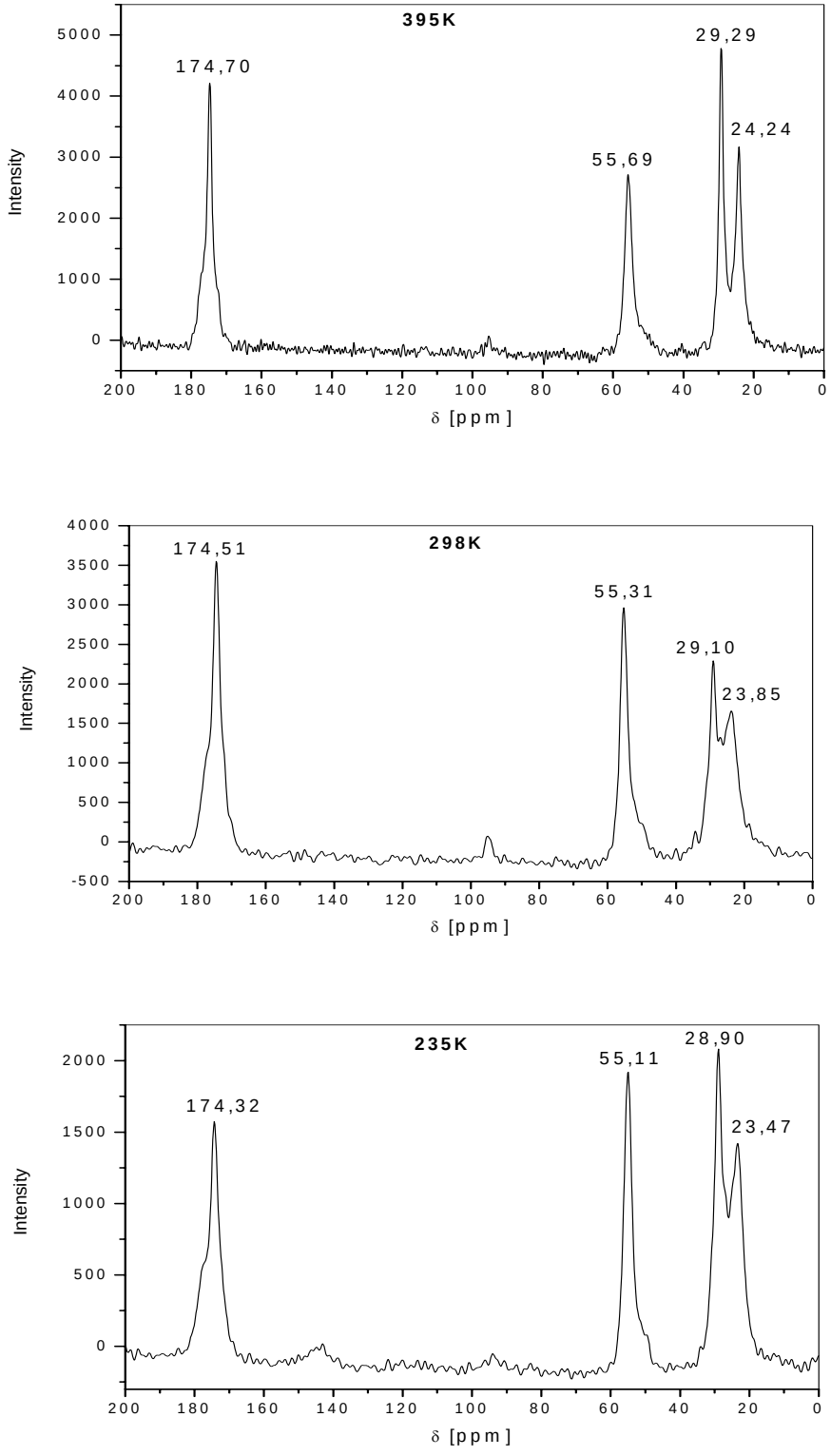

Figure 4.16: Solid-state NMR of PLGA (MD-1-48) (powder) at different temperatures.

Temperature dependent polarized optical microscopy was attempted as well. A drop-cast film of a 10 % (w/w) DMF solution of PLGA (PP8 purified) was used in special equipment, which allowed for low temperature measurements down to -85°C. There were some "frozen" lyotropic liquid crystalline structures identified but no change was observed in the temperature range of the endotherm in the film independent of different heating and cooling rates (2-10 K/min). IR or Raman measurements were not possible in these temperature ranges. But, these methods would mostly deliver information about changes in the secondary structure, which were excluded by solid state NMR. The lone example found for this phenomenon was published in 1999 for a poly (pentapeptide) of elastin, where a similar endotherm could not be clarified using similar approaches.[16] The solution of this problem seemed to be very challenging. Regardless, the transition was clearly a thermally induced transition that the polymer underwent.

Degradation studies:

The degraded material of "old" PLGA solutions in TFA was analyzed to identify possible degradation products. After a relatively short time period (2 h) after dissolving PLGA in TFA a drastic color change from colorless to dark brown appeared indicating a chemical structural change. Considerable effort was put into determining the identity of the degradation products. The evaporated brown residue was not soluble in chloroform or dichloromethane, but soluble in acetone wherein a proton NMR could be measured. NMR proved that polymer degradation occurred (not shown as spectra). Several mass spectroscopy experiments using the FD technique failed to elucidate the chemical structure of the unknown degradation product(s). Some prepared films of the different IR experiments in chapter 6 exhibited degradation. The IR spectrum was similar for all like the one illustrated in Figure 4.17.

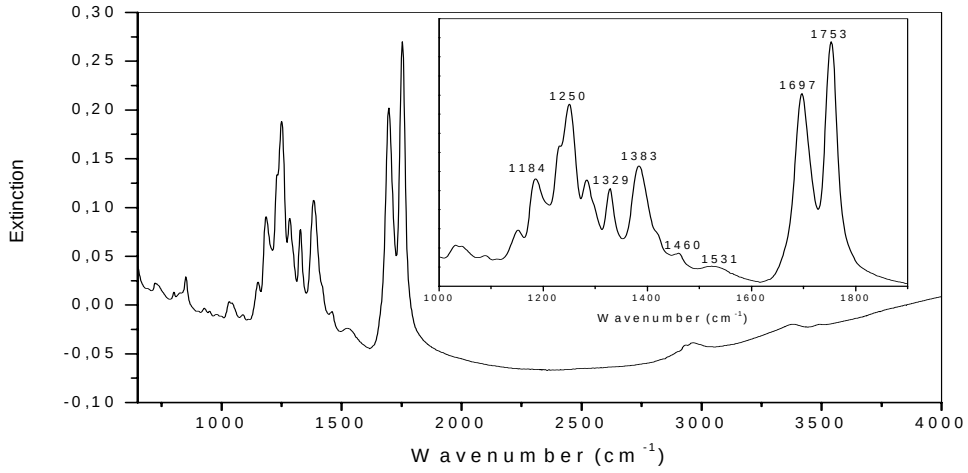

Figure 4.17: FTIR spectrum of a drop-cast film of degraded PLGA (PP1).

The spectrum showed a complete absence of the typical polypeptide sensitive bands like Amide I, II and V. A small residue of the Amide II band for a sheet structure was still observable at 1531 cm^{-1} meanwhile the Amide I band was completely absent. Some new, very intense bands were detected at the following wavenumbers, which were found to be stable until 200°C: 1753, 1697, 1383, 1329, 1250, and 1184 cm^{-1}.

After the unintentionally degraded material was observed in films, a systematic study with intentionally degraded material was executed and analyzed. Samples, which were stored for long periods of time in TFA, brown residual degraded PLGA were taken, redissolved in TFA, spin coated on cover glass and stored over night in a Petri dish in a vacuum oven. The obtained films on glass were measured by ATR-FTIR yielding spectra as shown in Figure 4.18. The degradation was observed again, however the degraded product or mixture of products were slightly different compared to the previous example. A very broad hydrogen bonding band was observed in the Amide V region around 3500 cm^{-1}. The Amide II band of a helical structure was still present at 1560 cm^{-1}. The new bands were located at 1677, 1203, and 1143 cm^{-1} meanwhile the band at 1753 cm^{-1}, representing the carbonyl group of the side chain, was no longer present. That gives rise to the assumption that the degradation was further advanced than in the unintentionally degraded material which had less contact time with TFA. The possible degradation products were already described in chapter 3.3 during the MALDI-TOF spectral discussions.

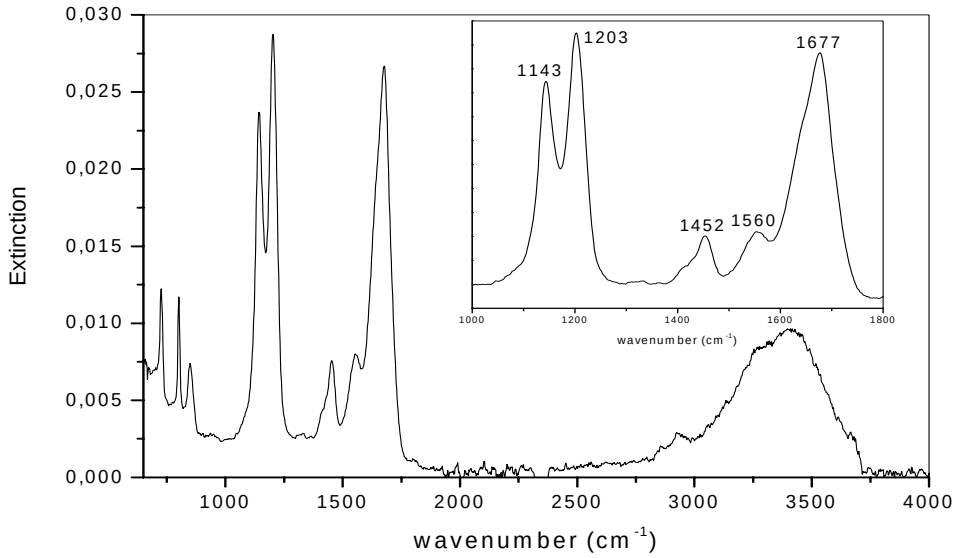

Figure 4.18: FTIR spectrum of brown residue (degraded PLGA) spin-coat on glass.

Some fresh samples of PLGA were prepared under the same conditions (spin coating etc.) to compare them to the degraded material (Figure 4.19). They exhibited a regular PLGA IR spectrum indicating a mixture of α-helix and β-sheet due to the Amide I bands at 1650 and 1632 cm^{-1}. The disappearance of the band at 1710 cm^{-1} gives rise to assume that maybe as first step of the degradation a decarboxylation of the carboxylic acid group of the side chain occurred.

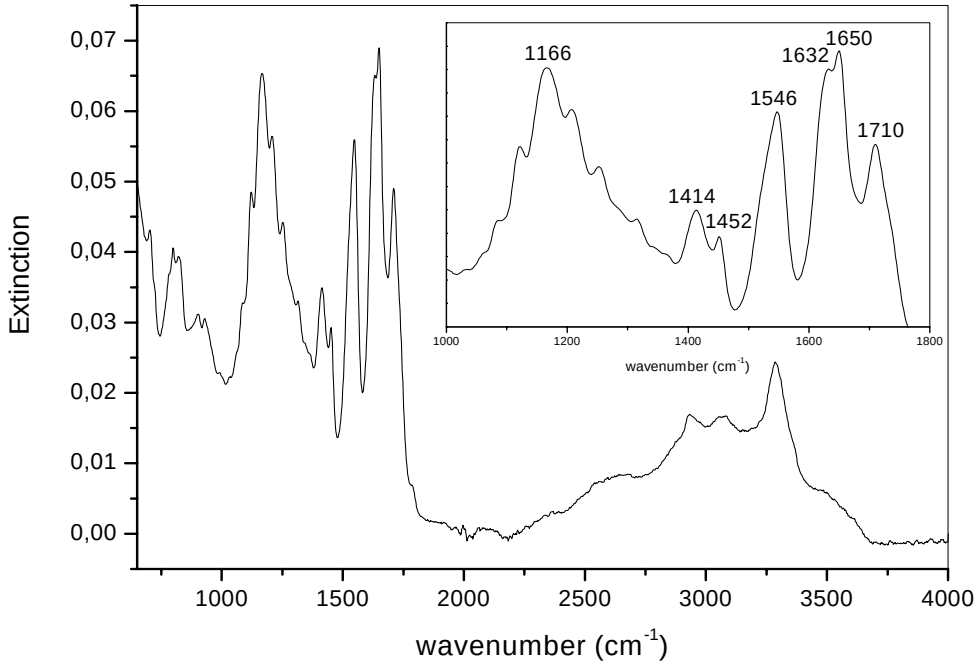

Figure 4.19: FTIR spectrum of non-degraded PLGA (PP3) spin-coat on glass.

4.4 Capillary Electrophoresis (CE)

CE has demonstrated tremendous potential for a wide range of applications as analytical separation technique, like quality control in food and beverage analytics, from small molecules that include inorganic ions, organic acids, amino acids, peptides, drugs, nucleosides, nucleotides, vitamins, steroids, and carbohydrates, to larger molecules such as hormones, proteins, nucleic acids, and even living cells. For instance, vitamins were previously separated by TLC, high pressure liquid or gas chromatography, based on differences in the compound polarity, which led to a different affinity to the solid phase making a simultaneous detection of different vitamins difficult.

Free zone capillary electrophoresis (CZE) is the simplest form of CE, which was chosen for the current work out of the different possible separation modes. The separation principle in CZE is based on the different electrophoretic mobility of the analytes in an applied electric field, which are mainly related to the different charge and mass of each species. CE analysis offers a range of advantages like short running times, low required sample and reagent amounts, and low cost compared to chromatography or conventional electrophoresis. However, CZE does not represent yet a conventional characterization method for synthetic polymers. The fundamental principle will be shortly described now.

The basic instrumental setup (Figure 4.20) consists of a high voltage power supply (0-30 kV), a fused silica (SiO_2) capillary, two buffer reservoirs, two electrodes, and an on-column detector. A specific amount of sample is introduced by controlling either the injection voltage or the injection pressure. After applying an electric field, each component in the sample zone migrates according to its own apparent mobility consisting of electrophoretic and electroosmotic mobility. Ideally, all sample components will be separated from each other to form individual zones of pure material. However, neutral molecules cannot be separated because they migrate at the velocity of the electroosmotic flow. Possible detection modes represent direct UV, indirect UV, fluorescence, or MS detection. The pH range between 2 and 12 is suitable for CE. At lower or higher pH values the current transport will be taken over by hydrogen or hydroxide ions, respectively. Schaeper and Sepaniak reviewed the influence of different parameters on the reproducibility of CE measurements in 2000.[17]

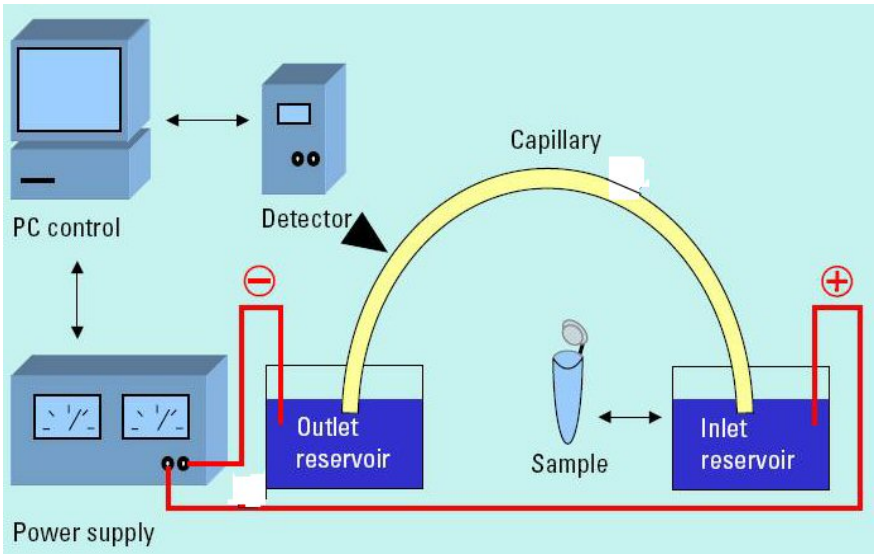

Figure 4.20: Basic components of a capillary electrophoresis system.[18]

The ion velocity is determined by dividing the traversed path length (capillary length from inlet to detector) by the migration time of the zone t_m as shown in equation 4.1.

$$v = \frac{l_{eff}}{t_m} \tag{4.1}$$

Where:

v = *ion velocity*

l_{eff} = *effective capillary length*

t_m = *migration time*

The apparent electrophoretic ion mobility depends on the ion velocity as shown here.

$$\mu_a = \frac{v}{E} = \frac{l_{eff}\, L_{tot}}{t_m V} \tag{4.2}$$

Where:

μ_a = *apparent electrophoretic mobility*

L_{tot} = *total capillary length*

E = *electric field strength*

V = *applied voltage*

The electrophoretic mobility is determined by the ratio of the driving electrical force to the frictional force approximated by Stokes law.

$$\mu = \frac{q}{6\pi r\,\eta} \tag{4.3}$$

Where:

μ = *electrophoretic mobility*

q = *charge*

$6\pi r$ = *ionic volume*

η = *dynamic viscosity of the electrolyte*

The viscosity of the medium is constant. The ion volume can be affected by the counterion or the complexing agent. The charge cannot be altered for fully dissociated ions (strong acids, small ions) and can be altered for weak acids and bases (pH dependent). The effective charge of a solute ion is the charge of the ion minus the fractional charge of the surrounding oppositely charged ions. The ion drags this portion of the double layer with it during the migration and migrates therefore slower than expected corresponding to its actual charge (electrophoretic effect).

The inner walls of fused silica capillaries possess an intrinsic negative charge due to the presence of weakly acidic silanol groups (pK_a~5.3), shown in Figure 4.21.

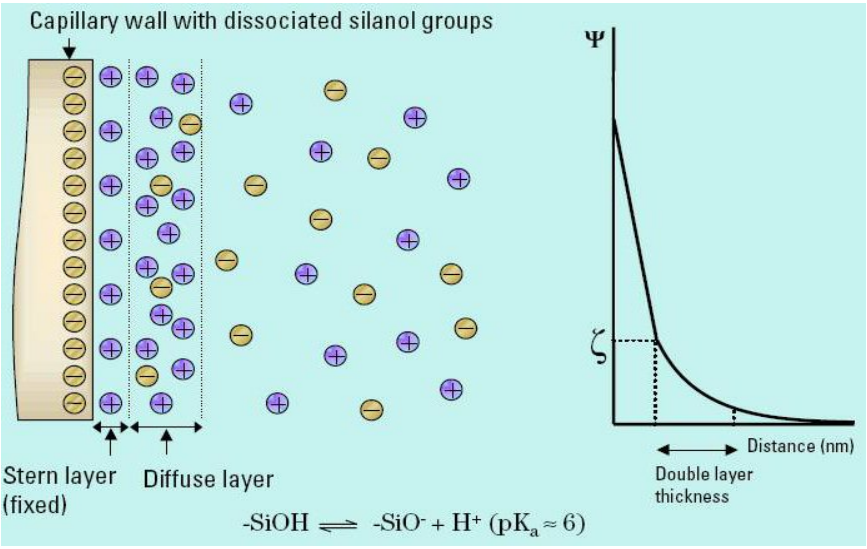

Figure 4.21: Illustration of the charge distribution and the zeta potential.[18]

A part of the cations remains fixed at the negative capillary wall by electronic attraction forming an electrical double layer (stern layer). The cation concentration decreases exponentially in dependence on the distance to the capillary wall in the diffuse "Gouy-

Chapman" layer. The coulomb interactions between the cations and the negative wall decreases and allow the diffuse layer to migrate to the anode upon the application of an electric field across the length of the capillary. The shearing of the diffuse layer over the stern layer induces the zeta potential, which represents an indirectly measurable parameter. The zeta potential decreases first linearly in the stern layer and then exponentially in the diffuse layer in dependence to the wall distance. The potential is largely dependent on the electrostatic nature of the capillary surface, and to a small extent, on the ionic nature of the buffer.[19]

An extremely flat (piston-shaped) flow profile occurs which leads to sharper peaks in CE compared to those of the pressure-driven (hydrodynamic) flow in liquid chromatography (LC) where the Hagen-Poiseuille force causes peak broadening. The resolution in CE is higher than in chromatography due to the absence of a laminar flow profile (Figure 4.22).

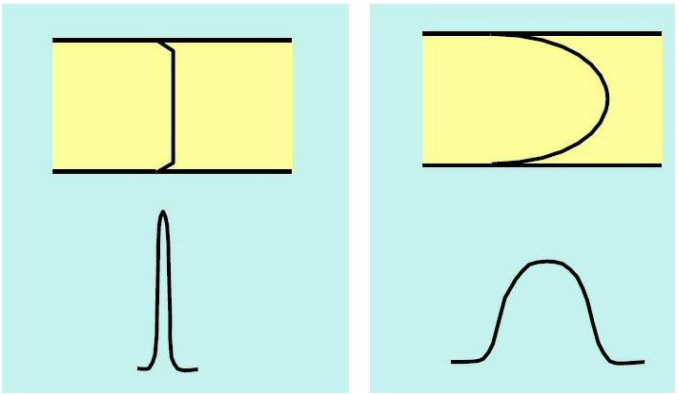

Figure 4.22: Effect of the flow profile on the zone width.[18]

The migration velocity of the EOF can be described in simplified form by means of the Helmholtz equation.

$$\mu_{EOF} = \frac{\varepsilon_0 \varepsilon \zeta}{4\pi\eta} \qquad (4.4)$$

Where:

μ_{EOF} = *electroosmotic flow*

ε = *dielectric constant of the buffer*

ε_0 = *dielectric constant of the vacuum*

ζ = *zeta potential (inversely proportional to buffer concentration and directly proportional to the number of wall charges)*

η = *viscosity constant of the buffer (inversely related to temperature)*

The EOF increases with the degree of dissociation of the surface silanol groups, i.e. with the pH value.

$$\mu_a = \mu_{EOF} + \mu_e \tag{4.5}$$

Where:

μ_a = *apparent mobility*

μ_{EOF} = *electroosmotic flow*

μ_e = *effective mobility*

The influence of the effective mobility on the apparent mobility of an ion is illustrated in Figure 4.23. There is no difference between the apparent mobility and the EOF for a neutral species. If the molecule carries a charge the apparent mobility is depending on the nature of the charge. An anion migrates opposite to the direction of the EOF (countermigration) due to the attraction of the negative charge by the anode. As long the EOF is higher than the migration velocity of the anion; the ions will still migrate to the cathode. In contradiction, the cations are attracted by the cathode and the ion mobility is contributing additional to the EOF (comigration). The cations will be first detected in free zone capillary electrophoresis, then the neutral species, and as last the anions. The use of UV active neutral markers helps to identify and calculate the EOF.

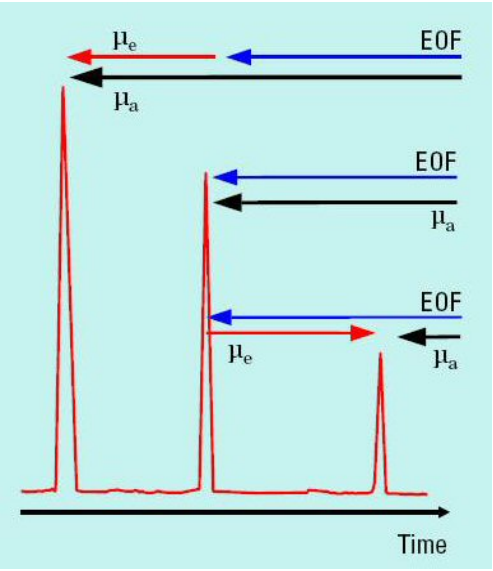

Cation with a positive μ_e

Neutral without μ_e

Anion with a negative μ_e

Figure 4.23: The influence of the effective mobility on the apparent mobility.[18]

The detector is placed near the outlet end of the capillary at the cathode side. In the current work a UV detector was used. The extinction of the UV detection is defined according to the Lambert-Beer law.

$$E = \lg (I / I_0) = \varepsilon c d \qquad (4.6)$$

Where:

E = Extinction
I = Light intensity after the sample
I_0 = Light intensity before the sample
ε = Extinction coefficient
c = Sample concentration
d = Sample thickness

The CE analysis of underivatized amino acids by direct UV detection was only barely described.[20] CE was therefore mainly performed for amino acids with precolumn, postcolumn, and on-column derivatization techniques with UV chromophores[21,22] or fluorophore reagents [23-27] to improve sensitivity and was reviewed by Smith et al.[28]

Poly(styrene sulfonates) were the first CE separated synthetic polyelectrolyte because of no interaction with the surface of the fused-bare silica capillaries, commercial availability with low dispersities and different molecular masses, and full dissociation even at low pH values. Their molecular detection limit in CE was determined to be 8000 g/mol.[29-32]

Proteins and polypeptides exhibit identical electrophoretic mobilities and can therefore not be separated in free solution without using a sieving matrix because of the constant charge to size ratio. Polypeptides were detected by UV absorption or by LIF after derivatization with a fluorescent reagent.[33] The high selectivity of CE was ideally combined with the detection strength of a LIF detector. Conductivity detectors were also found to be helpful due to the UV inactivity of many samples.[34-36]

The electrophoretic separation of proteins in untreated fused silica capillaries possesses another disadvantage due to the interaction of the protein with the silanol groups on the inner capillary wall. Many studies attempted buffer modifiers or neutrally coated capillaries to eliminate or suppress the protein/wall interaction. Lauer and McManigill [37] stated that CZE is possible if the coulomb repulsion between protein and the capillary

overcome the adsorption by raising the pH of the buffer solution above the isoelectric point of the protein. The work of the past decades was reviewed by Kasicka et al. [38]

The identification of the peaks was conducted for poly(glycine), poly(valine), poly(lysine) and poly(alanine) as end-charged homopolypeptides by comparing them to commercially available oligomers. If not all oligomeric peptides are commercially available, Cottet commonly assigned the peaks by assuming a regular distribution of the peptides starting from the dipeptide.[39]

The current work focuses on the free zone capillary electrophoresis (CZE) of PLGA with different molecular weights in an aqueous buffer system. The obtained homopolypeptides show a broad molecular weight distribution due to the lack of control over the active chain end during the polymerization. Capillary electrophoresis was successfully investigated as a new characterization method for oligomeric polypeptides. If a size separation was demanded, the system would have to be switched to gel electrophoresis, which was not the focus of this work.

High demands of purity are required to obtain a reliable and reproducible separation. A lot of effort was put into the finding of stable conditions for current, EOF etc. The capillary was rinsed by an investigated flushing procedure consisting of 1 M NaOH, 0.1 M NaOH, MQ water, and pure buffer after each sample measurement. A neutral UV active EOF marker (acetone) was added every time to control the stability and the consistence of the buffer system.

Six different amino acids as small molecule system were used as test compounds for the system development of the new installed CE device in the institute. L-aspartic acid, L-glutamine, γ-L-methyl glutamate, L-glutamic acid, L-asparagin, and L-alanine were measured in a sodium borate buffer at pH 10, in a 50 µm fused silica capillary at 25°C in a concentration of 5 g/l for all amino acids. The identification of the single amino acids was conducted by comparison to the separately measured electropherograms of each compound. A possible aggregation of the amino acid chains could be excluded by dynamic light scattering studies (DLS) of the prepared solutions. A similar amino acid separation in a borate buffer was achieved by Sulman et al. in a borate buffer with pH 9.18.[40] Figure 4.24 shows the obtained separation of the amino acids by CZE.

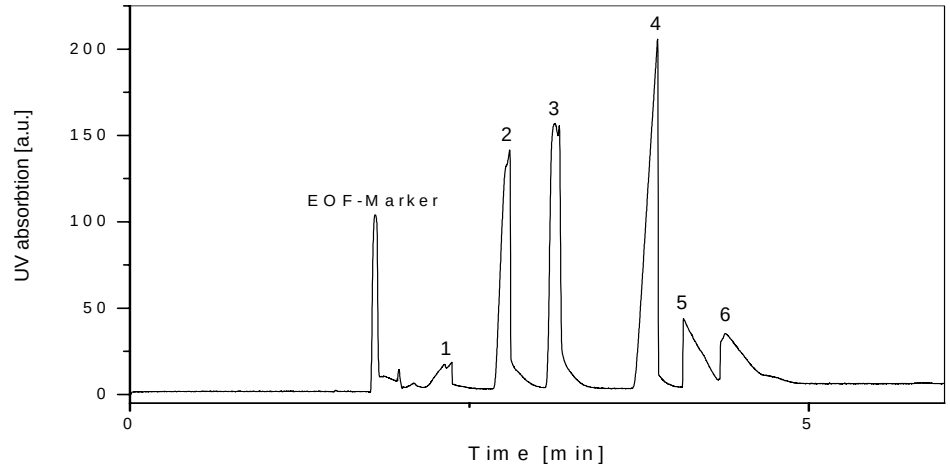

Figure 4.24: CE spectrum of six different amino acids:

1: L-alanine 2: L-glutamine 3: L-asparagine

4: γ-methyl-L-glutamate 5: L-glutamic acid 6: L-aspartic acid

5 g/l, sodium borate buffer (pH 10), fused silica capillary (50 µm), 25°C, UV-detection (191 nm), 30 kV, 50 mbar for 10s.

The aqueous basic sodium borate buffer at pH 10 could be successfully applied to investigate a reproducible separation of PLGA as shown in Figure 4.25. The charge density separation of PLGA was the first ever obtained for PLGA by CZE.

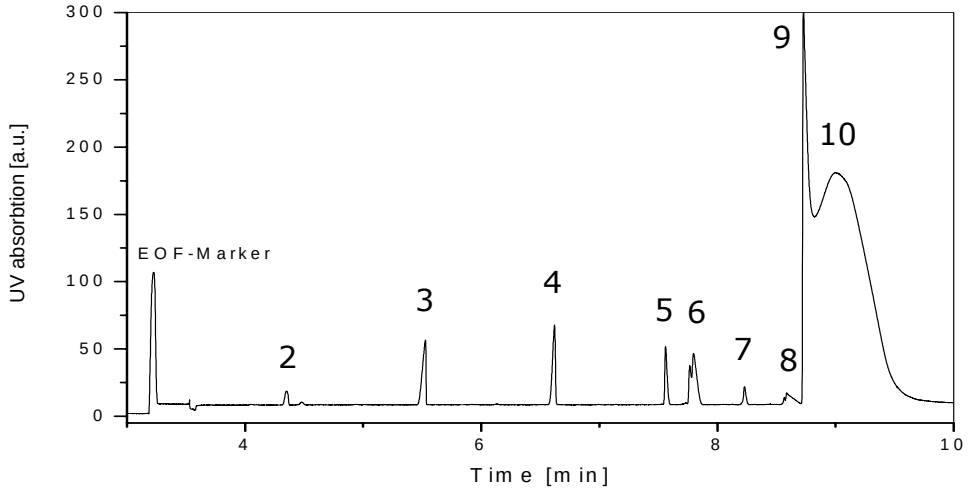

Figure 4.25: CE spectrum of PLGA (PP12), 5 g/l, sodium borate buffer (pH 10), fused Silica capillary (50 µm), 25°C, UV-detection (191 nm), 30 kV, 50 mbar for 10s.

The PLGA sample PP12 was polymerized with n-hexyl amine as initiator. The obtained oligomeric separation by charge density depends decisively on the chain length of the polypeptide chain. There is one negative charge per unit caused by the deprotonated carboxylic acid group of the side chain. The differences in charge density detected in the electropherograms were induced by the incorporation of the initiator molecule. The longer the polymer chain becomes the more the charge density approaches to the same value as shown in Table 4.7. High molecular weight polypeptides can therefore not be separated by CZE because the charge density becomes constant leading to one broad peak if the influence of the incorporated initiator vanishes.

Table 4.7: The calculated charge density (M/Q) in dependence of the chain length.

Chain length	1	2	3	4	5	6	7	8	9	10
Charge density	229	179	162	153	148	145	142	141	139	138

The concentration dependence of the obtained PLGA separation was analyzed by varying the concentration from 5 g/l down to 0.5 g/l. All other important parameters for the sample amount injected like injection time and pressure and the general running conditions were kept constant. The obtained separation, shown in Figure 4.26, exhibited the same behavior but a concentration of 2 g/l should not be diluted more to allow qualitative analysis. An increase of the injection time from 10s to 30s and finally to 60s resulted in a considerable overload of the capillary and led to peak broadening.

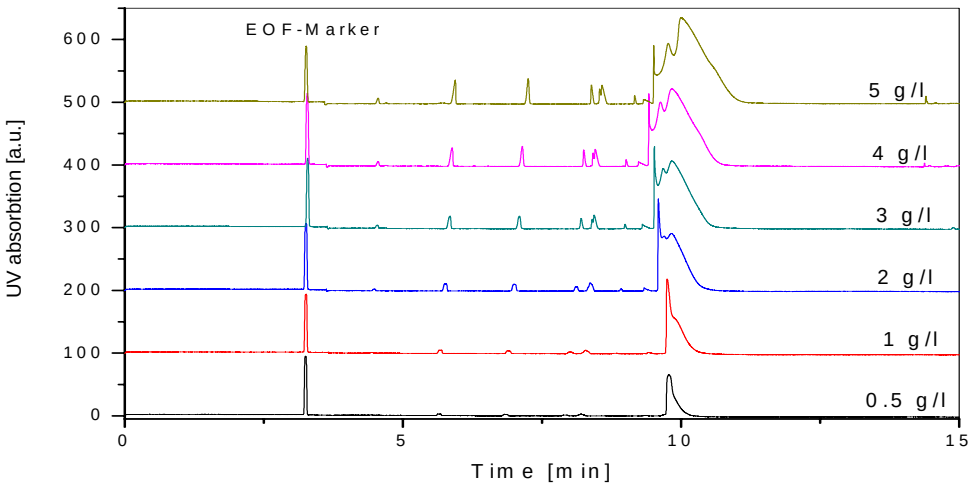

Figure 4.26: CE spectrum of PLGA (PP12), different concentrations (5, 4, 3, 2, 1, and 0.5 g/l) in sodium borate buffer (pH 10), fused silica capillary (50 µm), 25°C, UV-detection at 191 nm, 30 kV, 50 mbar for 10s.

A confirmation for the oligomeric separation was achieved by measuring another PLGA sample (MD-1-48), which was purified by soxhlet extraction after the synthesis. This purification led to the loss of the oligomeric fraction like shown in chapter 4.3. The CE electropherograms exhibited the same separation, but without the oligomers marked as 2-8 in Figure 4.25. The different voltage applied, 15 kV instead 30 kV, led to a lower EOF resulting in a shift of the time scale for the separation. The qualitative analysis remained still similar. A precise identification of the oligomers was difficult for the following reasons. There were no oligomers commercially available of PLGA to compare them following the most common identification procedure.[39] The more precise coupling of a nanospray ESI-mass detector to the CE device required a change of the buffer system because the borate buffer has not a sufficient volatility to ensure compatibility with the MS detection. The most applied acetate buffer was not suitable because it led to complete different electropherograms where the running conditions could unfortunately not be investigated to obtain a reasonable separation like for the borate buffer.

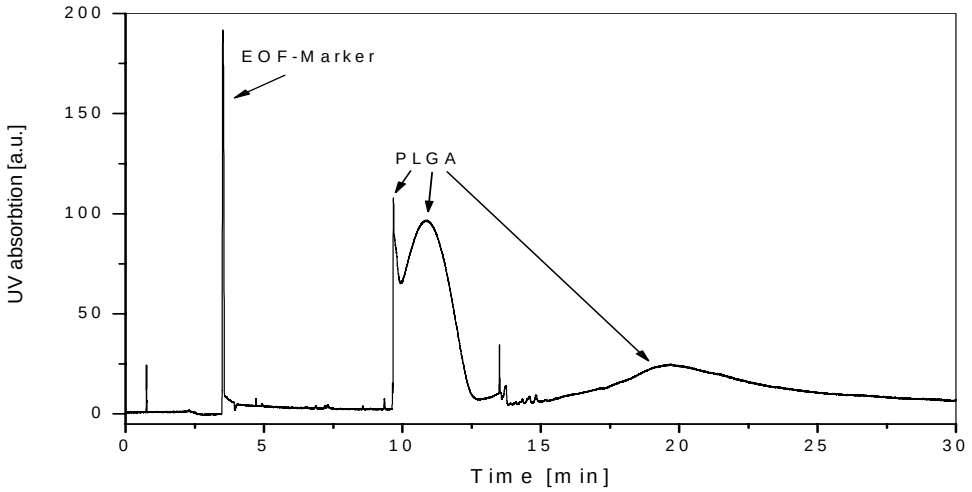

Figure 4.27: CE spectrum of PLGA (MD-1-48), 5 g/l in sodium borate buffer (pH 10), 15kV, fused silica capillary (50 µm), 25°C, UV-detection (191 nm), 50 mbar for 10s.

The analysis of a PLGA sample (PP6) polymerized using a different initiator, 3-methoxy-propyl amine instead n-hexyl amine, led to severe problems in CE like blocking of the capillary and unstable current. PP6, possessing the same degree of polymerization, was determined to aggregate more easily than PP12 by DLS. The difference was assumed to depend on increased hydrogen bonding by the incorporated initiator at the beginning of each chain. The following DLS studies attempted to investigate a suitable borate buffer system in which the aggregation of the polypeptide chains can be avoided by the addition of different additives. UV-VIS measurements were conducted to detect possible shifts in the UV absorption of the buffer.

First, the influence of the concentration of PP6 was analyzed. Aggregation was still detected even at 1 g/l. 0.5 g/l was free of aggregates, but this concentration was, like for PP12, to low to deliver a reliable CE separation.

Secondly, different salts were added to break up the aggregation. LiBr seemed to be suitable because a salt concentration of 3 g/l showed no aggregation in a polymer solution of 5 g/l, but the UV-VIS spectrum proved a shift of the UV absorption of the pure borate buffer at 190 nm up to 220 nm. Also a high current increase (200 µA) was observed due to the high salt content, which was already discussed in literature to cause localized heating of the sample zone and poor peak shape.[41] Replacing LiBr by NaCl led to UV absorption at 195 nm, which would be still acceptable compared to the stronger UV active bromide anion, but the current kept unstable. The observation, that the current was too high but stable for LiBr, led to the proposition to use LiCl as a possible promising system, even if the salt content would still cause problems. In the current work, a change to organic additives was preferred to avoid an increase of the current by the salts.

A small volume of HFIP, a known hydrogen bond disruptor, was used to break up the aggregation. 5 % (v/v) HFIP in a polymer solution of PP6 (2 g/l) was determined by DLS to be free of aggregates. Lower HFIP volumes did not disrupt the aggregates; higher volumes of HFIP caused insolubilities for PP6. The obtained separations, shown in Figure 4.28 at two different injection times, were unfortunately not exhibiting a good separation of PP12. The addition of HFIP surely changed the EOF and led again to current instabilities.

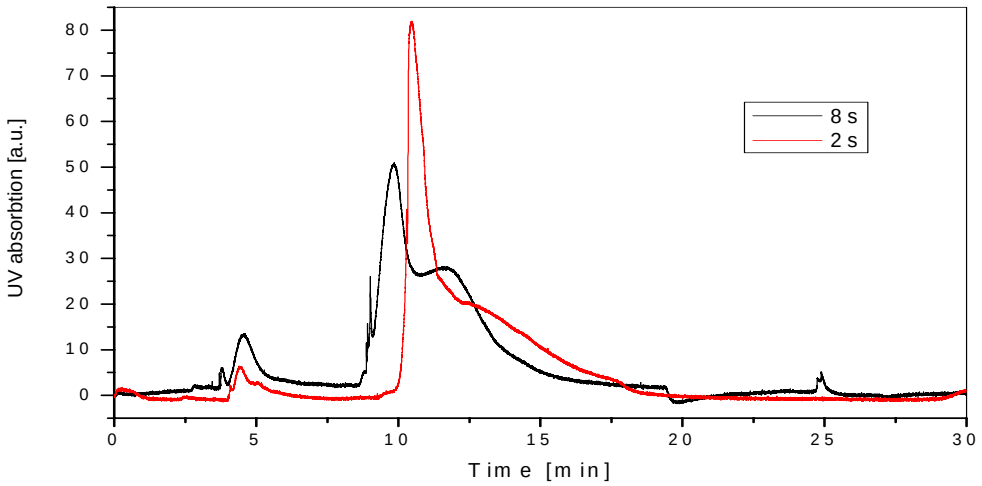

Figure 4.28: CE spectrum of PLGA (PP6), 2 g/l in sodium borate buffer (pH 10) + 5 % (v/v) HFIP, fused silica capillary (50 µm), 25°C, UV-detection at 191 nm, 30kV, 50 mbar for two different injection times (8 and 2s).

In conclusion the method of capillary electrophoresis seems to be a powerful tool to investigate a charge density separation of PLGA. The transformation of suitable buffer systems and conditions to other polymeric systems, even if just the initiator as the beginning of the chain is different, already led to another electrophoretic behavior. A broad application to other polymers requires therefore every time again an own system development, which is quite time consuming and very challenging. However, the obtained CZE separation of PLGA (PP12) clearly confirms the general applicability of the method to separate oligomeric polypeptides in an aqueous buffer.

For future research, it can be interesting to investigate the influence of different additives on the resolution of the separation and the further investigation of a mass spectroscopy suitable buffer system to allow a better identification of the obtained oligomeric signals.

A long time project would be the investigation of a buffer system in an organic non-aqueous buffer system, which is far more difficult than an aqueous buffer. Most of the polypeptides are insoluble in water and have very low solubility in organic solvents. The investigation of this new organic buffer system would offer to expand the CZE method to a broad number of other polypeptides.

References:

[1] K. Kovacs, J. Kovacs, *J. Am. Chem. Soc.*, **1963**, *85*, 1839 (95)

[2] E. R. Blout, R.H. Karlson, *J. Am. Chem. Soc.*, **1956**, *78*, 941 (69)

[3] W. E. Hanby, S. G. Waley, J. Watson, *J. Chem. Soc.*, **1950**, 3239 (6)

[4] V. Bruckner, K. Kovacs, J. Kovacs, *Naturwissenschaften*, **1952**, *39*, 330 (277)

[5] V. Bruckner, K. Kovacs, J. Kovacs, *Experienta*, **1954**, *10*, 166 (280)

[6] J. Nyilasi, Z. Kovats, *Acta Chim. Acad. Sci. Hungary*, **1952**, *2*, 451 (279)

[7] M. Green, M. A. Stahmann, *J. Biol. Chem.*, **1952**, *197*, 771

[8] M. Frenkel, A. Berger, *J. Org. Chem.*, **1951**, *16*, 1513

[9] A. Berger, E. Katchalski, *J. Am. Chem. Soc.*, **1951**, *73*, 4084

[10] E. R. Blout, R. H. Karlson, P. Doty, B. Hargitay, *J. Am. Chem. Soc.*, **1954**, *76*, 4492

[11] E. R. Blout, R. H. Karlson, P. Doty, B. Hargitay, *J. Am. Chem. Soc.*, **1956**, *78*, 497

[12] D. Ben-Ishai, A. Berger, *J. Org. Chem.*, **1952**, *17*, 1564 (5)

[13] E. Katchalski, *Methods in Enzymology*, **1957**, *3*, 540 (284)

[14] M. Idelson, E. R. Blout, *J. Am. Chem. Soc.*, **1958**, *80*, 4631-4634 (285)

[15] A. Wada, *Mol. Phys.*, **1960**, *3*, 409 (286)

[16] J. C. Rodriguez-Cabello, M. Alonso, *Macromol. Chem. Phys.*, **1999**, *200*, 1831

[17] J. P. Schaeper, M. J. Sepaniak, *Electrophoresis*, **2000**, *21*, 1421

[18] *Chemstation Software Manual CD*, **Agilent company**

[19] J. E. Melanson, N. E. Baryla, C. A. Lucy, *Trends analyt. Chem.*, **2001**, *20*, 365

[20] C. W. Klampfl, W. Ahrer, *Electrophoresis*, **2001**, *22*, 1579

[21] E. Skocir, J. Vindevogel, P. Sandra, *Chromatographia*, **1994**, *39*, 7

[22] S. Terabe, Y. Ishihama, H. Nishi, K. Otsuka, *J. Chromatogr.*, **1991**, *545*, 359

[23] S. Oguri, K. Yokoi, Y. Motohase, *J. Chromatogr. A*, **1997**, *787*, 253

[24] A. Taga, S. Honda, *J. Chromatogr. A*, **1996**, *742*, 243

[25] M. Albin, R. Weinberger, E. Sapp, S. Moring, *Anal. Chem.*, **1991**, *63*, 417

[26] T. Ueda, R. Mitchell, T. Kuwana, A. Nakamoto, *J. Chromatogr.*, **1992**, *593*, 265

[27] E. A. Arriaga, Y. Zhang, N. J. Dovichi, *Anal. Chim. Acta*, **1995**, *299*, 319

[28] J. T. Smith, *Electrophoresis*, **1999**, *20*, 3078

[29] J. B. Poli, M. R. Schure, *Anal. Chem.*, **1992**, *64*, 896

[30] M. Minarek, B. Gas, E. Kenndler, *Electrophoresis*, **1997**, *18*, 98

[31] H. Cottet, P. Gareil, *J. Chromatogr. A*, **1997**, *772*, 369

[32] H. Clos, H. Engelhardt, *J. Chromatogr. A*, **1996**, *802*, 149

[33] K. C. Chan, G. M. Janini, H. J. Issaq, *J. Chromatogr.*, **1993**, *622*, 269

[34] Y. Xue, *Chem. Educ.*, **1996**, 1

[35] H. Engelhardt, W. Beck, T. Schmitt, *Kapillarelektrophorese*, **1994**, Vieweg Verlag

[36] H. Engelhardt, O. Grosche, *Adv. Polym. Sci.*, **2000**, *150*, 190

[37] H. H. Lauer, D. McManigill, *Anal. Chem.*, **1986**, *58*, 166

[38] V. Kasicka, *Electrophoresis*, **1999**, *20*, 3084

[39] R. Plasson, H. Cottet, *Anal. Chem.*, **2005**, *77*, 6047

[40] O. V. Manaenkov, A. I. Sidorov, E. M. Sulman, *J. Anal. Chem.*, **2003**, *58*, 979

[41] K. D. Altria, M. A. Kelly, B. J. Clark, *J. Chromatographia*, **1996**, *43*, 153

Chapter 5

Poly (L-cysteic acid)

5.1 Synthesis

The synthesized PSCBC and PSBC were synthesized as potential intermediates that could lead to poly(cysteic acid). Poly(cysteic acid) was chosen as an interesting promising candidate for comparable studies to PLGA in the current work because their chemical structures are mostly similar, but the incorporation of a heteroatom sulfur in the side chain could offer better properties for film preparations, fiber extrusions, crystallizations, and solubility. It has been shown in the literature that an oxidation from the thioester or thioether to poly(cysteic acid) is relatively difficult due to a possible degradation of the polypeptide backbone. The common deprotection method using sodium in liquid ammonia was discussed and reviewed in detail for polypeptides and proteins by Schön.[1] However, it has been proven by Gertner et al. that PSBC can not be reduced completely with sodium in liquid ammonia without yielding impurities.[2,3] Spencer et al. confirmed that phosphonium iodide in glacial acetic acid was also not suitable for the reduction.[4] The acidic reduction of PSCBC with sodium in liquid ammonia yielded in pure poly(cysteine).[5] Berger and Katchalski used a mixture of formic acid and H_2O_2 as reagent, which was chosen for an attempt to reduce PSCBC to poly(cysteic acid) in the current work.[5]

The method was first applied in a test reaction with a small molecule reacting to the corresponding free sulfonic acid as shown in Figure 5.1.

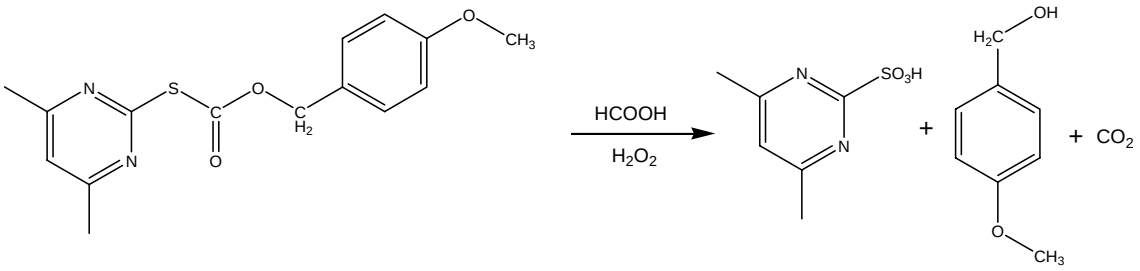

Figure 5.1: Test reaction for the oxidation with formic acid and H_2O_2.

Experimental procedure:

2 g (6.57 mmol) of p-methoxybenzyl-S-(4,6-dimethylpyrimidine-2-yl) thiocarbonate in 40 ml 90% (v/v) formic acid and 4 ml 30% (v/v) H_2O_2 were stirred until a clear solution was obtained (50 min). The solution turned translucent yellow after the p-methoxybenzyl-S-(4,6-dimethylpyrimidine-2-yl) thiocarbonate (yellow powder) was added to the reaction mixture. The reaction solution was heated up and changed the color several times over orange to dark red finally. The dark red solution was reduced in

vacuo and yielded dark red oil. After adding of 20 ml water a brown solution with very viscous red oil was obtained. Freeze drying led to highly viscous brownish oil, which was insoluble in acetone. TLC in 8:2 Hexane–EtOAc and NMR studies proved that side products were still present. After unsuccessful precipitations in hexane or diethylether, a salt was formed by adding NaOH and possible organic impurities were extracted by diethylether. The water phase was finally acidified to neutral pH and freeze dried. The brown precipitate has proven to be pure by ^{1}H-NMR in $CDCl_3$.

^{1}H-NMR ($CDCl_3$): 1.66 (CH_3), 3.74 (SO_3H), 6.76 (CH, aromatic)

The methoxy group of the test compound was confirmed to be non-oxidizable by a test reaction with anisole.

After confirming the utility of this oxidation reaction with small molecules, the procedure was applied for the reaction of PSCBC to poly(cysteic acid) as shown in Figure 5.2. 500 mg of PSCBC yielded 220 mg of a light brown powder, which was purified by soxhlet extraction in $CHCl_3$ for two days to remove benzyl alcohol. 68 mg of the purified product was obtained (MD-1-47).

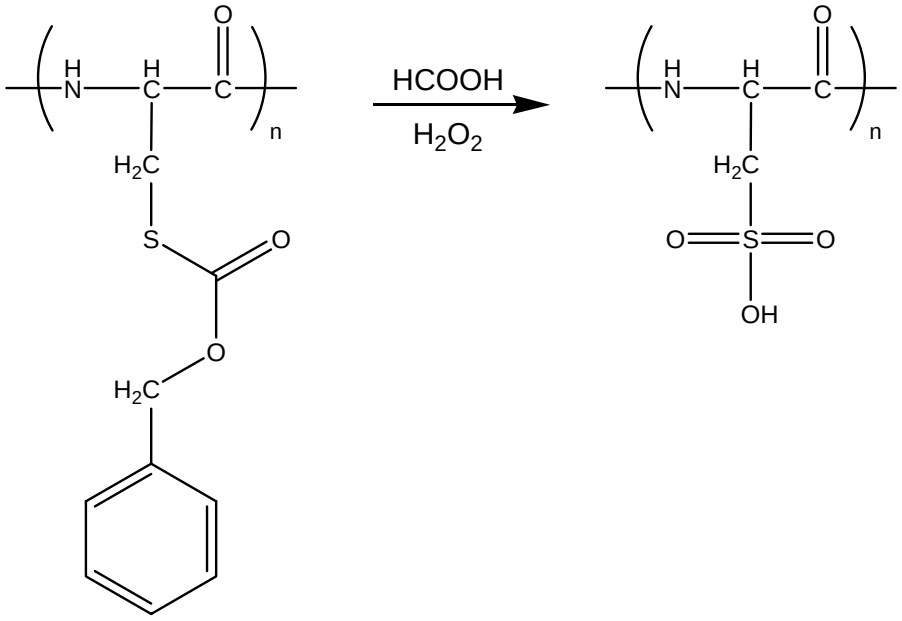

Figure 5.2: Saponification of PSCBC to Poly(cysteic acid).

5.2 Characterization

The product (MD-1-47) was not soluble in DMF, $CHCl_3$, THF, and was partially soluble in water, MeOH, and EtOH. The number of non-dissolved particles was increasing in this order from water to ethanol. The sulfonic acid should normally be soluble in water due to a high hygroscopic character, but there is a considerable risk of forming disulfide bridges during the reaction, which would decrease the solubility in water. Thermal analysis by TGA (heating rate 10 K/min, 25-900°C) indicated a degradation temperature of 170°C. Two different TGA-MS studies (heating rate 5 and 10 K/min, mass detection 0-150 g and 0-80 g) assumed an incomplete reaction by showing aromatic fragments from the benzyl group. The detection and identification of the assumed disulfide bonds was attempted by UV-VIS and Raman spectroscopy. The disulfide UV-VIS absorbance is supposed to be at 250 nm, stated for diethyl disulfide.[6] The appearance of the band at 250 nm cannot be taken as serious proof for the formation of disulfide bonds because the IR spectrum showed that the conversion from PSCBC was incomplete and residual benzyl groups were still present in the sample, which are also highly UV-VIS absorbent around 250 nm. The UV-VIS can not differentiate clearly between UV absorptions caused by benzyl or disulfide groups. Raman spectroscopy was attempted to identify S-S bonds in the obtained polymer. A comparison with all kind of different low molecular weight compounds containing a disulfide bond could not give definitive and reliable proof of the disulfides. Some compounds like L-cystine showed a highly intense band at 500 cm^{-1}, but for more complex compounds it is very difficult to identify the disulfide bond due to overlapping with other signals at this place.

Concluding, it has to be noted that the procedure from Katchalski et al. [5] could not be confirmed and their published results have to be discussed more in detail due to the lack of techniques, which could really prove the appearance of a free sulfonic acid group. The salt formation and titration experiments done by Katchalski et al. could give a positive result due to their qualitative character, which agrees with the obtained incomplete conversion where some side chain groups definitely exhibit a free sulfonic acid group but some portion may remain unprotected. Even if the reaction was repeated under inert atmosphere using a previously degassed solution did not succeed in improving the synthesis. Further studies to monitor the reaction by NMR or IR may help to determine the reaction progress. The following paragraph summarizes several other approaches, which could help to solve the problem of incomplete conversion in the future. They were not attempted in this work due to time limitations and the focus of the dissertation.

The previously described deprotection of the ester group followed by the oxidation of the resulting thiol in one reaction step were found to be relatively difficult and may have caused the incomplete reaction. It is proposed to do the reaction in two steps, the deprotection to the thiol, and the oxidation to the sulfonic acid.

The first methods used in the past for the selective removal of the S-protecting group suffered from a number of disadvantages: e.g. low yields, racemization and side reactions such as splitting of peptide bonds.[7] Katchalski et al. succeeded in removing the carbobenzoxy protecting group in high yields without causing racemization. They applied an excess of sodium methoxide (5 equiv.) for 5-10 min. at room temperature under nitrogen which caused rapid alcoholysis with almost quantitative liberation of the free thiol group, determined by titration.[5,8] Ghelis et al. followed a different approach by cleaving the ester group in boiling TFA, though this method may lead to decomposition of the polymer.[9] The application of basic conditions is desirable to avoid immediate formation of disulfide bonds.

The oxidation of thiols to sulfonic acids is quite challenging because mild oxidation conditions are necessary to avoid oxidative cleavage of the peptide backbone. The most common oxidizing agents like $KMnO_4$ can unfortunately not be applied because it is a too strong oxidizer. Röder et al. used N_2O_4 as oxidizing agent for alkane thiols (n=1-8) because it is a liquid at room temperature but has a boiling point of 21°C. Residual solvent can easily be removed simply by heating the system. It was possible to use N_2O_4 as both solvent and reactant, but these leaded to poor yields. A more efficient way was to dissolve the thiol in a low boiling solvent, e.g. petroleum ether or THF and introduce a gently stream of N_2O_4 into the solution.[10] Lowe and Bodwell followed another approach to use DMSO for the oxidation of small molecular thiols.[11,12] Katchalski et al. have oxidized poly(cysteine) by hydrogen peroxide, in the presence of cupric ions, which could also offer an attractive route.[5] Dithiothreitol (DTT) could maybe help as protective reagent to prevent disulfide formation during the reactions.[13]

References:

[1] I. Schön, *Chem. Rev.*, **1984**, *84*, 287

[2] M. Frankel, D. Gertner, *J. Chem. Soc.*, **1961**, *83*, 463

[3] E. Katchalski, A. Berger, *Bull. Res. Council Israel*, **1952**, *2*, 314

[4] E. R. Blakely, A. K. Sumner, E. Y. Spencer, *Canad. J. Technol.*, **1952**, *30*, 258

[5] A. Berger, J. Noguchi, E. Katchalski, *J. Am. Chem. Soc.*, **1956**, *78*, 4483

[6] M. Hesse, H. Meier, B. Zeeh, *Spektroskop. Meth. in der org. Chemie*, **1996**, 9

[7] S. Sarid, A. Patchornik, *Israel J. Chem.*, **1963**, *1*, 63

[8] M. Sokolovsky, M. Wilchek, A. Patchornik, *J. Am. Chem. Soc.*, **1963**, *86*, 1202

[9] L. Zervas, I. Photaki, N. Ghelis, *J. Am. Chem. Soc.*, **1963**, *85*, 1337

[10] T. Kramer, T. Röder, *Synth. Comm.*, **2004**, *34*, 297

[11] O. G. Lowe, *J. Org. Chem.*, **1976**, *41*, 2061

[12] S. H. Lipton, C. E. Bodwell, *J. Agric. Food Chem.*, **1973**, *21*, 235

[13] W. W. Cleland, *Biochemistry*, **1964**, *3*, 480

Chapter 6
Poly (L-glutamic acid)-TFA films

PBLG has been deposited as a uniform film with the molecules adopting a helical conformation on different substrates like glass by solvent evaporation with or without induced orientation by shearing the solution layer during the evaporation. The obtained films exhibited ordered spherulites visible under polarized light. Even the use of "coil solvents" like DCA yielded films of the polymers in helical conformations. Increasing the acidity of the solvent did not disrupt the hydrogen bonding, which led to the helical morphology, in fact, solvents like methane sulfonic acid (MSA) lead to decomposition.[1,2,3,4]

Considerably less is known for thin film preparation of PLGA. Previously, PLGA films were successfully prepared by spin coating from TFA solutions on glass.[5] The current work utilizes drop-casting to produce thick films on silica substrates. Table 1 gives an overview of the different PLGAs synthesized during the diploma thesis, which were investigated initially.[5] It is notable that these polymers were not purified by soxhlet extraction. These samples, therefore, included a larger fraction of oligomers than the PLGA studied at later stages of this research. Some of the "old" samples were purified later by soxhlet extraction and will be designated as "PPX purified" in the experiments.

Table 6.1: Overview of the different PLGAs synthesized during the diploma thesis.

Sample	Degree of Polymerization *	Molecular Mass [g/mol]
PP1	41	5300
PP2	32	4200
PP3	62	8100
PP4	20	2700
PP5	25	3300
PP6	46	6000
PP7	22	3000
PP8	33	4400
PP9	40	5300
PP10	43	5600
PP11	48	6300
PP12	58	7600

* The degree of polymerization was calculated by the ratio of the ^{1}H-NMR integrals of backbone to initiator signals.

A first film series on silica substrates was prepared by drop-casting of 1.25 % (w/w) solutions in TFA from different samples of PLGA (PP1, PP9, and PP10). The samples were not heated to aid in the dissolution of the polymeric material to avoid possible degradation of the polymers. The silica substrates were placed in open Petri dishes standing in the hood. The evaporation of the solvent was performed at RT overnight. Uniform, translucent films were commonly obtained without any observable defects on the surface. Temperature dependent FTIR measurements were executed in order to detect the secondary structure starting at RT and to determine if there will be a change in the conformation as the temperature was elevated. The following temperatures were measured with the same sample in a continuous in-situ measurement: RT, 50, 75, 100, 125, 150, 175, 200, 210, 220, and 225°C. The film thickness of all films was in the range of 2-3 µm determined by a mechanical α-stepper. The room temperature spectrum was shown in Figure 6.1, separately from the temperature dependent curves, to allow a better identification of the initial conformation. The results were identical and reproducible for all films produced by this procedure. The secondary structure determined to be a β-sheet conformation according to the characteristic Amide I and II band signals at 1631 and 1529 cm^{-1}, respectively. The annealing process did obviously not induce any conformational change as shown below by the spectra in Figure 6.1. The total intensity of the different bands decreased due to the onset of degradation at 200°C.

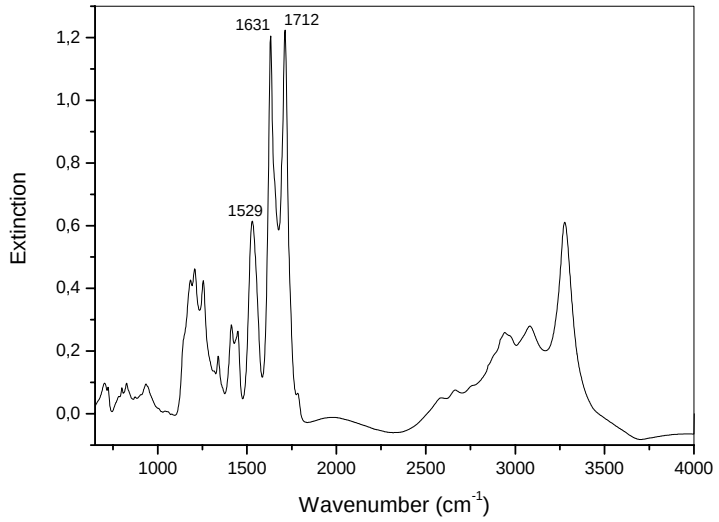

a)

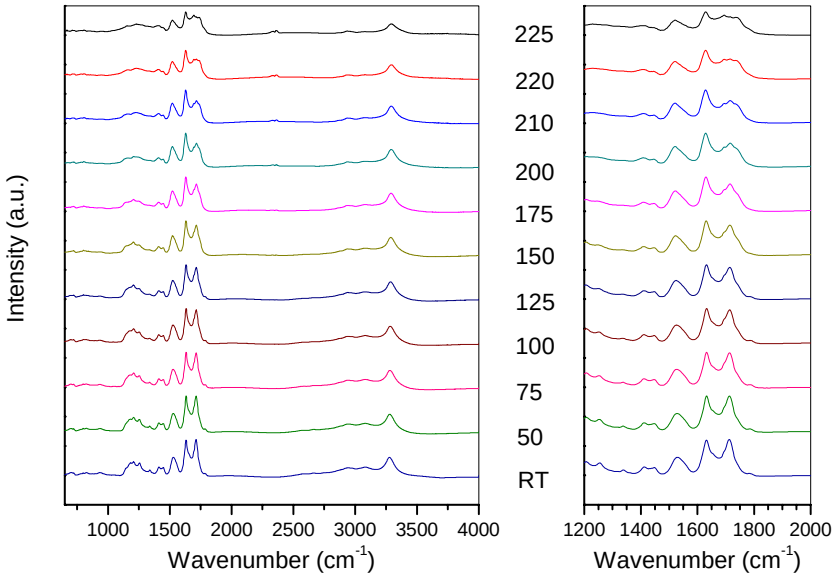

b)

Figure 6.1: a) FTIR-spectrum of a drop-cast PLGA film (PP1; 1.25 % (w/w) in TFA), RT. b) Temperature dependent FTIR spectra from RT up to 225°C.

The effect of the following parameters on the film properties were analyzed in a second series of experiments:

a) The film thickness was reduced.
b) The evaporation procedure (storage in the hood or in the vacuum oven).
c) Removal of the water content of TFA by adding a small amount of TFA-anhydride (0.05 % (v/v)).

Films were drop-cast in the second series from a 1.25 % (w/w) TFA solution on silica. The evaporation was slowed down to 3 days by using closed Petri dishes placed in vacuo. The film thickness was successfully reduced to 1 µm for all films in the second series. The spectra obtained demonstrated a clear correlation between the film thickness and the conformation of the polymer. The thinner films exhibited a mixture of β-sheets and α-helices, which were stable over the investigated temperatures. The fraction of each conformation was calculated by a Gaussian deconvolution of the overlapping Amide I bands. The ratio of the areas delivered the percentage of each conformation present. Figure 6.2 and 6.3 show that this ratio of secondary structures remained constant and no structural change was observed.

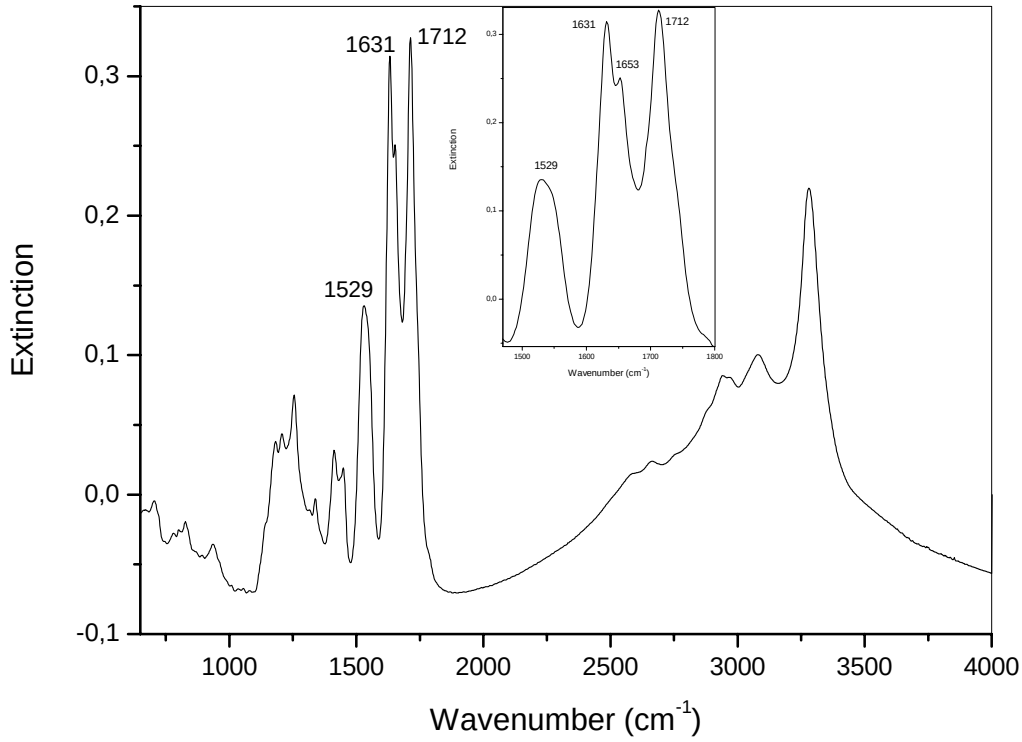

a)

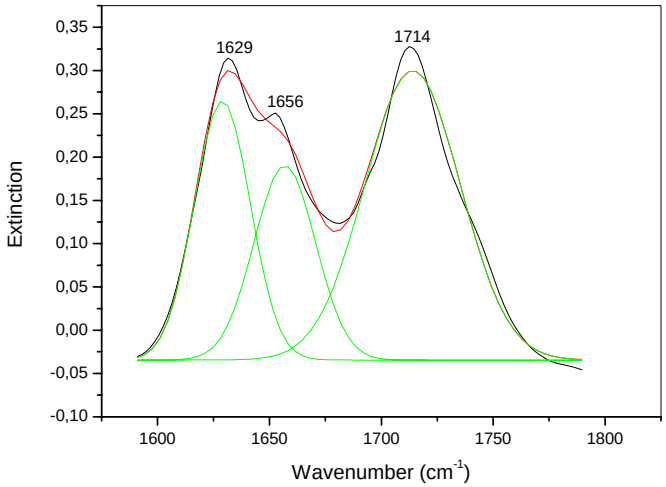

Peak	Area	Center	Width
1	9.3844	1628.9	25.002
2	7.7379	1656.9	27.487
3	17.867	1714.0	42.624

helix : sheet = 0.45 : 0.55

b) c)

Figure 6.2: a) FTIR-spectrum of a drop-cast PLGA film (PP1; 1.25 % (w/w) in TFA) at RT. b) Gauss peak deconvolution of the RT spectrum in the range 1600-1800 cm^{-1}. c) Integration results for the deconvoluted peak areas.

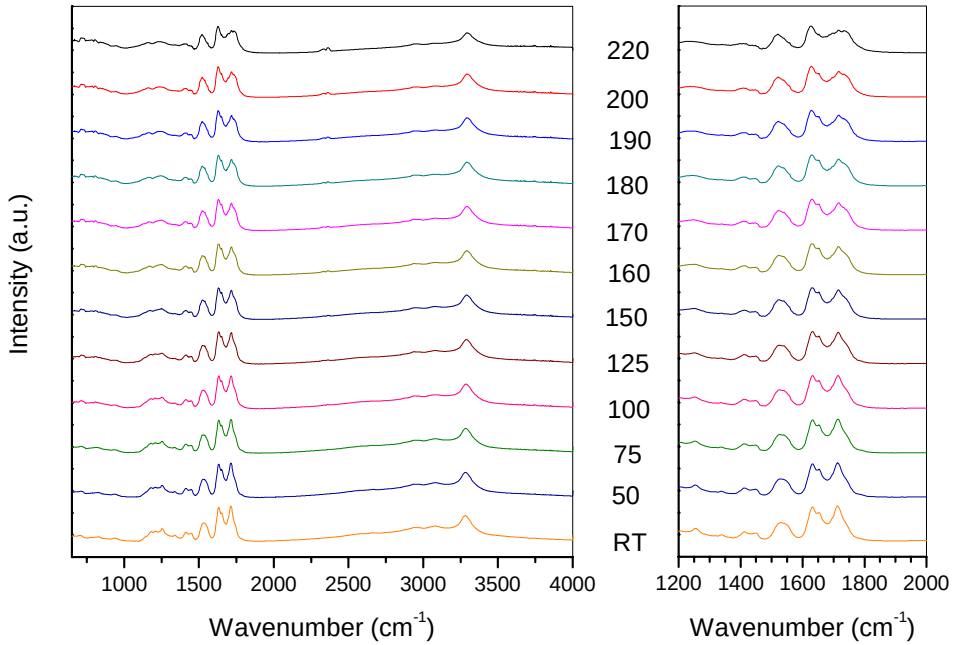

Figure 6.3: Temperature dependent FTIR spectra of a drop-cast film of PLGA (PP1; 1.25 % (w/w) in TFA) from RT up to 220°C.

The effect of the water content of TFA was analyzed, while all of the other parameters remained fixed. TFA anhydride (0.05 % (v/v)) was added to remove water from the highly hygroscopic TFA. The corresponding spectra and calculations are shown in Figure 6.4.

Reducing the water content led to a higher fraction of β-sheet conformation in the film as compared to the untreated TFA system. The obtained mixture of conformations was stable throughout the temperature range investigated. The different ratios of conformations obtained indicate that the water content of the TFA may induce changes in the film morphology of PLGA drop-cast films. It was that PLGA dissolved much better in TFA than in really dry TFA (with added anhydride). Obviously, the water supported the dissolving process by solving the formed salts consisting of the TFA anion and the protonated polypeptide chain.

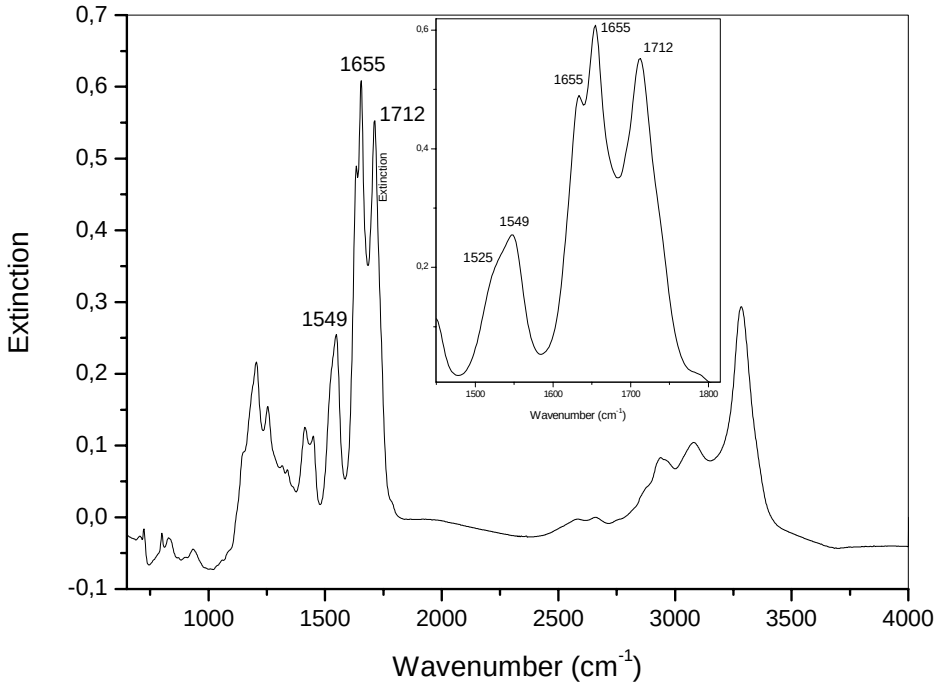

a)

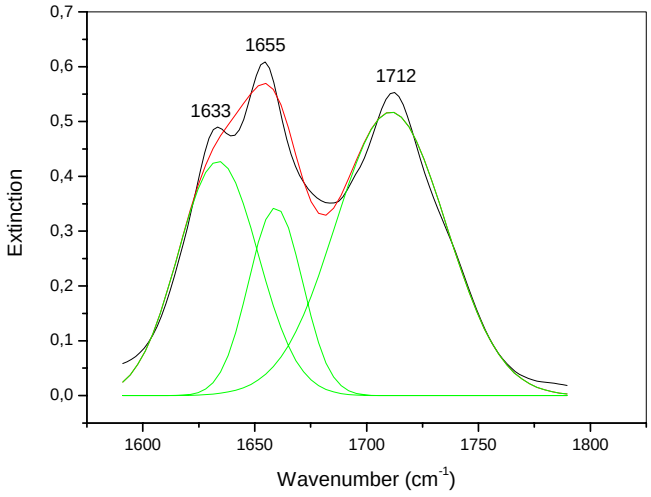

b)

Peak	Area	Center	Width
1	19.125	1633.6	35.694
2	10.366	1659.3	24.131
3	31.891	1710.8	49.188

helix : sheet = 0.35 : 0.65

c)

Figure 6.4: a) FTIR-spectrum of a drop-cast film of PLGA (PP10; 1.25 % (w/w) in TFA + 0.05 % (v/v) TFA anhydride) at RT.
b) Gauss peak deconvolution of the RT spectrum in the range 1600-1800 cm^{-1}.
c) Integration results for the deconvoluted peak areas.

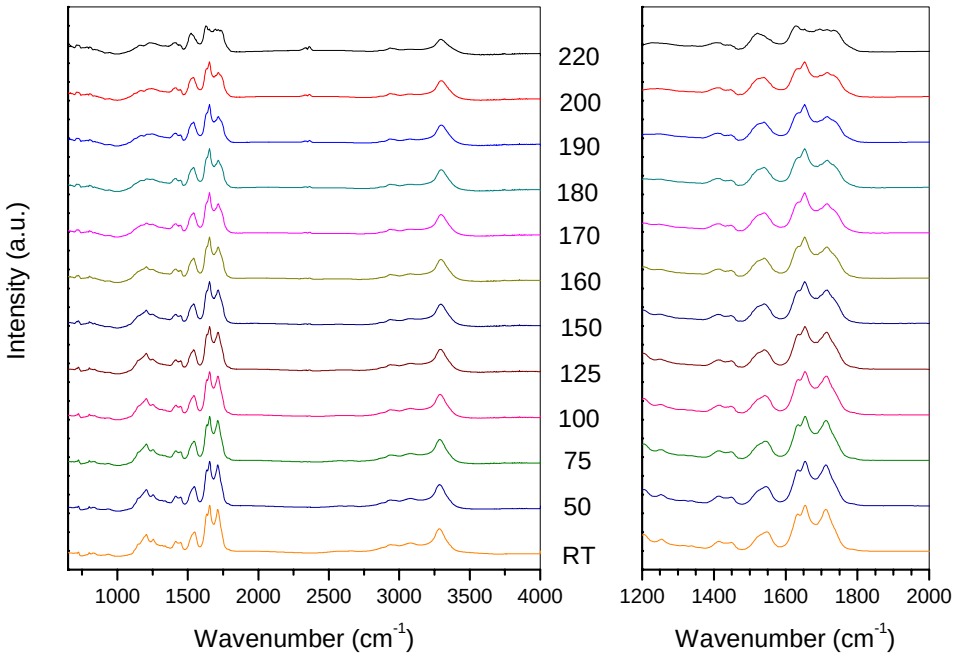

Figure 6.5: Temperature dependent FTIR spectra of a drop-cast film of PLGA (PP10; 1.25 % (w/w) in TFA + 0.05 % (v/v) TFA anhydride), RT to 220°C.

A third film series was investigated under the conditions of earlier work.[5] The films were spin-cast from a 1.25 % (w/w) TFA solution of PLGA (PP10) on silica. Temperature dependent FTIR studies were measured with the following temperatures: RT, 50, 75, 100, 125, 150, 160, 170, 180, 190, 200, 210, and 220°C.

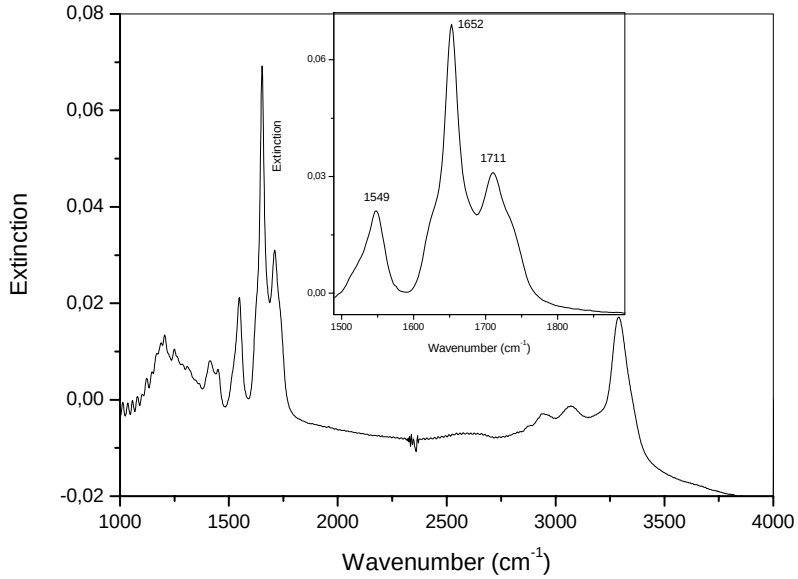

Figure 6.6: FTIR-spectrum of a spin-cast film of PLGA (PP10; 1.25 % (w/w) in TFA),RT.

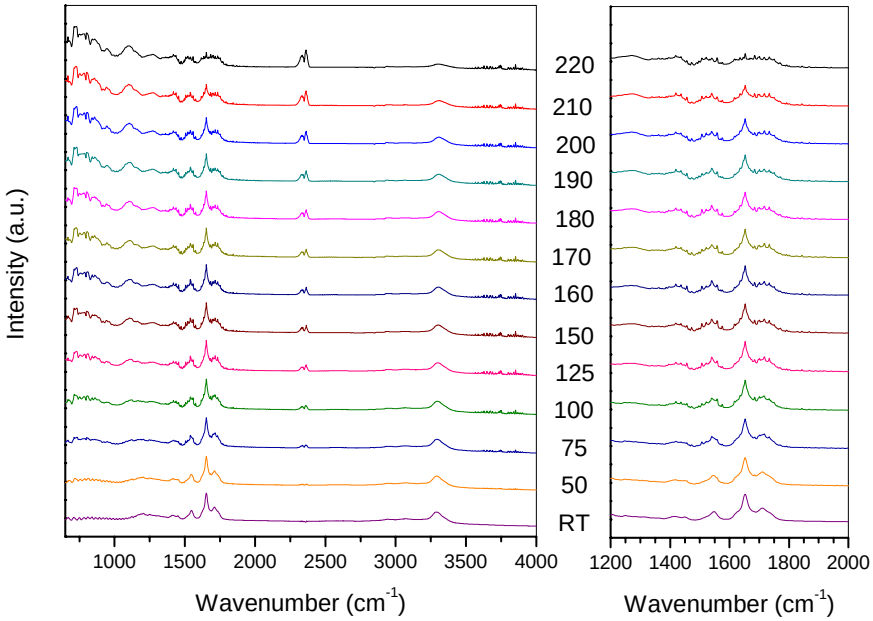

Figure 6.7: Temperature dependent FTIR spectra of a spin-cast film of PLGA (PP10; 1.25 % (w/w) in TFA) from RT up to 220°C.

The spectra obtained showed a film with only helical confirmation without any indication of β-sheet conformation. The reduced evaporation time and the applied rotational forces may be contributing factors. The film thickness produced by spin-coating, which lies approximately in the nm range, may also play a crucial role. Unfortunately the signal to noise ratio in IR measurements were so low that the recording of a reliable IR spectrum with very thin films became difficult. A spectrum clearly indicating a helical conformation is shown in Figure 6.6.

The storage of the substrates during solvent evaporation seemed to have little to no effect on the conformation of the PLGA. Films were prepared from both solvent systems (TFA and TFA treated with TFA anhydride) every time under both conditions (hood and vacuum oven) without a significant observable change. The purification of the substrates did not effect the results. The silica substrates used in these experiments were cleaned by soaking them for 30 minutes in TFA, 15 min in MQ-water in an ultrasonic bath (USB) and were finally 15 min in ethanol in an USB. Some new unused silica substrates were cleaned without the TFA treatment in order to assure the validity of the regular cleaning procedure. No difference was observed for the film results with different cleaning procedures. The contact angles of the substrates against water were measured by drop shape analysis to explore the hydrophilicity of the surface. Glass substrates showed a

highly hydrophilic character (5-8°) in contrast to fresh silica (30-40°) and TFA cleaned reused silica (60-80°).

Polarized optical microscopy studies showed ribbon-like structures in drop-cast PLGA (PP7) films from 2 % (w/w) solutions on cover glass, which were temperature stable until the degradation temperature was passed. The following pictures in Figure 6.8 were collected by using the heating stage of an optical microscope in dynamic heating experiments.

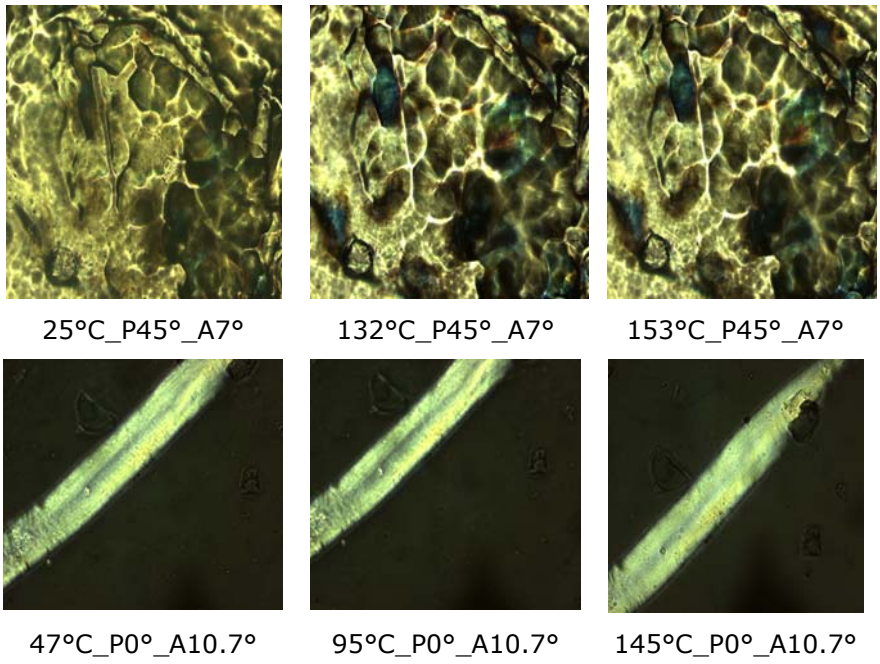

Figure 6.8: POM pictures of a drop-cast PLGA film (PP7) on cover glass. (Magnification is 20x in the first row, 50x on the second row). Polarizer and analyzer angles are given together with the corresponding temperatures.

FTIR dichroism studies were attempted for PLGA (PP7) drop-cast films prepared from TFA, DMA, TMU, and NMP solutions by using polarized infrared radiation in order to detect a possible orientation in the films. Unfortunately the IR spectra exhibited identical intensities for the dichroism sensitive bands regardless of the orientation of the polarized radiation sent through the sample in transmission. Therefore, no dichroic ratio could be calculated indicating that the helices or sheets are totally randomly distributed. This assumption was confirmed by X-ray diffraction measurements of the TFA drop-cast films. Different approaches were attempted to determine if there is any long range order present in the drop-cast films.

Two different samples of PLGA (PP7 and PP12) were drop-cast in an open Petri dish from a 1 % (w/w) solution in TFA. The obtained films were rolled, placed in a glass capillary, and measured in a 2-dimensional in-situ temperature dependent XRD experiment with the following temperatures: 30°C, 100°C, 150°C, 170°C, 190°C, and back to 30°C. PP7 exhibited the best results, illustrated in Figure 6.9.

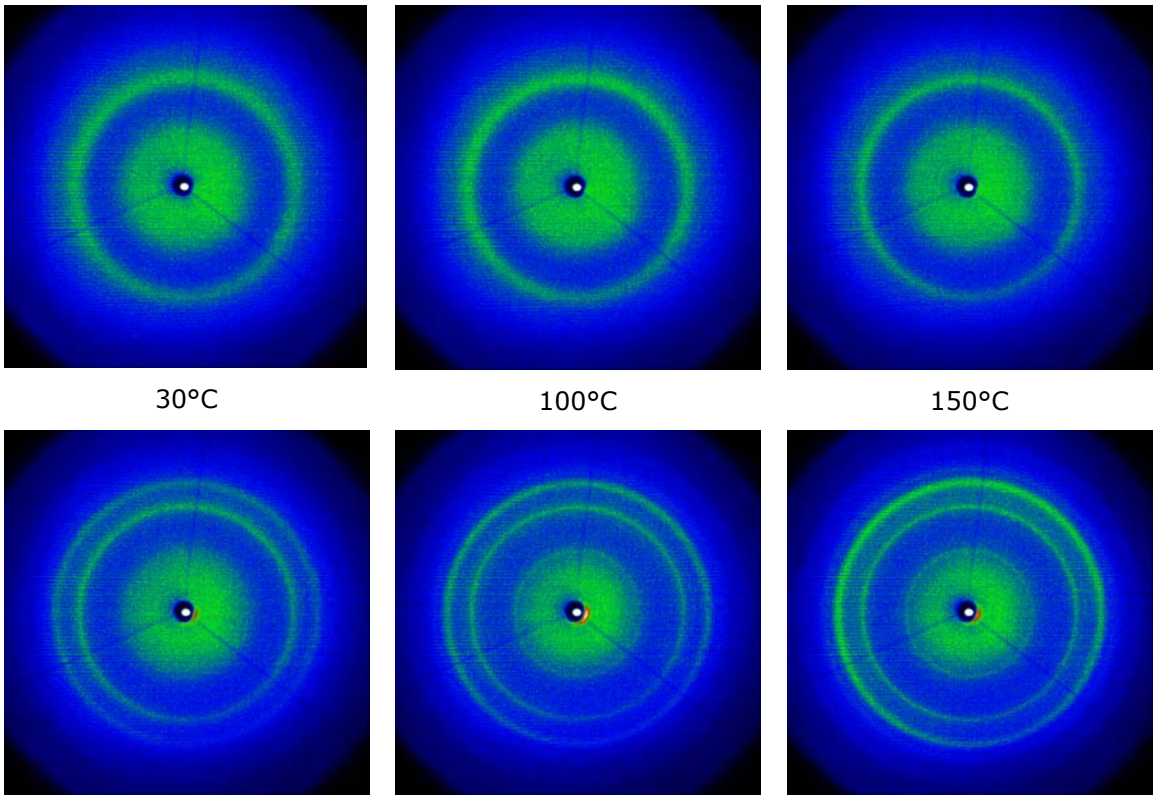

Figure 6.9: 2D-WAXS pictures of a drop-cast film of PLGA (PP7), rolled in a glass capillary at different temperatures in an in-situ annealing experiment.

An increase of the total number of reflexes observed increased with temperature. At the beginning of the experiment there was only one diffuse ring detectable, but at 170°C a second ring and at 190°C even a third diffuse ring appeared. This indicated an increase in the molecular order as the temperature increased, which persisted after cooling the specimen back to room temperature. A long-range order or an increased orientation could not be observed in IR dichroism studies. The appearance of the small intense reflection close to the beam stop is caused by a slightly thermal movement of the sample itself in the capillary.

Temperature dependent IR studies on films prepared from PLGA solutions (PP8) of both TFA solvent systems (dried / not dried) on silica, glass, or copper did not reveal any long range order or change of the spectra dependent on the temperature. The spectra (not shown) exhibited only a broad amorphous halo with a located maximum at 17-20° (2 θ). Concluding, neither drop-casting nor spin coating were suitable to induce a long-range orientation of the ordered local segments of helices and sheets.

PLGA (PP9) was coated once from 20 g/l TFA solutions on aluminum plates as coating material in the offset printing process. The sample imaged by IR-laser showed a very strong contrast, although the printing run length was only around 25 pages because most probably the polymer film was washed out by ink and fountain water during the printing.

PLGA films were reproducible prepared from the "coil" solvent TFA. The influence of the film preparation method (spin-coating versus drop-casting), solvent water content, film thickness, and substrate material was investigated. No polypeptide films were produced consisting of a coil conformation under the conditions investigated. Even the application of a solvent like TFA, which disrupts the hydrogen bonding leading to a coil conformation in solution, delivered exclusively α-helix and β-sheet conformations, as a pure conformation or as mixtures of both. No changes in the secondary structures of the polypeptide films were observed as a function of temperature, which means that not enough thermal energy could be added to the system to melt the helix before thermal degradation of the material itself would occur. The X-ray diffraction patterns of different films prepared from several solvents exhibited no long range order. Future studies should examine slower evaporation processes to increase the order of the PLGA films.

References:

[1] H. R. Kricheldorf, E. T. K. Haupt, *Int. J. Biol. Macromol.*, **1983**, *5*, 237

[2] M. Idelson, E. R. Blout, *J. Am. Chem. Soc.*, **1958**, *80*, 4631-4634

[3] M. Rinaudo, A. Domard, *Biopolymers*, **1975**, *14*, 2035

[4] M. Rinaudo, A. Domard, *Biopolymers*, **1976**, *15*, 2185

[5] M. Dietz, *Diploma Thesis*, **2004**, Mainz, *MPIP*

Chapter 7
Poly (L-glutamic acid)-Crystallizations

7.1 Introduction

The formation of lyotropic crystalline systems were reported in literature for PBLG and other poly(γ-alkyl-L-glutamate)s in a variety of common organic solvents.[1,2,3] The liquid crystalline phase occurred at a critical concentration, which was strongly dependent upon the identity of the solvent, molecular weight of the polymer and temperature. The association in aggregating solvents was partially to inter hydrogen bonding between end residues that did not sustain the helical conformation, as well as from dipolar interactions.[4,5] These findings were in agreement with Flory´s theory that increased flexibility of side chains favors solubility of the helical conformation.[6] In concentrated solutions in solvents that favored the helical conformation, isotropic solutions of poly(glutamates) became biphasic as observed by Robinson et al. [2,7] High molecular weight polymers formed lyotropic liquid crystals at lower concentrations than low molecular weight polymers. Solutions of poly(glutamates) with DP < 100 exhibited to a much lesser extent liquid crystal character.[8] Thermotropic cholesteric mesophases were reported for copoly(glutamates) based on PBLG and γ-alkyl-L-glutamates (n=8,10,12,14 and 16).[9] Transformation of a crystalline phase was detected as a first order transition in DSC measurements and was determined to be reversible in both the heating and cooling cycles.

The group of Mori published a series of studies about PLGA and its liquid crystalline character in the following helical solvents DMF, DMA, DMI (1,3-dimethyl-2-imidazolidone), NMP, NMF (n-methylformamide) which gave rise to be attempted during our work.[10-19] Higher molecular weight polymers produced via different polymerization (AM-Mechanism) possessed higher solubilities than presented in the current work. The lower solubilities of the polymers prepared for this study were especially noticed during the molecular weight characterization of PMLG, PSLG and their corresponding copolymers. The PLGA prepared for this study could not be dissolved in as high of a concentration as was used by Mori (30 % (w/w)). A maximum solubility of 5-10% (w/w) was possible, even with heating and stirring for a week. PLGA lyotropic cholesteric liquid crystals and the corresponding phase diagrams of PLGA in the solvents DMA, NMA, DMF, NMF, NMP, DMI were intensively studied in solution by Mori et al. [10-16,19] Some of these proposed lyotropic solvent systems were used for film preparations of PLGA on glass in the current work. The films were analyzed by POM and the pictures exhibited good liquid crystalline structures as shown in Figure 7.1.

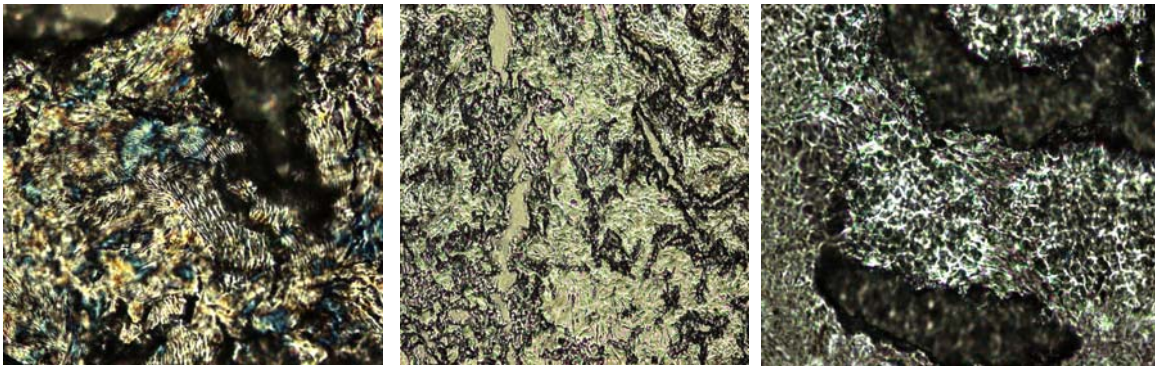

75° P, 2.6° A, DMA, 50x 75° P, 11.7° A, NMP, 50x 75° P, 1.1° A, TMU, 50x

Figure 7.1: POM pictures of lyotropic liquid crystals of PLGA in different solvents. The solvent, magnification, polarizer and analyzer angle is described below the pictures.

Keith et al. pioneered the crystallization investigations for PLGA by studying the solid state structure of PLGA and its alkaline earth salts.[20] Keith, Padden et al. reported that such polypeptides exit as the β-sheet in the crystalline form. Lamellar single crystals of alkaline earth salts of PLGA were grown by precipitation from dilute aqueous solution and studied by optical and electron microscopy and by X-ray and electron diffraction. The calcium, strontium and barium salts were crystallized in the β-sheet above room temperature and could be converted to crystals of the β-sheet PLGA by washing in dilute hydrochloric acid. The magnesium salt, on the other hand, was crystallized in the α-helix at or below room temperature, but could not be converted into crystals of PLGA by washing with dilute HCl. The crystalline lamellae were thin (25-60 Å in β-sheet crystals and about 100 Å in α-helix crystals). It was found by the disparity between crystal thickness and molecular length that the molecules crystallize by folding at the upper and lower surfaces of the crystals. PLGA was determined to be extremely soluble in the presence of monovalent counterions such as sodium or ammonium. Keith decided to investigate the influence of alkaline earth salts since doubly charged cations were expected to provide electrostatic links between carboxylate ions on different molecules and thus encourage precipitation of the polymer. Chain folded crystals were detected of both the α-helix and β-sheet. The earth alkaline salts were obtained by slowly heating the aqueous solutions containing sodium or ammonium PLGA and a soluble salt of the corresponding alkaline earth in a large excess (> 10x) of the alkaline earth metal in the form of an acetate or nitrate. They used another method for the preparation of the α-helical Mg salt. Ethanol, a nonsolvent, was added to a solution of NaPLGA and Mg acetate.[21]

The first crystallization studies for poly(glycine), poly(alanine), and poly(tyrosine) were conducted by casting films on glass and allowing the solvent to evaporate slowly. Mixtures of TFA and TFE (trifluoroethanol), with water as nonsolvent, were utilized for casting the films yielding ribbon-like crystals. Films cast from solutions containing TFA clung tenaciously to glass surfaces, even those coated with an evaporated layer of carbon. In all, 20 solvent systems were investigated to determine the best solvent for crystal growth.[22]

It is noteworthy that the X-ray powder patterns indicated an amorphous morphology. However, it must be emphasized that “amorphous” X-ray patterns of polypeptides or proteins and polymers like poly(ethylene), poly(propylene), poly(propyleneoxide) and poly(caprolactone) do not have the same meaning. The X-ray pattern yields information on the long range order (or disorder) of the polymer, which in the case of most synthetic polymers is closely connected to the short range (or local) order of the polymer chains. Local order in this case refers to the conformations of individual monomers in short chain segments. However, proteins may possess a high degree of local order combined with a low degree of long range order. In such a case most chain segments possess the most energetically favorable conformation; however this conformation varies with the nature and sequence of the amino acid units. The chain segments having different conformations are linked to each other by one, two or more amino acids with unfavorable conformations. Thus the entire chain possesses a long range disorder, although more than 90% of all monomer units exist in highly ordered local conformations. Furthermore the packing of several polypeptide chains may be disordered despite a high degree of conformational order (e.g. packing of helices). Thus it may happen that techniques, like ^{13}C-CP/MAS NMR and IR, which mainly identify the conformations of polypeptides, indicate a highly ordered secondary structure, whereas the X-ray pattern manifests a predominantly amorphous character of the sample. These two levels of information must be taken into account, when both methods are combined for the characterization of proteins.[23]

Films can possess high crystallinity or liquid crystalline behavior at high concentrations. Orientation in films can be induced due to the surface properties of the substrate like different wettability on silica or glass or by stroking/shearing of the cast solution during the evaporation of the solvent. The ordered spherulites obtained will be visible in a polarizing microscope and can be analyzed by X-ray experiments.[24,25]

The degree of crystallinity is then given by Equation 7.1.

$$\%\chi = \frac{I_c}{I_a + I_c} \times 100 \qquad (7.1)$$

I_c and I_a are the total intensity scattered by the crystalline and amorphous regions, respectively. The scattered intensity was commonly measured in a finite range, typically 2θ=2-32° using $CuK_{\alpha 1+2}$ X-ray radiation (1.5418 Å). However, at higher scattering angles the intensity curve for a semi-crystalline polymer often becomes more or less featureless due to distortions.

The radial (2θ) broadening of the reflections is due to a small crystallite size. Braggs Law, shown in equation 7.2, requires that reflection occurs only at the angle θ. However this condition was derived for an infinite crystal but for finite crystals the reflections have a finite width.

$$n\,\lambda = 2\,d\,\sin\theta \qquad (7.2)$$

This is especially true because with polymers, the ordered regions may extend only a few unit cells in each direction. The crystallite size becomes the dominant effect in the broadening of the reflections. The width at half height (B_{hkl}) was determined from the spectra for each particular hkl reflection. B_{hkl} is related approximately to the crystallite size (L_{hkl}) through the Scherrer equation. The crystal dimensions are typically in the range 30-200 Å.

$$L_{hkl} = \frac{0.9\,\lambda}{B_{hkl}\,\cos\theta} \qquad (7.3)$$

θ: Bragg angle of the reflection.

B_{hkl}: Width at half height, expressed in radians.

The broadening of the signals leads to significant overlap of the reflections. The small crystallites are also significantly distorted, with the result that relatively few reflections are observed at d < 2Å. With so few reflections it is not possible to apply the statistical methods that are used to solve the structures of crystals of low molecular weight compounds, for which significantly more Bragg reflections are commonly observed. Therefore, the only way to solve structures is by trial and error. The unit cell must first be predicted and then a model has to be constructed, which gives the best agreement between the observed and calculated intensities.

7.2 The model system PBLG

PBLG was used as model system. After several unsuccessful attempts to produce uniform films, uniform films were drop-cast from $CHCl_3$ solutions.

Solutions of PBLG (MD-1-2) 5 % (w/w) and 2.5 % (w/w) $CHCl_3$ were drop-cast on freshly cleaned silica substrates. All films exhibited highly uniform thicknesses, but most of the films proved to be too thick for IR measurements due to low transmission of the samples. The only sample thin enough to be measured was ca. 6.3 µm thick. A temperature dependent IR series was measured in transmission. The spectra are shown in Figure 7.2 and did not reveal any change of the secondary helical structure dependent upon the temperature.

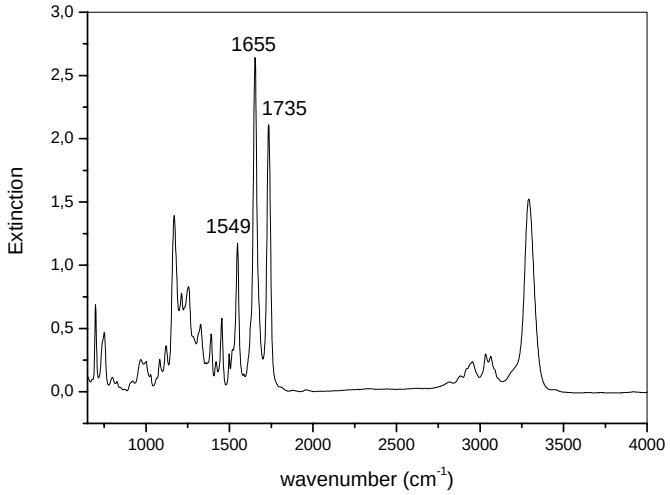

a)

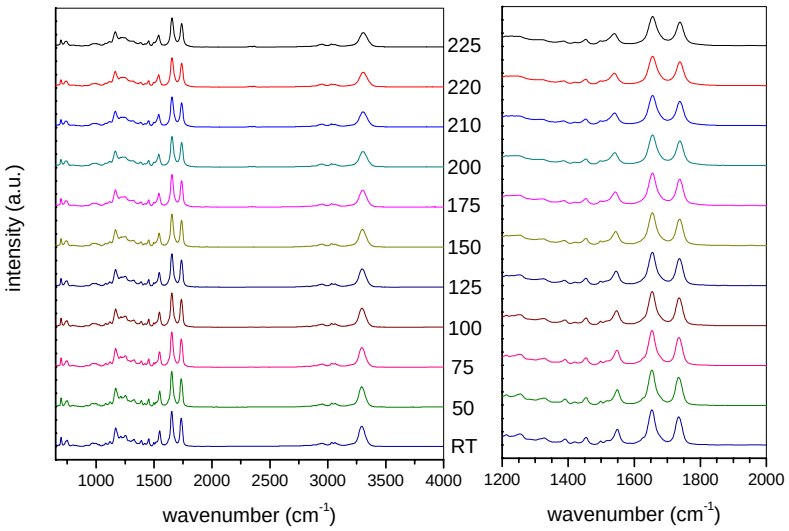

b)

Figure 7.2: a) FTIR-spectrum of a drop-cast film of PBLG (2.5 % (w/w) in $CHCl_3$) at RT. b) Temperature dependent FTIR spectra from RT up to 225°C on silica.

The same solution was used to prepare PBLG films on copper to conduct temperature dependent XRD patterns. No melting of the helix was detected. The spectra were consistent with the results of Floudas et al. who mechanically extruded fibers of PBLG.[26]

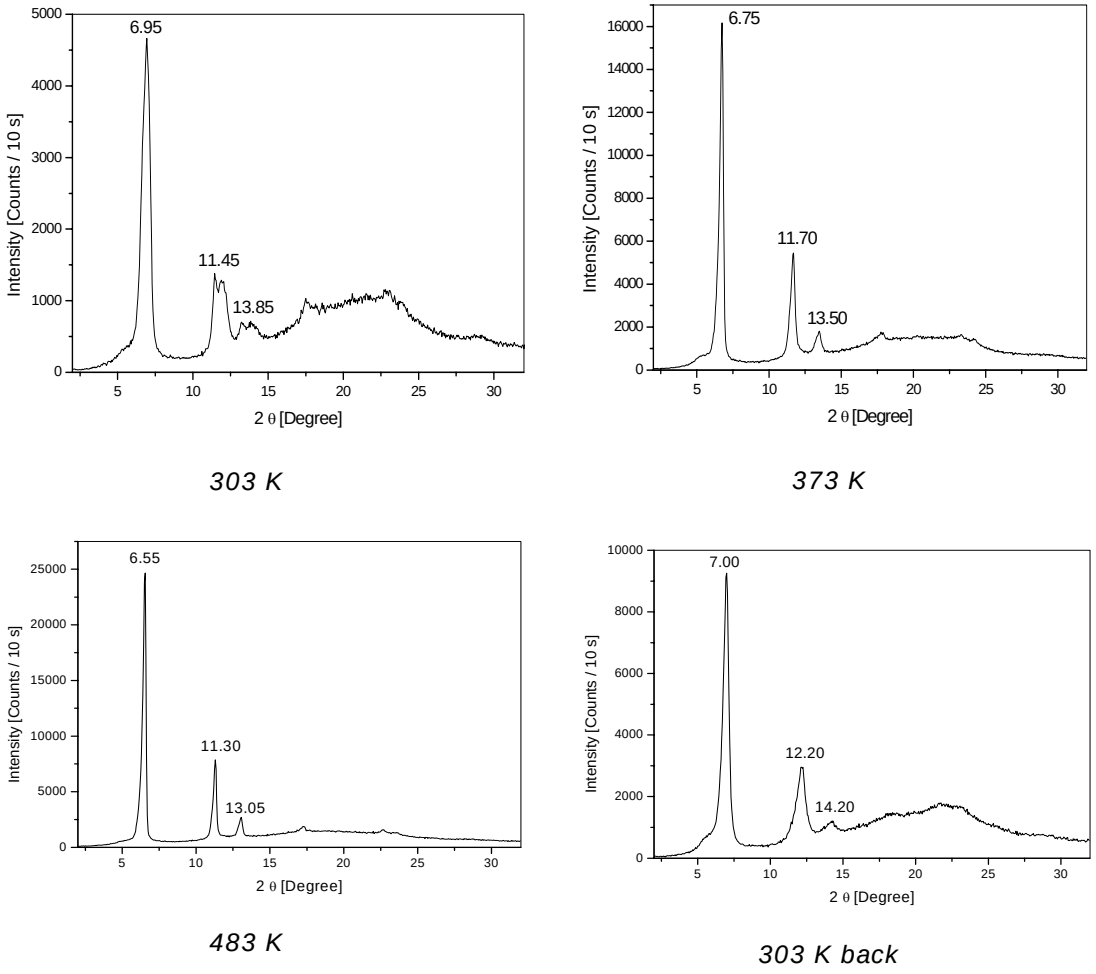

Figure 7.3: Temperature dependent WAXS of a drop-cast film of PBLG solutions (2.5 %wt in $CHCl_3$); 0.025 step scan with 10 s.

Temperature dependent XRD of drop-cast films of 2.5 % (w/w) PBLG solutions in $CHCl_3$ were measured on glass and on silica with a 0.03 step scan with 4s.

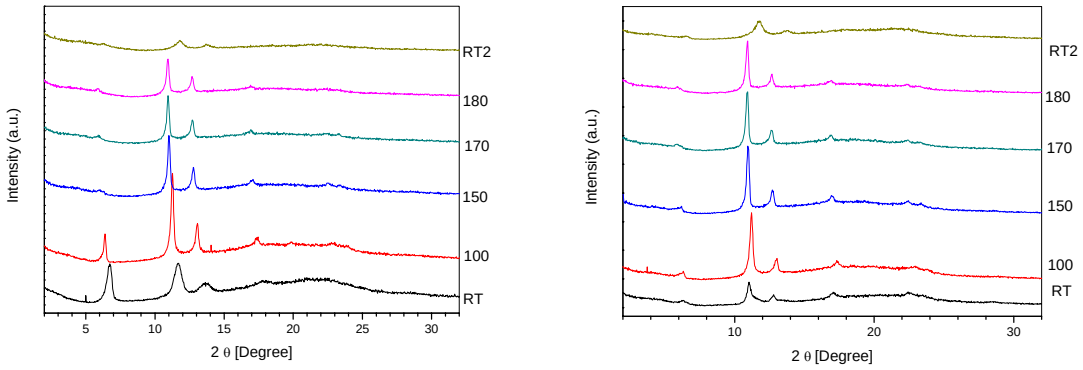

Figure 7.4: Temperature dependent WAXS of a drop-cast film of PBLG from a 2.5 % (w/w) $CHCl_3$ solution on glass (left) and on silica (right); 0.03 step scan with 4s.

Only intensity variations are observable but no significant changes ruling out the occurrence of any structural reorientation or phase transition.

7.3 Hydrogen-bonded complexes of PLGA with pyridine

In 1988, Kato and Frechet discovered that mesogenic structures could be obtained by self-assembly of pyridine and carboxylic acid fragments through the formation of intermolecular hydrogen bonds. This novel family of supramolecular thermotropic liquid crystals, based upon hydrogen bonded complexes, was prepared by an evaporation technique from a pyridine solution containing an equimolar amount of H-bonding donor and acceptor moieties followed by drying in vacuum at elevated temperatures. The successful formation of a hydrogen bonding complex between the carboxylic acid and the pyridine moieties was confirmed by infrared spectroscopy. The OH stretching band appeared at 2500 and 1900 cm^{-1} due to the strong hydrogen bonding of the complex.[27-33]

PLGA is not soluble either in pyridine or water, but was found to be soluble in various mixtures of pyridine and water. A significant amount of water was required to dissolve the formed pyridinium. The formation of the hydrogen-bonded complex is shown in Figure 7.5. The azeotropic point for a pyridine-water mixture is around 58.7 % pyridine.

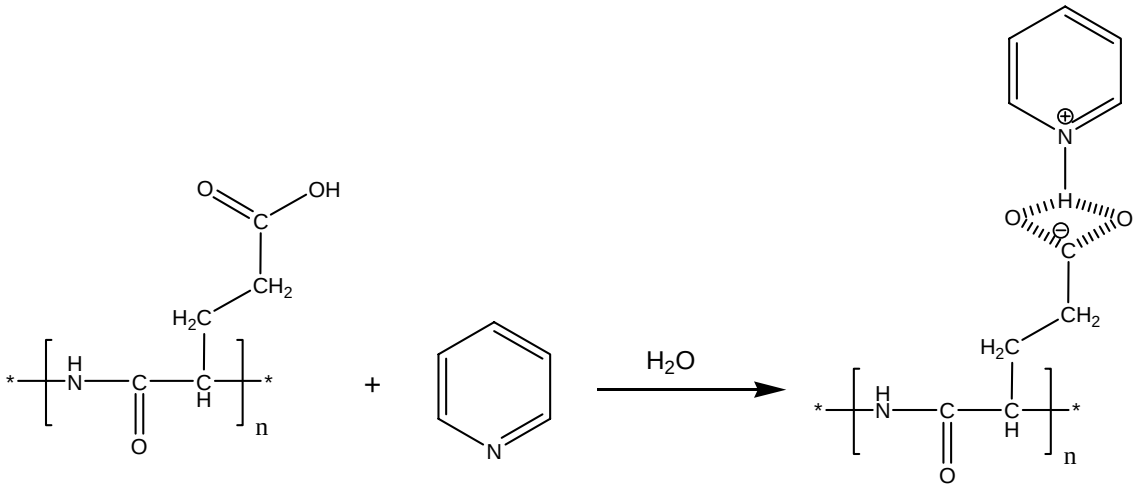

Figure 7.5: Formation of a hydrogen bonded complex between PLGA and pyridine in H_2O.

The first film preparation attempts were conducted with a PLGA solution of 10 g/l in a mixture of 3/1 (v/v) of pyridine/water. The solutions were drop-cast either on glass or silica substrates. The substrates were stored in closed Petri dishes during the evaporation of the solvent. One layer of solution was placed at the beginning on the top of the surface. The solvent mixture was removed after one day. The hydrogen bonded complex was adhered strongly to the glass surface and was not possible to remove it from the substrate surface. The XRD analysis was performed without determining a change to the original powder spectrum. The films prepared on silica were in contradiction easily removed from the substrate. The XRD analysis of the films on silica was performed in

reflection without removing the films from the substrate. The films exhibited a partially crystalline pattern with an amorphous halo and several very sharp crystalline reflections on the top of the halo. The spectra of MD52 and MD57 are shown in Figures 7.6 and 7.7 as examples. The position of the crystalline signals are marked in the spectra and transformed to the corresponding d-spacings according to Equation 7.2.

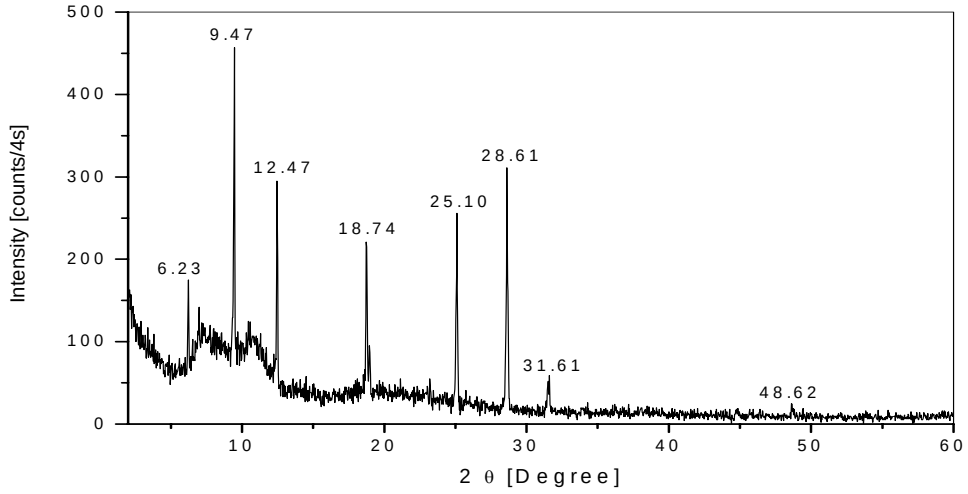

Figure 7.6: XRD pattern of a drop-cast PLGA film prepared from pyridine/water mixture (3/1) on a silica substrate [MD52]; 0.03 step scan with 4s.

Table 7.1: Crystalline Bragg reflections of MD52 in 2 θ with corresponding d-spacings.

2 θ [Degree]	6.23	9.47	12.47	18.74	25.10	28.61	31.61	48.62
D-spacing [A]	14.15	9.31	7.08	4.72	3.54	3.11	2.82	1.87

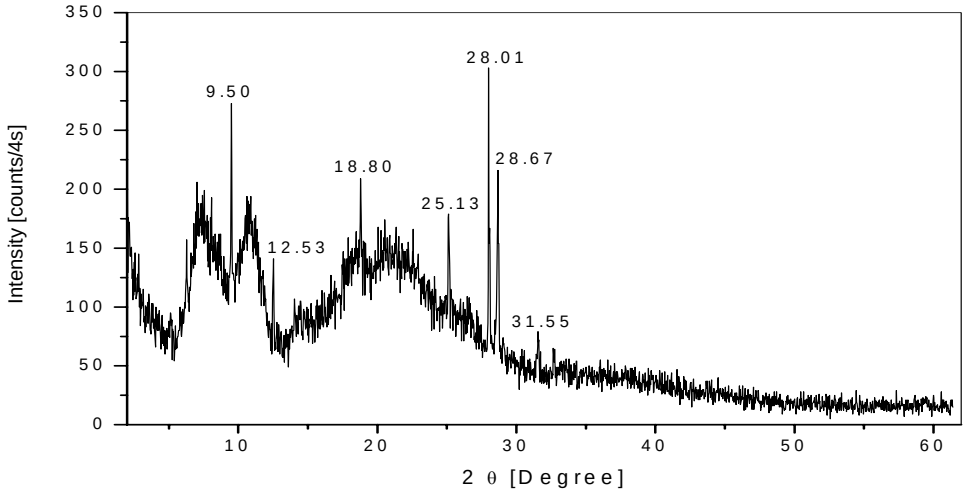

Figure 7.7: XRD pattern of a drop-cast PLGA film prepared from a 3/1 (v/v) pyridine/water mixture on a silica substrate [MD57]; 0.03 step scan with 4s.

Table 7.2: Crystalline Bragg reflections of MD57 in 2 θ with corresponding d-spacings.

2 θ [Degree]	9.50	12.53	18.80	25.13	28.01	28.67	31.55
D-spacing [A]	9.28	7.05	4.71	3.53	3.18	3.11	2.83

Film MD56 can be defined as almost completely crystalline, proven by the absence of the amorphous halos and by the appearance of many sharp crystalline signals. Figure 7.8 shows a temperature dependent XRD measurement of MD56. The film was annealed in a copper heating stage.

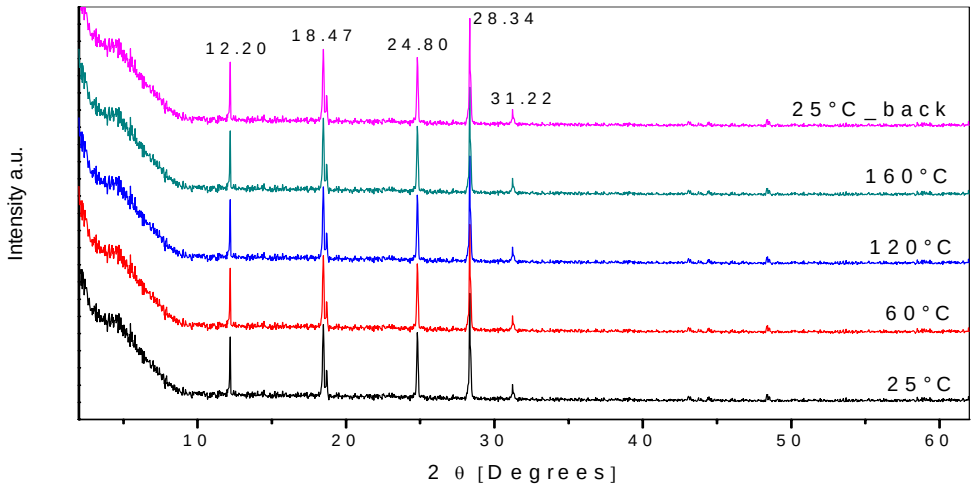

Figure 7.8: Temperature dependent XRD pattern of a drop-cast PLGA film prepared from a 3/1 (v/v) pyridine/water mixture on a silica substrate [MD56]; 0.03 step scan with 4s.

Table 7.3: Crystalline Bragg reflections of MD56 in 2 θ with corresponding d-spacings.

2 θ [Degree]	12.20	18.47	24.80	28.34	31.22
D-spacing [A]	7.24	4.79	3.58	3.14	2.86

The crystalline signals listed in Table 7.3 did not shift in position, nor did the shape of the peak or the intensity ratio change as the temperature was varied. The annealing process was stopped at 160°C to avoid a possible degradation of the sample whose degradation temperature was determined by TGA to be at approximately 200°C.

The obtained PLGA-pyridine complex was investigated by a variety of techniques.

The thermal behavior was analyzed by TGA, TGA-MS and DSC measurements. TGA and TGA-MS were different than the same measurements on the original powder spectrum of PLGA. The TGA shown in Figure 7.9 was measured with a heating rate of 10 K/min and had two steps instead of one step. The first step represented a significant mass loss whereby the second one represented the already known thermal degradation of PLGA (T_{d2}) at 235°C. The first step located at 135°C had a mass loss of ca. 20%, which corresponded to the evaporation of pyridine as confirmed by TGA-MS. The TGA-MS spectrum shown in Table 7.10 was measured from 25-300°C with a mass detection from 0-100g and a heating rate of 5K/min. Pyridine signals at 79, 80 g and aromatic fragments of 51 and 52 g indicated the removal of pyridine.

Table 7.4: Thermal degradation temperatures measured by TGA
(Heating rate: 10 K/min, N_2, 25-900°C).

PLGA film prepared from 70/30 (v/v) of pyridine/water mixtures	Degradation Temperature T_d [°C]	Percentage [%]
40 g/l	135	97
(W-6288)	235	79
10 g/l	135	98
W-6289	235	88

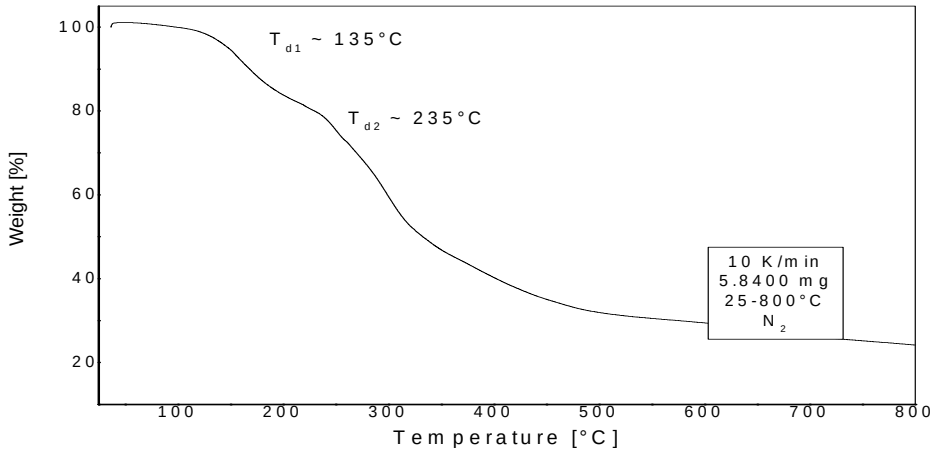

Figure 7.9: TGA of the PLGA-pyridine complex.

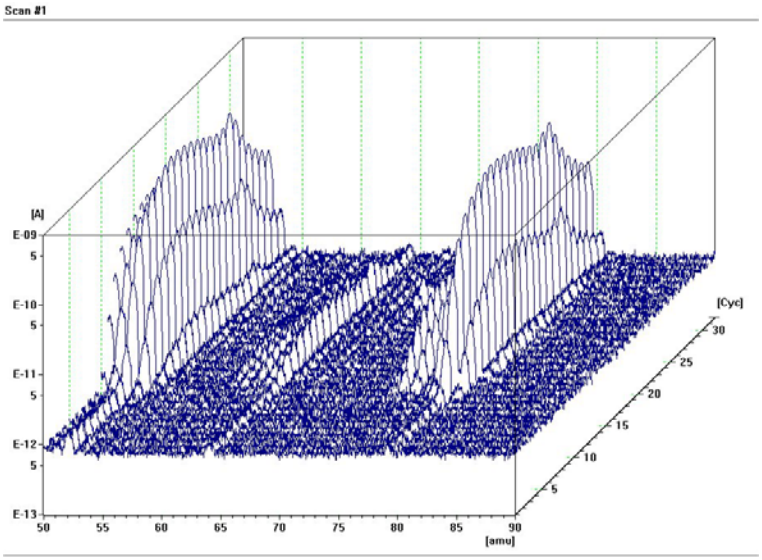

Figure 7.10: TGA-MS measurement of the PLGA-pyridine complex prepared from 40 g/l solution of a 3/1 (v/v) mixture of pyridine/water (EM-730).

The TGA-MS interpretation in combination with the temperature dependent XRD measurement of MD56 illustrated that the hydrogen bonded complex of PLGA with pyridine was crystallizing in a specific manner and remained constant even after the complete loss of pyridine by annealing. The pyridine stabilized therefore the ordered arrangement of the PLGA chains without being incorporated in the crystal structure.
The DSC trace exhibited two irreversible endotherm located at 100°C and 160°C in the first heating run and a glass transition at 87°C in the second heating run.

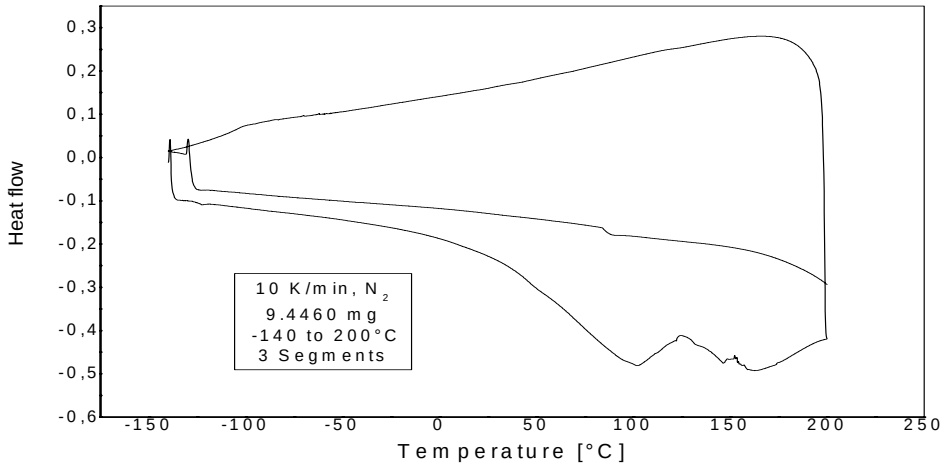

Figure 7.11: DSC trace of the solid PLGA-pyridine complex cast from a 40 g/l solution.

The secondary structure of the complex was investigated by IR spectroscopy. The spectrum of MD56 after the temperature dependent XRD series is shown in Figure 7.12. The Amide I at 1655 cm^{-1} and Amide II band at 1550 cm^{-1} allowed for an assignment of a pure helical structure. The formation of the hydrogen bonding complex was also confirmed by the hydrogen bonding which was located around 1900 and 2500 cm^{-1}. These bands decreased substantially during the annealing process confirming the removal of pyridine from the complex. The IR spectrum showed no other difference to the PLGA films prepared from other solvents.

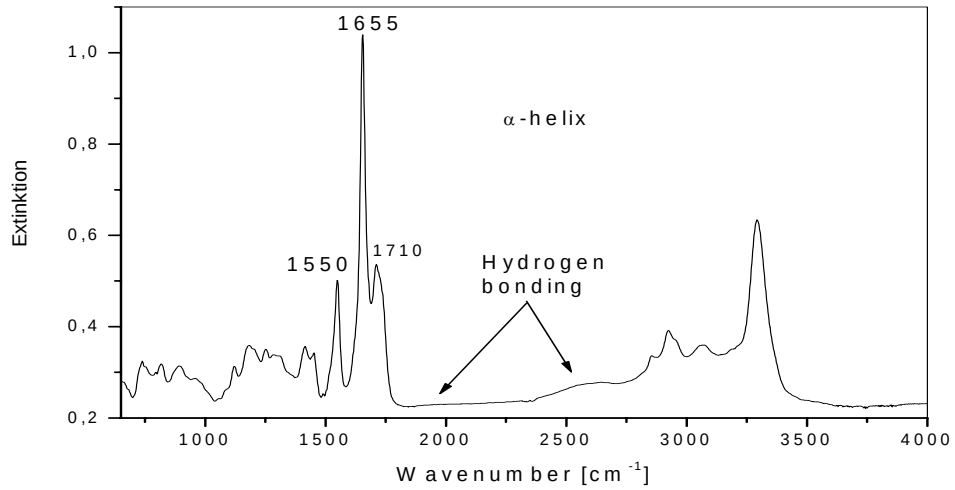

Figure 7.12: FTIR spectrum of a drop-cast PLGA film prepared from a 3/1 (v/v) pyridine/water mixture on a silica substrate [MD56] after annealing.

The complex was not soluble in TFA, glacial acetic acid, or D_2O. Alkaline D_2O dissolved the complex, but liberated pyridine as evidenced by smell. However, ^{1}H-NMR spectroscopy was attempted because PLGA itself was commonly measured in alkaline D_2O, but the pyridine reduced the resolution greatly.

After the first successful attempts a systematic study was conducted varying the parameters concentration and solvent mixture ratios of pyridine and water. The concentrations 5, 10, 20, and 40 g/l and the solvent mixture ratios 1/1, 3/2, 7/3, 4/1, and 9/1 (v/v) of pyridine/water were investigated for film preparation by drop-casting on silica. The concentration of 10 g/l was applied for each of the different solvent mixtures. The film thicknesses were expected to increase by casting three layers of solution on the substrate. The films were prepared in half closed Petri dishes and took one day to be prepared. The results were similar to the former ones. The films were partially crystalline, but without a reliable dependence on the solvent composition or the concentration. These parameters were therefore not decisive for the crystallization process of PLGA. One remarkable observation represented the physical properties of the films. The more crystalline the films were the more opaque they became. The most crystalline films were no longer able to be removed from the substrate in one piece. They could only be scratched off the substrate as a crystalline powder. The amorphous films, in contradiction, were easily peeled from the substrate. These amorphous films were translucent and flexible, but were not elastic.

One of the translucent flexible amorphous films of PLGA prepared from pyridine/water mixture 4/1 (v/v) was analyzed by 2D-SAXS and 2D-WAXS. The 2D-SAXS exhibited no scattering peaks and the 2D-WAXS showed only a diffuse ring without further orientation (picture not shown).

Polarized optical microscopy studies were performed to analyze the crystallization. A 10 g/l PLGA solution in a 3/1 (v/v) mixture of pyridine/water was analyzed on a glass slide. The pictures shown in Figure 7.13 exhibit some ribbon like structures in the liquid state. The structures remained unchanged during a fast evaporation process to the solid state.

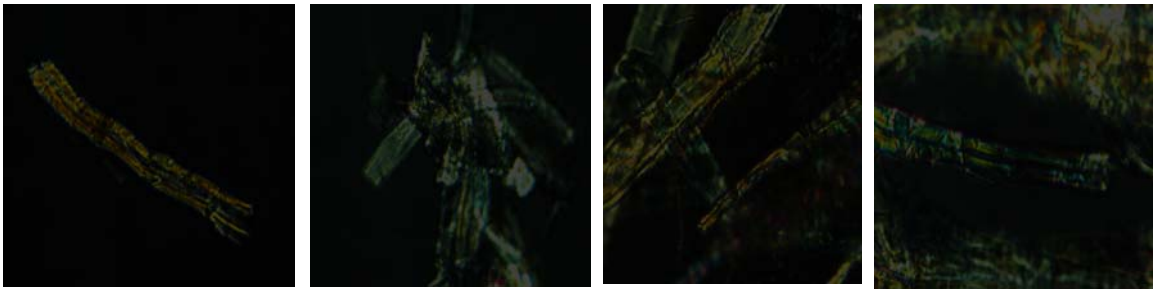

Figure 7.13: POM pictures of a 10 g/l PLGA solution in a 3/1 (v/v) pyridine/water mixture, observed with a magnification of 50x and under crossed polarizers.

A slow evaporation process on a glass substrate yielded in nice large spherulites as shown in Figure 7.14. The pictures observed with different magnifications prove a highly ordered structure on the macroscopic order.

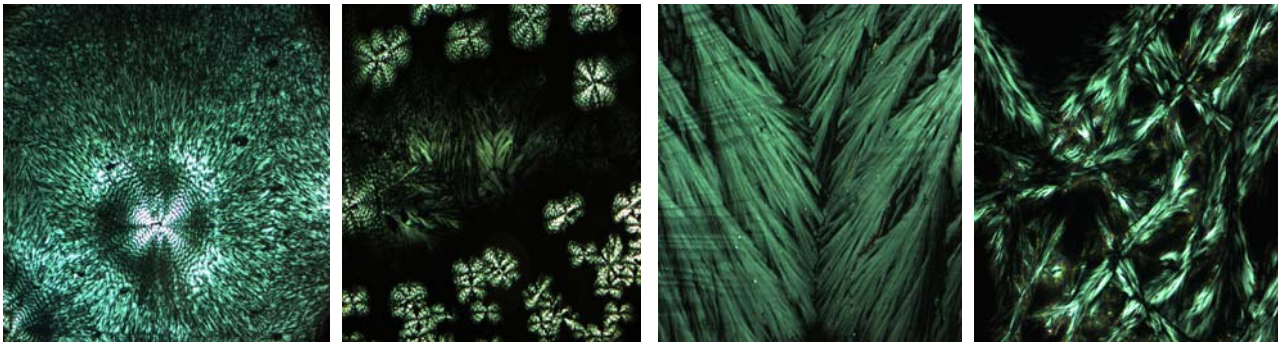

5x ***5x*** ***50x*** ***50x***

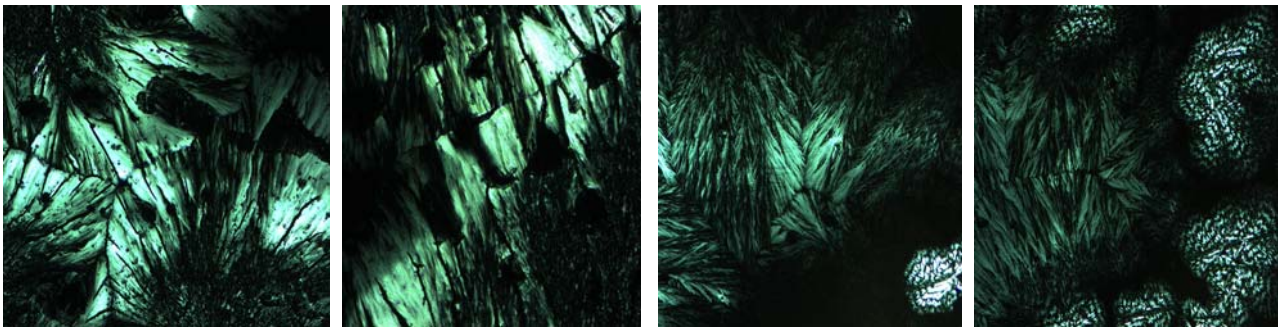

10x ***10x*** ***10x*** ***10x***

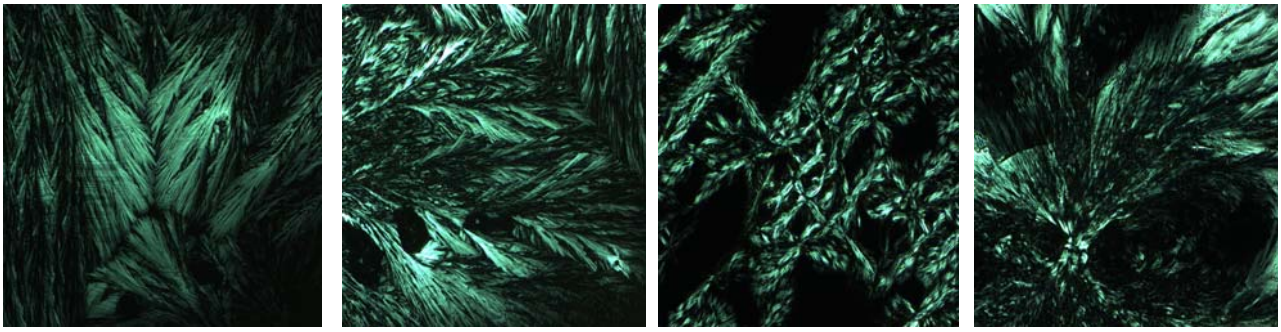

20x ***20x*** ***20x*** ***20x***

Figure 7.14: POM pictures of a slowly drop-cast film of a 10 g/l PLGA solution in a 3/1 (v/v) pyridine/water mixture on glass, observed under crossed polarizers. Magnification is given below the pictures.

The solution which yielded the large spherulites after the evaporation of the solvent was measured in a glass capillary in a transmission XRD experiment to analyze if there were crystal nuclei present. The obtained spectrum did not show crystalline ordered signals and was amorphous like the original PLGA powder exhibiting only a short distance order.

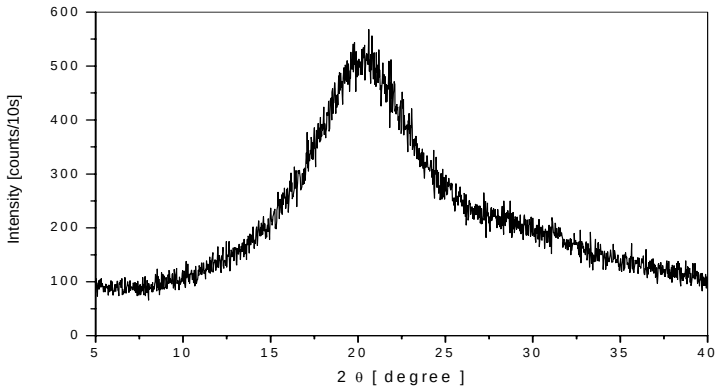

Figure 7.15: XRD pattern of PLGA in a 3/1 (v/v) mixture of pyridine/water, measured as liquid in a glass capillary by a 0.02 step scan with 10 s.

After these first approaches to produce crystalline films of PLGA from pyridine/water mixtures the film preparation procedure was changed to analyze the kinetics of the crystallization. The following films were prepared on silica substrates placed in half opened Petri dishes. These were put in a slightly opened vacuum desiccator which had paraffin oil at the bottom in a glass container. This set-up was successfully used to extract organic solvent very slowly to give the system enough time to crystallize out.

A series of experiments were conducted with a 10 g/l PLGA solutions of a 3/1 (v/v) pyridine/water mixture on silica. The three solution layers were added to the surface before the solvent of the former layer was completely evaporated. The sample was kept in the liquid state to investigate if this would enhance the crystallization process.
The films exhibited a partially crystalline character as shown in Figure 7.16. A pure crystalline film could not be obtained by this procedure.

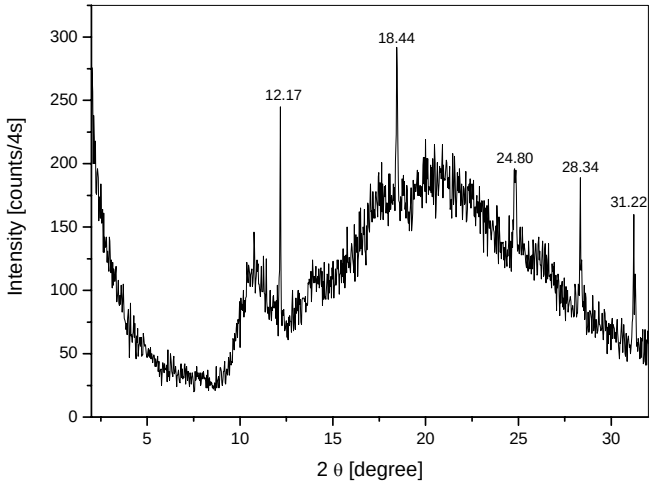

Figure 7.16: XRD pattern of a drop-cast PLGA film prepared from a 3/1 (v/v) pyridine/water mixture on a silica substrate [MD90]; 0.03 step scan with 4s.

Table 7.5: Crystalline Bragg reflections of MD90 in 2 θ with corresponding d-spacings.

2 θ [Degree]	12.17	18.44	24.80	28.34	31.22
D-spacing [A]	7.25	4.80	3.58	3.14	2.86

Experiments at lower temperature (ice water bath) did not improve the crystallization. Also the films were of poor quality because the evaporation rate of the solvent was too slow. The solvent at times did not evaporate completely sometimes to yield a solid film.

7.4 Hydrogen bonding disrupting solvent systems

The new crystallization procedure (vacuum desiccator) was attempted as well with other solvent systems of PLGA which had not given rise to crystalline films before. The solvents investigated were all known hydrogen bonding interrupting solvents. The solvents were mostly known to form lyotropic liquid crystalline solutions with PLGA in a defined concentration range at room temperature. Former film preparation studies had only given amorphous films. It was hoped that crystalline films containing a long range order could be prepared utilizing these solvent systems. All the film experiments were performed on silica substrates dried in the vacuum desiccator. Three layers of solution were put on the surface without waiting for complete evaporation of the former solution layer. The concentration of the solution was 10 g/l for the solvents DMF, DMA, TMU, and NMP. The films consisted of crystalline material for all solvent systems. The crystalline X-ray diffraction patterns shown in Figure 7.18-7.24 were all similar to the pyridine/water solvent experiments. The secondary structure of all films was detected by IR spectroscopy.

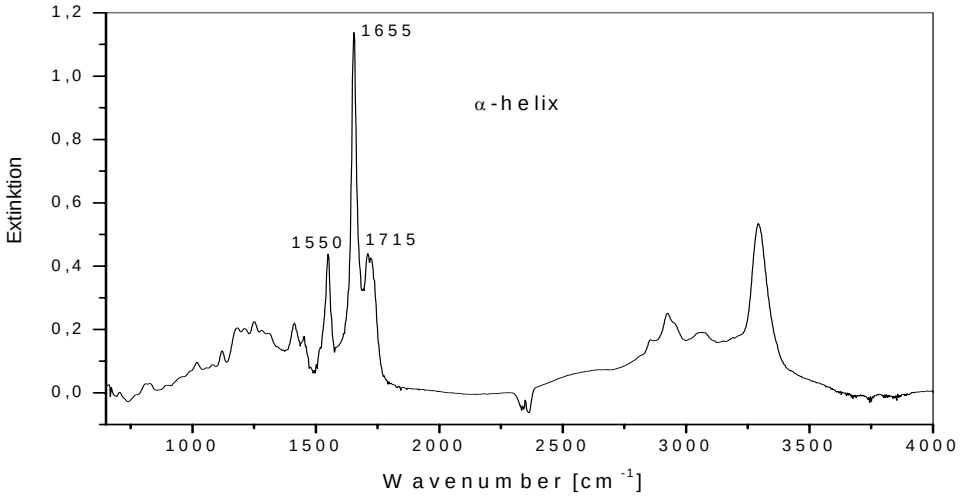

Figure 7.17: FTIR spectrum of a drop-cast PLGA film prepared from TMU solution (10 g/l) on a silica substrate [MD100].

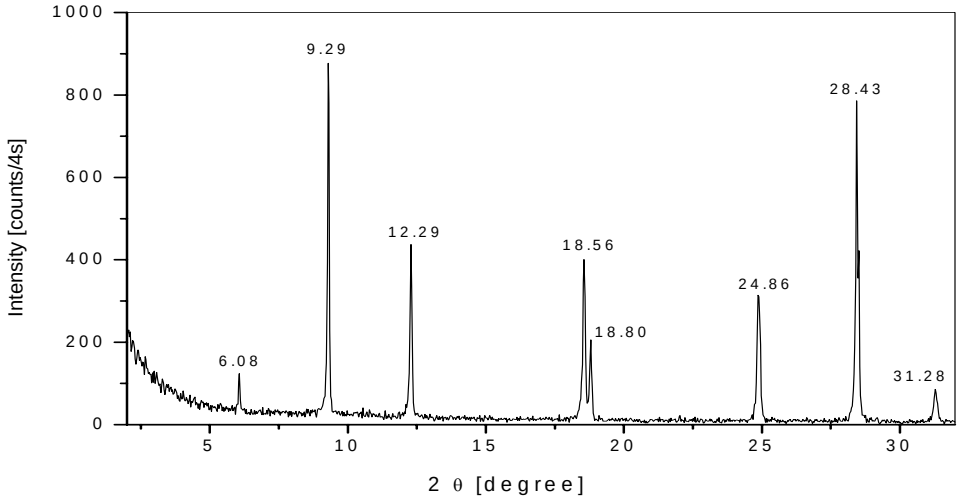

Figure 7.18: XRD pattern of a drop-cast PLGA film prepared from TMU solution (10 g/l) on a silica substrate [MD101]; 0.03 step scan with 4s.

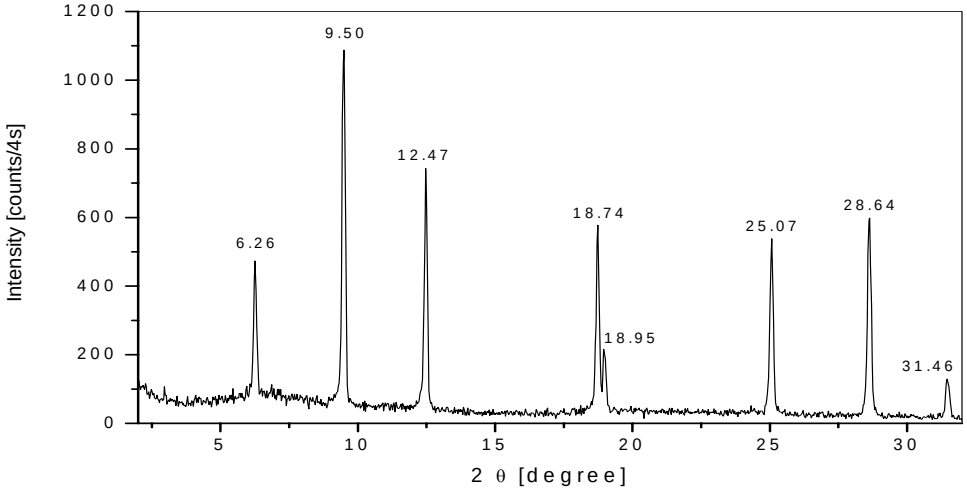

Figure 7.19: XRD pattern of a drop-cast PLGA film prepared from TMU solution (10 g/l) on a silica substrate [MD100]; 0.03 step scan with 4s.

Figure 7.18 and 7.19 show two of the numerous highly crystalline films prepared from TMU solutions of PLGA. The amorphous halo was absent and the diffraction pattern consisted exclusively of crystalline signals which were more numerous than as observed for the hydrogen bonding complex. The film MD100 was measured again with a smaller step scan of 0.02 and increased time of 5s, shown in Figure 7.20.

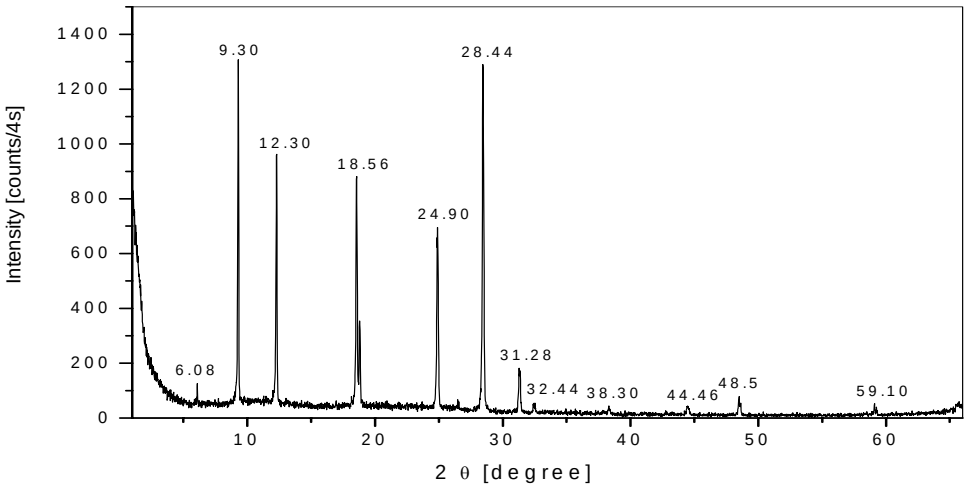

Figure 7.20: XRD pattern of a drop-cast PLGA film prepared from TMU solution (10 g/l) on a silica substrate [MD100]; 0.02 step scan with 5s.

DMF solutions of PLGA produced less crystalline samples compared to TMU as shown in Figure 7.21. The number of crystalline reflections is reduced and the amorphous halo is still recognizable. The IR spectrum is further given in Figure 7.22 representing a helical structure due to the Amide I and II band at 1650 and 1550 cm^{-1}.

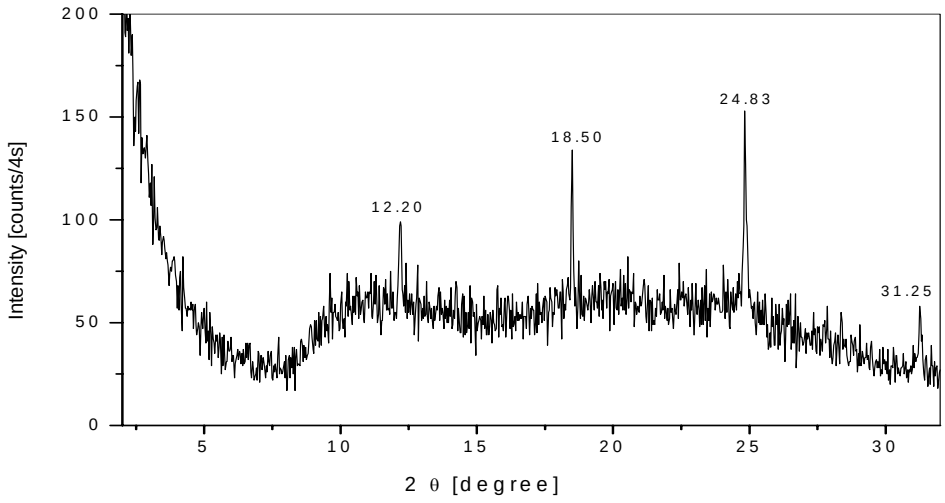

Figure 7.21: XRD pattern of a drop-cast PLGA film prepared from DMF solution (10 g/l) on a silica substrate [MD98]; 0.03 step scan with 4s.

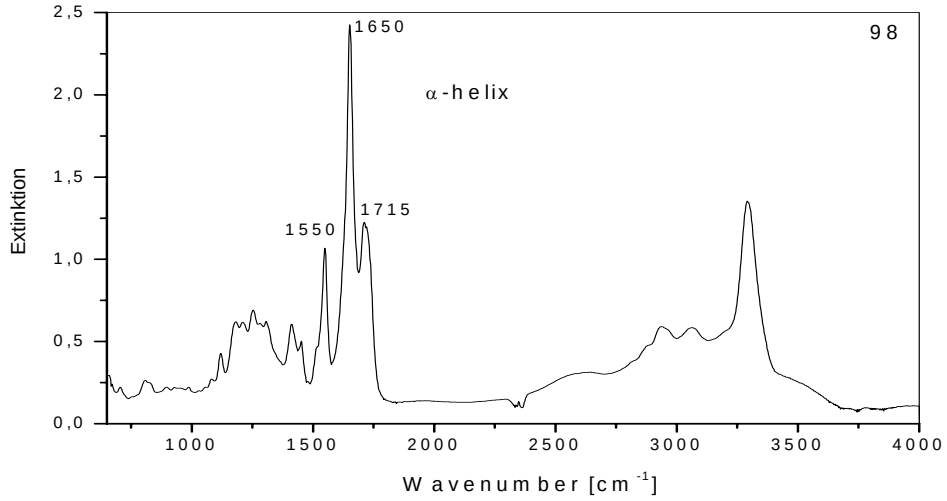

Figure 7.22: FTIR spectrum of a drop-cast PLGA film prepared from DMF solution (10 g/l) on a silica substrate [MD98].

PLGA solutions of NMP and DMA also led to crystalline films on silica as shown in Figure 7.23 and 7.24. The IR spectra were similar to the previous examples exhibiting a helical structure (not shown).

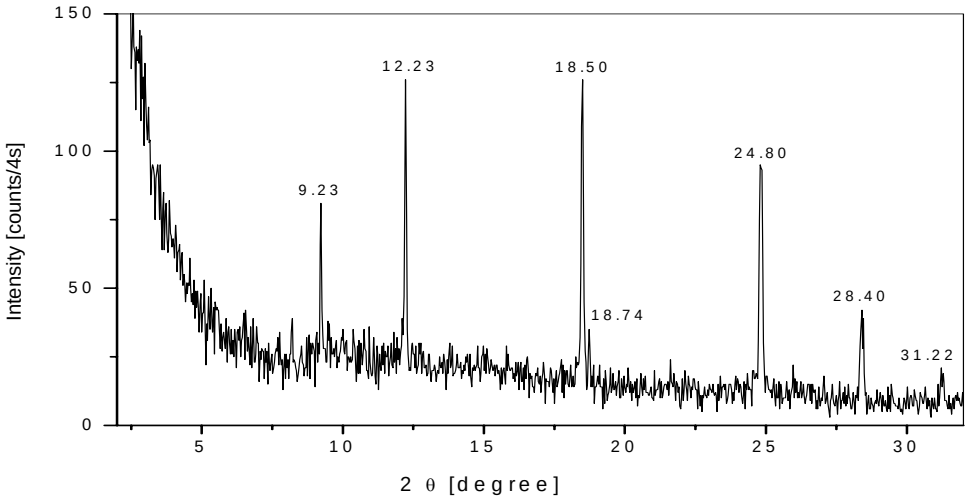

Figure 7.23: XRD pattern of a drop-cast PLGA film prepared from NMP solution (10 g/l) on a silica substrate [MD103]; 0.03 step scan with 4s.

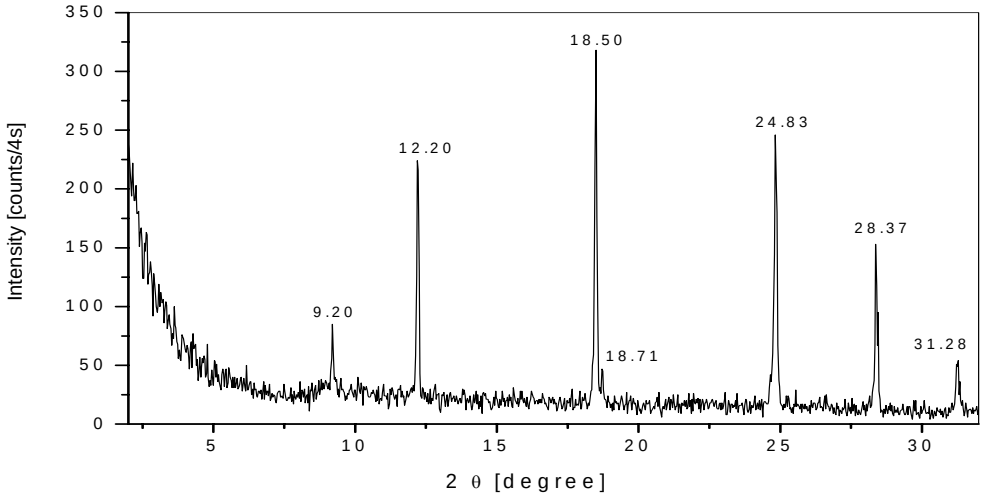

Figure 7.24: XRD pattern of a drop-cast PLGA film prepared from DMA solution (10 g/l) on a silica substrate [MD102]; 0.03 step scan with 4s.

The films prepared on silica could not be analyzed in transmission by the optical microscope. They were measured in reflectance mode exhibiting crystalline structures.

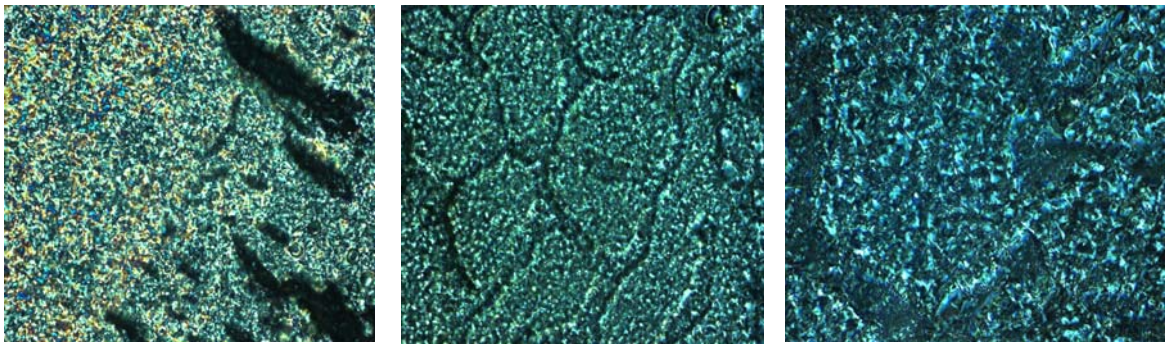

MD101, TMU, 20x | MD101, TMU, 10x | MD101, TMU, 20x

Figure 7.25: POM pictures measured in reflection of crystalline PLGA films. The solvent and the magnification is described below the pictures.

The 2 θ values together with their corresponding d-spacings of the different crystalline films of PLGA were summarized in Table 7.6 and 7.7 proving a high uniformity of all systems. They will be analyzed more in detail in chapter 7.5.

Table 7.6: 2 θ values of the different crystalline films of PLGA.

2 θ values				
PLGA				
DMF	**DMA**	**NMP**	**TMU**	**P/W**
			6.26	
	9.2	9.23	9.5	9.26
12.2	12.2	12.23	12.47	12.29
18.5	18.5	18.5	18.74	18.56
	18.71	18.74	18.95	
24.83	24.83	24.8	25.07	24.92
	28.37	28.4	28.64	28.46
31.25	31.28	31.22	31.46	31.31
				44.51
				48.44

Table 7.7: d-spacings of the different crystalline films of PLGA.

d-spacings [A]				
PLGA				
DMF	**DMA**	**NMP**	**TMU**	**P/W**
			14.08	
	9.59	9.56	9.28	9.52
7.24	7.24	7.22	7.08	7.18
4.78	4.78	4.78	4.72	4.77
	4.73	4.72	4.67	
3.58	3.58	3.58	3.54	3.56
	3.14	3.13	3.11	3.13
2.85	2.85	2.86	2.84	2.85
				2.03
				1.87

The roughness of the different films was investigated by AFM. Two samples, one amorphous film prepared from 50/50 (v/v) mixture of pyridine/water, and a second highly crystalline PLGA film (MD100) prepared from 10 g/l TMU solution were used. AFM was determined to be unsuitable because the roughness of the film surface is more than 0.5 µm. The analysis was continued with a confocal optical microscope (nanofocus) in order to obtain information about the topography of the films. The experiments confirmed a surface roughness of 0.5 µm for the crystalline PLGA (TMU) film. The amorphous film was more uniform with a reduced roughness of 0.3 µm (left column of Figure 7.26). The crystalline sample exhibited a non-uniform surface with crystalline domains and amorphous domains, in contradiction, to the amorphous hydrogen bonded complex film (middle column of Figure 7.26). This led to the increased film surface roughness illustrated by the 3-D pictures on the right column of Figure 7.26.

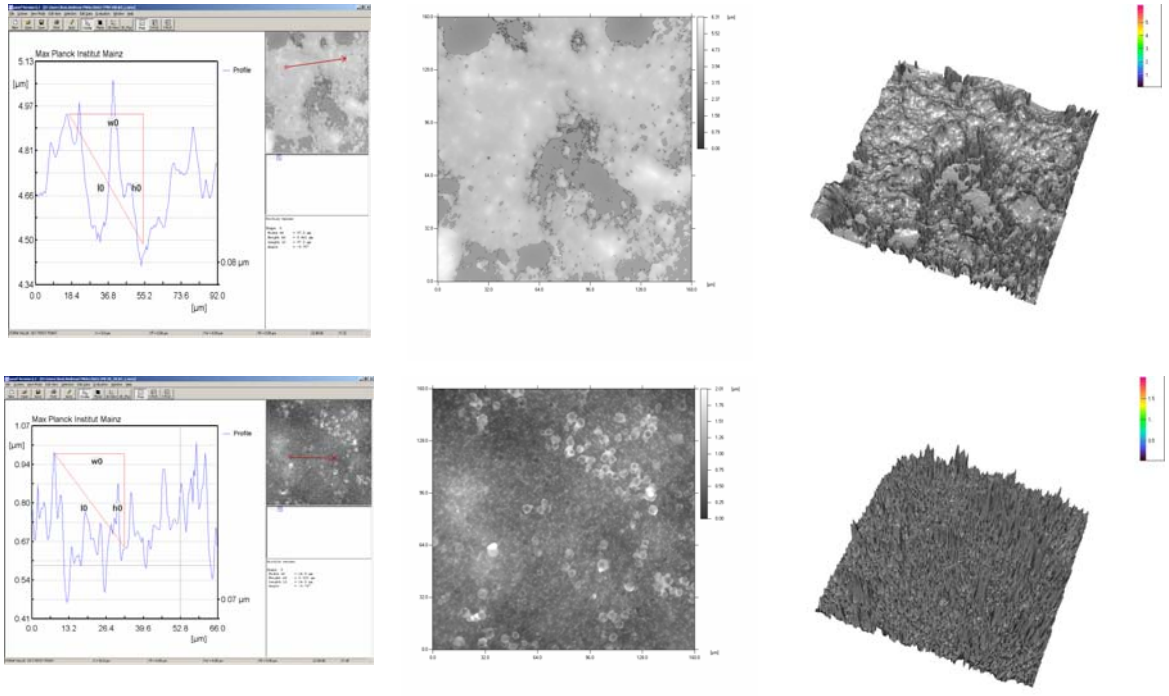

Figure 7.26: Confocal microscopy studies of a crystalline PLGA_TMU film (top) and an amorphous PLGA film of a 50/50 (v/v) pyridine/water mixture (bottom).

Many studies were attempted to prepare crystalline films on glass substrates, but this seemed to be more challenging than on silica. The conditions used to prepare films on silica did not lead to similar results on glass. A reason for this different behavior could be presumably the different wettability of the surfaces. The water contact angle measurements showed that the surface of glass (5°) was quite hydrophilic compared to the very hydrophobic surface of silica (80°).

7.5 Crystallization of other polymer systems

The desiccator method was applied to other synthesized polypeptides in order to investigate if the crystallization method can be transferred and was a general treatment for a broader spectrum of polypeptides.

PSCBC (MD-1-50) and PBLG (MD-1-45) films prepared by drop-casting were attempted from 10 g/l solutions in DMF or mixtures of $CHCl_3$ and DMF on silica in the vacuum desiccator. PBLG did not produce good films over a concentration range of 1 g/l to 20 g/l. However, PSCBC yielded sharp crystalline diffraction patterns as shown in Figure 7.28. The crystalline refinement was similar to the other systems. Surprisingly for these crystalline structures the IR spectrum exhibited a β-sheet structure as shown in Figure 7.27 in agreement with the literature for polypeptides with a heteroatom in the side chain.

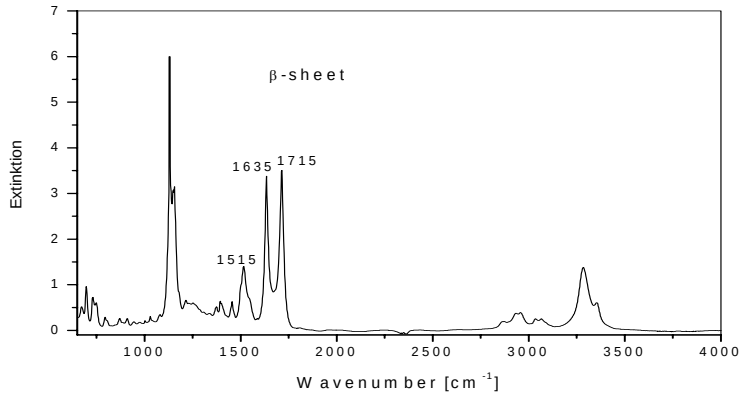

Figure 7.27: FTIR spectrum of a drop-cast PSCBC film prepared from DMF solution (10 g/l) on a silica substrate [MD106].

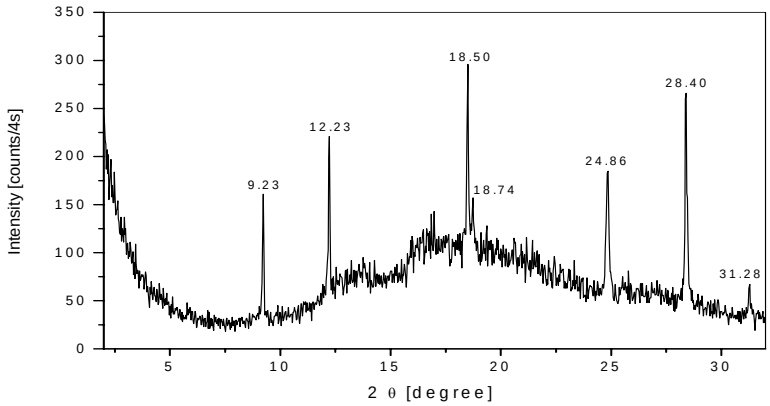

Figure 7.28: XRD pattern of a drop-cast PSCBC film prepared from DMF solution (10 g/l) on a silica substrate [MD106]; 0.03 step scan with 4s.

These results reexamined many times for reproducibility and reliability because it was bothersome that different secondary structures yielded in the same crystal structure. This was unexpected because if the secondary structure was different the spatial arrangement of the atoms should be different as well, but they were not.

The evaporation time was assumed up to this point to play the decisive role for achieving crystalline films on silica. However, residual solutions (7/3 (v/v) mixture of $CDCl_3$/TFA-d) of NMR test tubes of PSCBC and PSBC were applied for drop casting on silica in a Petri dish. The film casting required just one day at room temperature for the evaporation of the solvent in contradiction to the desiccator studies, which needed at least two weeks for complete solvent evaporation. The films showed again the same crystalline refinement in XRD (Figure 7.29 and 7.30) and the β-sheet structure in IR (not shown).

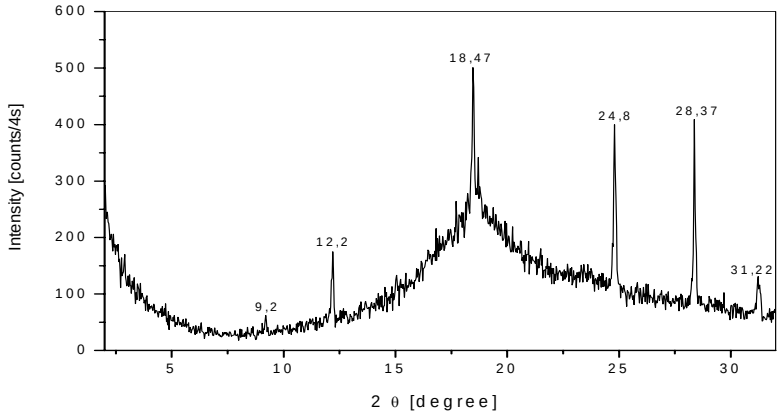

Figure 7.29: XRD pattern of a drop-cast PSBC film prepared from a 7/3 (v/v) $CDCl_3$/TFA-d mixture on a silica substrate [MD135]; 0.03 step scan with 4s.

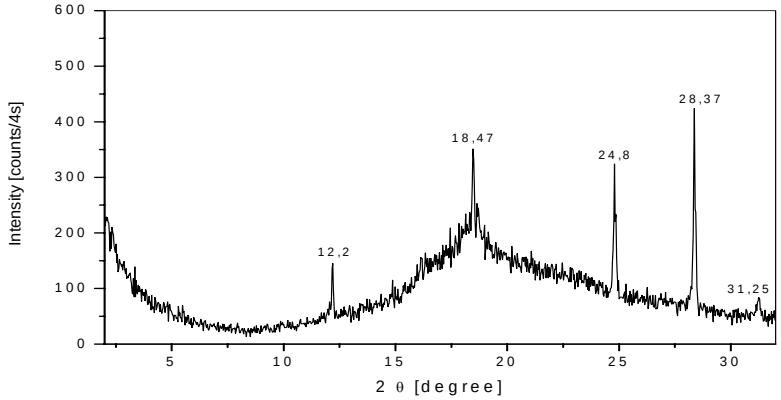

Figure 7.30: XRD pattern of a drop-cast PSCBC film prepared from a 7/3 (v/v) $CDCl_3$/TFA-d mixture on silica [MD140+141]; 0.03 step scan with 4s.

If it is assumed that the evaporation kinetics (evaporation time) were not critical for the crystal growth, the choice of an appropriated solvent becomes very important. All examined solvents are strong hydrogen bonding interrupters. One must consider that the presence of aggregates may inhibit the crystallization of polypeptides. The dynamic light scattering studies of PBLG and PLGA in DMF indicated aggregated chains. Stirring at 60°C for 24 h led to a complete disruption of the aggregates. This was observed as well in the crystallization process where the DMF films exhibited a much lower degree of crystallinity as compared to TMU. The ability of the solvent to break up aggregation should be considered decisive for the crystal growth. This explains why these crystals have not been previously reported. Most researchers have focused on more common helical solvents where aggregation is prevalent ($CHCl_3$, THF, toluene etc.). The crystals, which were known from PLGA, were produced as salts (Mg, Na, K, Ba).[22] There are strong electronic repulsions between the side chains in the liquid state which hinders aggregation by hydrogen bonding. This would confirm that the crystal growth is independent of the secondary structure. The different d-spacings summarized in chapter 7.4 in Table 7.7 exhibit two different series of crystalline reflexes each with a factor of two between the single spacings, which indicate that the crystalline films consist of a mixture of two different regular layered structures. Unfortunately, there is no more information available about the nature or the chemical structure of these assumed layered structures so that every chemical proposition would be highly hypothetic. Further crystallization studies will have to solve this mystery. IR measurements could not prove the existence of a two phase system because there was always just one pure phase (helix or sheet) present at similar XRD patterns. The possibility one phase is crystallizing out from a mixture of two ordered secondary structures can be therefore excluded.

7.6 Analysis of possible side products

The current work to investigate possible small molecule impurities which could crystallize out, leading to these highly crystalline XRD patterns, will be summarized here. The sharpness of the crystalline signals gave rise to assume a small molecule because for a polymer seem the patterns to be too sharp. Additional it is curious that the crystalline reflexes are not changing their position, intensity or shape upon heating during the temperature dependent XRD measurements.

Small molecule halides formed by residual bromide ions from the saponification process of PLGA can be excluded because PLGA was purified after the synthesis by soxhlet extraction. Another argument against halides represents the fact that also PSCBC and PSBC crystallized with the same XRD patterns. There was no halide present during their synthesis at all. Pyridine hydrobromide and pyridine bromide perbromide (pyridine $HBr*Br_2$) were however checked. It was commercially available as crystalline powder which was so hygroscopic that after 2 min a clear solution was obtained. The material could not be measured in X-ray, but literature data were different to our samples. The following experiment proved definitely the absence of low molecular weight halides by using an $AgNO_3$ solution test procedure. The silver nitrate solution was dropped in a PLGA solution of a pyridine/water mixture. There was no characteristic precipitation of a silver halide detected. Afterwards some drops of an aqueous sodium bromide solution were added to yield a precipitate to check the $AgNO_3$. The yellow precipitate formed immediately and was equal to the control; where aqueous sodium bromide and silver nitrate were mixed.

Diketopiperazines are a class of possible crystalline cyclic organic compounds that result from peptide bonds between two amino acids to form a lactam. A diketopiperazine was the first peptide to have its complete three dimensional structure described by Robert Corey in the 1930s. Their synthesis was intensively studied by different scientists [34-36] and as cyclodipeptides they can be found as degradation product of oligo- and polypeptides which are easily formed even at room temperature.[37,38] They can also exist as side or even as main products in NCA polymerizations.[39-42]

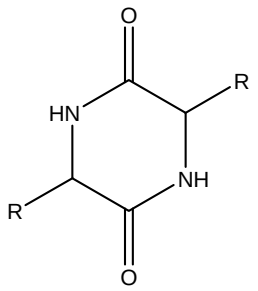

Figure 7.31: 2,5-Diketopiperazine or also called 2,5-dioxopiperazine

The carbonyl signals of all cyclopeptides appear 1.5-4.0 ppm upfield of the carbonyl signals of the corresponding polypeptides and can be therefore used for their detection and identification in ^{13}C-NMR spectra in mixtures with oligo- and polypeptides.[43] The glycine derivative was commercially available and the IR and Raman spectra were compared without a significant indication for its presence. The XRD of a drop cast film of a DMF solution of this crystalline compound exhibited signals at 14.87, 15.08, and 30.59 (2 θ) which were not consistent with our samples. The NMR and IR spectra of the crystalline films could not provide any proof for the presence of these compounds.

Another possible side product class represented n-hexyl ammonium salts formed by the initiator during the polymerization. The carbon dioxide evolution could lead to the corresponding carbonate and the applied drying agent $MgSO_4$ for the organic layer in the triphosgene method would lead to the sulfate. N-hexyl ammonium sulfate was synthesized by reacting n-hexyl amine with sulfuric acid. N-hexyl ammonium carbonate was produced by bubbling CO_2 gas through a wet THF solution of n-hexyl amine. Both white compounds were successfully obtained. Their XRD patterns were shown in Figure 7.32 and 7.33 whereby the sulfate represented a typical layered structure. The signal refinement was not matching with our crystalline spectra.

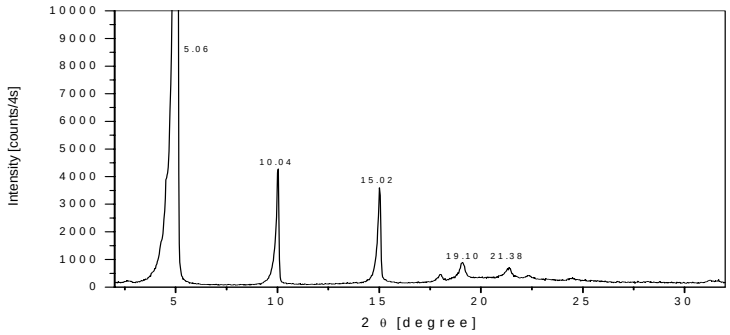

Figure 7.32: XRD powder pattern of n-hexyl-ammonium sulfate; 0.03 step scan with 4s.

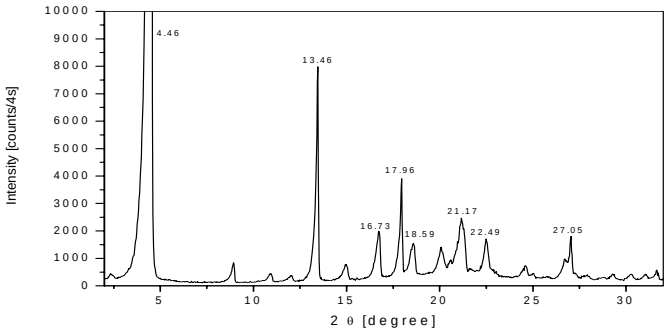

Figure 7.33: XRD pattern of n-hexyl-ammonium carbonate; 0.03 step scan with 4s.

An assumed small molecule, which crystallizes out, should be extractable by different solvents because the PLGA itself is insoluble in most of the common organic solvents. Extraction experiments were executed by using acetone, MeOH, THF, ACN, EtOH, and EtOAc without obtaining a highly crystalline small molecular compound.

Another possibility could be that the polymerization proceeded via γ-peptide bonds instead of α-peptide bonds formation (linkage on the carboxylic acid group in the side chain). This could lead to crystalline linear compounds chemically identical to the regular polypeptide chains illustrated in Figure 7.34. This is improbable because PSCBC and PSBC can not form this linkage, but the crystal structure is the same. This should exclude this possible side reaction.

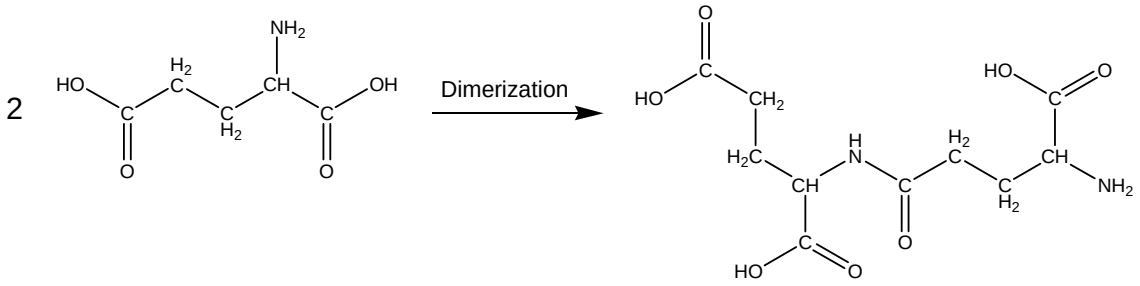

Figure 7.34: γ-peptide bond formation instead of α-peptide bonds.

Different databases were used for the identification of possible side products, impurities or any material, which could have caused these crystalline refinements.[44,45] The examined compounds were p.e. n-hexyl ammonium salts (iodide, bromide, hydrogen arsenate, hydrogen phosphate, and hydrogen phosphate hydrate), silicon oxide (SiO_2), silica (Si), 2,5 – diketopiperazines (Glycine anhydride), glutamic acid hydrochloride, D,L-glutamic acid, D,L-glutamic acid hydrate, β-PLGA, pyridine hydrobromide (pyridine_HBr), and pyridine bromide perbromide (pyridine_HBr*Br_2). Nothing was matching with the obtained crystalline patterns.

HPLC fractionation of PLGA was performed to check for small molecule impurities which could give rise to the observed crystallizations.

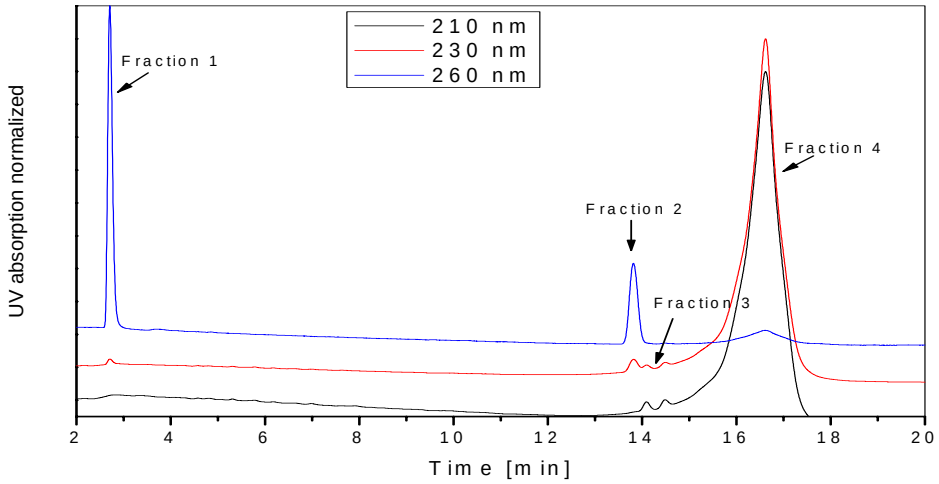

Figure 7.35: HPLC fractionation of PLGA powder by running a gradient from a mixture of 5 % ACN, 95 % H_2O, and 0.1 % TFA to 30 % ACN, 70 % H_2O, and 0.1 % TFA.

The interpretation of Figure 7.35 must be carefully conducted. Each UV-wavelength spectrum was normalized to give maximum intensity for the most intense peak. The maximum value was kept constant for all three detection wavelengths. However, the absolute intensity differed significantly, especially for the 260 nm spectrum where Fraction 1 and 2 were most recognizable. Figure 7.35 gives a qualitative, but not a quantitative result because the UV absorption coefficients of the different fractions were unknown and the absolute intensity could therefore not be related easily to the concentration in solution.

Table 7.8:
ESI-MASS (fraction 1) of PLGA fractionated by HPLC in the solvent system 70% (v/v) H_2O, 30% (v/v) ACN, 1% (v/v) TFA.

M/Z (Mass / Charge)	Intensity [%]
209*	22.79
225	15.50
255	100.00
263*	7.89
402*	8.72

Table 7.9:

ESI-MASS (fraction 2) of PLGA fractionated by HPLC in the solvent system 70% (v/v) H_2O, 30% (v/v) ACN, 1% (v/v) TFA.

M/Z (Mass / Charge)	Intensity [%]
153*	23.06
158*	50.46
214*	47.83
225	14.27
282	69.63
352*	33.11
355*	21.12
360	13.93
402*	30.02
406*	100.00
413*	16.21
431*	31.96
435	28.88

Table 7.10:

ESI-MASS (fraction 3) of PLGA fractionated by HPLC in the solvent system 70% (v/v) H_2O, 30% (v/v) ACN, 1% (v/v) TFA.

M/Z (Mass / Charge)	Intensity [%]
153*	18.66
207*	14.52
209*	9.42
225	6.40
282	7.22
333*	17.34
352*	27.05
360	58.98
406*	100.00
407*	16.97
431*	28.10

Table 7.11:

ESI-MASS (fraction 4) of PLGA fractionated by HPLC in the solvent system 70% (v/v) H_2O, 30% (v/v) ACN, 1% (v/v) TFA.

M/Z (Mass / Charge)	Intensity [%]
153	15.98
158	7.31
209	35.62
214	11.87
263	7.76
333	27.85
352	40.18
406	59.82
413	18.26
431	8.68
478	11.42
496	31.51
561	100.00
614	27.85
697	10.96
709	10.05

The signals marked with * were present in all fractions of PLGA and, therefore, were not be dependent on a small molecule impurity, which could crystallize out instead of the polymer. The ESI-Mass spectroscopy was measured in exactly the same solvent mixture as the HPLC fractionation was conducted. The HPLC started the gradient with a mixture of 5 % ACN, 95 % H_2O, and 0.1 % TFA, raising the polarity of the solvent mixture by increasing the percentage of ACN finally to 30 % ACN, 70 % H_2O, and 0.1 % TFA. Four fractions were obtained as shown in Figure 7.35 whereby fraction 4 represents PLGA. The first three fractions exhibited a different sensitivity depending on the UV detection wavelength. Fraction 1 and 2 had a higher UV absorbance at 260 nm compared to 210 nm. Fraction 3 and 4 were nearly invisible by increasing the wavelength from 210 to 260 nm corresponding to the UV activity of the polypeptide backbone. There is normally no UV absorbance at 260 nm of the backbone. Fraction 1 and 2 may consist of residual PBLG chain units which were not saponified. A phenyl ring would be highly absorbing in the range of 260 nm. Benzyl alcohol from the deprotection reaction and n-hexyl amine were injected and were determined to be not responsible for any of the fractions. The ESI-Mass spectra did not provide any evidence that pointed to the presence of small crystalline impurities. Most of the signals of the first three fractions are also present in fraction 4.

GPC studies were conducted to compare the PLGA powder with the highly crystalline PLGA film prepared from TMU (MD101). The measurements did not show a difference between the systems. The molecular weight distributions were similar and did not give rise to different molecular weight distributions as would be expected if a cleavage of polypeptide chain had occurred, which could then crystallize.

Crystalline and amorphous PLGA films were removed from silica substrates to measure the material in ^{1}H-NMR. The chemical structure was exactly the same compared to the original PLGA powder (spectra not shown).

Solid state NMR spectra comparison between a PLGA powder and a drop-cast film of a pyridine/water mixture, shown in Figure 7.36 and 7.37, did not exhibit big differences due to the secondary structure.

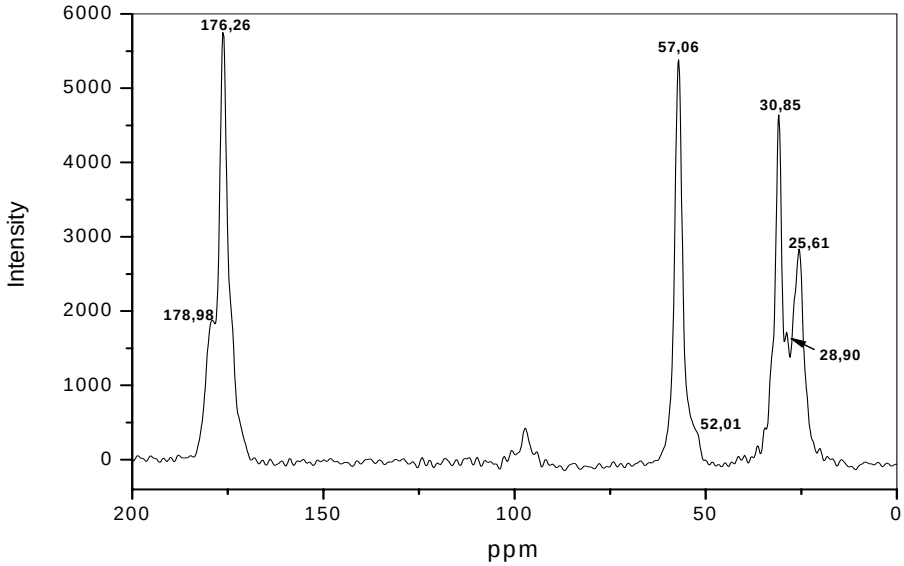

Figure 7.36: Solid state NMR spectrum of PLGA (powder).

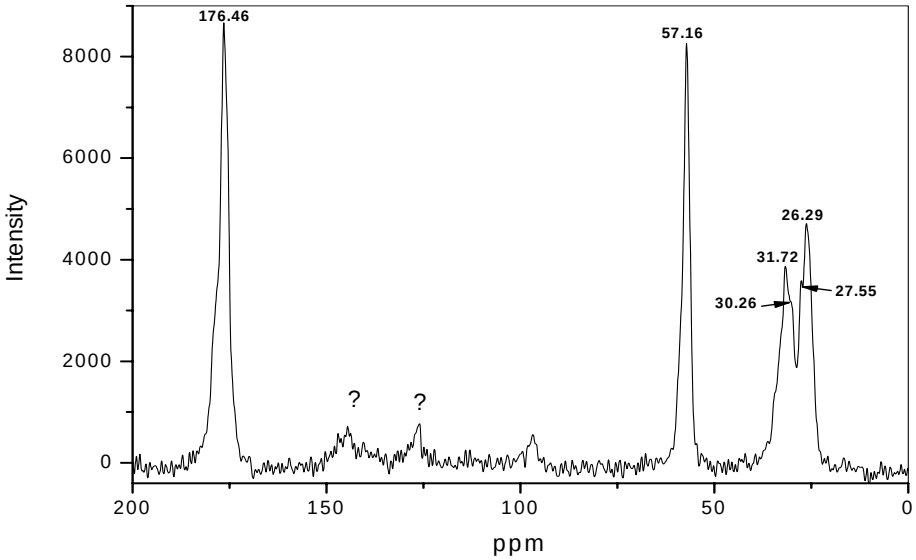

Figure 7.37: Solid state NMR spectrum of a PLGA film prepared from a 7/3 (v/v) pyridine/water mixture on silica.

Detailed experiments carried out to investigate the origin of the crystalline structure observed. It was unclear if the crystalline structure of the prepared films could be the result of locked-in lyotropic liquid crystals from solution because all the solvent systems exhibit lyotropic liquid crystallinity. For this purpose defined concentrations (1, 5, and 10 g/l) of PLGA in the solvents TMU, DMA, DMF, NMP and of PSCBC in DMF were prepared. Glass substrates with a fixed metal ring on the top were prepared to allow for larger amounts solution on the glass substrate. The evaporation of the solvent was controlled by weighing the substrate and by POM. If the assumption was correct that the lyotropic liquid crystalline state led to the crystallization process, changes would be expected to be observable. The results of the POM did not support the formation of a liquid crystalline phase.

In conclusion, there could be nothing found as impurity or small molecule, which crystallizes out instead of the polymer. All attempted experiments were met with little success.

References:

[1] C. Robinson, J.C. Ward, R. B. Beevers, *Disc. Faraday Soc.*, **1958**, *25*, 29

[2] C. Robinson, *Trans. Faraday Soc.*, **1956**, *52*, 571

[3] A. Elliot, E. J. Ambrose, *Discuss. Faraday Soc.*, **1950**, *9*, 246

[4] H. Block, *Poly (gamma-benzyl-L-glutamate) and other glutamic acid containing polymers, Vol. 9*, Gordon and Breach, **1983**

[5] P. Rohrer, H. G. Elias, *Makromol. Chem.*, **1972**, *151*, 281

[6] P. J. Flory, W. J. Leonard, *J. Am. Chem. Soc.*, **1965**, *87*, 2102

[7] W. H. Daly, P. S. Russo, I. I. Negulesco, *unpublished results*

[8] D. S. Poché, *Ph.D. Dissertation*, Louisiana State University, **1990**

[9] J. Watanabe, T. Nagase, *Polymer J.*, **1987**, *19*, 781

[10] T. Mori, S. Tonegawa, N. Tsuji, *Chem. Express*, **1991**, *6*, 731
T. Mori, A. Morofuji, R. Tanaka, *Polymer J.*, **1979**, *11*, 721

[11] T. Mori, *Kobunshi Ronbunshu*, **1983**, *40*, 767

[12] T. Mori, *Kobunshi Ronbunshu*, **1982**, *39*, 105

[13] T. Mori, *Kobunshi Ronbunshu*, **1979**, *36*, 183

[14] T. Mori, *Kobunshi Ronbunshu*, **1979**, *36*, 189

[15] T. Mori, *Kobunshi Ronbunshu*, **1981**, *38*, 493

[16] T. Mori, *Kobunshi Ronbunshu*, **1980**, *37*, 717

[17] T. Mori, M. Koga, *Chem. Lett.*, **1989**, *4*, 289

[18] T. Mori, *Polymer J.*, **1985**, *17*, 1145

[19] T. Mori, K. Watanabe, A. Toyofuku, *Chem. Express*, **1993**, *8*, 541

[20] H. D. Keith, *Biopolymers*, **1971**, *10*, 1099

[21] H. D. Keith, G. Giannoni, F. J. Padden, *Biopolymers*, **1969**, *7*, 775

[22] F. J. Padden, H. D. Keith, *J. Appl. Phys.*, **1965**, *36*, 2987

[23] H. Pivcova, V. Saudek, P. Schmidt, D. Hlavata, J. Plestil, F. Laupretre, *Polymer J.*, **1987**, *28*, 991

[24] A. Elliott, E. J. Ambrose, *Disc. Faraday Soc.*, **1950**, *9*, 246

[25] A. Elliott, G. D. Fasman, *Poly-α-amino Acids*, New York, **1967**, Dekker Inc.

[26] G. Floudas, *Biomacromolecules*, **2004**, *5*, 81
G. Floudas, *Prog. Polym. Sci.*, **2004**, *29*, 1143

[27] H. Kihara, T. Kato, T. Uryu, J. M. J. Frechet, *Chem. Mater.*, **1996**, *8*, 961

[28] T. Kato, J. M. J. Frechet, P. G. Wilson, T. Saito, *Chem. Mater.*, **1993**, *5*, 1094

[29] T. Kato, N. Hirota, A. Fujishima, J. M. J. Frechet, *J. Polym. Sci. A Polym. Chem.*, **1996**, *34*, 57

[30] T. Kato, N. Mizoshita, K. Kishimoto, *Angew. Chem. Int. Ed.*, **2006**, *45*, 38

[31] T. Kato, J. M. J. Frechet, *J. Am. Chem. Soc.*, **1989**, *111*, 8533

[32] T. Kato, J. M. J. Frechet, *Macromol. Symp.*, **1995**, *98*, 311

[33] T. Kato, J. M. J. Frechet, *Liquid Crystals*, **1993**, *14*, 5, 1311
[34] P. M. Fischer, *J. Peptide Sci.*, **2003**, *9*, 9
[35] C. J. Dinsmore, D. C. Beshore, *Tetrahedron*, **2002**, *58*, 3297
[36] I. L. Karle, H. C. J. Ottenheyn, B. Witkop, *J. Amer. Chem. Soc.*, **1974**, *96*, 539
[37] A. Gmaurer, *Chem. Comm.*, **1971**, 39
[38] K. Titlestad, *Chem. Comm.*, **1971**, 1527
[39] L. Bilek, J. Derkoscg, H. Micheld, F. Wessely, *Monatsh. Chem.*, **1953**, *84*, 717
[40] P. Rosenmund, K. Kaiser, *Angew. Chem.*, **1970**, *82*, 137
[41] M. Rothe, D. Mühlhausen, *Angew. Chem. Int. Ed. Engl.*, **1976**, *88*, 338
[42] H. R. Kricheldorf, K. Bösinger, *Makromol. Chem.*, **1976**, *177*, 1243
[43] H. R. Kricheldorf, *Org. Magn. Res.*, **1980**, *13*, 52
[44] *JCPDS*, **1997**, International Centre for diffraction data
[45] *JCPDS*, **1996**, International Centre for diffraction data

Chapter 8
Fiber extrusions

8.1 Introduction

Fibers from liquid crystalline polymers with greatly enhanced orientation and strength have been spun from liquid crystalline solutions or melts. The lyotropic system of PBLG in chloroform was the first detected polymer system to exhibit a liquid crystalline phase. In 1950, Elliot and Ambrose reported that the concentrating of a solution of PBLG in a helical solvent resulted in a birefringent phase with a high optical rotation.[1] However, only a fraction of main chain liquid crystalline polymers can form fibers with high thermal and thermo-oxidative stability. Therefore, liquid crystalline polymer fibers consist of aromatic chemical structures in order to retain their linearity and rigidity. Although main chain liquid crystalline polymers with flexible spacers have also been studied, it is evident that the mechanical properties and thermal stability are drastically reduced after the number of flexible units in the main chain liquid crystalline polymers exceeds two.[2]

Fibers spun from the lyotropic state usually employ a wet or dry-jet wet spinning method, while those spun from thermotropic liquid crystalline polymers are spun from the melt. The wet spinning process, named for the aqueous solutions that are often used as coagulating agents, is employed mostly for lyotropic polymers in nonvolatile solvents. The extruded material or extrudate is immersed directly in a non-solvent bath, where fiber coagulation and solution extraction take place. Molecular weight is a major contributing factor that determines the strength of the fibers produced. In order to produce fibers with adequate tensile strength to utilized in industrial applications, the intrinsic viscosity of the polymer must exceed 4 dl/g.[2]

In 1972 the first commercially available high performance organic fiber, poly(p-phenylene terephthalamide), known as PPTA or *Kevlar*, was produced by a dry-jet wet fiber spinning process by DuPont. It would be almost 20 years before any other high performance fibers were available. Fiber spinning could be carried out even at moderate temperatures (around 80-95°C). Although Kevlar fibers possessed high crystallinity based on WAXD and density measurements, the nature of the crystal morphology was still in question.[2] Fibers from isotropic solutions of aromatic polymers exhibited different structures than those formed from anisotropic solutions because limited order is induced via the fiber spinning process. Therefore, heat treatment plays an important role in the structural development. *Technora* was the most important commercial aromatic polyamide fiber (1985) with unique fiber properties like chemical and impact resistance.[2]

8.2 Results and discussions

In the current study, attempts were made to extrude fibers from lyotropic liquid crystalline solutions of PSCBC in DMF or PLGA in TMU in an aqueous coagulation bath. All attempts to prepare fibers via solvent extrusion met with limited success. The low molecular weights of the polymeric material, which never exceeded a degree of polymerization of 100 due to synthetic limitations, may be a determining factor. Another factor that may limit fiber production via this method is the low rigidity of the polypeptide backbone compared to Kevlar due to the absence of the phenylene group. The combination of a quite flexible backbone and low molar mass give rise to solutions with low viscosity, which also hampered attempts to induce orientation by shearing the sample between two glass plates.

Mechanical extrusion of the polymeric materials was attempted by heating the powders to temperatures just below the onset of degradation to produce macroscopically oriented filaments. The degradation temperature for the polymers PLGA, PSBC, and PSCBC were previously determined by TGA. Floudas et al. noticed during the work with PBLG that a temperature much higher than the glass transition (T_g) is required to induce a softening of the material, [3] but PLGA was found to be non-extrudable even at high temperatures. However, PSBC and PSCBC were successfully extruded for the first time to fibers. The different extrusion behavior could be related to the thermal behavior as observed in DSC where PLGA did not exhibit a glass transition in contradiction to PSBC and PSCBC, which were at 31°C and 47°C, respectively. Annealing of the polymers above T_g of the amorphous polymer sections obviously helped to soften the material enough to become extrudable.

Two dimensional SAXS and WAXS measurements were used to characterize the fibers produced from the extrusion experiments. SAXS measurements did not reveal any orientation in large scale dimensions. The WAXS measurements were suitable to detect an orientation of the obtained fibers along the vertical direction. PSCBC was only measured at RT and exhibited, as shown in Figure 1, two equatorial reflections in the 2D image. The integration of the image delivered the 1D plot (Figure 8.1). Two halos were detectable at the positions 5.22 and 18.18 2 θ corresponding to the d-spacings 16.88 and 4.87 Å. The patterns were comparable to the described XRD powder patterns of the different poly(glutamates) in chapter 3.3. The weak intensity of the second halo could not be assigned to a lower crystallinity than the second one in Figure 8.2. It indicated that in one case (Figure 8.1) more single polypeptide chains were aligned in a parallel direction to the incident X-ray beam during the X-ray measurement in the size dimension of local domains than in the second case (Figure 8.2). The amorphous halo was just

showing an average over a defined number of small local domains consisting of single chains (intramolecular distances like the identity periods, 5.4 Å for a α-helix and 7.27 Å for a β-sheet). The first sharper peak corresponds most likely to intermolecular distances.

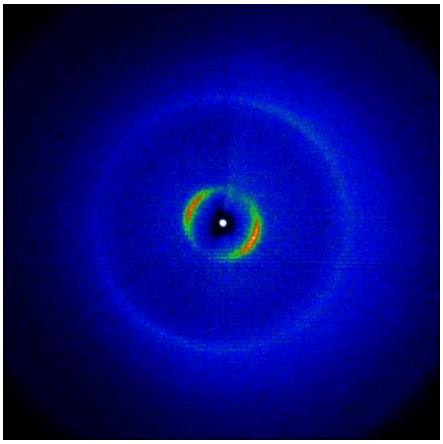

PSCBC fiber at 30°C

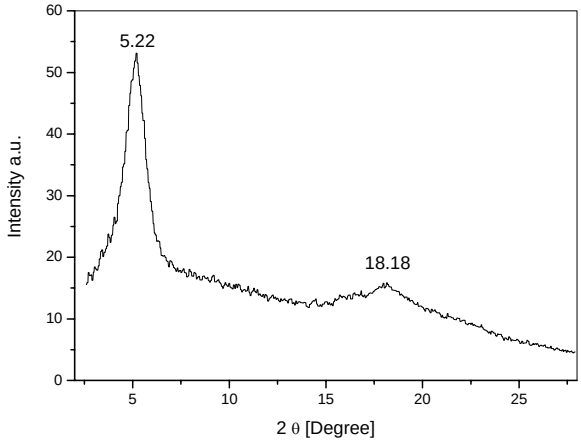

Figure 8.1: Extruded fiber diagram of PSCBC (2D-WAXS left, 1D-WAXS right).

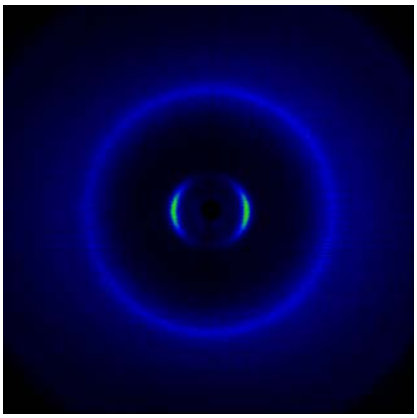

PSBC fiber at 30°C

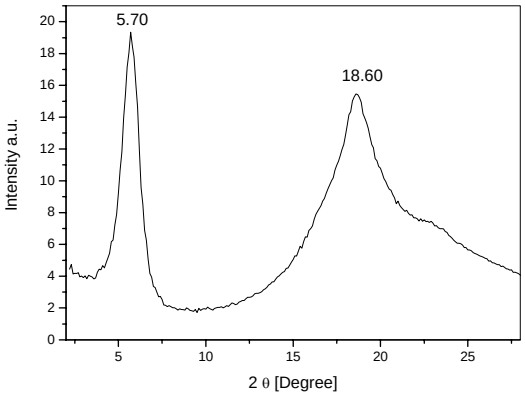

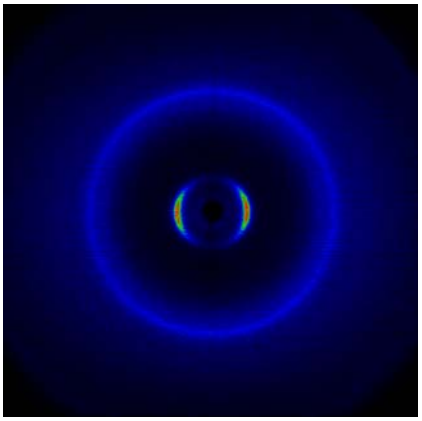

PSBC fiber at 170°C

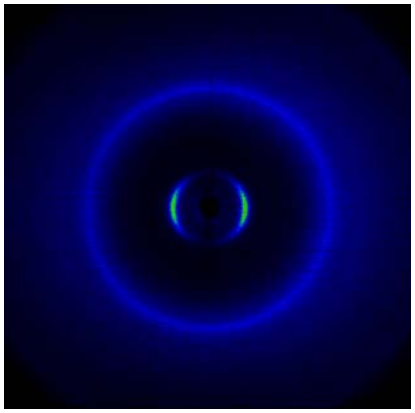

PSBC fiber back at 30°C

Figure 8.2: 2D-WAXS fiber images of PSBC together with a 1D plot.

A temperature dependent series were measured for the extruded PSBC fiber applying the following temperatures: 30, 40, 50, 60, 70, 80, 90, 100, 120, 140, 160, 170 and back to 30°C. Figure 8.2 proved that the orientation of the fiber could be reversibly increased by annealing up to 170°C. As soon as the fiber was cooled down to room temperature the orientation partially vanished again. The room temperature 1D plot exhibited like in Figure 8.1 two halos at 5.70 and 18.60 2 θ, corresponding to d-spacings of 15.46 and 4.76 Å. The intramolecular 4.76 Å spacing was also detected in the crystalline films of PLGA described in chapter 7.

References:

[1] A. Elliott, E. J. Ambrose, *Discuss. Faraday Soc.*, **1950**, *9*, 46

[2] D. R. Salem, *Structure formation in polymeric fibers*, **2001**, Hanser Publ., Munich

[3] P. Papadopoulos, G. Floudas, H. A. Klok, I. Schnell, T. Pakula, *Biomacromolecules*, **2004**, *5*, 81

Chapter 9
General conclusions and outlook

A series of different γ-esters of PLGA and poly (L-cysteine) derivatives were successfully synthesized by living anionic ring-opening polymerization. The NCA monomers were obtained by reacting phosgene substitutes with the commercially available amino acid derivatives with the exception of octadecyl-L-glutamate, which was synthesized from L-glutamic acid. The NCA polymerization was successfully adapted from literature for the synthesis of PSCBC and PSBC, which have not been prepared by phosgene substitutes previously. All polypeptides were purified by soxhlet extraction due to the low solubility of the products. The chemical structures were confirmed by ^{1}H- and ^{13}C-NMR spectroscopy and the thermal properties were characterized by TGA and DSC. XRD powder patterns found these compounds to be amorphous for all of the polymers obtained. The molecular weight characterization by common techniques like GPC, light scattering (DLS and SLS), viscosimetry, osmometry etc. were very challenging due to very low solubility and high tendency of the polymers to form aggregates in solution. Finally, all the polymers could be successfully characterized by one of the aforementioned techniques. The molecular weights of some polymers were obtained by viscosity measurements in the highly acidic solvent DCA, which was able to inhibit the aggregation of the polypeptide chain. The secondary structure in the solid state was analyzed by using different conformational sensitive techniques. The powders were characterized by IR-, Raman-, and solid state NMR spectroscopy; the prepared polypeptide films exclusively by IR spectroscopy. The order of the prepared films was analyzed by DSC, POM and X-ray diffraction. The polypeptides with different ordered states (helix, β-sheet) in the solid state at room temperature were applied to investigate a conformational change to the disordered coil structure by annealing.

The first film preparation attempts were focused on the preliminary results obtained during earlier work. The drop-casting procedure was successfully applied for TFA solutions of PLGA to produce uniform bulk films of a thickness between one and five micrometers on silica substrates. The analysis of the films by XRD exhibited that no long range order or orientation is present in the samples even if they all possessed a helical microstructure, which was confirmed by IR spectroscopy. The absence of IR dichroism indicated absence of orientation phenomena. The coil solvent TFA delivered constantly a helical or a β-sheet structure in the solid state depending on the water content of the solvent which was observed for the first time to exhibit a high influence on the crystallization process for PLGA. Temperature dependent in-situ IR measurements were examined to analyze if a helix-coil transition occurs, but there could be no solvent system

determined, which resulted in a disordered coil structure in the solid state. General parameters like solvent systems, evaporation conditions, concentration, substrates etc. were investigated for the preparation of uniform bulk films. PLGA films prepared from TFA solutions were once tested as coating material for printing tests and showed a strong contrast limited to a short running length because the film was most probably washed out by fountain water and/or ink under the printing procedure. The determined wettability change observed in the earlier work for this system was caused by the onset of degradation of the material and not by a conformational change of the polypeptide backbone.

For further film preparations other solvent systems were applied due to the lack of a long range order in the TFA system and the high volatility of the solvent. New crystallizations were successfully obtained on silica prepared by drop-casting of solutions of PLGA in DMF, DMA, TMU, NMP, and pyridine/water mixtures, respectively. PSCBC in DMF, $CDCl_3$/TFA-d, and PSBC in $CDCl_3$/TFA-d exhibited the same crystalline diffraction patterns like PLGA. The long range order in the X-ray diffraction pattern is proven by extremely sharp crystalline signals, which are not changing the shape or the position of the peak by increasing the temperature up to 160°C. The substrate seems to play a decisive role because the crystalline structures were not obtainable on glass. The crystal structure consists probably of two different layered structures based on the intensity ratios of the two series of crystalline signals in the X-ray diffraction patterns. The source of the layered structure remains unclear and needs further studies to investigate the spatial arrangement of the chains in more detail. The secondary structure was still not changing upon heating even if a highly crystalline diffraction pattern occurs. Concluding that even the newly investigated crystallization did not show a helix-coil transition in the solid state by annealing, the phenomenon known in solution has to be claimed as unachievable in the solid state based on the results of this work. One reason could be that the melting temperature of the helix is higher than the degradation temperature. To exclude other sources for the XRD patterns, extractions were attempted with common organic solvents to extract a possible small crystallizable molecule. These attempts were negative. The molecular weight distribution and the polydispersity were analyzed by GPC and the crystalline films were similar to the PLGA powder. A HPLC fractionation of the PLGA powder was accomplished to search for small molecule impurities, which cannot be detected by GPC, because their low molecular weights will remain unrecognized. Three additional fractions obtained by HPLC fractionation were analyzed by ESI-mass spectroscopy without proving a small molecular compound. A possible formation of salts consisting of halides could be excluded due to the negative result of a test reaction with silver nitrate solution. No sign for a degradation product or other small molecules was determined by analyzing the chemical structure (NMR), functional groups (IR) or the

thermal behavior (DSC, TGA). Different crystallographic databases contained no data for known crystalline compounds with a similar crystalline refinement. A remaining open question represents the observation that the same crystalline pattern can be reproducibly prepared with exhibiting two different ordered secondary structures (helix and β-sheet). After the investigation that the evaporation time cannot be decisive for the crystal growth, the choice of a strong hydrogen bonding interrupting solvent is most probably the key to support and induce the crystallization process. The linkage between aggregation behavior on the one side and the crystallization process of polypeptides on the other side could offer great opportunities for future crystallization studies of this important polymer class.

Materials and Instruments

Temperature calibration:

The temperature calibration for glass and silica substrates placed on a copper holder for temperature dependent XRD patterns was conducted using a thermo couple wire placed in a small hole on the corresponding surface. The apparent temperatures on silica needed no correction; however the temperatures of the glass substrates were 5 degrees lower than indicated. The temperatures for measurements on glass had therefore to be increased by 5°C during in-situ XRD measurements.

Capillary Electrophoresis (CE):

Different fused-silica capillaries were used with a diameter of 50 or 75 µm and a capillary length between 40 and 100 cm. The current should be kept below 100 µA. The electropherograms were recorded by the "G1600AX" device (Agilent Company), equipped with a Diode Array detector.

FTIR-Spectroscopy:

The FTIR spectra were recorded by the „Magna-IR 850" spectrometer (Nicolet Company) in transmission. The temperature dependent FTIR series of the drop-cast films were accomplished with at least 100 scans per measurement in a nitrogen flushed chamber.

NMR-Spectroscopy:

All ^{1}H-NMR and ^{13}C-NMR spectra were recorded by different devices from the Bruker Company (DPX 250 or AV300). All spectra were calibrated against the corresponding deuterated NMR solvent like DMF-d_7: 2.91 ppm, D_2O: 4.67 ppm or $CDCl_3$: 7.25 ppm.

Spin-Cast Films:

Polypeptide films were spin-cast by the „Delta 80" device (Süss Mikrotec Company).

Thermal gravimetric analysis (TGA):

TGA measurements were accomplished by the „TG 50" device (Mettler Company) with a heating rate of 10 K/min.

TGA-MS:

The coupling of TGA with mass spectroscopy was accomplished by the „TGA/SDTA-851" device (Mettler Company) and the „Quadstar 422" mass spectrometer (Pfeiffer Company).

Differential Scanning Calorimetry (*DSC*):

DSC of powders and films were measured by a „DSC 30" device (Mettler Company) with different heating rates (2-20 K/min).

Chemicals:

All chemicals were purchased from Sigma-Aldrich and were used without further purification unless otherwise stated.

^{13}C-CP MAS solid state NMR:

All ^{13}C-CP MAS spectra have been recorded on a Bruker ASX machine operating at ^{1}H and ^{13}C Larmor frequencies of 500.13 MHz and 125.76 MHz, respectively. Using a commercial Bruker 4 mm double-resonance probe at a spinning frequency of 10 kHz, the contact time was set to 2 ms with 10 s relaxation delays between two successive transients. For each sample, at least 1024 scans were averaged.

Raman-Spectroscopy:

The Raman spectra were recorded by the „RFS 100/S" spectrometer (Bruker Company).

X-ray diffraction (XRD):

The XRD patterns were measured in reflection by the „PW 1820" diffraction device with a vertical goniometer (Philips Company) or with the „D8 Advance 2" diffraction device (Bruker). Both equipments used a scintillation detector ($CuK_{\alpha 1+2}$ wavelengths, 40 kV, 30 mA).

UV-Spectroscopy:

The UV spectra were recorded by the „Lambda 2" spectrometer (Perkin Elmer Company).

Gel Permeation Chromatography (GPC):

The GPC measurements were accomplished with the following devices and parameters: Column GRAM (porosity 10^3, 10^4, 10^6 Å; particle size 10 µm; dimensions 0.8*30 cm), Pump Waters 515, Detectors ERC RI-101 and UV S-3702 (SOMA), solvent DMF (60°C, 1 ml/min)

HPLC:

The HPLC spectra were recorded by a device of the Agilent Company. A quaternary gradient pump "HP 1100" was used. The solvents and other conditions are described in the corresponding section.

Viscosimetry:

The inherent viscosity was determined by an Ubbelohde viscometer coupled to a Schott device in different solvents described in the corresponding sections.

Light Scattering (DLS and SLS):

The light scattering measurements were accomplished by the “SP81” Goniometer equipped with an “ALV 5000” correlator. The laser wavelength was 632.8 nm (He/Ne).

MALDI-TOF spectroscopy:

MALDI-TOF spectra were recorded by the “Time-of-flight MS Reflex III” device (Bruker Company).

Mass spectroscopy:

The FD-mass measurements were recorded by the “MAT 95” device (Finnigan Company) and the ESI-mass measurements were recorded by the “QTos Ultima 3” device (Micromass/Waters Company).

Optical Microscopy:

Optical microscopy studies were accomplished using the “Axiophot” device (Zeiss Company).

Confocal optical microscopy:

Confocal optical microscopy studies were accomplished using the “Axiovert 200M” device (Zeiss Company).

Abbreviations

A_2	Second Virial Coefficient
AcOH	Acetic acid
ACN	Acetonitrile
B_{hkl}	Width at half height
CD	Circular Dichroism
CE	Capillary Electrophoresis
CZE	Free Zone Capillary Electrophoresis
d	Doublet (^{1}H-NMR spectra)
Da	Dalton
DCA	Dichloro Acetic Acid
DCTB	*trans*-2-[3-(4-*tert*-Butylphenyl)-2-methyl-2-propenylidene]malononitrile
DLS	Dynamic Light Scattering
DMA	Dimethylacetamide
DMF	Dimethyformamide
DMI	1,3-Dimethyl-2-Imidazolidone
DMSO	Dimethyl Sulfoxide
dn/dc	Refractive Index Increment
DP	Degree of Polymerization
DSC	Differential Scanning Calorimetry
DTT	Dithiothreitol
EOF	Electroosmotic Flow
ESI	Electrospray Ionization
EtOH	Ethanol
EtOAc	Ethylacetate
Et_2O	Diethylether
FA	Formamide
FD	Field Desorption
FTIR	Fourier Transform Infrared Spectroscopy
g	Gram
GPC	Gel Permeation Chromatography
h	Hour
HCl	Hydrochloric Acid
HFIP	Hexafluoroisopropanol
H_2O_2	Hydrogen Peroxide
$KMnO_4$	Potassium Permanganate
KOH	Potassium Hydroxide

M	Molar Mass
MALDI-TOF	Matrix Assisted Laser Desorption Ionization-Time of Flight
MeOH	Methanol
mg	Milligram
min	Minute(n)
mL	Milliliter
M_n	Number Average Molecular Weight
M_w	Weight Average Molecular Weight
MSA	Methane Sulfonic Acid
MWD	Molecular Weight Distribution
NCA	N-Carboxyanhydride
NMF	n-Methylformamide
NMP	N-methylpyrrolidone
NMR	Nuclear Magnetic Resonance
N_2O_4	Dinitrogentetraoxide
ORD	Optical Rotational Dispersion
PBLG	Poly (γ-Benzyl-L-Glutamate)
PDI	Polydispersity Index
PEO	Polyethylenoxide
PLGA	Poly (L-Glutamic Acid)
POM	Polarized Optical Microscopy
ppm	Parts Per Million (10^{-6})
ROP	Ring-Opening Polymerization
RT	Room Temperature
s	Singlet (^{1}H-NMR spectra)
SAXS	Small Angle X-ray Scattering
SLS	Static Light Scattering
t	Triplett (^{1}H-NMR spectra)
TCNQ	7,7,8,8-Tetracyano quino dimethane
TFA	Trifluoroacetic acid
TGA	Thermal Gravimetric Analysis
THF	Tetrahydrofuran
TLC	Thin Layer Chromatography
TMS	Tetramethylsilane
TMU	Tetramethylurea
UV	Ultraviolet
WAXD	Wide Angle X-ray Diffraction
WAXS	Wide Angle X-ray Scattering
XRD	X-ray Diffraction

% (v/v)	Volume Percentage
% (w/w)	Weight Percentage
θ	Bragg Angle
χ	Degree of Crystallinity
$<R_g^2>_z^{1/2}$	z-Average of the Radius of Gyration
L_{hkl}	Crystallite Size
T_g	Glass Transition